NICKEL-ALKALI HETEROBIMETALLIC CATALYSTS FOR ETHYLENE POLYMERIZATION

by
Thi Viet Tran

A dissertation submitted to the Department of Chemistry,
College of Natural Sciences and Mathematics
in partial fulfillment of the requirements for the degree of

Doctor of Philosophy

in Chemistry

Chair of Committee: Dr. Loi H. Do

Committee Member: Dr. Olafs Daugulis

Committee Member: Dr. Eva M. Harth

Committee Member: Dr. Thomas S. Teets

Committee Member: Lars C. Grabow

University of Houston
August, 2020

ACKNOWLEDGEMENTS

I wish to express my sincere appreciation to my thesis advisor, Professor Loi Do, for patiently guiding, encouraging, and supporting me throughout my Ph.D. studies. As a member of the Do Research Group, I will always keep in mind Dr. Do's reminder that we should strive for the absolute best in our work and in our scientific presentations. I can proudly say that my time at the Dr. Do's Group has been an intellectually and personally enriching experience. I would like to thank all my committee members, Dr. Daugulis, Dr. Harth, Dr Teets, and Dr. Ghabow for many insighful suggestion and for the tough questions which motivated me to enhance my knowledge and broaden my research perspectives. I also want to acknowledge Dr. Daugulis, Dr. May, Dr. Wu, Dr. Coltart, Dr. Miljanic, and Dr. Cai, for fantastic chemistry lectures.

My sincere thanks also go to my group members: Amy, Dawei, Anh, Mike, Sohini, Huong, Dat, Eryn, and Abhipsa. My research and my life would have been more challenging without their generous helps.

My decision to come to US to pursue an advance degree in chemistry was largely due to the encouragement of my undergraduate mentors at BKU, Dr. Thanh Truong, Dr. Nam Phan, Dr. Tung Nguyen, Dr. Chung Nguyen, and Dr. Thai-Anh Nguyen. I am extremely grateful to them for the wonderful time we had together at BKU. Many thanks to my friends Quan Tran, Huong Nguyen, Trang Nguyen, and Ky Le.

Special thanks to Yennie, my wife, for coming into my life.

Finally, I would like to dedicate this thesis to my family and my in-laws. Words can not express how grateful I am to their continuous and unparalleled love, help and support.

ABSTRACT

Polyethylene (PE) is one of the most commonly used plastics in our society due to the low-cost of ethylene and their diverse applications. The physical, chemical, and mechanical properties of PE are influenced by its molecular weight, molecular weight distribution, and morphology. Production of PE using single-site transition metal based catalysts is advantageous over processes based on free radial chemistry because it allows synthesis of well-defined polymers. However, single site catalysts typically afford one type of polymer under a given set of reaction condition. To obtain different PE products, it is necessary change the reaction conditions or chemically modify the steric or electronic properties of the catalyst. The former could be difficult to do in an industrial plant setting, whereas the latter may consume a tremendous amount of labor, cost, and time.

To overcome these drawbacks, our group has been developing stimuli-responsive catalysts that are capable of yielding different polyethylene product from a universal catalyst platform. We have created several Ni or Pd catalysts that could switch reactivity by interchanging their pendant secondary cations.

In this thesis, we have prepared a new class of nickel phosphine-phenolate complexes bearing a pendant polyethylene glycol (PEG) chain to provide a binding pocket for secondary metals. In the presence of secondary alkali cations such as Li^+, Na^+, K^+, and Cs^+, our heterobimetallic complexes displayed significant enhancement in catalytic activity and thermal stability compared to that of their parent monometallic complex and afforded different types of PE depending on the alkali ions used. The nickel-lithium complex showed extraordinary activity at 40 ^oC and the nickel-cesium displayed a high thermal stability at 90 ^oC. We also took advantage of the tunability of our

nickel complex to synthesize bimodal PE in one-pot reactions. Polymerization of ethylene using our nickel complex in the presence of a mixture of Li/Na afforded polyethylene with bimodal molecular weight distributions, which was confirmed by GPC characterization.

Lastly, we have prepared a bulky variant of our nickel phosphine-phenolate-PEG catalyst. The introduction of bulkier substituents into the phosphine donor has led to a significant enhancement in catalyst thermal stability and polymer molecular weight.

TABLE OF CONTENTS

LIST OF ABBREVIATIONS

acac	acetylacetonate
$BAr^{F}_{4}^{-}$	tetrakis(3,5-trifluoromethylphenyl)borate
Bu	butyl
BHT	butylated hydroxytoluene
CF_3	trifluoromethyl
COD	1,5-cyclooctadiene
CuAAC	Copper-catalyzed azide-alkyne cycloaddition
d	doublet
DCM	dichloromethane
DMSO	dimethyl sulfoxide
DSC	differential scanning calorimetry
equiv	equivalence
Et	ethyl
ESI	electrospray ionization
FID	flame ionization detector
GC	gas chromatography
GPC	gel permeation chromatography
HRMS	high resolution mass spectroscopy
HDPE	high density polyethylene
IR	infrared (spectroscopy)
J	coupling constant
LDPE	low density polyethylene
m	multiplet or milli
m	meta
m/z	mass to charge ratio
Me	methyl
MeCN	acetonitrile
M_n	the number average molecular weight
min	minute
ml	millliter
mp	melting point

MSD	mass spectral detector
M_w	the weight average molecular weight
NMR	nuclear magnetic resonance
NO_2	nitro
o	ortho
OMe	methoxyl
OR	alkoxy
p	para
PE	polyethylene
PEG	polyethylene glycol
PEX	Cross-link polyethylene
Ph	phenyl
ppm	parts per million
PO	polyolefin
Py	pyridine
q	quartet
s	singlet
t	tert
TBTA	tris(benzyltriazolemethyl)amine
TCB	1,2,4-trichlorobenzene
TCE	tetrachloroethane
TOF	turnover number
TON	turnover frequency
UHMWPE	ultra-high molecular weight polyethylene

LIST OF FIGURES

LIST OF SCHEMES

LIST OF TABLES

Chapter 1. Catalyst Tuning Strategies

1.1. Introduction

Polyolefins (PO) are among some of the most commonly used plastics in our society with an annual production of about 150 million tons.[1] In general, POs possess many advantages in comparison with other natural or man-made materials such as their high tensile strength, chemical stability, corrosion resistance, innocuousness, lightweightness, flexibility, low production cost, and recyclability. These properties make POs suitable for numerous applications, such as packaging materials, storage containers, pipes, electronics, fabrics, and foams.[2-4]

Within the PO class of materials, polyethylene (PE) is manufactured with the largest volume, comprising more than 70 million tonnes produced yearly. The low-cost of ethylene and the diverse properties of PE make these polymers highly useful in commercial products. For example, in the packaging sector, high-density polyethylene (HDPE) is commonly used as containers and low-density polyethylene (LDPE) is commonly used as plastic wraps.[5-6] The applications of PE are strongly dependent on its physical, chemical, and mechanical properties. These properties are heavily influenced by the molecular weight distribution (MWD) and polymer microstructure (branching type, branching density, and block structure).[2, 7-9]

Greater than 70% of PE is being produced via transition metal catalyzed reactions.[9] Although early transition metal catalysts (e.g., Ti, Hf, Zr) have been used with much success, interests in late transition metal catalysts, particularly Ni and Pd, have increased due to their greater potential in copolymerizing ethylene with polar monomers.[3-4, 10-13] Ni and Pd-based catalysts have provided unique access to a variety of PE topologies ranging from highly linear crystalline to hyperbranched

amorphous polymers using only ethylene as a raw material.[14-15] Although heterogeneous catalysts are most commonly used in industry, single-site homogeneous catalysts have emerged as attractive alternatives due to their ability to access PEs with precise molecular weight and microstructures.[16] Brookhart's seminal report in 1995 that Ni and Pd diimine complexes are capable of producing branched high molecular weight polyethylene with activities rivaling many early transition metal counterparts (Figure 1.1)[17] has inspired researchers to develop improved variants. As a result, hundreds of new catalyst structures have been disclosed in the last two decades. Recently, research interests have shifted toward controlling the MWD and microstructures of PEs to broaden their commercial applications.[1]

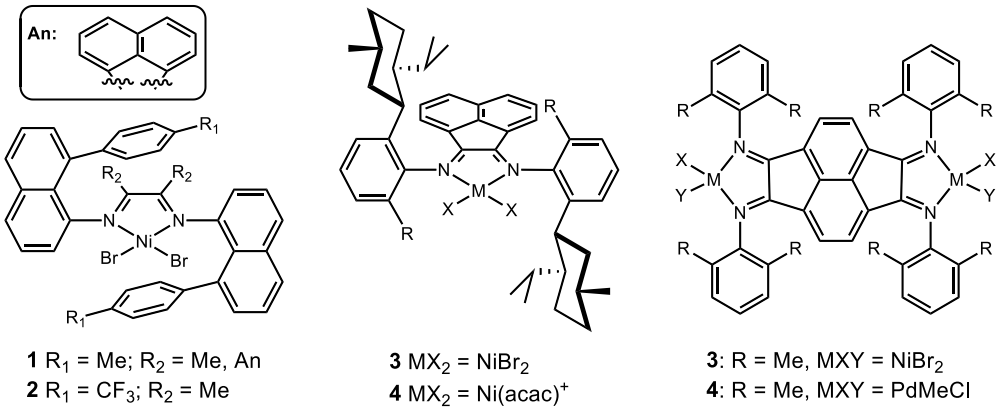

Figure 1.1. Representative examples of Ni and Pd based α-diimine complexes.

In general, single site catalysts produce one type of polymer under a given set of reaction conditions. Typically, to obtain different polymer products, the steric and electronic properties of the metal catalysts are tuned by modifying their supporting ligands. Unfortunately, this process can be labor, cost, and time intensive. To diversify polyethylene products from a common catalyst, researchers have developed several strategies to influence the polymerization process, including altering the reaction conditions (e.g., changing temperature, ethylene pressure), switching redox

states, adding Lewis acids, adding chain transfer agents, and controlling catalyst nuclearity. In this chapter, we will summarize the various strategies used by researchers to obtain tailor-designed POs from metal-catalyzed polymerization. We will then describe our group's catalyst design rationale and the main goals to be achieved in this research thesis.

1.2. Altering Reaction Conditions

Changes in reaction conditions such as temperature and ethylene pressure can significantly impact the polymerization process. For most Ni(II) and Pd(II) complexes with common chelating [N,N], [N,O], [N,P], and [O,P] ligands, increasing the reaction temperature increases catalytic activity and decreases polymer molecular weight, while increasing ethylene pressure tends to increase both activity and molecular weight. For Ni and Pd α-diimine complexes, the metal centers are able to "walk" on the growing polymer chains through rapid ß-H elimination reaction and reinsertion with opposite regio-chemistry. This process is so-called "chain walking" and is competitive with ethylene binding (Scheme 1.1). Increasing temperature typically increases the rate of chain-walking (a first-order process) relative to ethylene binding (a second-order process).[18] Therefore, the branching structure of the resulting polymer can be controlled by adjusting the reaction temperature and ethylene pressure (Scheme 1.2).[19]

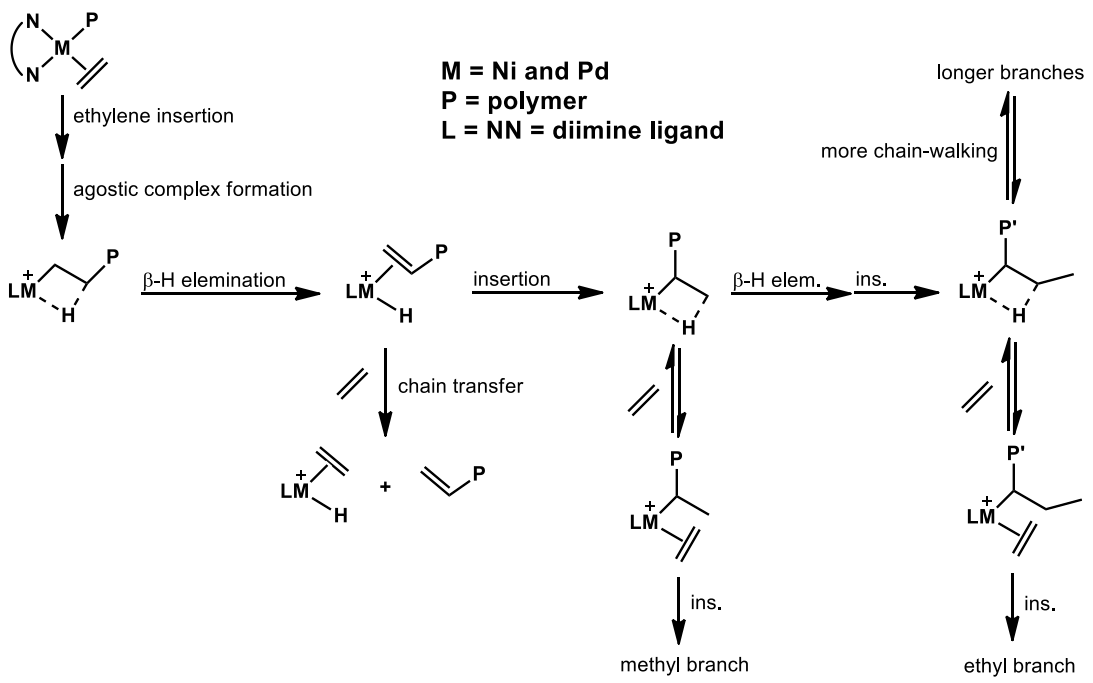

Scheme 1.1. Mechanism of chain walking in ethylene polymerization.

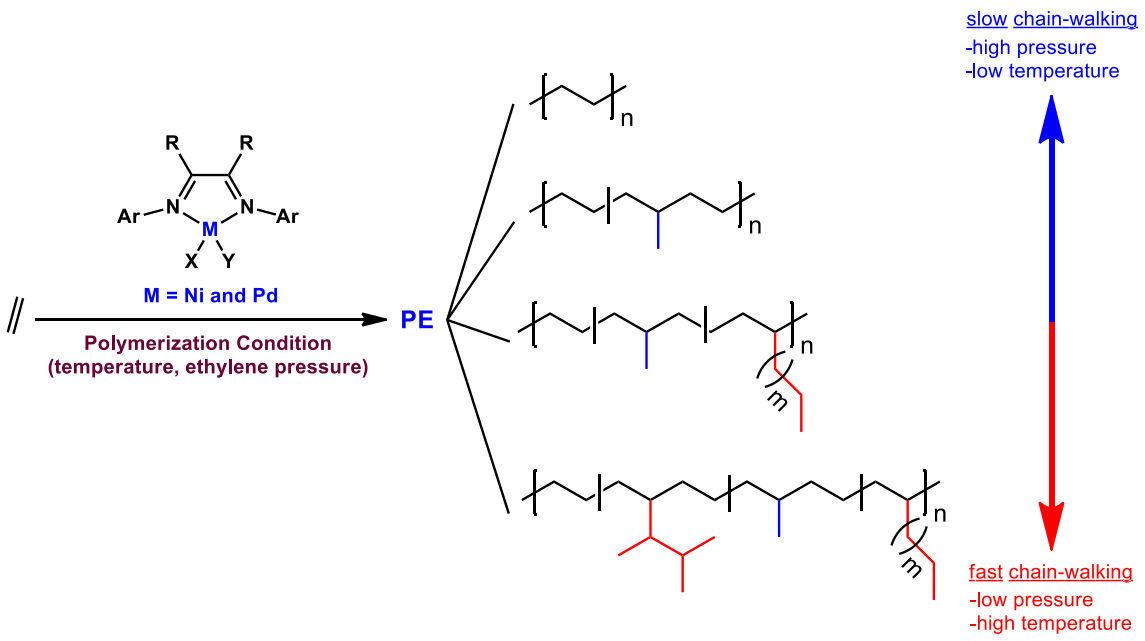

Scheme 1.2. Influence of reaction temperature and ethylene pressure on the branching structure of polymers produced.[19]

Coates' group has taken advantage of reaction condition switching to synthesize linear and branched multiblock copolymers directly from ethylene.[20] Using fluorinated aryl naphthyl α-diimine Ni complex **7** that is capable of performing living polymerization, they found that at high ethylene pressure and low reaction temperature (6 atm, -35 ^{o}C), complex **7** produced highly linear PE (LPE) (9 branches/1000 C, T_m = 128 ^{o}C). In contrast, at lower ethylene pressure and higher reaction temperature (1 atm, 20 ^{o}C), highly branched, amorphous PE (BPE) (112 branches/1000 C) was observed. By alternating between these two reaction conditions, they obtained the tetrablock copolymer $LPE_{55}BPE_{62}LPE_{58}BPE_{61}$ (the subscript specifies the M_n kg mol^{-1} of each individual PE block) with unique tensile strength (Scheme 1.3). This tetrablock copolymer can act as a compatibiliser for an 80:20 LDPE/HDPE blend. With an addition of just 5% of $LPE_{55}BPE_{62}LPE_{58}BPE_{61}$, the strain at break of the blend dramatically increased 553% in comparison to that of the uncompatibilised mixture, while maintaining similar yield stress at 13 MPa, (Figure 1.2).

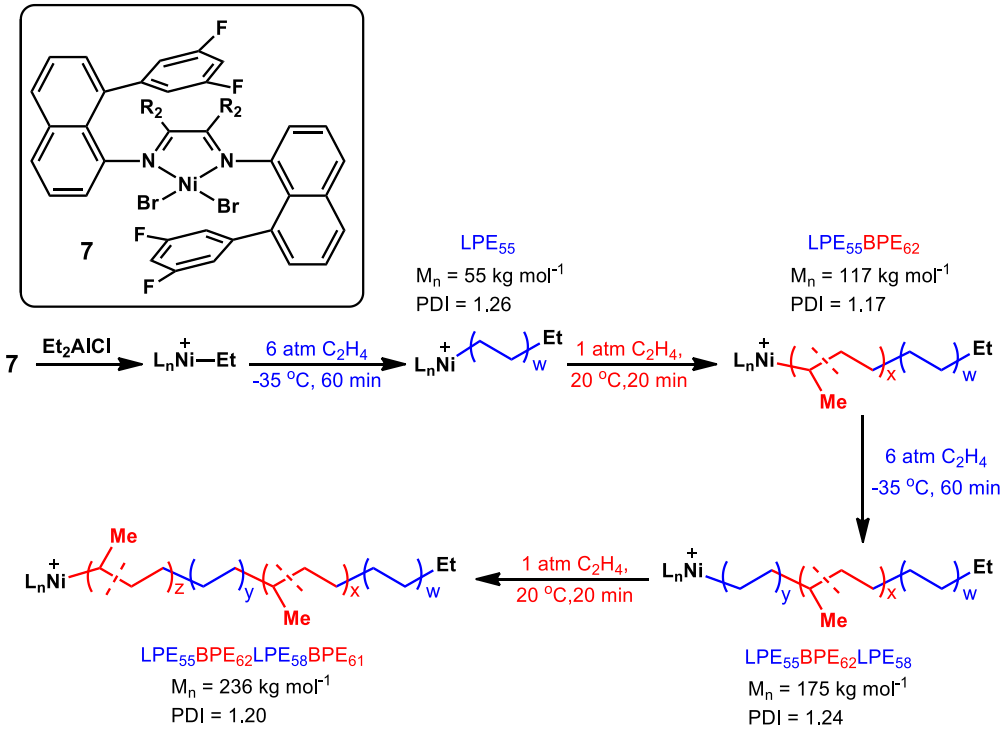

Scheme 1.3. Synthesis of multiblock copolymer using "sandwich"-type Ni complex **7**.

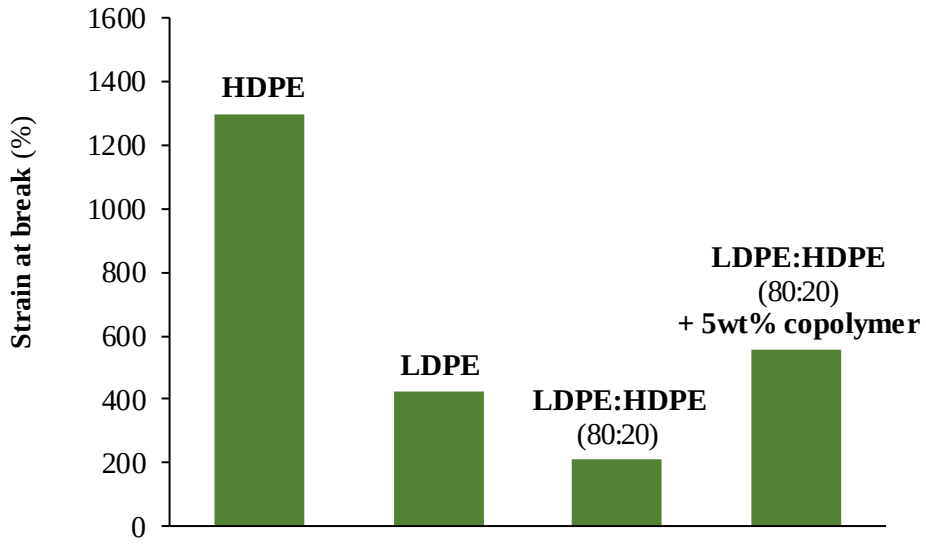

Figure 1.2. Strain at break of HDPE, LDPE, blend and compatibilised blend strained at a rate of 100% min^{-1}.[20]

1.3. Redox-switching

Redox control catalysis has been applied successfully in numerous metal catalyzed organic transformation, including polymerization.[21-23] The most common ligand design for redox-active complexes usually incorporates ferrocene (Fc) groups since they can be reversibly oxidized and reduced by conventional reagents such as AgOTf/$FcBAr^F_4$ as oxidant or Cp^*_2Fe/Cp_2Co as reductant. Intriguing results in lactide homo(co)polymerization catalyzed by many transition metal complexes, such as those based on yttrium, indium, cerium, titanium, zirconium, and iron, have been reported by Diaconescu, Byers, and Long.[24-27] Gibson et al. were among the first to introduce the concept of redox control in olefin polymerization (Figure 1.3).[28 29-30] Unfortunately, their Pd complexes and bis-ligand Ni complexes **12** were found to be inactive in ethylene polymerization. Although some Ni complexes were quite active, they produced butenes with trace amounts of higher oligomers (C_6 and C_8) instead of PE. Complex **9a** was the most active, displaying a TON of about 19.14×10^3 (mol ethylene/mol of catalyst). The oxidized form of **9a** exhibited similar reactivity as that of its parent, producing butenes with a TON of 16.43×10^3 (mol ethylene/mol of catalyst). Thus, negligible change in reactivity was observed upon redox switching. Gibson proposed that the MAO used to activate the pre-catalyst might have reduced the cationic iron(III)-ferrocene back to its neutral iron(II) form, which was confirmed by their control experiments.

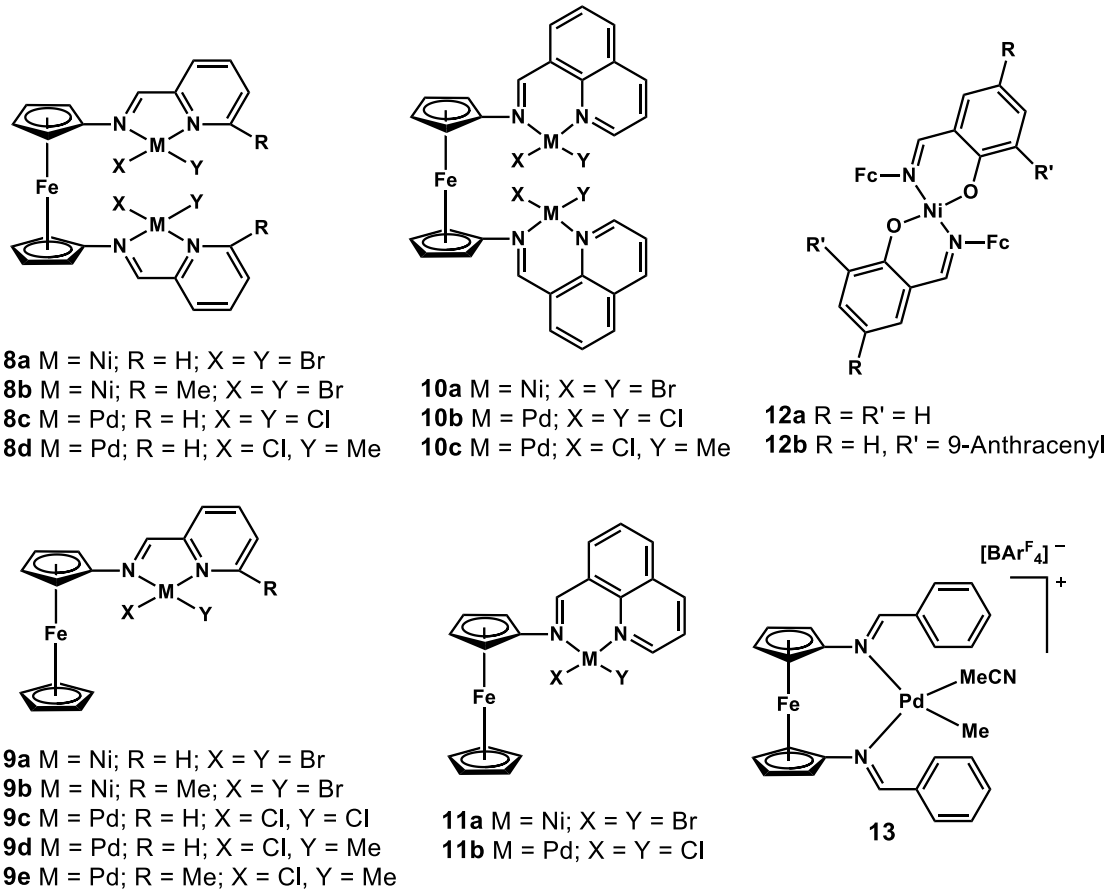

Figure 1.3. Ni and Pd complexes bearing ferrocene moieties introduced by the Gibson group.

1.3.1. Redox-Active Palladium Catalysts for Ethylene Polymerization

In 2015, Chen and his coworkers reported a series of Pd complexes bearing ferrocene-bridged phosphine sulfonate ligands with phenyl and *o*-MeO-C_6H_4 substituents (Scheme 1.4A).[31] For comparison, they also studied benzene-bridged phosphine-sulfonate Pd analogues for (Scheme 1.4B). Based on their cyclic voltammetry results, only the iron centers showed reversible redox activity. The Pd centers were not oxidized by treatment with AgOTf. In ethylene polymerization, both neutral (**14a-16a**) and oxidized (**14a^{ox}-16a^{ox}**) forms demonstrated high activity. They all produced linear PE (5-13 branches/1000 C) with narrow PDI. It has been shown previously that for Pd phosphine-sulfonate catalysts, electron poor complexes tend to undergo faster chain transfer

than their electron rich counterparts, which leads to PE with lower molecular weight. Unfortunately, in this case, the oxidized complexes showed dramatic decrease in both activity (4-6 fold) and molecular weight (3-5 fold). Because Pd black was observed after polymerization when the oxidized complexes were used, the authors hypothesized that the oxidation species is probably less stable than the neutral species at elevated reaction temperature (80 ^{o}C).

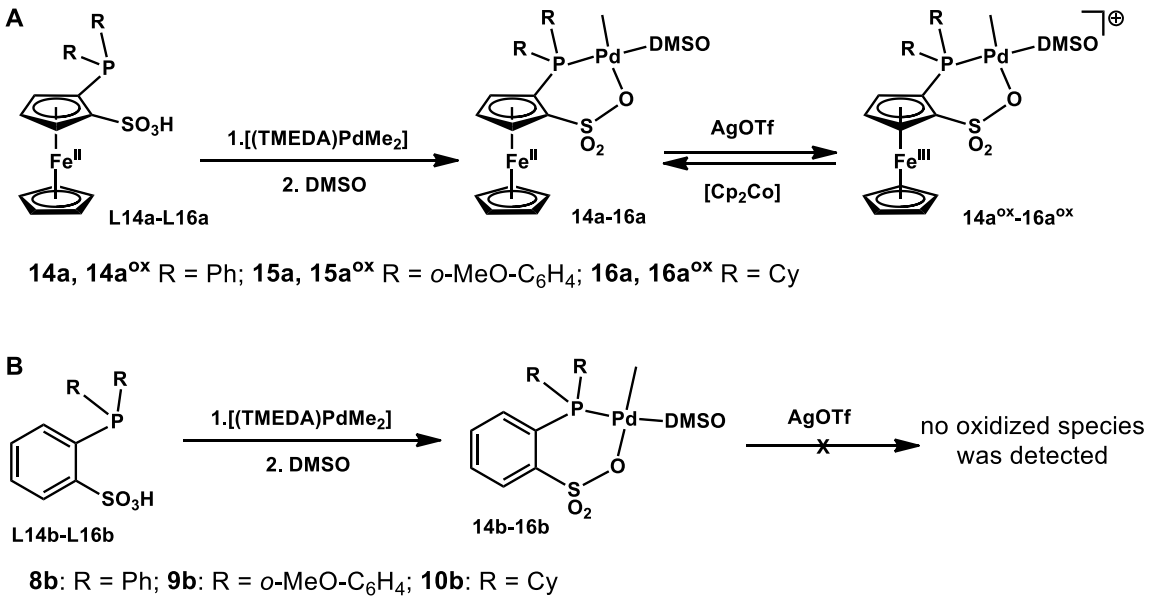

Scheme 1.4. Pd ferrocene-bridged catalysts and their benzene-bridged analogues.

In 2017, Chen's group introduced a Pd α-diimine catalyst bearing two ferrocenyl moieties which could be sequentially oxidized by $AgBAr^{F}_{4}$ (Scheme 1.5).[32] The oxidized species were analyzed in situ by NMR and IR spectroscopy and cyclic voltammetry. All three complexes were active in ethylene polymerization, affording the highest activity and PE molecular weight at 40 ^{o}C. The activity trend followed the order **17**-CN > [**17**-CN]$^{+}$ > [**17**-CN]$^{2+}$, whereas the polymer molecular weight trend followed the order [**17**-CN]$^{+}$ > **17**-CN > [**17**-CN]$^{2+}$. Because polymer molecular weight is determined by the relative rates of ethylene insertion over the rates of chain transfer. It is likely that these two events are affected differently in the different complexes

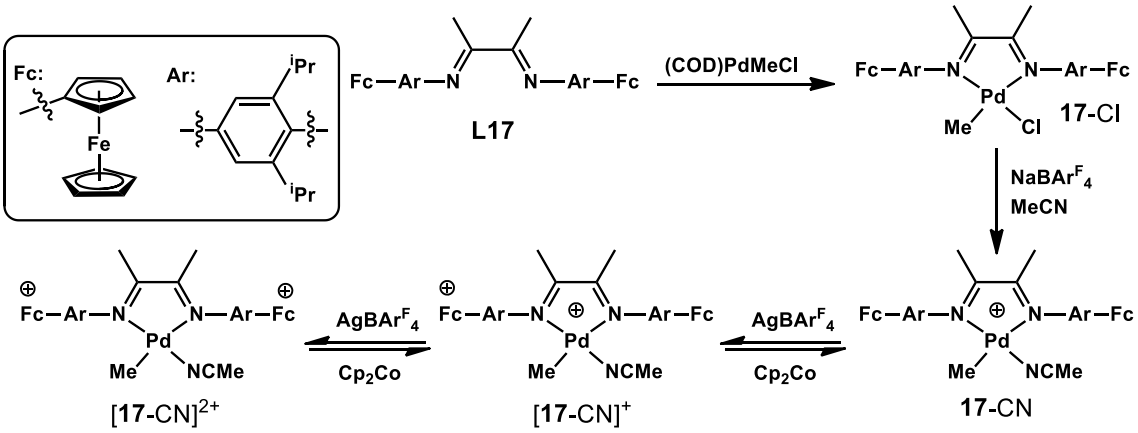

Scheme 1.5. Pd complexes bearing two ferrocenyl moieties introduced by Chen's group.

Later, in 2019, the Long group reported similar Pd complexes bearing different backbone and linkers (Figure 1.4). These complexes were also active and possess redox switchable behavior in ethylene polymerization, showing trends similar to those reported by Chen.

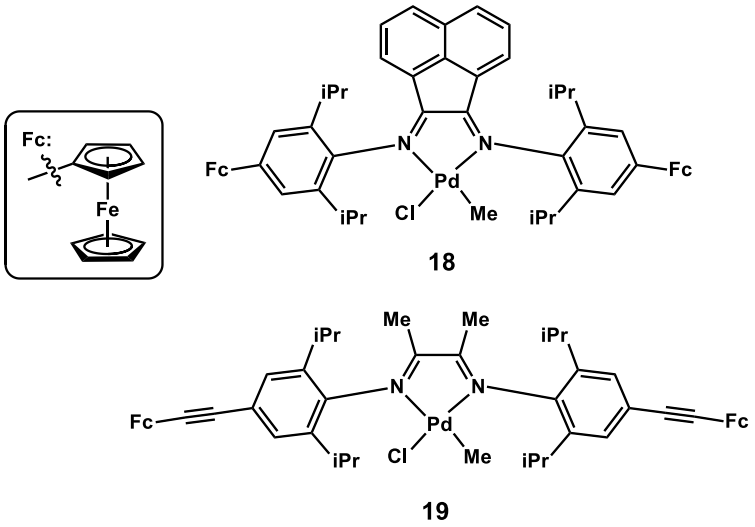

Figure 1.4 Long's redox active Pd catalysts for ethylene polymerization.

1.3.2. Redox-Active Nickel Catalysts for Ethylene Polymerization

Redox switching in olefin polymerization was successfully demonstrated using Ni complexes Long's group in 2016.[15] Their Ni α-diimine complex **20** (Figure 1.5) produced high molecular weight PE with ∼30% more branches (114 branches/ 1000 C) than that produced by **20** (88 branches/ 1000C) in the presence of 1 equiv of cobaltocene as a reductant. The reduced catalyst gave polymers with increased methyl branches (54.9% → 62.8%) and branches that were six carbons or longer (9.2% → 10.4%), while the percentage of *sec*-butyl branches decreased (5.3% → 0.9%). Furthermore, the branching density was found to decrease almost linearly upon the addition of reductant (Table 1). Interestingly, the polymer molecular weight was highest when 0.75 equiv of cobaltocene was added (M_w = 274 kg/mol), 26% higher than that produced by the Ni catalyst only (M_w = 217 kg/mol). However, the polymer MW decreased when more reductant was added (M_w = 200 kg/mol) (Table 1, entry 5).

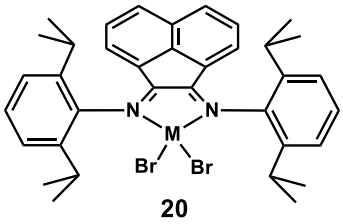

Figure 1.5 Ni complex used in Long's study

Table 1.1 Polymerization study for complex **20** in the presence and absence of cobalt reductant.

entry	[Co][b] (equiv)	yield (g)	M_w[c] (kg/mol)	M_w/M_n[c]	B[d]
1	0	1.75	217	1.54	114 (±1.9)
2	2.5	1.94	254	1.65	109 (±3.0)
3	5.0	1.95	271	1.77	104 (±0.5)
4	7.5	2.38	274	1.72	99 (±0.7)
5	10.0	1.78	200	2.04	88 (±2.8)

[a]Polymerization conditions: 10.0 μmol Ni catalyst, 148 mL of toluene, 2 mL of DCM, 20 °C, 15 psi ethylene, 30 min and 92 equiv of PMAO-IP. [b][Co] = cobaltocene. [c]Determine using triple detection GPC at 140 °C in 1,2,4-trichlorobenzene. [d]Branches per 1000 carbons.

In 2017, Long's group reported a series comprising three Ni complexes bearing two ferrocenyl moieties (Figure 1.6).[33] Although the pendant ferrocenyl substituents displayed sharp reversible peaks, the main ligand backbones showed different electrochemical properties: complex **21** displayed a quasi-reversible peak, complex **22** showed an irreversible reduction peak and complex **23** showed no significant electrochemical activity. These complexes were next investigated in ethylene polymerization. Upon addition of 2 equiv of $AgBAr^F{}_4$ as oxidant, the polymerization activity increased slightly. In contract, upon addition of 1 equiv of Cp_2Co as reductant, the activity dropped dramatically. The polymers produced by the catalysts in different oxidation states had similar molecular weight and branching density except for precatalyst **21**, which showed that the neutral and oxidized forms produced polymers with more branches (~40 branches/1000 C) than the reduced form (9 branches/1000 C) (Figure 1.7).

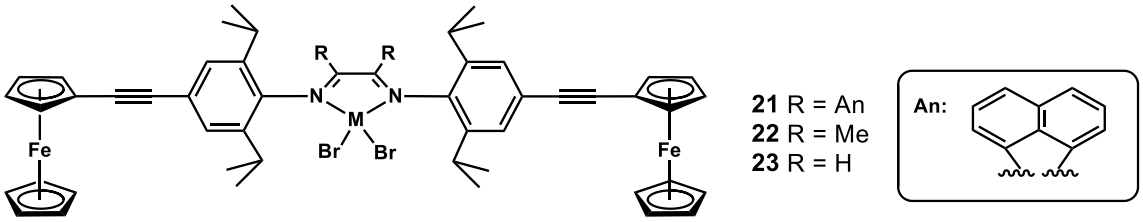

Figure 1.6 Ni complexes bearing two ferrocenyl side-arms.

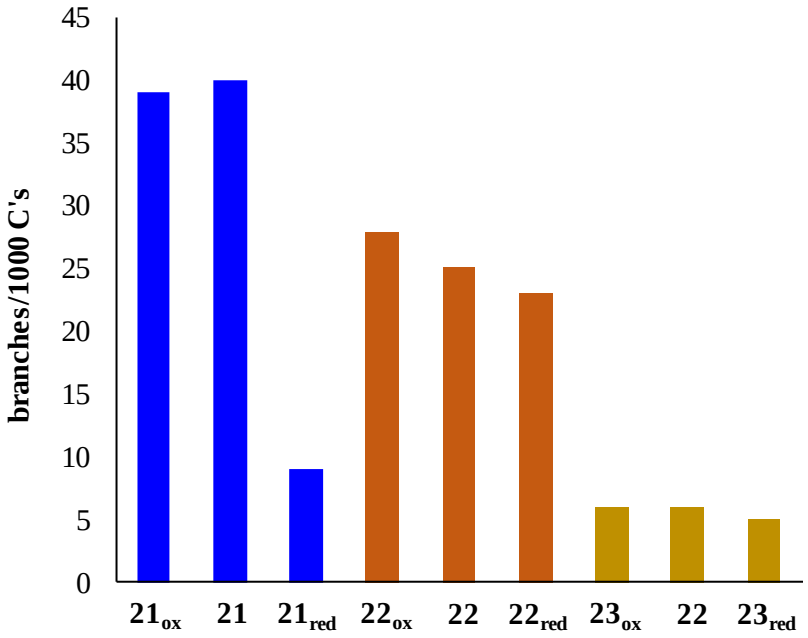

Figure 1.7. Branching density of PE produced by complexes **21**, **22**, and **23** in the presence/absence of an oxidant ($AgBAr^F{}_4$) or a reductant (Cp_2Co).[33] Polymerization conditions: 5.0 μmol catalyst, 98 mL of toluene, 2 mL of dichloromethane, 20 °C, 15 psi ethylene, 15 min, and 500 equiv of MMAO

Later, in 2018, Long's group introduced photoredox catalysis in olefin polymerization. They employed **20** as a catalyst, tris[2-phenylpyridinato-C^2,N] iridium(III) (*fac*-$Ir(ppy)_3$) as a photoreductant, and blue light as an external stimulus.[34] The polymerization of ethylene by precatalyst **20** was unaffected by the presence or absence of light and the resulting polymers displayed similar molecular weights. However, the branching density decreased as light exposure time increased (113 → 93 branches/ 1000 C) (Figure 1.8).

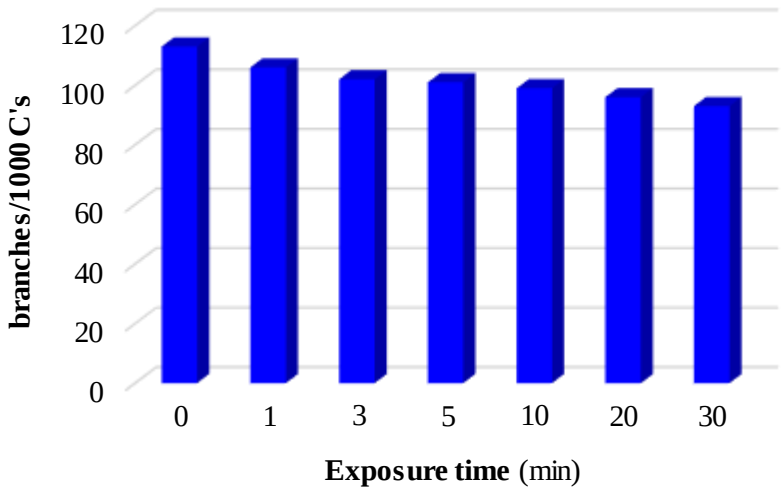

Figure 1.8. Plot of PE branching density versus light exposure time for polymerization containing fac-Ir(ppy).[34]

1.4. Lewis-Acid Binding

Lewis-acid assisted catalysis has been demonstrated to be highly versatile in various organic transformations. For example, the use of Lewis acid additives has been shown to improve the efficiency of Ru-catalyzed ring-closing metathesis reaction,[35] Pd-catalyzed C-N bond formation and C-H activation,[36-37] Ni-catalyzed cyanoesterification and cyanocarbamoylation,[38] Fe-catalyzed dehydrogenation,[39] and Co-catalyzed hydrogenation.[40-41] Lewis acids can interact with substrates to activate strong bonds, which can promote bond breaking or nucleophilic attack. Furthermore, when properly positioned, Lewis acids could help improve product selectivity.[42] The concept of Lewis acid-assisted catalysis has also been explored in olefin dimerization, oligomerization, and homo- and co-polymerization.[37, 43-48] Because the applications of Lewis acid additives in olefin polymerization is still limited, we would like to simply classify this strategy into two main categories: metal cation Lewis acids and boron Lewis acids.

1.4.1. Boron Lewis Acid Binding

In 2007, Bazan and coworkers reported a Ni alkoxy imine complex that can form a mixture of two zwitterionic isomers upon addition of 2 equiv of $B(C_6F_5)_3$ (Scheme 1.6).[49] The notable feature of the Ni center is that it is supported by a C=C double bond that was further confirmed by X-ray characterization. Ethylene polymerization results showed that pre-catalyst **24** is not active, while the mixture of complexes **25a** and **25b** produced linear PE with a TOF of 450 (kg polymer mol_{Ni}^{-1} h^{-1}) and a broad PDI (5.8). Surprisingly, an additional of 6 equiv of $B(C_6F_5)_3$ resulted in a four-fold increase in catalytic activity and significantly reduced PDI (2.5). The authors hypothesized that excess $B(C_6F_5)_3$ could scavenge impurities in the reaction mixture. However, recent publications showed that the η^3-*allyl* Ni bond is relatively stable under high reaction temperature and ethylene pressure, thus, $B(C_6F_5)_3$ in this case may also serve as an activator.

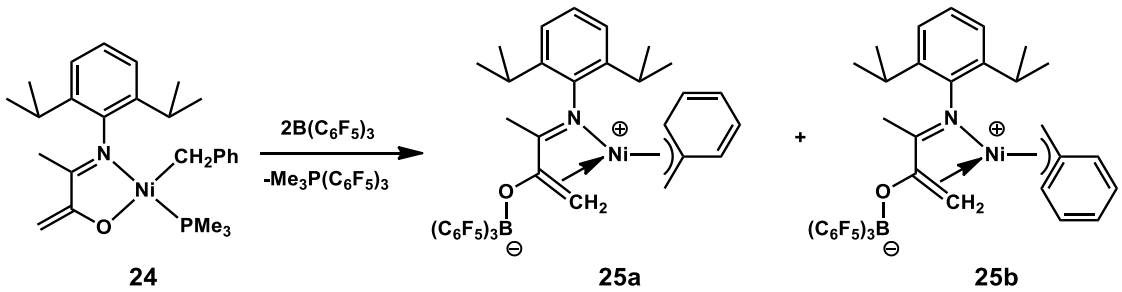

Scheme 1.6. Zwitterionic isomers of Ni complex introduced by Bazan's group.

In 2012, Jordan's group introduced Pd complexes bearing [P,O] ancillary ligands (Scheme 1.7)[50-51] that are able to react with $B(C_6F_5)_3$ to switch the hybridization of the O donors from sp^3 to sp^2, leading to a significant change in catalytic reactivity. The borane adducts **26b** and **27b** were characterized by X-ray crystallography to confirm their proposed zwitterion structures. The coordination of $B(C_6F_5)_3$ is suggested to weaken the Pd-O bonds and increase the degree of

positive charge on the Pd centers, resulting in enhancement of both chain growth and chain transfer rates. This hypothesis was supported by ethylene polymerization studies using complex **26b,** which showed an increase in polymer yield and significant decrease in polymer molecular weight compared to that by **26a**. Interestingly, addition of borane to the Pd phosphine phosphonate complex **27a** resulted in significant improvement in both catalytic activity and PE molecular weight. Several possibilities can account for these observations, such as the chain growth rate increased more than the chain transfer rate or the catalyst lifetime is longer compared to that of **27a** without borane.

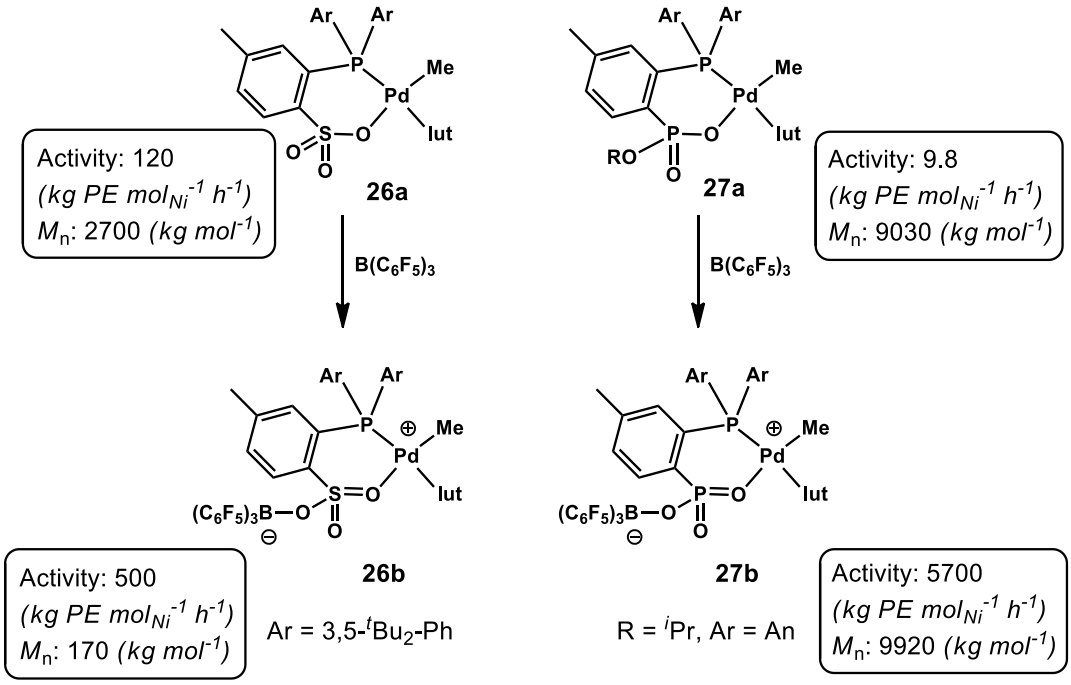

Scheme 1.7. Phosphine sulfonate and phosphine phosphonate Pd complexes.

In 2014, Jordan reported a novel Pd phosphine complex that contains both sulfonate and phosphonate ester moieties (Figure 1.10).[44] Without coordination of $B(C_6F_5)_3$, the sulfonate group is better donor than the phosphonate ester because the anionic sp^3 O donor is more Lewis basic than the neutral sp^2 O donor of the phosphonate group. When $B(C_6F_5)_3$ was added, it formed an

adduct with the sulfonate group and generated the phosphine phosphonate chelated complex **28b**. The structures of complex **28a** and its adduct **28b** were characterized by NMR spectroscopy and X-ray crystallography. Ethylene polymerization studies showed that both complexes afforded oligomers comprising both toluene-soluble and toluene-insoluble fractions with similar activity.

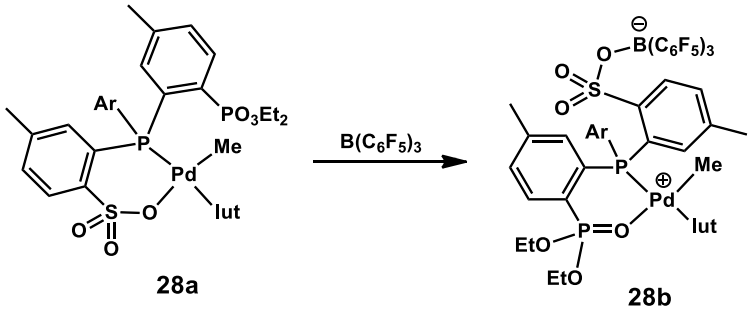

Figure 1.9. Phosphine Pd complex bearing both sulfonate and phosphonate moieties.

The phosphine sulfonate ligand above both bind borane at positions that are relatively far away from the active metal centers. Therefore, the catalyst tuning effect of boranes is primarily electronic in nature. In 2019, M. Chen et. al. reported pyridazine imine Ni complexes that have a boron coordination site adjacent to the metal center (Figure 1.11).[52] Chen's complexes displayed low activity and produced PE products with medium molecular weights, low branching density, and broad PDI. In general, addition of Lewis acid additives enhanced the polymerization rate, reduced polymer molecular weight, increased branching density and narrowed the PDI (Table 1.2). The steric hindrance at the Ni centers is increased by chelation of the boron agents.

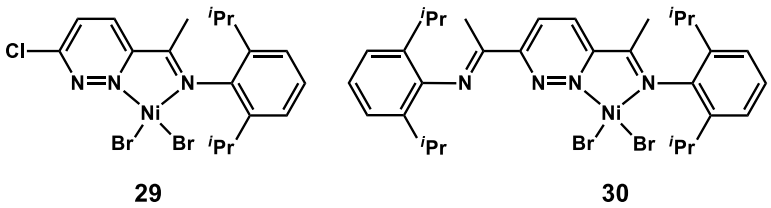

Figure 1.10. Pyridazine imine Ni complexes.

Table 1.2 Ethylene polymerization using Ni precatalyst **32** and **33**.[a]

entry	cat.	additive[b]	activity[c]	M_n[d] (10^3)	M_w/M_n[d]	B[e]
1	**29**	-	120	23.8	9.6	13
2	**29**	BCl_3	300	9.6	3.3	50
3	**29**	$BF_3.Et_2O$	1920	4.2	2.6	65
4	**29**	$B(C_6F_5)_3$	580	7.8	3.2	54
5	**30**	-	60	21.2	6.9	25
6	**30**	BCl_3	80	8.2	3.4	29
7	**30**	$BF_3.Et_2O$	1160	4.5	3.2	71
8	**30**	$B(C_6F_5)_3$	500	7.9	3.0	45

[a]Polymerization conditions: 10.0 μmol Ni precatalyst, 2 mL CH_2Cl_2, 18 mL toluene, 250 equiv MAO, ethylene 8 atm, 1 h, 30 °C. [b]10 equiv boron additive. [c]kg polymer mol_{Ni}^{-1} h^{-1}. [d]Determined by GPC using polystyrene standards.[e]B = branches/1000 C, determined by ^1H NMR in $C_2D_2Cl_4$ at 120 °C.

Recently, Changle Chen reported two examples of Ni and Pd complexes bearing phosphine sulfonate supporting ligands (Figure 1.12).[53] Similar to Min Chen's complexes, Changle Chen's complexes enhanced productivity and reduced PE molecular weight upon addition of $B(C_6F_5)_3$. For Ni catalyst **32a**, increase in branching density was also observed (12 → 28 branches/1000 C). For Pd catalyst **31a**, up to a 670-fold increase in chain transfer rate was observed in ethylene polymerization upon addition of $B(C_6F_5)_3$.

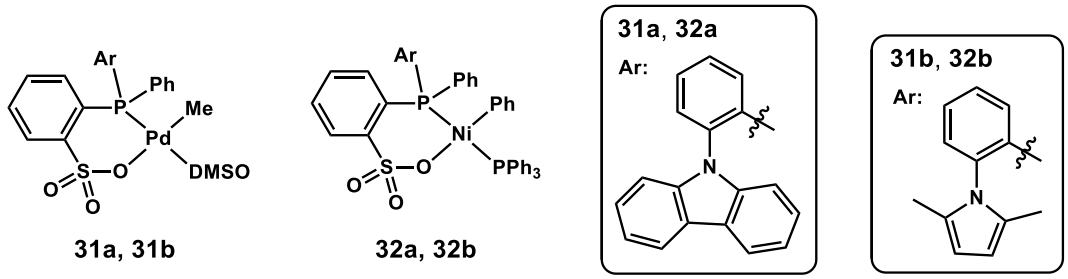

Figure 1.11 Phosphine-sulfonate Pd and Ni catalysts bearing carbazolyl and pyrrolyl substituents.

1.4.2. Secondary Metal Binding

The concept of secondary metal binding was explored in the early days by Brookhart and co-workers. In 2003, they reported several Ni complexes that are capable of chelating Li cation to their pendant methoxy ether moieties (Figure 1.12).[54] In ethylene homopolymerization studies, they observed that bimetallic complexes **33** and **34** were more productive than monometallic complex **33**. A similar trend was observed for the copolymerization of ethylene and hexyl acrylate. The incorporation of LiCl (complex **33**) was proposed to increase the electrophilicity of the Ni center, which led to higher catalyst activity. To enhance the electrophilicity of catalyst **33** even further, anion exchange was conducted with $NaB(C_6F_5)_4$ to give complex **34**, which displayed greater activity than that of its parent. The structure of **34** was confirmed by X-ray crystallography.

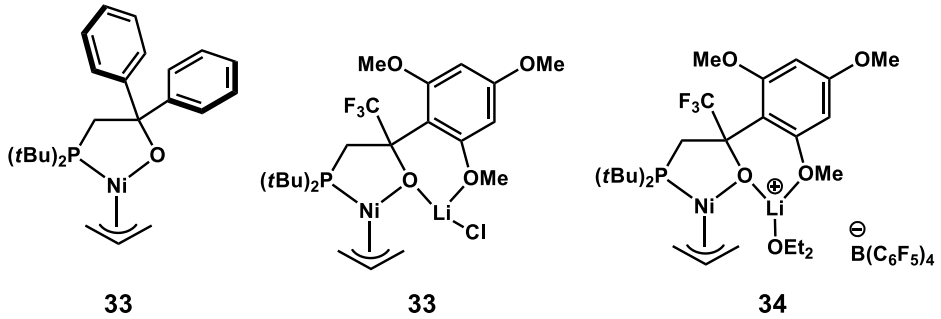

Figure 1.12. Examples of Ni bimetallic catalysts for olefin polymerization reported by Brookhart and co-workers.[54]

In 2005, Nagashima and co-workers introduced a azanickellacyclic complex bearing a second diimino chelation site (Figure 1.13).[55] Introduction of secondary metals to this diimine moiety resulted in formation of heterobimetallic complexes which displayed different behaviors toward ethylene polymerization. Upon activation by MAO (200 equiv), Ni-$ZnBr_2$ and Ni-$CoBr_2$ bimetallic complexes (**37a** and **37b**) produced PE with increased yields and molecular weights, giving

monomodal molecular weight distributions. In contract, polymerizations catalyzed by Ni-$FeBr_2$ and Ni-$NiBr_2$ gave bimodal distributions, and polymers with reduced yield and molecular weight compared to that of their mononuclear counterpart **36**. The bimodal polymer profiles suggested that both Fe and Ni centers were capable of polymerization. For this ligand design, the primary benefit of second metal coordination was proposed to increase the catalyst's stability by making its structure more rigid.

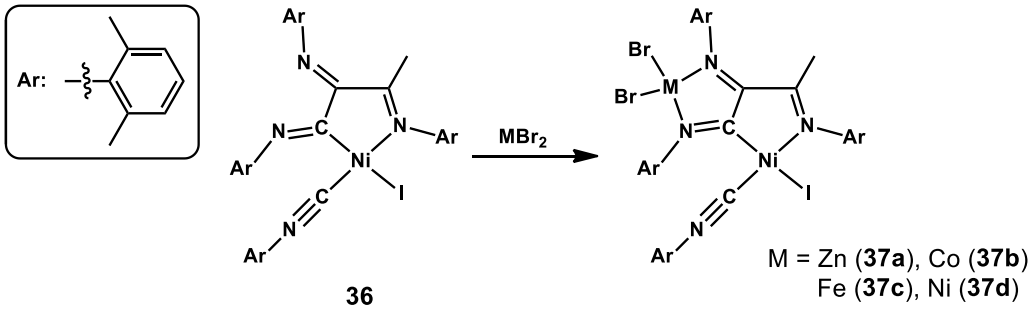

Figure 1.13 Azanickellacyclic complex.

Later, in 2016, Tonks and co-workers observed similar trends in ethylene polymerization with phenoxy imine Ni complexes containing a 2,2'-bipyridine pendant group (Figure 1.14).[56] Polymer yield and molecular weight were found to increase in the presence of excess amounts of $ZnCl_2$, which presumably abstracted pyridine and increased the steric bulk of the Ni center by chelating to the bipyridine. Other Lewis acids such as $AlCl_3$ and $CuCl_2$ were also tested and found to be less effective. The polymerization activity of these mono- and bimetallic complexes, in general, are quite poor (maximum-10 kg PE mol_{Ni}^{-1} h^{-1}).

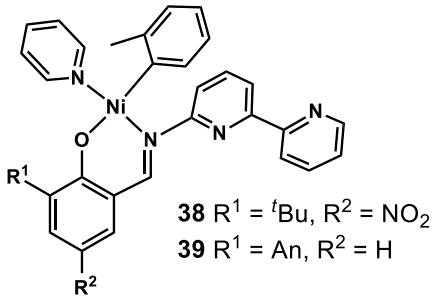

Figure 1.14. Ni complexes supported by phenoxy imine backbone bearing 2,2'-bipyridine pendent moiety.

From 2015 to 2019, the Do group introduced a series of Ni and Pd complexes supported by conventional ligand platforms that feature mono or bis polyethylene glycol (PEG) side chains (Figure 1.15).[46, 57-60] The PEG chains were designed to selectively capture alkali cations (Li^+, Na^+, K^+, and Cs^+).

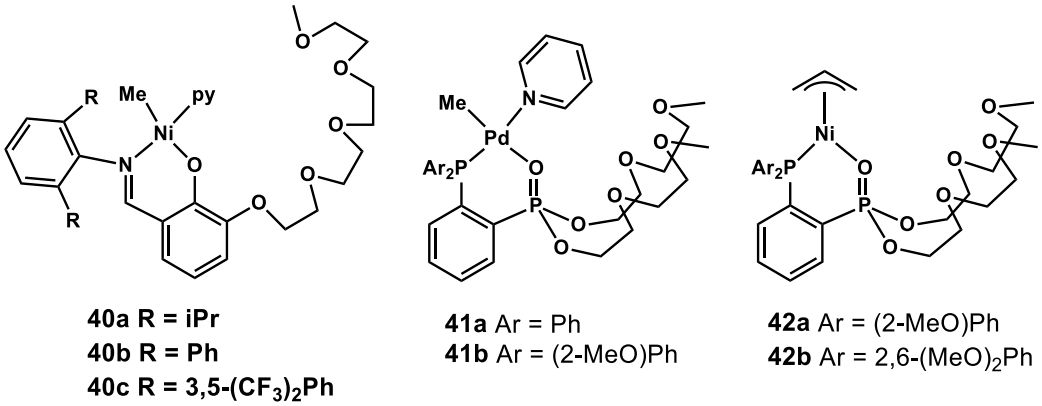

Figure 1.15. Ni and Pd complexes containing PEG chain side-arms.

All of the nickel complexes exhibited unique changes to their reactivity upon addition of different alkali metals. Complexes **40** became more active and produced PEs with distinct properties, and complexes **41** displayed greater thermal stability. Complex **42** was capable of chelating many other cations such as Mg^{2+}, Ca^{2+}, Co^{2+}, Cu^{2+}, Zn^{2+}, Sn^{2+}, Al^{3+}, Bi^{3+}, Ga^{3+}, Sc^{3+}, and La^{3+} in tetrahydrofuran. In most cases, the recruitment of secondary metals resulted in increased

polymer yield. However, the polymer products displayed similar properties (molecular weight, branches, and PDI). Co^{2+} and Zn^{2+} were found to provide the most favorable effects for **42**, giving a 10.6- and 6.7-fold enhancement in ethylene polymerization activity in THF, respectively. In addition, the impact of different counteranions was also examined. Interestingly, $CoCl_2$ was found to be less active than $Co(OTf)_2$, while $ZnCl_2$ was more active than $Zn(OTf)_2$. These results demonstrated that the broad chelation ability of PEG chains allows the generation of a diverse assortment of heterometallic species, which could all display unique and distinct catalytic properties.

In 2018, the Do group introduced a series of Ni carboxamidate triazole catalysts that were active for ethylene polymerization (Compound **43**, Figure 1.6).[61] Based on this platform, they incorporated a pendant picolyl donor ring to create a binding pocket for secondary metals **(**Figure 1.6).[48] Polymerization studies for complex **44a** by itself furnished PE with molecular weight of about 2.8×10^3 kg/mol. Surprisingly, the incorporation of $ZnCl_2$ into **44a** generated PEs with multimodal molecular weight distributions after 2 h. GPC analysis of the polymer products showed that the mixtures contained three main peaks: peak I associated with M_w = up to $\sim10^3$ kg/mol, peak II associated with M_w = up to $\sim10^4$ kg/mol and peak III associated with M_w = up to $\sim10^5$ kg/mol (Figure 1.17). Prolonging the reaction time increased both catalytic activity and amount of higher molecular weight polymers.

43a Ar = 2,6-(*i*Pr)$_2$Ph
43b Ar = 2,6-(Ph)$_2$Ph
43c Ar = 2,6-[3,5-(CF$_3$)$_2$Ph]$_2$Ph

44a Ar = 2,6-(*i*Pr)$_2$Ph
44b Ar = 2,6-(Ph)$_2$Ph
44c Ar = 2,6-[3,5-(CF$_3$)$_2$Ph]$_2$Ph

Figure 1.16. Ni carboxamidate triazole complexes and Ni carboxamidate triazole complexes bearing a pendent picolyl donor as a secondary binding site.

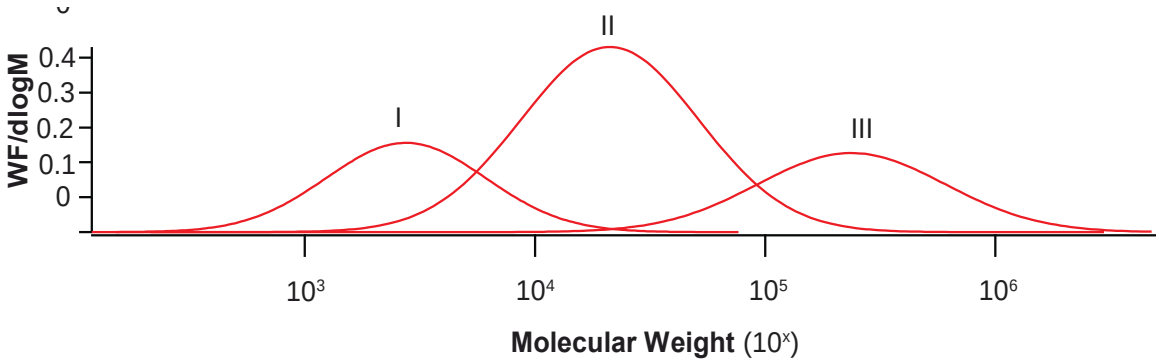

Figure 1.17. GPC data fitting of PEs produced by **44a**/$ZnCl_2$ after 2h.[48] *Reproduced with permission from Xiao, D.; Do, L. H. Organometallic* ***2018,*** *37, 3079-3085. DOI:10.1021/acs.organomet.8b00454. Copyright © 2018 American Chemical Society.*

1.5. Self-Assembly of Caged Catalysts

This strategy was first introduced in ethylene polymerization by Jordan's group in 2010. Their Pd phosphine sulfonate complex was able to convert between complexes with different nuclearity (Scheme 1.8).[62] In toluene, tetranuclear complex **46** generated low MW PEs (M_w = 7.87×10^3 kg/mol) with a narrow PDI (2.6). However, in hexane, **46** gave polymer products containing primarily high MW components (M_w up to 1×10^6 kg/mol) with minor amounts low MW components and broad PDI (60). It was proposed that the tetranuclear structure **46** was maintained in hexane, but in toluene it most likely dissociated into mononuclear complexes **45** that have poor steric shielding of the Pd centers. The extremely broad PDI of **46** in hexane, suggested that perhaps

an equilibrium mixture of catalyst species might exist in solution.[61] Interestingly, after treating with cryptand Krypt211 to trap the lithium cation, complex **46** dissociated into mononuclear species **47** which afforded only ethylene oligomers (C_4-C_{18}). The authors proposed that the free $ArSO_3^-$ moiety in complex **47** has significantly enhanced its chain transfer rate in ethylene homopolymerization.

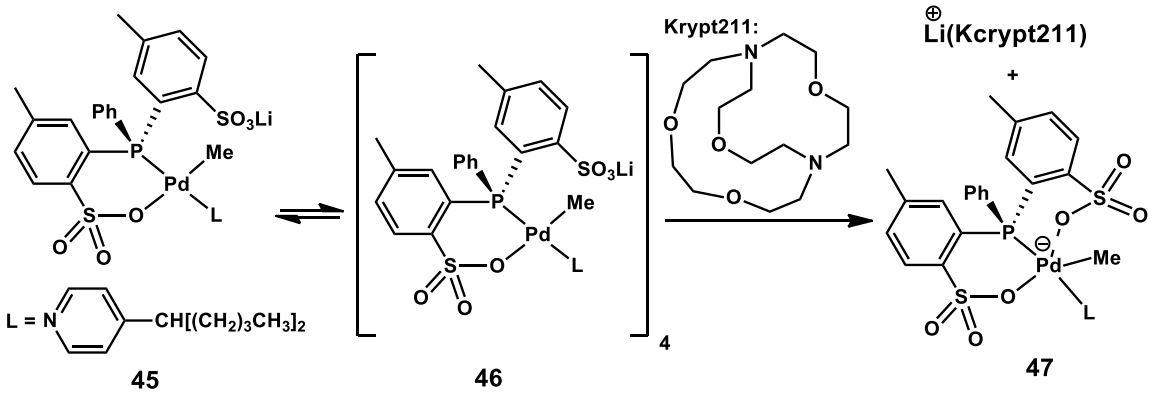

Scheme 1.8. Pd complexes that are able to switch between different species with different nuclearity.

Based on this platform, many interesting Pd caged catalysts for ethylene polymerization was reported by Jordan's group in the past several years (Figure 1.18).[63-64] Derivatives **48** and **49** displayed similar behavior in ethylene polymerization to that of compound **46** (Figure 1.18A). The zinc cage complex **49** showed improvement in thermal stability in comparison with previous lithium analogues **46**, **48** and **49**. However, because of the reactivity of zinc with Lewis bases, cage complex **50** is chemically more susceptible to disassembly. For instance, in methanol, the tetranuclear complex **50** was completely converted into trinuclear complex **51** with the ancillary 4-*tert*-butylpyridine shifted from palladium to zinc (Figure 1.18B).

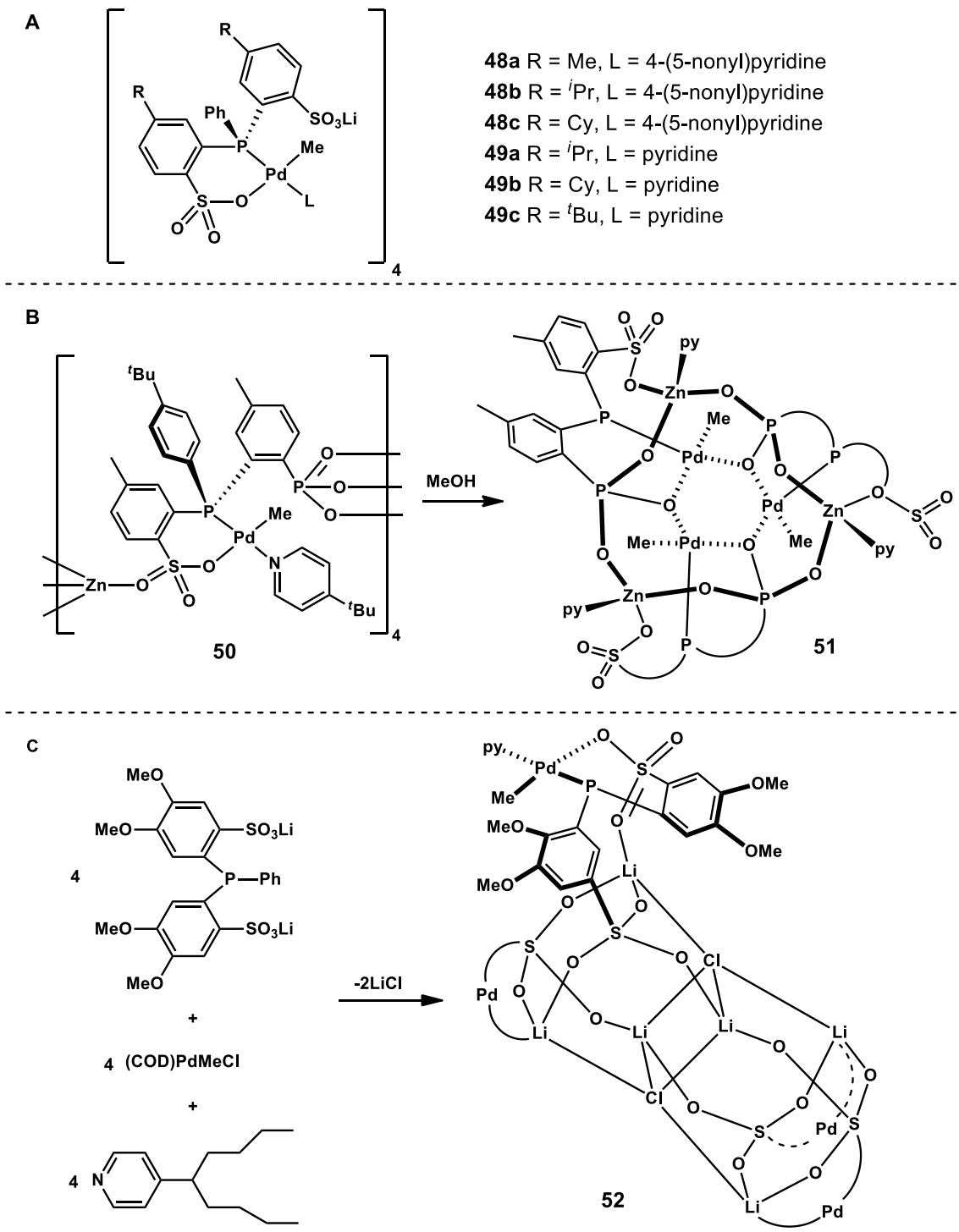

Figure 1.18. Self-assembled Pd caged complexes introduced by the Jordan group.

In 2019, Jordan group reported a novel tetrameric caged structure with a rhomboidal Li_2Cl_2 unit inserted within a cluster (Figure 1.18C).[65] The caged complex **52** was found to be more robust in ethylene polymerization (hexane, 80 ^{o}C, 410 psi ethylene), producing high MW PE (M_w up to 1.47×10^6) with narrower PDI (2.3), in comparison to previous caged compounds ($6.6 \leq PDI \leq 60$).

1.6. Chain Transfer Agents

Chain transfer agents (CTAs) have been successfully applied in ethylene polymerization for many early transition and lanthanide metal catalysts, particularly for living catalysts to increase the number of polymer chains generated per active metal center. CTAs are not commonly used for group 10 transition-metal based catalysts. However, Tonks et. al. reported the use of dialkyl zinc reagents as CTAs for Ni diimine complexes in 2014 (Figure 1.19A) and Guironnet (Figure 1.19B) introduced silanes as CTAs for Pd diimine complexes in 2017. Tonks' group demonstrated that complex **53b** in the presence of various concentration of $ZnEt_2$ and ethylene pressure can fine-tune the molecular weight of PEs across extremely wide ranges (M_n = 5400 – 140000 kg/mol). In work by Guironnet's group, they showed that precise control over the rate of chain transfer of Pd catalyst **54** in ethylene polymerization could be achieved by varying the concentration and substituents of the silane. In both cases, zinc-based and silane-based CTAs are highly efficient, giving no negative impact on catalytic reactivity.

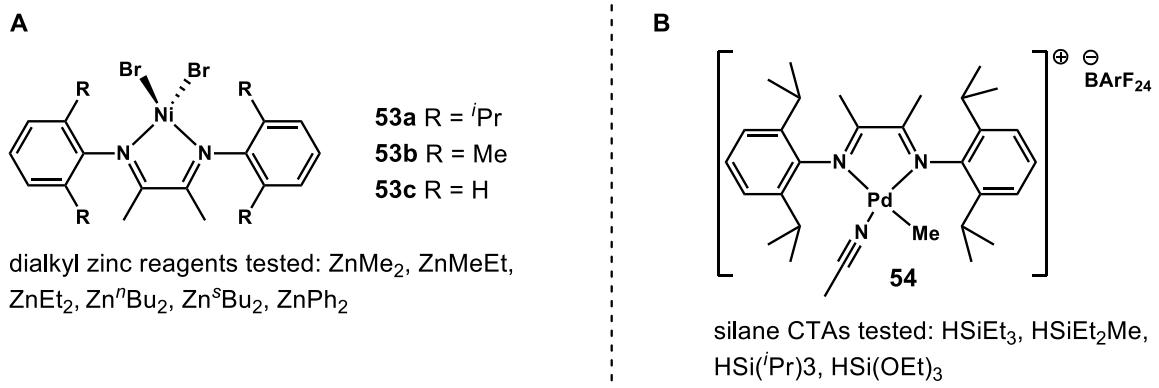

Figure 1.19. Dialkyl zinc and silane compounds as effecient CTAs for group 10 transition-metal based catalysts.

1.7. Our Catalyst Design Approach

Of the strategies discussed above, we favor the cation-switching approach because it provides the broadest range of catalyst tuning capability. Borane-tuning has limited range because only a handful of trisubstituted boranes are commercially available. Redox-tuning can usually only toggle between 2-3 oxidation states. Catalyst self-assembly is highly solvent dependent and can be difficult to control. Finally, use of CTAs can change polymers' MW but not their microstructure or MW distribution. One of the major challenges in designing cation-switchable catalysts is to create metal binding groups that give robust/predictable structures and position secondary cations in close proximity to the catalyst center. Once a suitable catalyst design is achieved, interchanging cations is operationally simple. In addition, we also proposed that the secondary cations can serve as binding sites for polar functional groups in the copolymerization of ethylene and polar monomers (Scheme 1.9). However, copolymerization studies are beyond the scope of this dissertation.

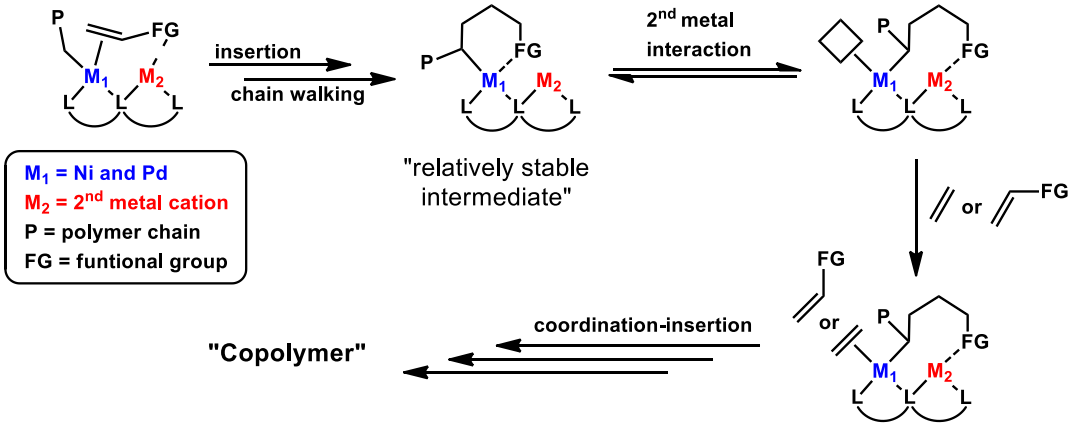

Scheme 1.9. Proposed interaction of second metal cation and polar functional group in the copolymerization of ethylene and polar monomer.

1.8. Scope of the Dissertation

In this work, we focused on bimetallic structures in which the metal centers are bridged by phenolate donors to enforce short metal-metal distances and enable cooperative reactivity. Specifically, we have designed a series of Ni catalysts supported by phenoxyphosphine ligands featuring polyethylene glycol (PEG) chains as secondary metal binding groups (Figure 1.20). The phenoxyphosphine ligand was chosen because the corresponding nickel complexes are known to produce polymers and copolymers with high activity. The PEG was chosen because it can selectively chelate alkali metals over nickel. The following chapters will describe synthesis and characterization of Ni catalysts, olefin polymerization studies, and efforts to synthesize bimodal PE.

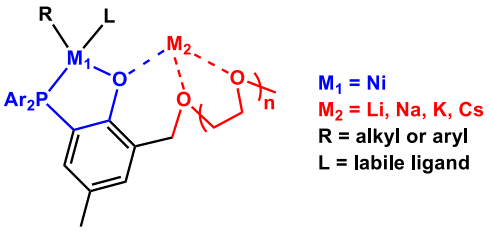

Figure 1.20. General structure of Ni phenoxyphosphine PEG complexes used in this study.

Chapter 2. Development of Highly Productive Nickel-Sodium Phenoxyphosphine Ethylene Polymerization Catalysts and Their Reaction Temperature Profiles

This work have been previously published.

Reproduced with permission from Tran, T. V.; Nguyen, Y. H.; Do, L. H. *Polym. Chem.*, **2019**, *10*, 3718-3721. DOI:10.1039/C9PY00610A.

2.1. Introduction

As discussed in Chapter 1, to enable the incorporation of pendant alkali ions to nickel phenoxyphosphine complexes, we attached polyethylene glycol (PEG) chains to the *ortho* positions of their phenolate rings (Scheme 2.1). We preferred using alkali cations as the secondary metal because alkali ions are redox inactive and do not compete with nickel for ethylene binding. Furthermore, because they are hard Lewis acids, they are capable of forming relatively stable metal-ligand interactions with hard Lewis-bases such as those present in polar monomers. We propose that this alkali-polar functional group interaction could open up the stable six-membered metallocyclic species formed during ethylene and polar olefin copolymerization (Scheme 1.9). In this chapter, the secondary metal investigation was focused on sodium ions due to their favorable properties.[46, 57]

2.2. Synthesis of Nickel Phenoxyphosphine-Polyethylene Glycol Complexes

2.2.1. Ligand Synthesis

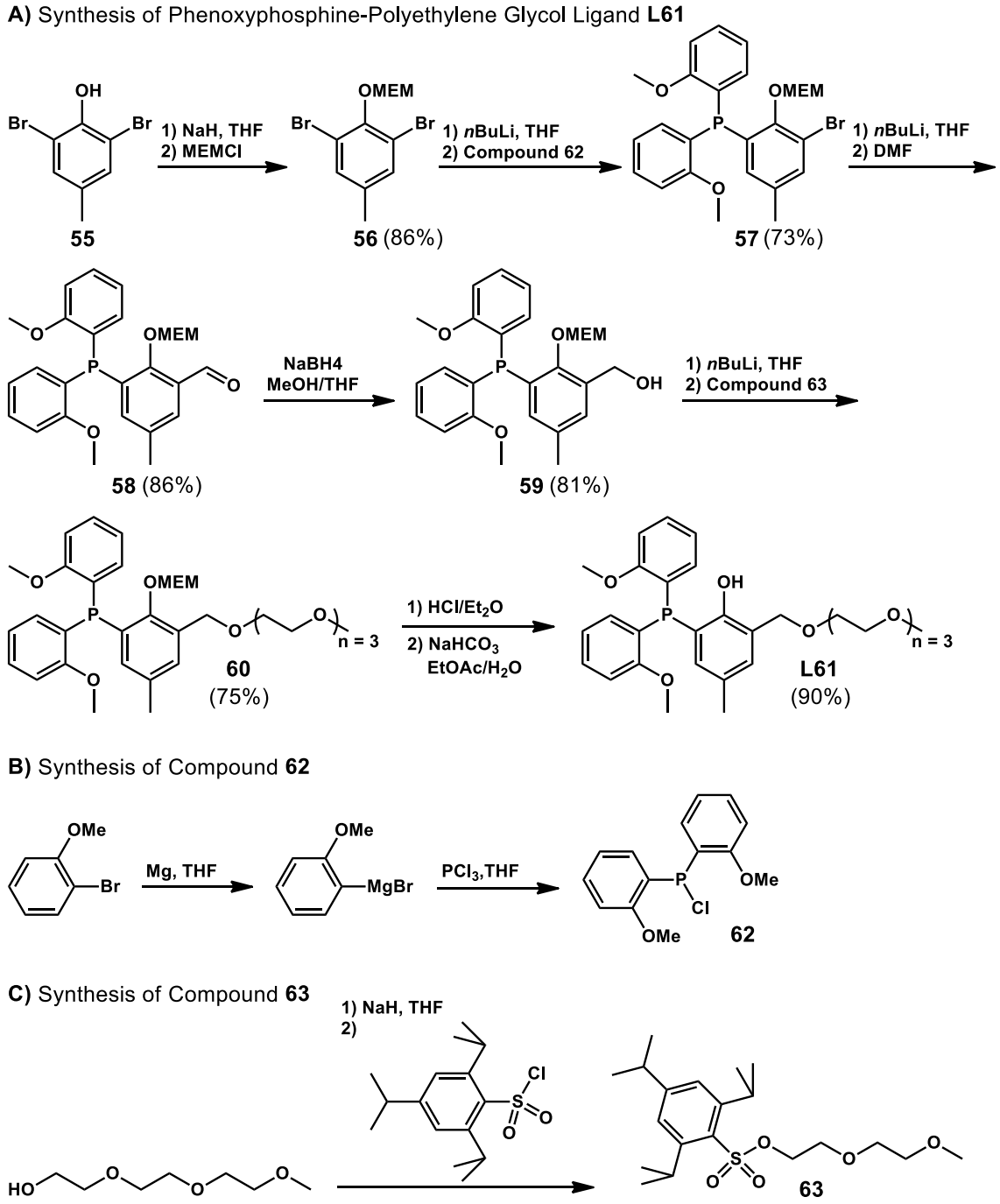

Scheme 2.1. Synthesis of ligand **L61** and compound **62** and **63**.

The multi-step synthesis of dinuclearting phenoxyphosphine-PEG ligand **61** was outlined in Scheme 2.1.[46] Starting from 2,6-dibromo-4-methylphenol **55**, we first protected the phenol group with 2-methoxyethoxymethyl ether (MEM) to give compound **56**. The resulting product was then lithiated with 1 equiv of *n*BuLi and treated with **62** to give phosphine **57**. Lithiation of **57**, followed by nucleophilic attack of DMF and reduction with sodium borohydride yielded alcohol **59**. Finally, alkylation with compound **63**, followed by deprotection with HCl in Et_2O afforded the final ligand **L61** with an overall yield of about 7-11 %.

2.2.2. Catalyst Synthesis

To obtain nickel complex **Ni11**, **L61** was deprotonated by sodium hydride in THF and then reacted with $NiPhBr(PMe_3)_2$ to afford the desired product as a yellow solid in gram scale and good yield (1.12 g, 75 %). For control studies, we also prepared the conventional nickel phenoxyphosphine complex featuring *ortho tert*-butyl group (**Ni^{t}Bu**) using the same metallation procedure (Scheme 2.2).[66]

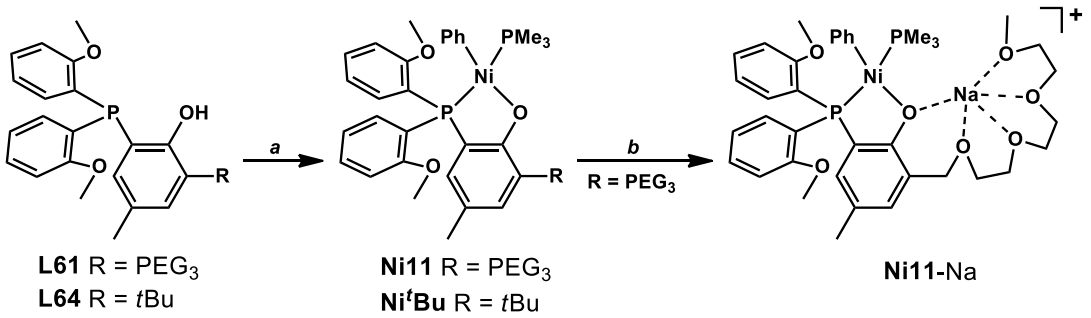

Scheme 2.2. Synthesis of nickel phenoxyphosphine complexes. Step a: 1) NaH, THF, 2) $NiPhBr(PMe_3)_2$; Step b: $NaBAr^F{}_4$. PEG3 = $CH_2(OCH_2CH_2)_3OCH_3$.

2.3. Metal Binding Study

To determine whether Na^+ can coordinate to **Ni11**, we carried out metal titration studies by UV-visible absorption spectroscopy. We observed that when aliquots of $NaBAr^F{}_4$ (where $BAr^F{}_4^-$ = tetrakis(3,5-bis(trifluoromethyl)phenyl)borate)[67] were added to a solution of **Ni11** in Et_2O, the optical band at ~370 nm gradually decreased while the optical band at ~330 nm increased (Figure 2.1). The appearance of isosbestic points at 326 and 359 nm suggests that the addition of Na^+ to **Ni11** led to the formation of a new optically active species. The optimal Ni:Na binding stoichiometry was determined to be 1:1 by Job Plot studies (Figure 2.2).[68]

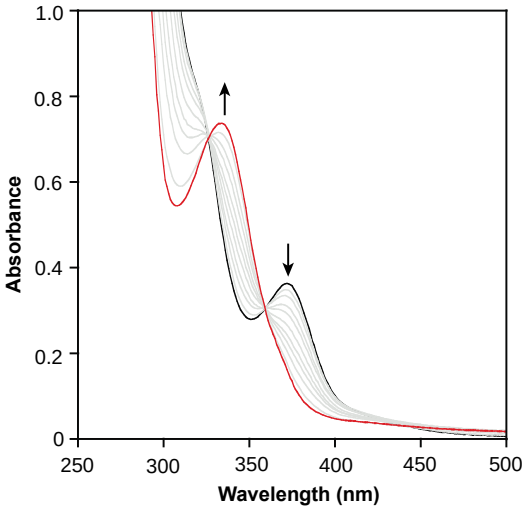

Figure 2.1. UV-vis absorbance spectra of complex **Ni11 (**100 μM in Et_2O) after the addition of various aliquots of $NaBAr^F{}_4$. The starting trace of **Ni11** is shown in black and the final trace (+ 1.0 equiv of Na^+ relative to Ni) is shown in red.

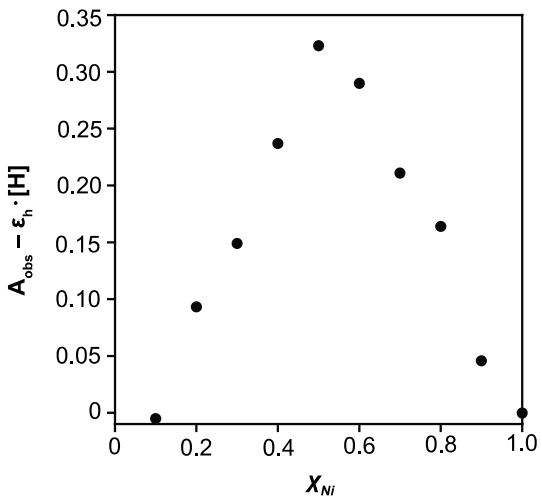

Figure 2.2. Job Plot showing the coordination interactions between complex **Ni11** and $NaBAr^F{}_4$. The peak maximum occurs at χNi = 0.5, which suggests that the optimal nickel:sodium binding stoichiometry is 1:1. The y-axis value (Aobs – εh·[H]t) is proportional to the concentration of the nickel-sodium complex **Ni11**-Na. The x-axis is the molar ratio of nickel (χNi = [**Ni11**]/([**Ni11**]+[Na^+])). The full data is given in Table 2.2.

To obtain structural characterization, we grew single crystals of the nickel-sodium complex by layering pentane over a toluene/Et_2O solution of **Ni11** and $NaBAr^F{}_4$ (1:1). Its X-ray structure revealed a heterobimetallic complex with the composition NiNa(phenoxyphosphine-PEG)Ph(PMe_3) (**Ni11**-Na, Figure 2.3). The Ni centre is four-coordinate, in which the phenyl group is coordinated *trans* relative to the phosphorus donor P1. Presumably, this orientation is preferred due to metal-π interactions between the adjacent sodium ion and phenyl ring (C30–C31). The sodium is ligated by four PEG oxygen atoms and a phenolate donor.

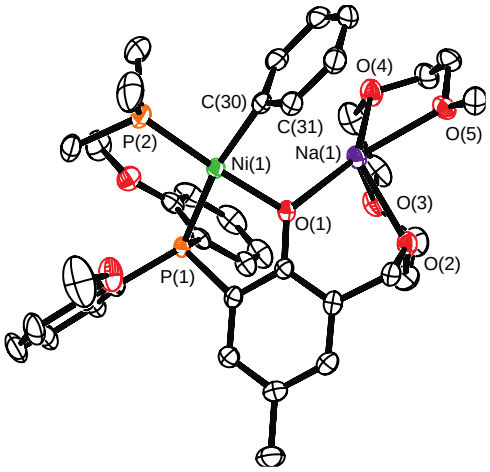

Figure 2.3. X-ray structure of complex **Ni11**-Na (ORTEP view, displacement ellipsoids drawn at 50% probability level). Hydrogen atoms and the $BAr^F{}_4^-$ anion have been omitted for clarity.

Although complex **Ni11** itself could not be crystallized for X-ray diffraction analysis, the structure of the related mononickel **Ni^{t}Bu** showed that the Ni centre is square planar but the coordinated phenyl group is *cis* relative to P1 (Figure 2.4). Interestingly, when a solution of **Ni^{t}Bu** in Et_2O was treated with up to 4 equiv of $NaBAr^F{}_4$, no UV-visible absorption changes were observed (Figure 2.5), indicating that there are no coordination interactions between complex **Ni^{t}Bu** and Na^+.

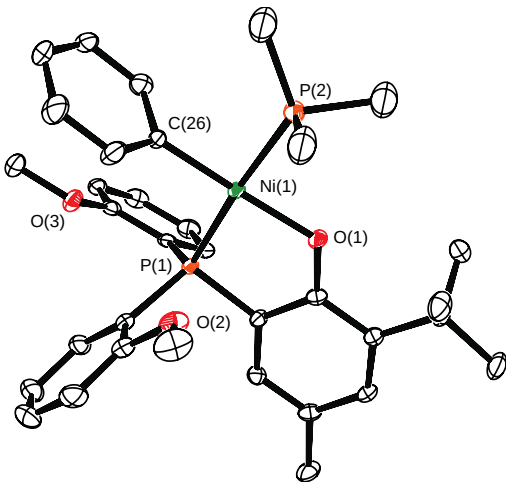

Figure 2.4. X-ray structure of complex **Ni^{t}Bu** (ORTEP view, displacement ellipsoids drawn at 50% probability level). Hydrogen atoms and pentane solvent have been omitted for clarity. Atom colors: green = nickel, orange = phosphorus, red = oxygen, black = carbon.

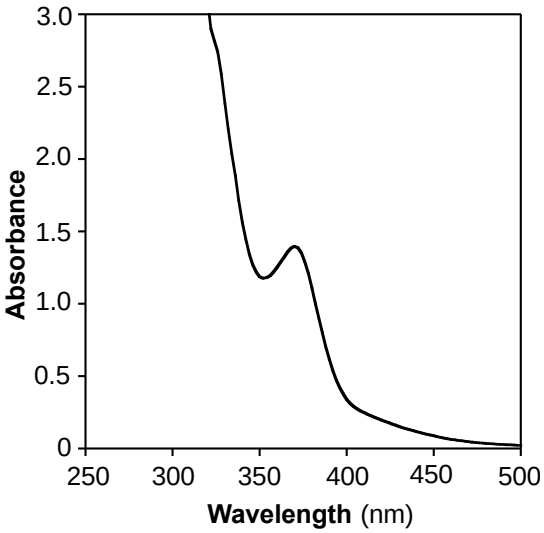

Figure 2.5. UV-vis absorbance spectra of complex **Ni^{t}Bu** (100 μM in Et2O) after the addition of 4 equiv of $NaBAr^F{}_4$. The starting trace of **Ni^{t}Bu** before and after the addition of Na are identical, suggesting that sodium does not bind to the nickel complex.

2.4. Ethylene Polymerization Study

With our Ni complexes in hand, we tested their catalytic performance by first activation using $Ni(COD)_2$ (COD = 1,5-cyclooctadiene) and then exposure to 450 psi of ethylene at 30 °C for 1 h

in toluene. To minimize catalyst thermal decomposition, the polymerization studies in Table 2.1 were performed using a low catalyst concentration of 5 μM and with manual external cooling to maintain the desired reaction temperature. Under these conditions, complex **Ni^{t}Bu** produced linear polyethylene (PE) with an activity of 2.12×10^3 kg/mol·h (Table 2.1, entry 1). The addition of $NaBAr^F{}_4$ to **Ni^{t}Bu** had negligible effects on polymerization (activity = 1.88×10^3 kg/mol·h, entry 2), which further supports our observation that Na^+ does not bind to **Ni^{t}Bu**.

Table 2.1. Ethylene Polymerization Data[a]

Entry	Complex	Pressure (Psi)	Time (h)	Initial Temp. (°C)	Activity (Kg/Mol·h)
1	**Ni^{t}Bu**	450	1	30	2120
2	**Ni^{t}Bu**/Na^+	450	1	30	1880
3	**Ni11**	450	1	30	0
4	**Ni11**-Na	150	1	20	3780
5	**Ni11**-Na	300	1	20	8840
6	**Ni11**-Na	450	1	20	10800
7	**Ni11**-Na	450	0.5	30	25300
8	**Ni11**-Na	450	1	30	18100
9	**Ni11**-Na	450	2	30	15080
10	**Ni11**-Na	450	1	20	10800
11	**Ni11**-Na	450	1	40	14700
12	**Ni11**-Na	450	1	50	13000
13	**Ni11**-Na	450	1	60	9380

[a]Conditions: Ni catalyst (0.5 μmol), $NaBAr^F{}_4$ (1 μmol, if any), $Ni(COD)_2$ (4 μmol), 100 mL toluene. Temperature was controlled by manual external cooling when necessary to ensure that the reaction temperature does not exceed greater than 5°C from the starting temperature.

Surprisingly, when **Ni11** was tested under the same conditions as above, no polyethylene was obtained (Table 1, entry 3). We hypothesized that the free PEG chain in **Ni11** can self-inhibit by occupying open coordination sites at the Ni centre. However, when $NaBAr^F{}_4$ was added to **Ni11**, the resulting nickel-sodium **Ni11**-Na showed a remarkably activity of 1.81×10^4 kg/mol·h (entry

8), which is a ~8.5× increase in comparison to that of **Ni^{t}Bu**. The PE produced by **Ni^{t}Bu** and **Ni11**-Na both have low molecular weight (M_n = ~10^3) and narrow polydispersity (M_w/M_n = < 2.0), which is typical for this class of catalysts.[66, 69]

A comparison with several different Ni systems reported in the literature indicates that **Ni1**-Na is among one of the most *productive* (Table 2.11, note: different studies used different polymerization conditions).[69-77] Although the Ni diimine (**Ni1**)[70] and Ni tris(adamantyl)phosphine (**Ni9**)[77] complexes are extraordinarily active, our **Ni11**-Na complex achieved the highest turnover number (TON). For example, the TON for **Ni11-Na** was 646×10^3, whereas the TON for **Ni1** and **Ni9** were 400×10^3 and 216×10^3, respectively. Interestingly, catalysts **Ni1** and **Ni9** furnished PE with significantly higher molecular weights ($M_n \geq 10^5$) than **Ni11**-Na ($M_n \approx 10^3$). However, it is well established that higher M_n polymers could be obtained by increasing the steric bulk of the catalyst structure.[31, 78]

To investigate the polymerization behaviour of **Ni11**-Na further, we evaluated its reactivity as a function of pressure, time, and temperature. We found that when the ethylene pressure was increased from 150 → 300 → 450 psi (Table 2.1, entries 4-6), the catalyst activity also increased. The approximately linear correlation between pressure and polymerization rate suggests that the reaction is first-order in ethylene. At 150 psi and 20°C (Table 2.5), **Ni11**-Na showed relatively constant activity (average = 3.3 ×10^3 kg/mol·h) up to 3.0 h. However, at 450 psi and 30°C (Table 2.1), the activity gradually decreased from 2.5 ×10^4 (entry 7) to 1.5 ×10^4 kg/mol·h (entry 9) over the course of 2 h, which could be indicative of either catalyst decomposition or mass transport limitations. In the latter case, it is well documented that for highly active catalysts, precipitation of large amounts of polymer inside the reactor could dramatically slow down the polymerization process.[71, 77]

Finally, when we performed polymerizations at different temperatures (20 to 60°C, entries 8 and 10-13), we observed that the optimal temperature was 30 °C. We noted, however, that for some reactions the initial temperature spiked abruptly and were difficult to control. This large exotherm only occurred when the **Ni11**-Na complex was used. Polymerizations using the monometallic **Ni10** and **Ni11** complexes did not generate any additional heat.

To evaluate the thermal stability of the **Ni11**-Na complex, we measured the reaction temperature and polymer yields as a function of time. When a 100 μM toluene solution of the nickel-sodium catalyst was treated with $Ni(COD)_2$ and then exposed to 450 psi of ethylene, the reaction temperature rose from 20 to 159 °C in 4 min (Figure 2.6A). After this initial temperature increase, the solution cooled slowly back down to ~20 °C after 60 min. Interestingly, when the product yields were determined at 4 and 60 min, similar amounts of polymer were obtained (~10.4 and ~11.3 g, respectively), suggesting that the **Ni11**-Na catalyst was deactivated shortly after ~4 min. When the **Ni11**-Na concentration was lowered to 50 μM, the maximum reaction temperature was observed to be 122 °C after 5 min (Figure 2.6B). The rate of polymer formation remained relatively constant from 0-7 min but then dropped precipitously thereafter. In contrast, when the reactor temperature was maintained at 30°C during a 2 h polymerization run using 5 μM **Ni11**-Na, the amount of PE produced increased steadily (Figure 2.6C), suggesting that an appreciable amount of the catalyst loaded was still active after 2 h.

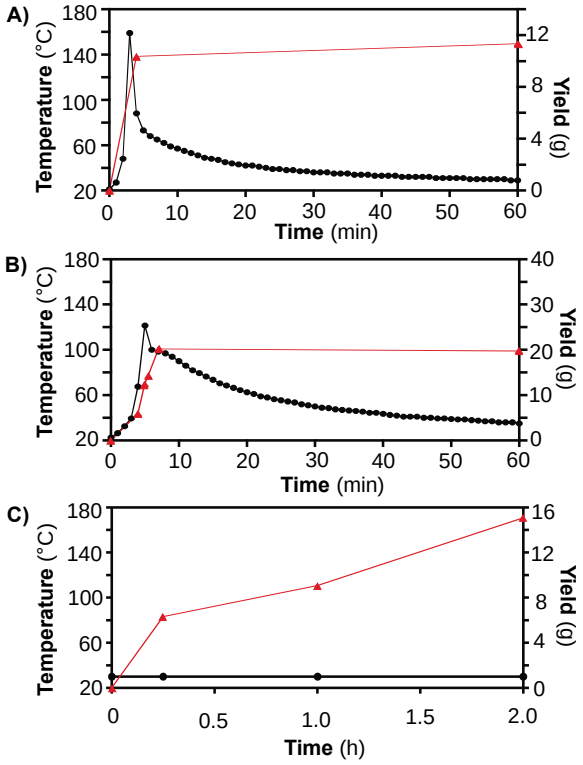

Figure 2.6. Plots showing the reaction temperatures (black dots) and polymer yields (red triangles) by the **Ni11**-Na complex at 100 µM (A) and 50 µM (B) catalyst concentrations. When external temperature control was applied (C), the **Ni11**-Na (5 µM) catalyst gave increasing amounts of PE up to the 2 h polymerization time. All reactions were performed under 450 psi of ethylene.

2.5. Conclusion

In summary, we have synthesized a new class of Ni phenoxyphosphine complexes featuring PEG side arms that can chelate secondary sodium ions. We have found that the **Ni11**-Na complexes are remarkably efficient catalysts for ethylene polymerization, demonstrating once again that the use of pendant Lewis acids is an effective strategy to enhance catalyst performance. This work also illustrates the importance of conducting detailed temperature studies to optimize polymerization processes. Although there are many reports that highly active catalysts can exhibit large exotherms,[71, 77, 79-80] seldom are their reaction temperature profiles provided. This information is useful because it allows us to predict the best reaction conditions to use for a given

catalyst. For example, by knowing the temperature threshold above which **Ni11**-Na decomposes, we were able to adjust our polymerization conditions to achieve one of the highest TON reported for a nickel catalyst. Although it is standard practice to disclose only the reactor temperature at the start of a reaction, we recommend also providing temperature data for the full polymerization time to gain insights into a catalyst's true thermal stability.

2.6. Experimental

General Procedures

Commercial reagents were used as received. All air- and water-sensitive manipulations were performed using standard Schlenk techniques or under a nitrogen atmosphere using a drybox. Anhydrous solvents were obtained from an Innovative Technology solvent drying system saturated with argon. High-purity polymer grade ethylene was obtained from Matheson TriGas without further purification. The $NaBAr^F_4$ salt was prepared according to a literature procedure.[67]

NMR spectra were acquired using JEOL spectrometers (ECA-400, -500, and -600) and referenced using residual solvent peaks. All ^{13}C NMR spectra were proton decoupled. ^{31}P NMR spectra were referenced to phosphoric acid. ^{1}H NMR spectroscopic characterization of polymers: each NMR sample contained ~20 mg of polymer in 0.5 mL of 1,1,2,2-tetrachloroethane-d_2 (TCE-d_2) and was recorded on a 500 MHz spectrometer using standard acquisition parameters at 120 °C. High-resolution mass spectra were obtained from the mass spectral facility at the University of Houston. Elemental analyses were performed by Atlantic Microlab. Gel permeation chromatography (GPC) data were obtained using a Malvern high temperature GPC instrument equipped with refractive index, viscometer, and light scattering detectors at 150 °C with 1,2,4-trichlorobenzene (stabilized with 125 ppm BHT) as the mobile phase. A calibration curve was

established using polystyrene standards in triple detection mode. All molecular weights reported are based on the triple detection method.

Synthesis and Characterization

Ligand **L64** was synthesized as depicted in Scheme 2.3 below:

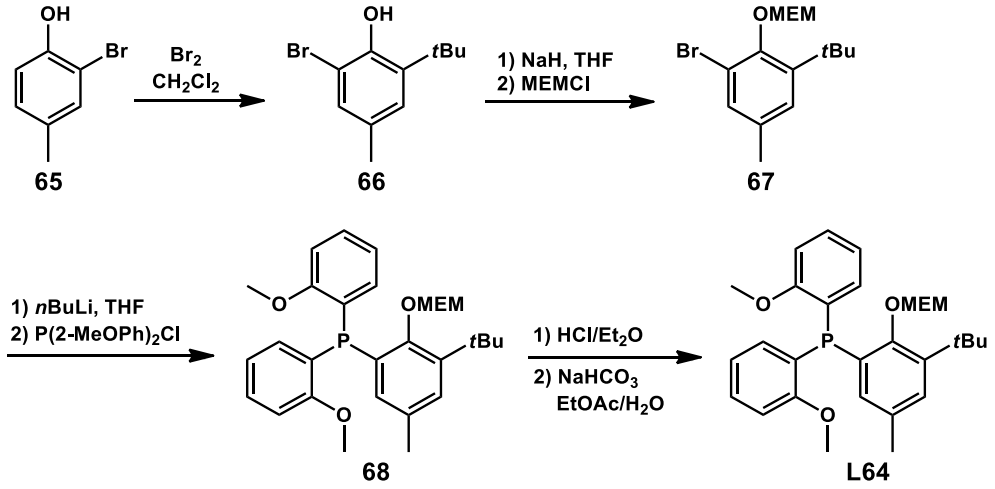

Scheme 2.3. Synthesis of ligand **L64**.

Preparation of Compound 62. This synthesis was modified from a reported procedure.[81] A 200 mL Schlenk flask was charged with magnesium turnings (1.2 g, 50 mmol, 2.5 equiv) under nitrogen in 50 mL of dry THF. The compound 2-bromoanisole (5.2 mL, 40 mmol, 2.0 equiv) was added to the reaction mixture and then stirred at RT for 3 h until the solution turned dark gray. The resulting Grignard reagent was slowly cannula transferred over a period of 45 min to a solution of PCl_3 (1.6 mL, 20 mmol, 1.0 equiv) in 100 mL of dry THF at -78 ^{o}C. After the addition was complete, the heterogeneous mixture was continued stirring and allowed to warm up to RT overnight. Finally, the solvent was removed under vacuum and the

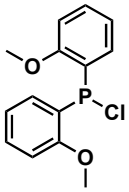

crude product was used in the next step without further purification. ^{31}P NMR ($CDCl_3$, 162 MHz): δ (ppm)= 69.94 (s), 62.56 (s).

Preparation of Compound 66. This synthesis was modified from a literature procedure.[82] The

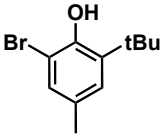

compound 2-*tert*-butyl-4-cresol (6.73 g, 40.95 mmol, 1.05 equiv) was dissolved in 100 mL of dry DCM in a 200 mL Schlenk flask. The flask was covered with aluminum foil and cooled to 0 ^{o}C. Bromine (2 mL, 39 mmol, 1.00 equiv) was added dropwise to the reaction flask and the mixture was allowed to warm to RT and stirred overnight. The reaction was quenched by the slow addition of cold H_2O (75 mL) and was then extracted into DCM (2×150 mL). The organic layers were combined, washed with aqueous $NaHCO_3$ (2×100 mL), H_2O (2×100 mL), dried over Na_2SO_4, filtered, and evaporated to dryness. The crude material was purified by silica gel column chromatography (20:1 hexane: ethyl acetate) to afford a white solid (9.50 g, 39.07 mmol, 95%). ^{1}H NMR ($CDCl_3$, 400 MHz): δ (ppm) = 7.16 (s, 1H), 7.01 (s, 1H), 5.64 (s, 1H), 2.26 (s, 3H), 1.40 (s, 9H). ^{13}C NMR ($CDCl_3$, 101 MHz): δ (ppm) = 148.21, 137.24, 130.30, 129.69, 127.46, 111.97, 35.36, 29.47, 20.68.

Preparation of Compound 67. To a mixture of **66** (9.50 g, 39.07 mmol, 1.0 equiv) in 100 mL of

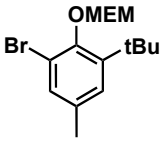

dry THF in a 200 mL Schlenk flask under nitrogen at -0 ^{o}C, small aliquots of NaH (60%, 2.34 g, 58.6 mmol, 1.5 equiv) were added and the mixture was stirred at RT for 2 h. The reagent 2-methoxyethoxymethyl chloride (MEMCl) (5.5 mL, 44.93 mmol, 1.15 equiv) was added and the solution was stirred overnight. The reaction was quenched by the slow addition of H_2O and the product was extracted into Et_2O (2×150 mL). The organic layers were combined, washed with H_2O (2×75 mL), dried over Na_2SO_4, filtered, and evaporated to dryness. The crude material was purified by silica gel column chromatography (20:1 hexane: ethyl acetate) to afford

a colorless oil (6.91 g, 20.86 mmol, 53%). ^{1}H NMR ($CDCl_3$, 400 MHz): δ (ppm) = 7.22 (d, J_{HH} = 1.8 Hz, 1H), 7.07 (d, J_{HH} = 1.8 Hz, 1H), 5.27 (s, 2H), 4.05 (m, 2H), 3.65 (m, 2H), 3.41 (s, 3H), 2.26 (s, 3H), 1.40 (s, 9H). ^{13}C NMR ($CDCl_3$, 101 MHz): δ (ppm) = 150.46, 145.06, 134.56, 132.14, 127.69, 117.74, 98.21, 71.72, 69.45, 59.18, 35.65, 30.94, 20.83. HRMS–ESI(+): Calc. for $C_{15}H_{23}BrO_3$ $[M+Na]^+$ = 353.0728, Found = 353.0853.

Preparation of Compound 68. To a solution of compound **67** (6.62 g, 20 mmol, 1.0 equiv) in 50

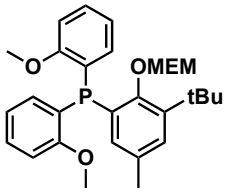

mL of dry THF in a 100 mL Schlenk flask under nitrogen at -78 ºC, nBuLi (1.6 M in hexanes, 12.8 mL, 20.5 mmol, 1.02 equiv) was added dropwise using a syringe pump. The reaction mixture was stirred at -78 ºC for 40 min. A solution of $P(2\text{-MeOPh})_2Cl$ (5.05 g, 18 mmol, 0.9 equiv) in 50 mL of dry THF was cannula transferred into the reaction mixture and stirred for another 40 min at -78 ºC, followed by naturally warming to RT. The reaction was quenched by the slow addition of H_2O and the product was extracted into Et_2O (3×75 mL). The organic layers were combined, washed with H_2O (2×50 mL), dried over Na_2SO_4, filtered, and evaporated to dryness. The crude material was purified by silica gel column chromatography (4:1 hexane: ethyl acetate) to afford a colorless oil (4.02 g, 8.09 mmol, 40%). This compound was used directly in the next step without further purification.

Preparation of Compound L64. Compound **68** (1.24 g, 2.5 mmol, 1.0 equiv) was dissolved in

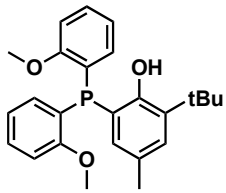

100 mL of MeOH and then 10 mL solution of 2 M HCl in Et_2O was added. The reaction mixture was stirred at RT overnight and then dried to remove solvent. The product was dissolved in 200 mL of EtOAc along and then combined with 50 mL of 1 M aqueous $NaHCO_3$. The mixture was stirred at RT for 30 min and the

product was extracted into Et_2O (2×100 mL). The organic layers were combined, washed with H_2O (2×100 mL), dried over Na_2SO_4, filtered, and evaporated to dryness. The crude material was purified by silica gel column chromatography (4:5 hexane: ethyl acetate) to afford a white solid (0.69 g, 1.68 mmol, 67%). ^{1}H NMR ($CDCl_3$, 500 MHz): δ (ppm) = 7.40 (d, J_{HH} = 11.5 Hz, 1H), 7.19 (ddd, J_{HH} = 7.4, 5.6, 1.7 Hz, 2H), 7.13 (d, J_{HH} = 1.8 Hz, 1H), 7.02 (td, J_{HH} = 8.1, 1.5 Hz, 2H), 6.97 (dd, J_{HH} = 5.4, 1.6 Hz, 1H), 6.70 (t, J_{HH} = 7.5 Hz, 2H), 6.37 (dd, J_{HH} = 8.1, 5.1 Hz, 2H), 3.07 (s, 6H), 1.92 (s, 3H), 1.51 (s, 9H). ^{13}C NMR ($CDCl_3$, 100 MHz): δ (ppm) = 161.04 (d, J_{CP} = 15.1 Hz), 156.56 (d, J_{CP} = 19.7 Hz), 135.36, 133.23, 133.0.3 (d, J_{CP} = 3.2 Hz), 130.24, 129.53, 128.42, 123.09 (d, J_{CP} = 2.8 Hz), 120.96, 119.28, 110.30, 55.71, 34.79, 29.54, 20.88. ^{31}P NMR ($CDCl_3$, 162 MHz): δ (ppm) = -51.71. HRMS–ESI(+): Calc. for $C_{25}H_{29}O_3P$ $[M+Na]^+$ = 431.1752, Found = 431.1887.

Preparation of Compound 56. Solid 2,6-dibromo-4-methylphenol (6.65 g, 25 mmol, 1.0 equiv)

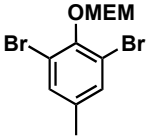

was dissolved in 100 mL of dry THF in a Schlenk flask under nitrogen and cooled to 0 ºC. Small aliquots of NaH (60%, 1.48 g, 37 mmol, 1.5 equiv) were added and the mixture was stirred at room temperature for 1 h. The reagent 2-methoxyethoxymethyl chloride (MEMCl) was added and the resulting solution was stirred overnight. The reaction was quenched by the slow addition of H_2O and the products were extracted into Et_2O (2×100 mL). The organic layers were combined, washed with H_2O (2×50 mL), dried over Na_2SO_4, filtered, and evaporated to dryness. The crude material was purified by silica gel column chromatography (2:1 hexane: ethyl acetate) to afford a clear oil (7.66 g, 21.64 mmol, 86%). ^{1}H NMR ($CDCl_3$, 500 MHz): δ (ppm) = 7.29 (s, 2H), 5.20 (s, 2H), 4.08 (m, 2H), 3.61 (m, 2H), 3.38 (s, 3H), 2.24 (s, 3H). ^{13}C NMR

($CDCl_3$, 126 MHz): δ (ppm) = 149.04, 136.91, 133.35, 117.97, 98.36, 71.77, 69.89, 59.19, 20.29. HRMS–ESI(+): Calc. for $C_{11}H_{14}Br_2O_3$ $[M+Na]^+$ = 374.9202, Found = 374.9332.

Preparation of Compound 57. To a solution of **56** (7.08 g, 20 mmol, 1.0 equiv) in 50 mL of dry

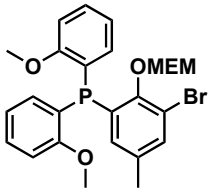

THF in a Schlenk flask under nitrogen at -78 ºC, nBuLi (1.6 M in hexanes, 12.8 mL, 20.5 mmol, 1.02 equiv) was added dropwise using a syringe pump. The reaction mixture was then stirred at -78 ºC for 40 min. A solution of P(2-MeOPh)$_2$Cl (5.05 g, 18 mmol, 0.9 equiv) in 50 mL of dry THF was cannula transferred to the reaction mixture and stirred for another 40 min at -78 ºC, followed by naturally warming to RT. The reaction was quenched by the slow addition of H_2O and the products were extracted into Et_2O (3×75 mL). The organic layers were combined, washed with H_2O (2×50 mL), dried over Na_2SO_4, filtered, and evaporated to dryness. The crude material was purified by silica gel column chromatography (3:1 hexane: ethyl acetate) to afford a colorless oil (6.82 g, 13.16 mmol, 73%). ^{1}H NMR ($CDCl_3$, 500 MHz): δ (ppm) = 7.36 (s, 1H), 7.32 (t, J_{HH} = 7.5 Hz, 2H), 6.86 (m, 3H), 6.83 (d, J_{HH} = 5.2 Hz, 1H), 6.63 (m, 2H), 6.49 (m, 1H), 5.30 (s, 2H), 4.02 (t, J_{HH} = 4.8 Hz, 2H), 3.72 (s, 6H), 3.52 (t, J_{HH} = 4.5 Hz, 2H), 3.34 (s, 3H), 2.12 (s, 3H). ^{13}C NMR ($CDCl_3$, 126 MHz): δ (ppm) = 161.33 (d, J_{CP} = 16.5 Hz), 161.20 (d, J_{CP} = 20.9), 154.24, 154.07, 135.61, 134.78, 134.50, 133.86, 132.94 (d, J_{CP} = 17.4 Hz), 132.81, 130.34, 124.31, 124.20 (d, J_{CP} = 13.7 Hz), 121.18, 117.34, 117.32, 110.22, 98.75 (d, J_{CP} = 9.4 Hz), 98.68, 71.81, 69.52 (d, J_{CP} = 4.3 Hz), 59.07, 55.75, 20.66. ^{31}P NMR ($CDCl_3$, 162 MHz): δ (ppm) = -35.90. HRMS–ESI(+): Calc. for $C_{25}H_{30}BrO_5P$ $[M+Na]^+$ = 541.0750, Found = 541.0940.

Preparation of Compound 58. To a solution of **57** (6 g, 11.58 mmol, 1.0 equiv) in 50 mL of dry

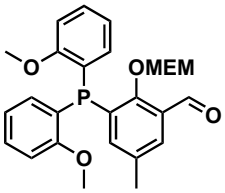

THF in a Schlenk flask under nitrogen at -78 ^{o}C, nBuLi (1.6 M in hexanes, 8.4 mL, 13.44 mmol, 1.16 equiv) was added dropwise using a syringe pump. The reaction mixture was stirred at -78 ^{o}C for 40 min. Dry DMF (5 mL, 65 mmol, 5.6 equiv) was added to the reaction mixture and stirred for another 40 min at -78 ^{o}C, followed by naturally warming up to RT. The reaction was quenched by the slow addition of H_2O and the product was extracted into Et_2O (3×75 mL). The organic layers were combined, washed with H_2O (2×50 mL), dried over Na_2SO_4, filtered, and evaporated to dryness. The crude material was purified by silica gel column chromatography (3:2 hexane: ethyl acetate) to afford a light yellow oil (4.67 g, 9.98 mmol, 86%). This compound was used directly in the next step without further purification.

Preparation of Compound 59. Compound **58** (4.67 g, 9.98 mmol, 1.0 equiv) was dissolved in

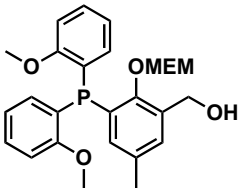

400 mL of MeOH and 80 mL of THF. Small aliquots of $NaBH_4$ (2 g, 54 mmol, 5.4 equiv) were added and the mixture was stirred at RT overnight. The reaction solvent was removed under vacuum and the residue was redissolved in Et_2O (100 mL). The ether layer was washed with H_2O (2×100 mL), dried over Na_2SO_4, filtered, and evaporated to dryness. The crude material was purified by silica gel column chromatography (1:3 hexane: ethyl acetate) to afford a white solid (3.8 g, 8.08 mmol, 81%). ^{1}H NMR ($CDCl_3$, 600 MHz): δ (ppm) = 7.33 (t, J_{HH} = 7.6 Hz, 2H), 7.20, (s, 1H), 6.87 (dd, J_{HH} = 8.4, 5.5 Hz, 2H), 6.84 (t, J_{HH} = 7.4 Hz, 2H), 6.62 (m, 2H), 6.51 (m, 1H), 5.29 (s, 2H), 4.62 (s, 2H), 3.88 (m, 2H), 3.72 (s, 6H), 3.57 (m, 2H), 3.36 (s, 3H), 2.14 (s, 3H). ^{13}C NMR ($CDCl_3$, 126 MHz): δ (ppm) = 161.21 (d, J_{CP} = 16.6 Hz), 157.74 (d, J_{CP} = 20.6 Hz), 135.24, 134.73, 134.37, 133.78,

132.59, 130.25, 129.79 (d, J_{CP} = 12.2 Hz), 124.29 (d, J_{CP} = 12.3 Hz), 121.08, 110.15, 99.92 (d, J_{CP} = 13.1 Hz), 71.50, 69.16, 61.02, 59.11, 55.74, 20.94. ^{31}P NMR ($CDCl_3$, 162 MHz): δ (ppm) = -38.50. HRMS–ESI(+): Calc. for $C_{14}H_{20}O_6$ $[M+Na]^+$ = 493.1751, Found = 493.1925.

Preparation of Compound 63. Triethylene glycol monomethyl ether (2.63 g, 16 mmol, 1.0 equiv)

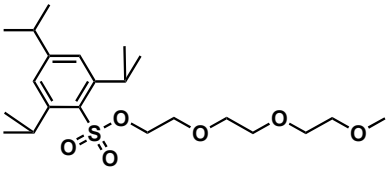

was dissolved in 100 mL of dry THF in a Schlenk flask under nitrogen and cooled to 0 ºC. Small aliquots of NaH (60%, 1 g, 25 mmol, 1.56 equiv) were added and the mixture was stirred at RT for 1 h. The reagent 2,4,6-triisopropylbenzenesulfonyl chloride (6.1 g, 20 mmol, 1.25 equiv) was added and the solution was stirred overnight. The reaction was quenched by the slow addition of H_2O and the product was extracted into Et_2O (2×100 mL). The organic layers were combined, washed with H_2O (3×50 mL), dried over Na_2SO_4, filtered, and evaporated to dryness. The crude material was purified by silica gel column chromatography (5:1 hexane: ethyl acetate to 1:3 hexane: ethyl acetate) to afford a colorless oil (5.14 g, 11.95 mmol, 75%). ^{1}H NMR ($CDCl_3$, 500 MHz): δ (ppm) = 7.16 (s, 2H), 4.14 (m, 4H), 3.71 (t, J_{HH} = 4.8 Hz, 2H), 3.59 (m, 6H), 3.50 (m, 2H), 3.34 (s, 3H), 2.89 (sep, J_{HH} = 6.9 Hz, 1H), 1.24 (m, 18H). ^{13}C NMR ($CDCl_3$, 126 MHz): δ (ppm) = 153.77, 150.93, 129.35, 123.84, 71.96, 70.78, 70.64, 68.87, 68.22, 59.12, 34.34, 29.67, 24.80, 23.65. HRMS–ESI(+): Calc. for $C_{22}H_{38}O_6S$ $[M+Na]^+$ = 453.2287, Found = 453.2442.

Preparation of Compound 60. To a mixture of **59** (3.8 g, 8.08 mmol, 1 equiv) in 100 mL of dry

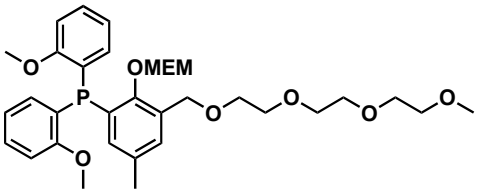

THF in a Schlenk flask under nitrogen at -0 ºC, small aliquots of NaH (60%, 1.3 g, 32.4 mmol, 4 equiv) was added. The reaction mixture was stirred at RT for 1 h. A

solution of compound **63** (5.23 g, 12.15 mmol, 1.5 equiv) in 50 mL of THF was cannula transferred into the reaction mixture and then stirred at RT overnight. The reaction was quenched by the slow addition of cold H_2O and the product was extracted into Et_2O (3×100 mL). The organic layers were combined, washed with H_2O (2×75 mL), dried over Na_2SO_4, filtered, and evaporated to dryness. The crude material was purified by silica gel column chromatography (1:1 hexane: ethyl acetate to 1:4 hexane: ethyl acetate) to afford a colorless oil (3.95 g, 6.07 mmol, 75%). This compound was used directly in the next step without further purification.

Preparation of Compound L61. Compound **60** (3.95 g, 6.07 mmol, 1 equiv) was dissolved in

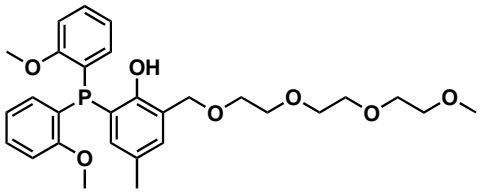

100 mL of MeOH and then treated with 10 mL of 2 M HCl in Et_2O. The reaction mixture was stirred at RT overnight. The solvent was removed under vacuum and the product was dissolved in 200 mL of EtOAc. A 50 mL solution of 1 M $NaHCO_3$ in H_2O was then added. The mixture was stirred at RT for 30 min and the product was extracted into Et_2O (2×100 mL). The organic layers were combined, washed with H_2O (2×100 mL), dried over Na_2SO_4, filtered, and evaporated to dryness. The crude material was purified by silica gel column chromatography (1:3 hexane: ethyl acetate) to afford a white waxy solid (2.9 g, 5.49 mmol, 90%). ^{1}H NMR ($CDCl_3$, 500 MHz): δ (ppm) = 7.32 (td, J_{HH} = 7.7, 1.5 Hz, 2H), 7.23 (d, J_{HH} = 1Hz, 1H), 6.97 (d, J_{HH} = 1.7 Hz, 1H), 6.85 (m, 4H), 6.77 (m, 2H), 6.52 (m, J_{HH} = 5.1, 1.9 Hz, 1H), 4.66 (s, 2H), 3.73 (s, 6H), 3.68 (m, 2H), 3.66 (m, 2H), 3.60 (m, 2H), 3.58 (m, 4H), 3.49 (m, 2H), 3.35 (s, 3H), 2.11 (s, 3H). ^{13}C NMR ($CDCl_3$, 126 MHz): δ (ppm) = 161.53 (d, J_{CP} = 26.8 Hz), 161.40 (d, J_{CP} = 5.5 Hz), 155.96 (d, J_{CP} = 29.7 Hz), 155.87, 134.34, 133.74 (d, J_{CP} = 6.6 Hz), 130.62, 130.22, 129.04 (d, J_{CP} = 9.6 Hz), 123.91, 122.57 (d, J_{CP} = 6.1 Hz), 121.04, 110.32, 71.98, 70.99, 70.76, 70.61, 70.40,

69.73, 59.11, 55.81, 20.71. ^{31}P NMR ($CDCl_3$, 162 MHz): δ (ppm) = -44.09. HRMS–ESI(+): Calc. for $C_{29}H_{39}O_7P$ $[M+Na]^+$ = 551.2175, Found = 551.2362.

Preparation of Complex NiPhBr(PMe)$_2$. This synthesis was modified from a literature procedure.[83] Inside the glovebox, Ni[COD]$_2$ (1.10 g, 4 mmol, 1 equiv) and PMe_3 (1 M in THF, 10 mL, 10 mmol, 2.5 equiv) were dissolved in 50 mL of dry Et_2O. PhBr (0.94 g, 6.0 mmol, 1.5 equiv) was added and the reaction mixture was stirred at RT for 6 h. The solution was filtered to remove a black solid and the filtrate was then dried completely under vacuum. The crude material was washed with cold Et_2O (-30 ^oC, 4×4 mL) to afford a bright orange solid (1.02 g, 3.17 mmol, 79%). ^{1}H NMR (C_6D_6, 500 MHz): δ (ppm) = 7.28 (dd, J_{HH} = 7.7, 1.1 Hz, 2H), 6.91 (t, J_{HH} = 7.5 Hz, 2H), 6.75 (m, 1H), 0.78 (t, J_{HH} = 3.9 Hz, 18H). ^{31}P NMR (C_6D_6, 202 MHz): δ (ppm) = -14.78.

Preparation of Complex Ni^{t}Bu. Inside the glovebox, ligand **L64** (0.164 g, 0.4 mmol, 1.0 equiv) was dissolved in 10 mL of THF. Small aliquots of NaH (60%, 0.32 g, 0.8 mmol, 2.0 equiv) were added and the mixture was stirred at RT for 2 h. The solution was filtered to remove excess NaH and then combined with a solution of NiPhBr(PMe$_3$)$_2$ (0.122 g, 0.38 mmol, 0.95 equiv) in 5 mL of benzene. The resulting mixture was stirred at RT overnight. The precipitate formed was removed by filtration and the filtrate was dried under vacuum. The crude material was dissolved in a mixture of 15 mL of pentane and 2 mL of toluene and the solution was filtered once again before evaporating to dryness. Finally, the resulting solid was washed with pentane (3×2 mL) and dried under vacuum to afford a yellow powder (0.11 g, 0.17 mmol, 45%). ^{1}H NMR (C_6D_6, 500 MHz): δ (ppm) = 7.56 (ddd, J_{HH}

= 11.1, 7.5, 1.3 Hz, 2H), 7.23 (d, J_{HH} = 7.5 Hz, 2H), 7.14 (d, J_{HH} = 2.0 Hz, 1H), 7.04 – 6.98 (m, 2H), 6.97 – 6.92 (m, 1H), 6.71 (t, J_{HH} = 7.4 Hz, 2H), 6.63 (t, J_{HH} = 7.5 Hz, 2H), 6.58 (d, J_{HH} = 7.3 Hz, 1H), 6.38 (dd, J_{HH} = 8.1, 4.4 Hz, 2H), 2.98 (s, 6H), 2.04 (s, 3H), 1.69 (s, 9H), 0.81 (d, J_{HH} = 8.8 Hz, 9H). ^{13}C NMR (C_6D_6, 152 MHz): δ (ppm) = 174.11 (d, J_{CP} = 26.3 Hz), 160.74 (d, J_{CP} = 5.5 Hz), 150.92 (d, J_{CP} = 32.6 Hz), 137.70 (d, J_{CP} = 9 Hz), 137.09 (d, J_{CP} = 2.8 Hz), 133.99 (d, J_{CP} = 5.4 Hz), 130.85, 130.72, 130.47, 125.22, 121.86 (d, J_{CP} = 6.8 Hz), 120.47 (d, J_{CP} = 8.3 Hz), 120.29, 119.86, 118.69, 118.20, 110.66 (d, J_{CP} = 4.4 Hz), 54.88, 35.13, 29.54, 20.60, 12.47 (d, J_{CP} = 23.8 Hz). ^{31}P NMR (C_6D_6, 202 MHz): δ (ppm) = 15.08 (d, J_{PP} = 320.9 Hz), -13.64 (d, J_{PP} = 320.7 Hz). Anal. Calcd for $C_{34}H_{42}NiO_3P_2$: C, 65.94; H, 6.84. Found: 65.68; 6.99.

Preparation of Complex Ni11. Inside the glovebox, ligand **L61** (1.12 g, 2.11 mmol, 1.0 equiv) was dissolved in 50 mL of dry THF. Small aliquots of NaH (60%, 0.17g, 4.22 mmol, 2.0 equiv) were added and the mixture was stirred at RT for 2 h. The mixture was filtered to remove excess NaH and then a solution of $NiPhBr(PMe_3)_2$ (0.65 g, 2.02 mmol, 0.96 equiv) in 20 mL of benzene was added. The resulting mixture was stirred at RT overnight. The next day, the solution was filtered to remove the precipitate and the filtrate was dried completely under vacuum. The crude material was dissolved in a mixture of 40 mL of pentane and 4 mL of benzene. Another filtration was performed to remove the precipitate and the filtrate was dried once again. Finally, the resulting solid was washed with pentane (3×5 mL) and dried to under vacuum to afford a yellow powder (1.12 g, 1.51 mmol, 75%). ^{1}H NMR (C_6D_6, 500 MHz): δ (ppm) = 7.64 (m, 2H), 7.37 (d, J_{HH} = 1.7 Hz, 1H), 7.24 (d, J_{HH} = 7.7 Hz, 2H), 7.06 (dd, J_{HH} = 8.0, 4.4 Hz, 1H), 7.02 (m, 2H), 6.74 (t, J_{HH} = 7.4 Hz, 2H), 6.66 (t, J_{HH} = 7.5 Hz, 2H), 6.61 (m, 1H), 4.87 (s, 2H), 3.74 (m, 2H), 3.60 (m, 2H), 3.50 (m, 2H), 3.44 (m, 4H),

3.30 (m, 2H), 3.07 (s, 3H), 2.95 (s, 6H), 2.03 (s, 3H), 0.81 (d, 9H). ^{13}C NMR (C_6D_6, 152 MHz): δ (ppm) = 173.39 (d, J_{CP} = 26.8 Hz), 160.77 (d, J_{CP} = 4.8 Hz), 150.91 (d, J_{CP} = 29.7 Hz), 137.05, 133.93 (d, J_{CP} = 6.3 Hz), 132.86, 131.74, 131.00, 127.16 (d, J_{CP} = 9.5 Hz), 125.22, 120.46, 120.39, 120.31, 120.07, 119.71, 117.92, 117.54, 110.52 (d, J_{CP} = 3.8 Hz), 72.09, 70.99, 70.85, 70.80, 70.63, 69.89, 69.82, 58.42, 54.81, 20.45, 11.50 (d, J_{CP} = 24.7 Hz). ^{31}P NMR (C_6D_6, 202 MHz): δ (ppm) = 13.74 (J_{PP} = 319.5 Hz), -12.74 (J_{PP} = 318.1 Hz). Anal. Calcd for $C_{38}H_{52}NiO_7P_2$: C, 61.72; H, 6.82. Found: 61.63; 6.96.

Metal-Binding Studies

***UV-Vis Absorption Spectroscopy: Metal Titration*.** Stock solutions of **Ni11** and $NaBAr^F{}_4$ were prepared inside an inert nitrogen-filled glovebox. A 500 μM stock solution of **Ni11** were obtained by dissolving 25 μmol of **Ni11** in 50 mL of Et_2O. A 10 mL aliquot of this 500 μM solution was diluted to 50 mL using a volumetric flask to give a final concentration of 100 μM. The 3.0 mM stock solution of $NaBAr^F{}_4$ was obtained by dissolving 30 μmol of $NaBAr^F{}_4$ in 10 mL of Et_2O using a volumetric flask. A 3.0 mL solution of **Ni11** was transferred to a 1 cm quartz cuvette and then sealed with a septum screw cap. A 100 μL airtight syringe was loaded with the 3.0 mM solution of $NaBAr^F{}_4$. The cuvette was placed inside a UV-vis spectrophotometer and the spectrum of the **Ni11** solution was recorded. Aliquots containing 0.1 equiv of $NaBAr^F{}_4$ (10 μL), relative to the nickel complex, were added and the solution was allowed to reach equilibrium before the spectra were measured (about 20−30 min). The titration experiments were stopped after the addition of up to 1.0 equiv of $NaBAr^F{}_4$.

UV-Vis Absorption Spectroscopy: Job Plot Studies. Stock solutions of **Ni11** (500 μM) and $NaBAr^F{}_4$ (500 μM) in Et_2O were prepared in separate volumetric flasks inside the drybox. Stock solutions of **Ni11** and $NaBAr^F{}_4$ were combined in different ratios to give 10 different samples, each having a final volume of 3.0 mL. The samples were recorded by UV-vis absorption spectroscopy at RT.

The UV-vis spectral data were analyzed according to the method reported by Hirose.[68] In our case, the host (H) is **Ni11**, the guest (g) is Na^+, and the complex (C) is **Ni11**-Na. Since the sodium salt has no absorption in the 300-500 nm range, we used this simplified expression to analyze the data: $A_{obs} - \varepsilon_h \cdot [H]_t = (\varepsilon_C - a \cdot \varepsilon_h) \cdot [C]$, where A_{obs} = observed absorbance, a = constant, ε_h = molar absorptivity of host **Ni11**, ε_C = molar absorptivity of **Ni11**-Na, $[H]_t$ = starting concentration of host **Ni11**, and [C] = observed concentration of **Ni11**-Na. Since [C] is proportional to $A_{obs} - \varepsilon_h \cdot [H]_t$, a Job Plot was constructed by plotting $A_{obs} - \varepsilon_h \cdot [H]_t$ vs. χ_{Ni} (the mole ratio of **Ni11** = [**Ni11**]/([**Ni11**]+[Na^+])).

Table 2.2. Data and Calculations Used for Job Plot[a]

χ_{Ni}	**Volume of Stock Soln of H** (mL)	**Amount of H Added** (mol)	**Final Conc. of H** (M)	A_h (calculated)	A_{obs} (@330 nm)	A_{obs}-A_h
1.0	3.000E-03	1.500E-06	5.000E-04	2.663E+00	2.663E+00	-2.040E-04
0.9	2.700E-03	1.350E-06	4.500E-04	2.396E+00	2.350E+00	4.576E-02
0.8	2.400E-03	1.200E-06	4.000E-04	2.130E+00	1.966E+00	1.637E-01
0.7	2.100E-03	1.050E-06	3.500E-04	1.864E+00	1.653E+00	2.108E-01
0.6	1.800E-03	9.000E-07	3.000E-04	1.598E+00	1.308E+00	2.896E-01
0.5	1.500E-03	7.500E-07	2.500E-04	1.331E+00	1.008E+00	3.234E-01
0.4	1.200E-03	6.000E-07	2.000E-04	1.065E+00	8.275E-01	2.375E-01
0.3	9.000E-04	4.500E-07	1.500E-04	7.988E-01	6.497E-01	1.491E-01
0.2	6.000E-04	3.000E-07	1.000E-04	5.325E-01	4.393E-01	9.315E-02
0.1	3.000E-04	1.500E-07	5.000E-05	2.663E-01	2.714E-01	-5.174E-03

[a]The molar absorptivity of H (ε_h) at 330 nm = 5325 $M^{-1}cm^{-1}$. Stock solution of H is 500 µM.

Polymerization Studies

General Procedure for Ethylene Polymerization.

Inside the drybox, the Ni complex **Ni11** (0.5 μmol) and $NaBAr^F{}_4$ (1 μmol) were dissolved in 10 mL of toluene in a 20 mL vial and stirred for 10 min. Solid $Ni(COD)_2$ (4 μmol) was added and stirred until a clear solution was obtained (4–5 min). The mixture was loaded into a 10 mL syringe equipped with an 8-inch stainless steel needle. The loaded syringe was sealed by sticking the needle tip into a rubber septum and brought outside of the drybox. To prepare the polymerization reactor, 90 mL of dry Ar-saturated toluene was placed in an empty autoclave. The autoclave was pressurized with ethylene to 80 psi, stirred for 5 min, and then the reactor pressure was reduced to 5 psi. This process was repeated three times to remove trace amounts of oxygen inside the reaction vessel. The reactor was then heated to the desired temperature and the catalyst solution was injected into the autoclave through a side arm. The autoclave was sealed and purged with ethylene at 40 psi (no stirring) three times. Finally, the reactor pressure was increased to the desired pressure, and the contents were stirred vigorously. To stop the polymerization, the autoclave was vented and cooled in an ice bath. A solution of MeOH (600 mL) was added to precipitate the polymer. The polymer was collected by vacuum filtration, rinsed with MeOH, and dried under vacuum at 80 °C overnight. The reported yields are average values obtained from duplicate or triplicate runs.

Special Notes:

- To obtain consistent polymer yields from run to run, the amount of catalyst used in each run must be kept as consistent as possible. Since 0.5 μmol of the **Ni11** catalyst weighs only 0.37 mg, it is extremely difficult to weigh out exactly this amount using a standard analytical balance.

To minimize errors due to weighing inconsistencies, we used a batch catalyst preparation method. First, we weighed out 37 mg (50 µmol) of the catalyst and then dissolved it into 50 mL of toluene. This solution was divided equally into 10 vials so that each vial contained 5 µmol of catalyst. Next, we combined each 5 µmol of catalyst with 20 mL of toluene and partitioned this 25 mL mixture into 10 vials so that each vial contained 0.5 µmol of catalyst. Finally, each vial was dried completely under vacuum and stored in a refrigerator inside the drybox until ready for use.

- For all polymerization reactions, except ones that were performed to determine the temperature profiles, the reaction temperature was controlled by manual cooling of the reactor with an air stream when the reactor increases more than 5°C above the starting temperature.
- To clean the Parr reactor, the vessel was washed with hot toluene (80 ^{o}C) to remove the polymer sample from the previous run and rinsed with acetone before drying under vacuum for at least 1 h to remove trace amounts of water.

Table 2.3. Comparison of Nickel Catalyst Activity[a]

Catalyst	Yield (g)				Activity (kg PE/mol Ni·h)
	Run 1	Run 2	Run 3	Average	
Ni10	0.89	1.22	-	1.06	2120
Ni10/NaBAr$^F{}_4$	1.17	0.72	-	0.94	1880
Ni11	0	0	0	0	0
Ni11/NaBAr$^F{}_4$	8.95	8.85	9.41	9.07	18100

[a]Polymerization conditions: Ni catalyst (0.5 µmol), NaBAr$^F{}_4$ (1 µmol, if any), Ni(COD)$_2$ (4 µmol), 100 mL toluene, 450 psi ethylene, 30 °C for 1 h.

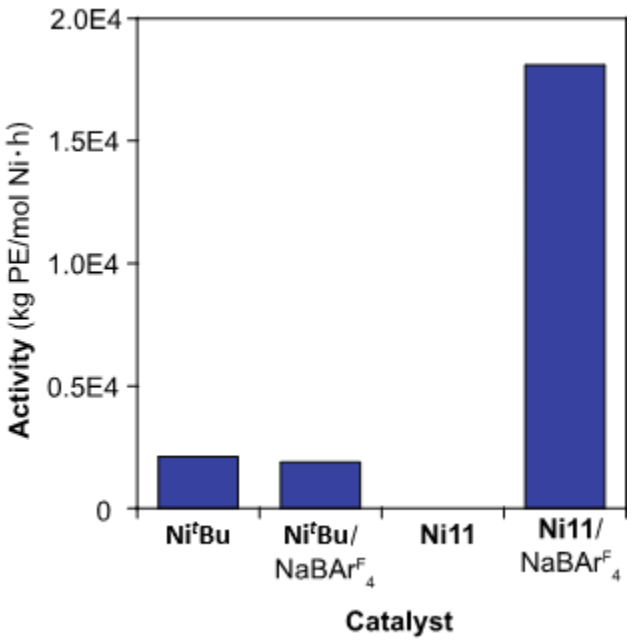

Figure 2.7. Comparison of catalyst activity between **Ni^{t}Bu** and **Ni11** with and without the addition of NaBAr$^F{}_4$. Full data shown in Table 2.3.

Table 2.4. Pressure Study of Ethylene Polymerization by **Ni11**-Na[a]

Pressure (psi)	**Yield** (g)				**Activity** (kg PE/mol Ni·h)
	Run 1	Run 2	Run 3	Average	
150	2.34	1.81	1.52	1.89	3780
300	4.77	4.86	3.62	4.42	8840
450	4.59	5.72	5.91	5.41	10800

[a]Polymerization conditions: Ni catalyst (0.5 μmol), $NaBAr^F{}_4$ (1 μmol), $Ni(COD)_2$ (4 μmol), 100 mL toluene, 20°C for 1 h at various ethylene pressures. Temperature controlled by manual external cooling when necessary.

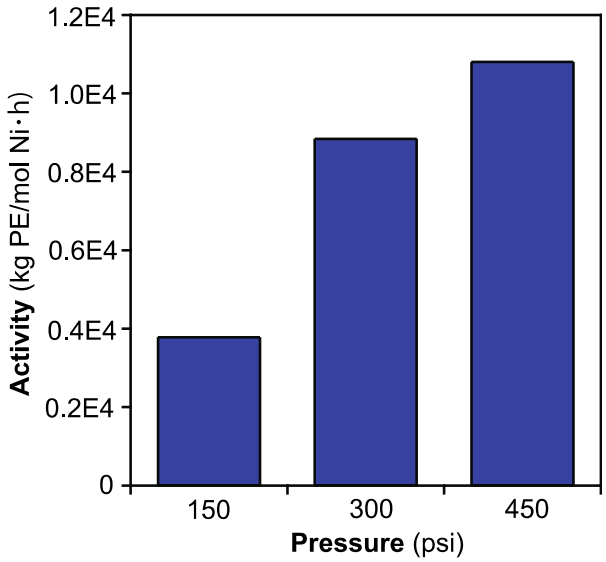

Figure 2.8. Activity vs. pressure plot of catalyst **Ni11**-Na in ethylene polymerization at 450 psi. The highest activity was observed at 450 psi. Full data shown in Table 2.4.

Table 2.5. Time Study of Ethylene Polymerization by **Ni11**-Na at 150 psi[a]

Time	**Yield** (g)				**Activity** (kg PE/mol Ni·h)	M_n[b] ($\times 10^3$)	M_w/M_n[b]
	Run 1	Run 2	Run 3	Average			
0.25 h	0.425	0.418	0.356	0.400	3200	1420	1.4
1 h	2.34	1.81	1.52	1.89	3780	1590	1.4
2 h	3.08	3.75	3.19	3.34	3340	1550	1.5
3 h	4.21	3.63	5.45	4.43	2950	1580	1.4

[a]Polymerization conditions: Ni catalyst (0.5 μmol), $NaBAr^F{}_4$ (1 μmol), $Ni(COD)_2$ (4 μmol), 100 mL toluene, 150 psi ethylene, 20°C for various times as indicated. Temperature controlled by manual external cooling when necessary. [b]Determined by GPC in trichlorobenzene at 150 °C.

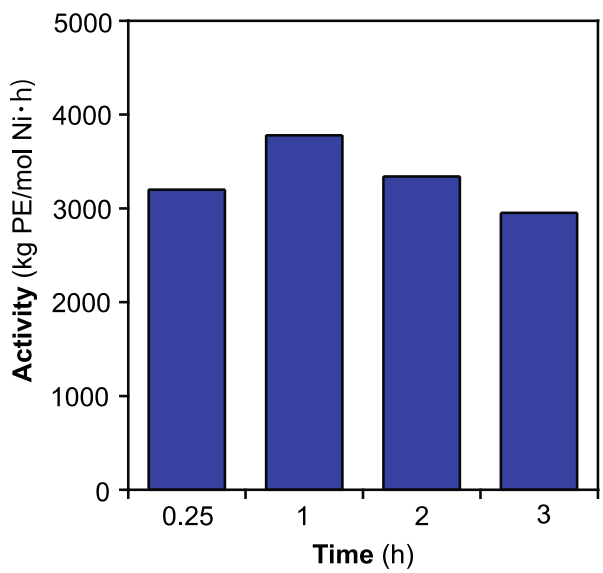

Figure 2.9. Activity vs. time plot of catalyst **Ni11**-Na in ethylene polymerization at 150 psi. The activity remained relatively constant over a 3 h time course. Full data shown in Table 2.5.

Table 2.6. Time Study of Ethylene Polymerization by **Ni11**-Na at Optimal Reaction Conditions[a]

Time	**Yield** (g)				**Activity** (kg PE/mol Ni·h)
	Run 1	Run 2	Run 3	Average	
0.5 h	6.92	5.71	-	6.32	25300
1 h	8.95	8.85	9.41	9.07	18100
2 h	14.37	15.80	-	15.08	15080

[a]Polymerization conditions: Ni catalyst (0.5 μmol), $NaBAr^F{}_4$ (1 μmol), $Ni(COD)_2$ (4 μmol), 100 mL toluene, 450 psi ethylene at 30 °C for various times as indicated. Temperature controlled by manual external cooling when necessary.

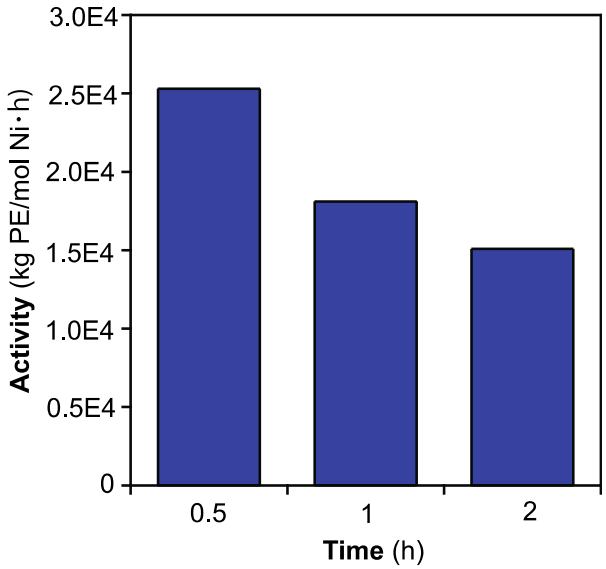

Figure 2.10. Activity vs. time plot of catalyst **Ni11**-Na in ethylene polymerization under optimal reaction conditions. The activity decreased gradually over the 2 h time course. Full data shown in Table 2.6.

Table 2.7. Temperature Study of Ethylene Polymerization by **Ni11**-Na at 150 psi[a]

Temperature (°C)	**Yield** (g)				**Activity** (kg PE/mol Ni ·h)	M_n[b] ($\times 10^3$)	M_w/M_n[b]
	Run 1	Run 2	Run 3	Average			
RT	2.34	1.81	1.52	1.89	3780	1590	1.4
30	4.06	4.14	2.86	3.69	7380	1400	1.3
40	3.81	3.63	4.26	3.90	7800	1380	1.4
50	4.27	5.24	4.21	4.57	9140	850	1.6
60	2.52	3.86	3.14	3.17	6340	830	1.7

[a]Polymerization conditions: Ni catalyst (0.5 µmol), $NaBAr^F{}_4$ (1 µmol), $Ni(COD)_2$ (4 µmol), 100 mL toluene, 150 psi ethylene, 1 h at various temperatures. Temperature controlled by manual external cooling when necessary. [b]Determined by GPC in trichlorobenzene at 150 °C.

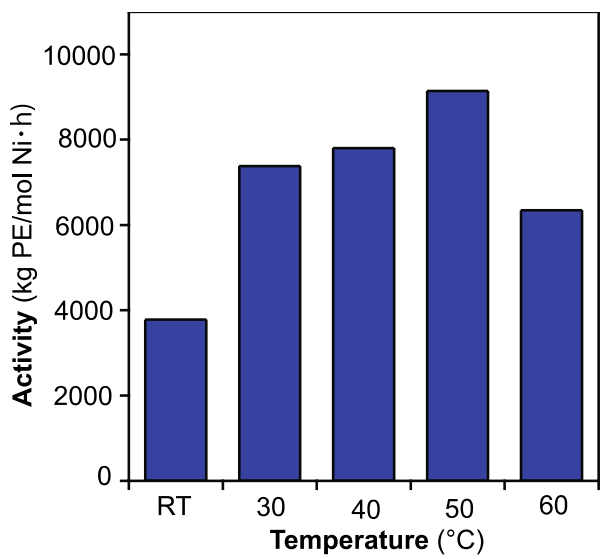

Figure 2.11. Activity vs. temperature plot of catalyst **Ni11**-Na in ethylene polymerization at 150 psi. The activity was optimal at ~50 °C. Full data shown in Table 2.7.

Table 2.8. Temperature Study of Ethylene Polymerization by **Ni11**-Na at 450 psi[a]

Temperature (°C)	**Yield** (g)				**Activity** (kg PE/mol Ni ·h)	M_n[b] ($\times 10^3$)	M_w/M_n[b]
	Run 1	Run 2	Run 3	Average			
RT	4.59	5.72	5.91	5.41	10800	1550	1.4
30	9.41	8.95	8.85	9.07	18100	1710	1.5
40	6.89	6.64	8.51	7.35	14700	1210	1.5
50	6.32	6.29	6.96	6.52	13000	1260	1.4
60	4.91	4.63	4.53	4.69	9380	1090	1.2

[a]Polymerization conditions: Ni catalyst (0.5 µmol), $NaBAr^F{}_4$ (1 µmol), $Ni(COD)_2$ (4 µmol), 100 mL toluene, 450 psi ethylene, 1 h at various temperatures. Temperature controlled by manual external cooling when necessary. [b]Determined by GPC in trichlorobenzene at 150 °C.

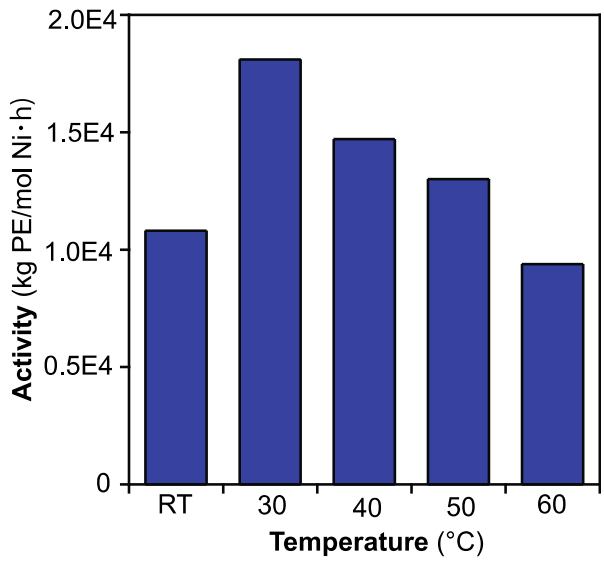

Figure 2.12. Activity vs. temperature plot of catalyst **Ni11**-Na in ethylene polymerization at 450 psi. The activity was optimal at ~30 °C. Full data shown in Table 2.8.

Table 2.9. Time-Dependent Catalyst Activity of **Ni11**-Na (100 μM)[a]

Time (min)	**Temperature** (°C)	**Yield** (g)			**Activity** (kg PE/mol Ni·h)
		Run 1	Run 2	Average	
4	159	10.80	9.90	10.35	31050
60	29	10.97	11.70	11.34	2268

[a]Polymerization conditions: Ni catalyst (5.0 μmol), $NaBAr^F{}_4$ (10.0 μmol), $Ni(COD)_2$ (20.0 μmol), 50 mL toluene, 450 psi ethylene, start reaction at 20 °C. Temperature *was not* controlled by manual external cooling.

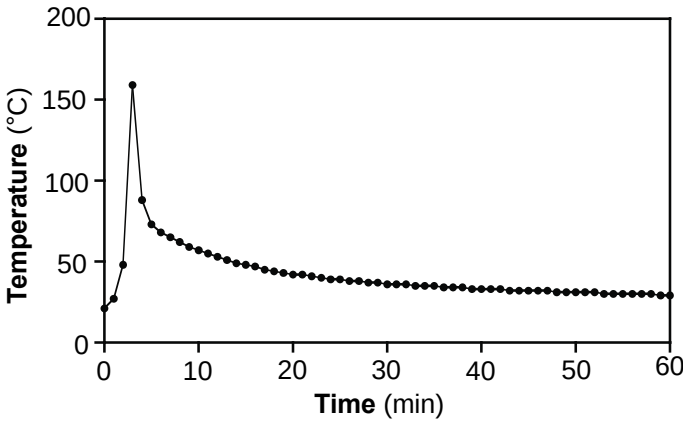

Figure 2.13. Temperature profile of ethylene polymerization (450 psi) by **Ni11**-Na (100 μM) over the course of 1 h. The temperature values represent the internal reactor temperatures and were recorded manually by reading the digital temperature gauge.

Table 2.10. Time-Dependent Catalyst Activity of **Ni11**-Na (50 μM)[a]

Time (min)	**Temperature** (°C)	**Yield** (g)			**Activity** (kg PE/mol Ni·h)
		Run 1	Run 2	Average	
4	60	5.60	6.30	5.95	17800
5	122	11.70	13.30	12.50	30000
5.5	110	13.70	14.90	14.30	31200
7	98	18.90	21.50	20.20	34630
60	35	20.70	18.80	19.75	3950

[a]Polymerization conditions: Ni catalyst (5.0 μmol), $NaBAr^F{}_4$ (10.0 μmol), $Ni(COD)_2$ (20.0 μmol), 100 mL toluene, 450 psi ethylene, start reaction at 20 °C. Temperature *was not* controlled by manual external cooling.

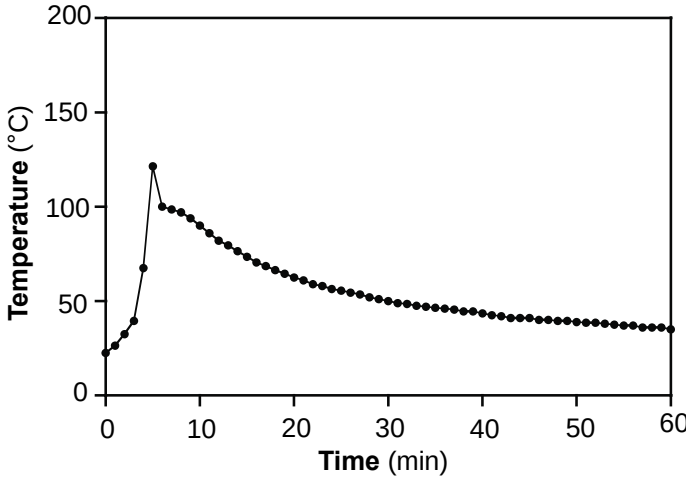

Figure 2.14. Temperature profile of ethylene polymerization (450 psi) by **Ni11**-Na (50 μM) over the course of 1 h. The temperature values represent the internal reactor temperatures and were recorded manually by reading the digital temperature gauge.

Table 2.11. Comparison of Nickel Ethylene Polymerization Catalysts Reported in the Literature

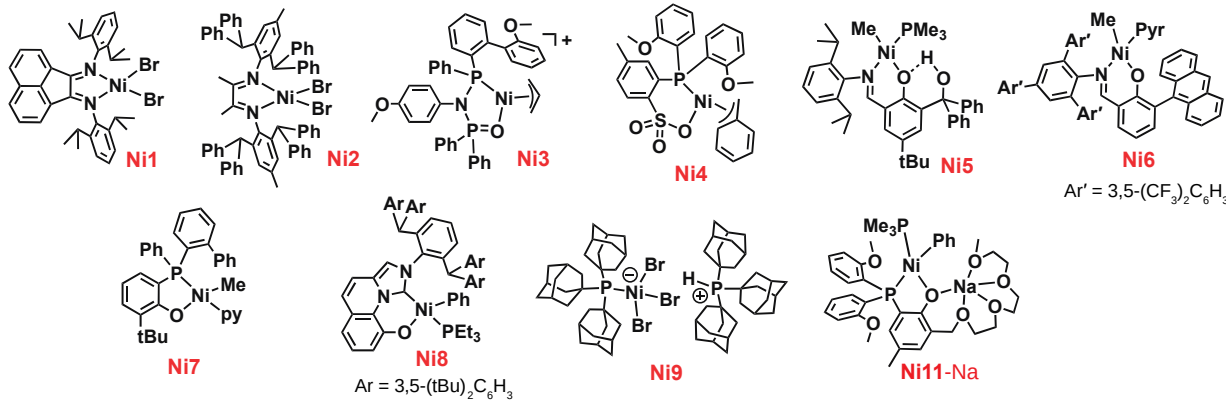

Complex (conc.)	C_2H_4 Press. (psi)	Temp. (°C)	Time (min)	Activity (kg PE/mol Ni·h)	TON ($\times 10^3$ mol ethylene/ mol Ni)	M_n	$\frac{M_n}{M_w}$	Reference (Compound name in original reference)
Ni1 (0.83 μmol/200 mL)	200	35	10	67200	400	337000	1.8	Brookhart (**4g**)[70]
Ni2 (1.57 μmol/100 mL)	100	100	10	2856	17	422000	1.2	Long (**2b**)[71]
Ni3 (5.00 μmol/20 mL)	118	25	60	260	9	188900	2.5	Chen (**Ni4**)[72]
Ni4 (20.0 μmol/30 mL)	300	25	120	163	12	1500	–	Jordan (**4a**)[73]
Ni5 (10.0 μmol/25 mL)	118	25	40	1184	28	6700	1.8	Marks (**1b**)[74]
Ni6 (5.00 μmol/100 mL)	580	30	40	1218	29	466100	1.6	Mecking (**2-CF3/Py**)[84]
Ni7 (5.00 μmol/100 mL)	145	30	20	2100	25	398000	1.5	Li (**2c**)[69]
Ni8 (2.5 μmol/8.5 mL)	580	30	30	1000	18	84000	2.0	Nozaki (**7c**)[85]
Ni9 (0.50 μmol/150 mL)	400	10	3.5	103600	216	1390000	1.4	Daugulis/Brookhart (**6**)[77]
Ni11-Na (0.50 μmol/100 mL)	450	30	60	18100	646	1710	1.5	This work

2.7. Crystallographic Data

X-ray Data Collection and Refinement

Single crystals suitable for X-ray diffraction studies were picked out of the crystallization vials and mounted onto Mitogen loops using Paratone oil. The crystals were collected at a 6.0 cm detector distance at –150 °C on a Brucker Apex II diffractometer using Mo Kα radiation (λ = 0.71073 Å). The structures were solved by direct methods using the program SHELXT and refined by SHELXLE. Hydrogen atoms connected to carbon were placed at idealized positions using standard riding models and refined isotropically. All non-hydrogen atoms were refined anisoptriocally.

Crystals of complex **Ni^{t}Bu** were grown by layering of pentane into a solution of the complex in toluene at -30 ^{o}C. The three methyl carbons (C32-C34) attached to the phosphine atom were refined in two parts due to positional disorder. The solvent molecule pentane was refined successfully without the use of any structural restraints.

Crystals of complex **Ni11** were grown by layering of pentane into a solution of the complex and $NaBAr^F{}_4$ in a mixture of toluene and Et_2O at -30 ^{o}C. The fluorine atoms attached to carbons C54, C61, and C69 were refined using positional disorder due to free rotation of the CF_3 groups.

Table 2.12. Crystal Data and Structure Refinement for **Ni^{t}Bu** and **Ni11**-Na

	Ni^{t}Bu·C_5H_{12}	**Ni11**-Na
Empirical Formula	$NiC_{34}H_{42}O_3P_2 \cdot C_5H_{12}$	$NiNaC_{38}H_{30}O_7P_2$ ($BC_{32}H_{12}F_{24}$)
Formula Weight	691.47	1625.64
Temperature (°C)	-150	-150
Wavelength (Å)	0.71073	0.71073
Crystal System	Triclinic	Monoclinic
Space Group	P_{-1}	$P2_1/c$
Unit Cell Dimensions		
a (Å)	11.0922(13)	21.7805(17)
b (Å)	11.6999(14)	17.3222(14)
c (Å)	15.9470(19)	19.7901(16)
α (°)	72.2620(10)	90
β (°)	71.2670(10)	102.5400(10)
γ (°)	81.6330(10)	90
Volume (Å^3)	1864.1(4)	7288.4(10)
Z, Calculated Density (Mg/m^3)	2, 1.232	4, 1.481
Absorption Coefficient (mm^{-1})	0.640	0.429
F(000)	740	3312
Theta Range for Data Collection (°)	1.403 to 25.027	1.516 to 27.554
Limiting Indices	$-13 \leq h \leq 10$	$-23 \leq h \leq 28$
	$-13 \leq k \leq 13$	$-24 \leq k \leq 22$
	$-18 \leq l \leq 18$	$-25 \leq l \leq 25$
Reflections Collected/ Unique	9114/ 6404	43028/16670
	[R(int) = 0.0106]	[R(int) = 0.0181]
Data/ Restraints/ Parameters	6404 / 30 / 418	16670 / 57 / 944
Goodness of Fit on F^2	1.085	1.053
Final R Indices	R_1= 0.0466	R_1= 0.0666
[I > 2σ(I)]	wR_2 = 0.1590	wR_2 = 0.1861
R Indices (All Data)*	R_1 = 0.0556	R_1 = 0.0779
	wR_2 = 0.2051	wR_2 = 0.2007
Largest Diff. Peak and Hole (e Å^{-3})	1.339 and -0.821	1.893 and -1.533

*$R_1 = \Sigma\, ||F_o|-|F_o||/\Sigma|F_o|$; $wR_2 = [\Sigma[w(F_o^2 - F_c^2)^2]/\Sigma[w(F_o^2)_2]]^{1/2}$; $GOF = [\Sigma[w(F_o^2 - F_c^2)_2]/(n-p)]^{1/2}$, where *n* is the number of reflections and *p* is the total number of parameters refined

2.8. Spectral Characterization

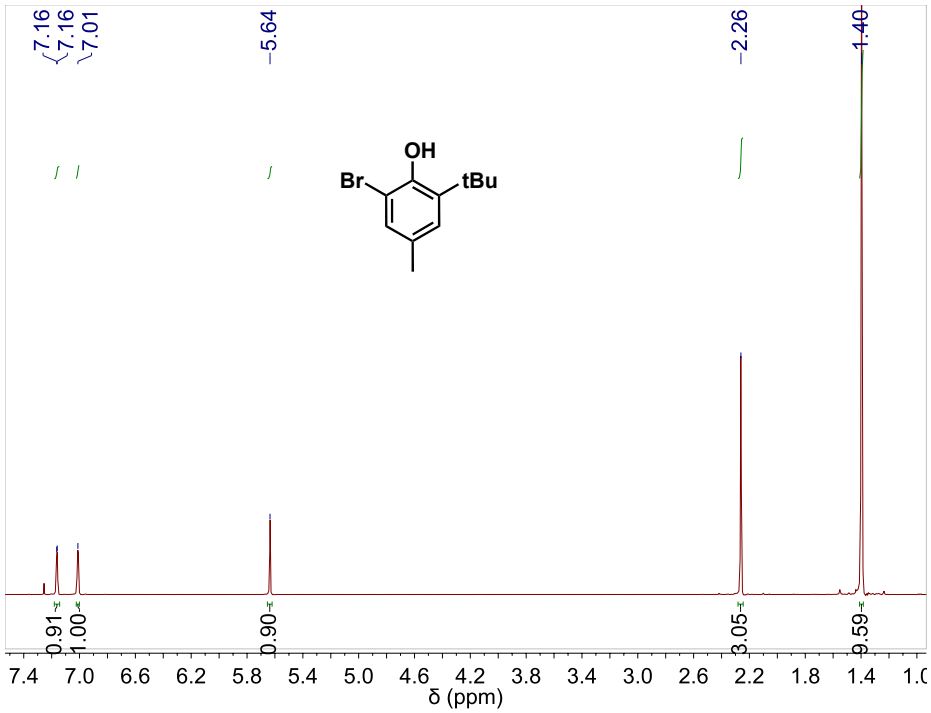

Figure 2.15. ^{1}H NMR spectrum ($CDCl_3$, 400 MHz) of compound **66**.

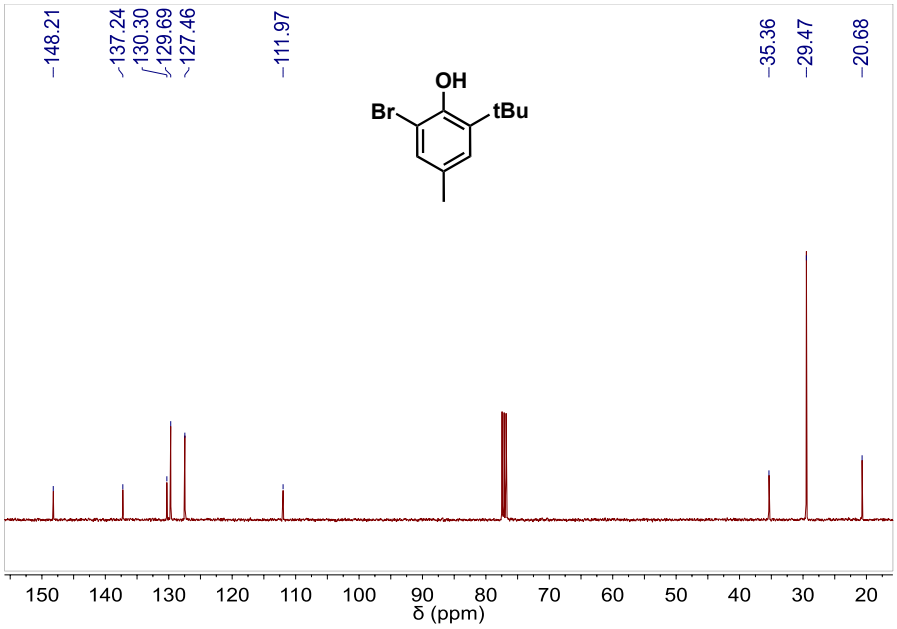

Figure 2.16. ^{13}C NMR spectrum ($CDCl_3$, 101 MHz) of compound **66**.

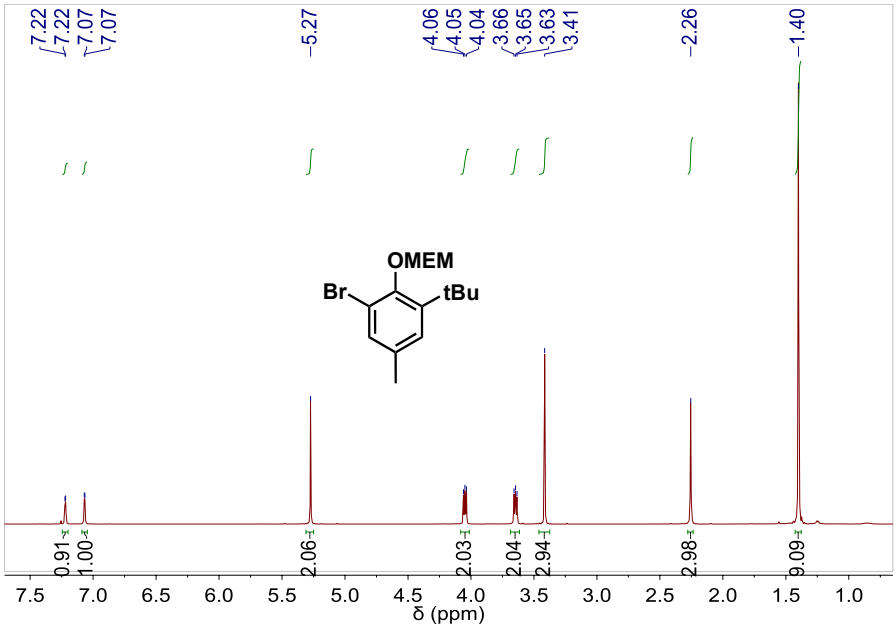

Figure 2.17. ^{1}H NMR spectrum ($CDCl_3$, 400 MHz) of compound **67**.

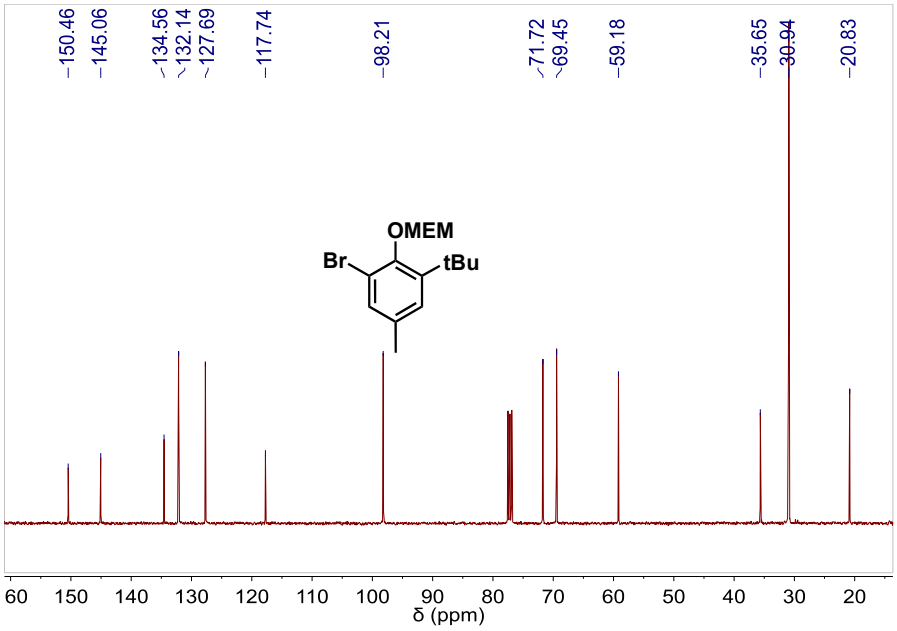

Figure 2.18. ^{13}C NMR spectrum ($CDCl_3$, 101 MHz) of compound **67**.

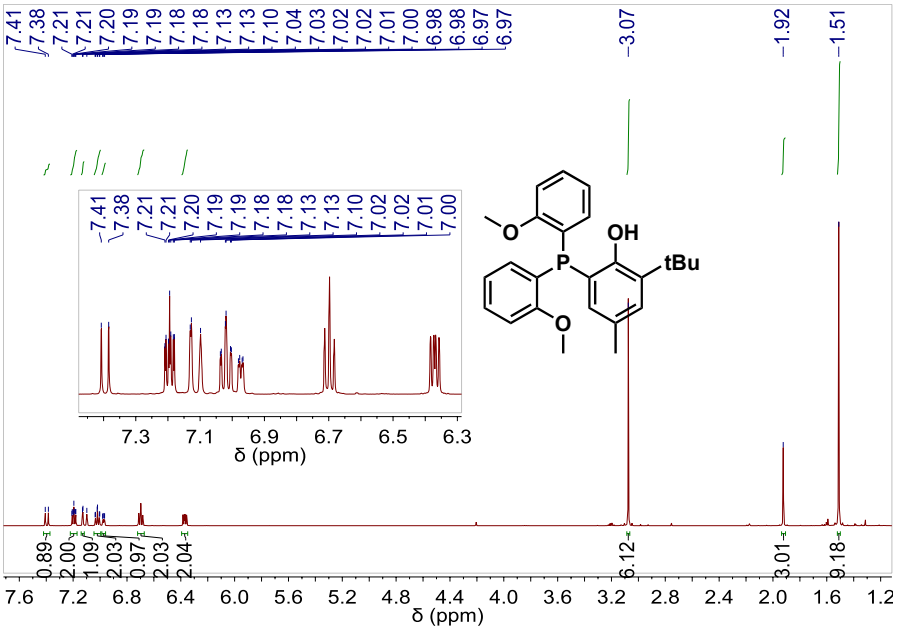

Figure 2.19. ^{1}H NMR spectrum ($CDCl_3$, 500 MHz) of compound **L64**.

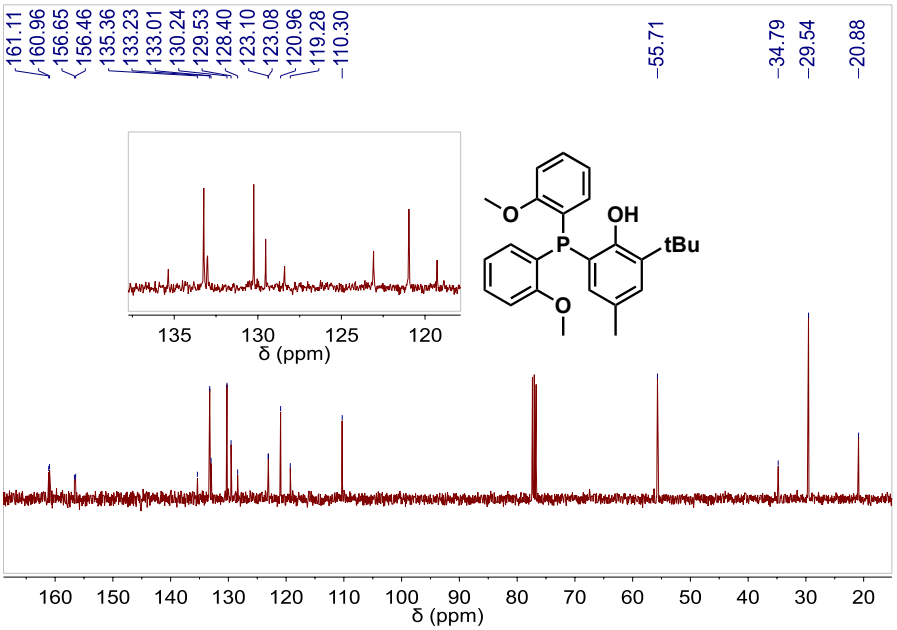

Figure 2.20. ^{13}C NMR spectrum ($CDCl_3$, 101 MHz) of compound **L64**.

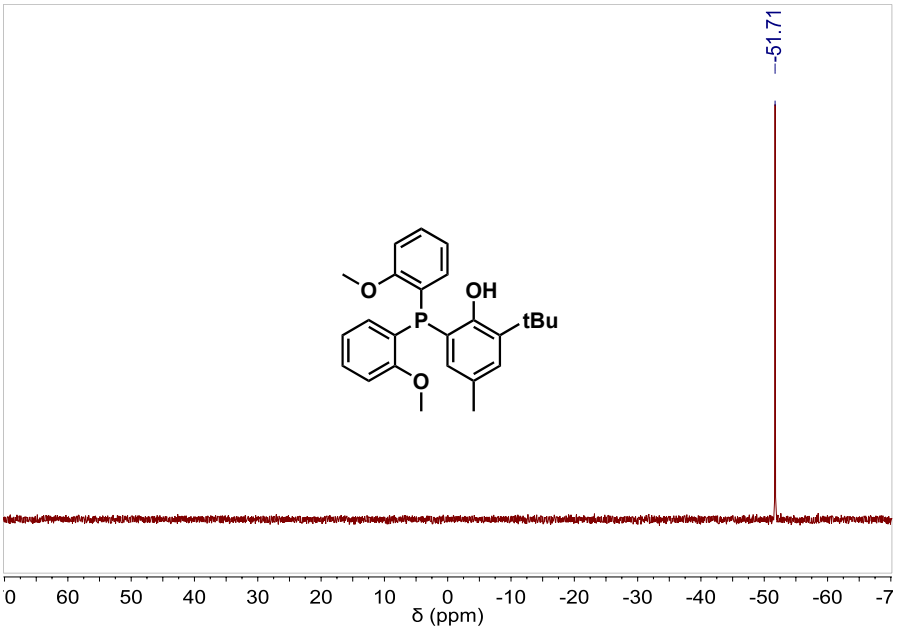

Figure 2.21. ^{31}P NMR spectrum ($CDCl_3$, 202 MHz) of compound **L64**.

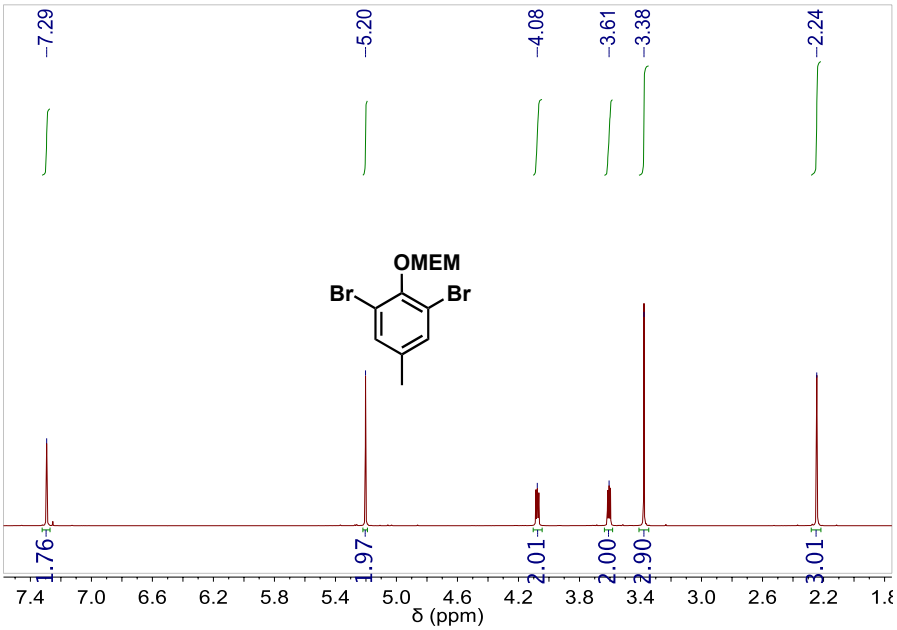

Figure 2.22. ^{1}H NMR spectrum ($CDCl_3$, 500 MHz) of compound **56**.

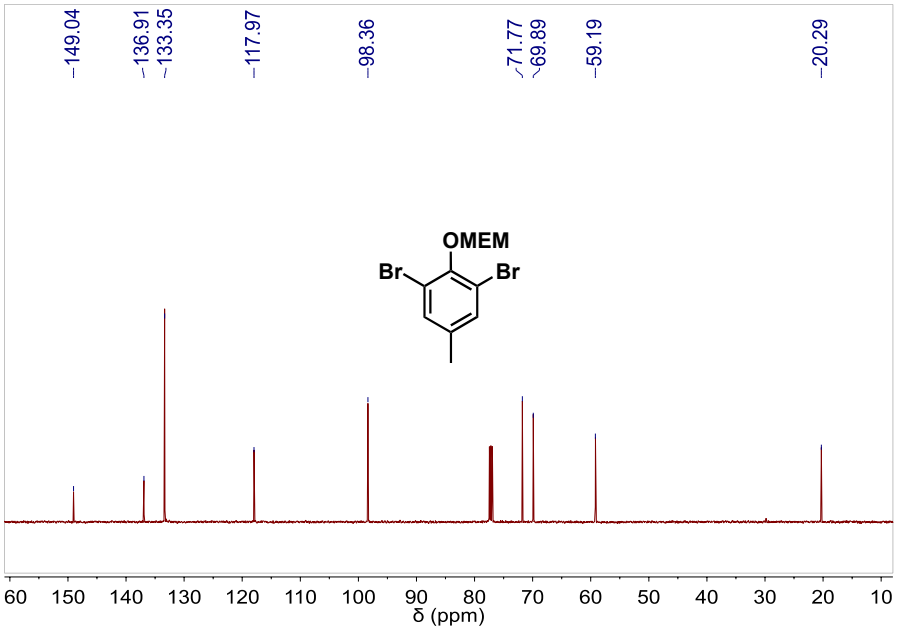

Figure 2.23. ^{13}C NMR spectrum ($CDCl_3$, 126 MHz) of compound **56**.

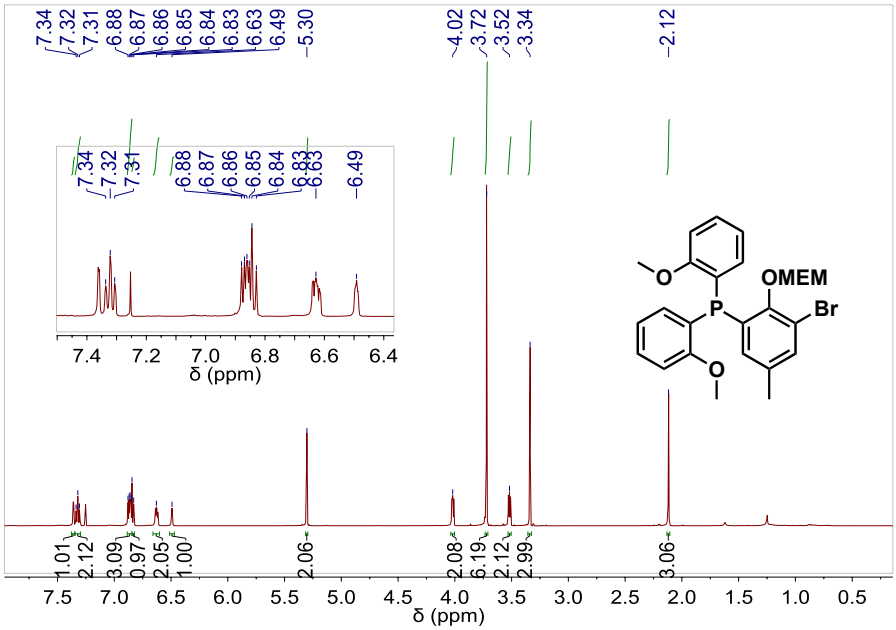

Figure 2.24. ^{1}H NMR spectrum ($CDCl_3$, 500 MHz) of compound **57**.

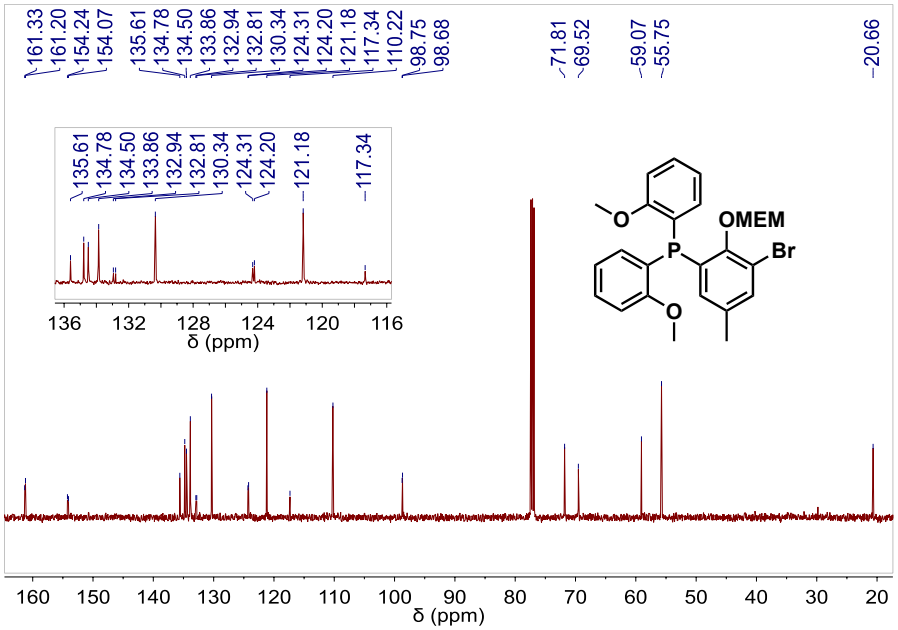

Figure 2.25. ^{13}C NMR spectrum ($CDCl_3$, 126 MHz) of compound **57**.

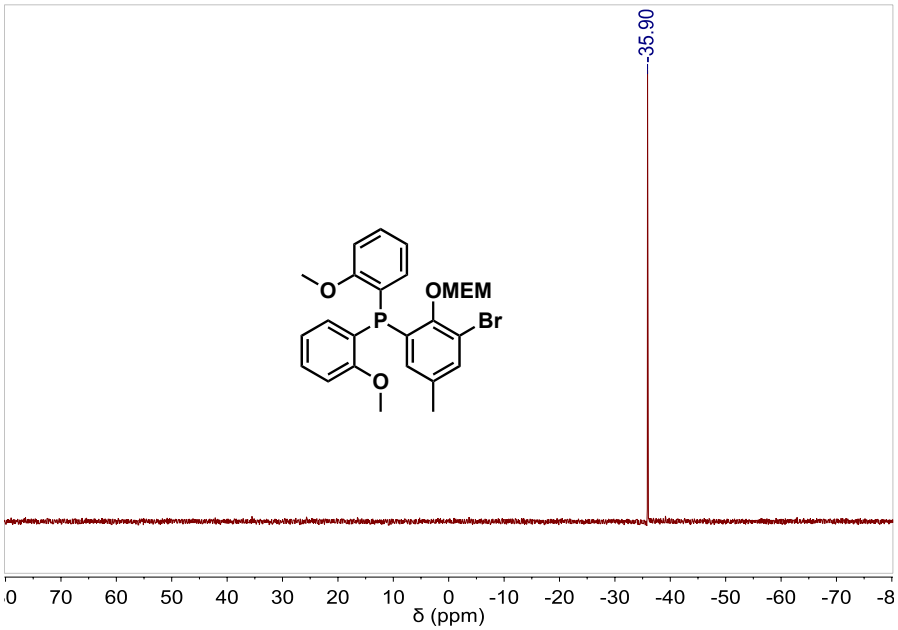

Figure 2.26. ^{31}P NMR spectrum ($CDCl_3$, 202 MHz) of compound **57**.

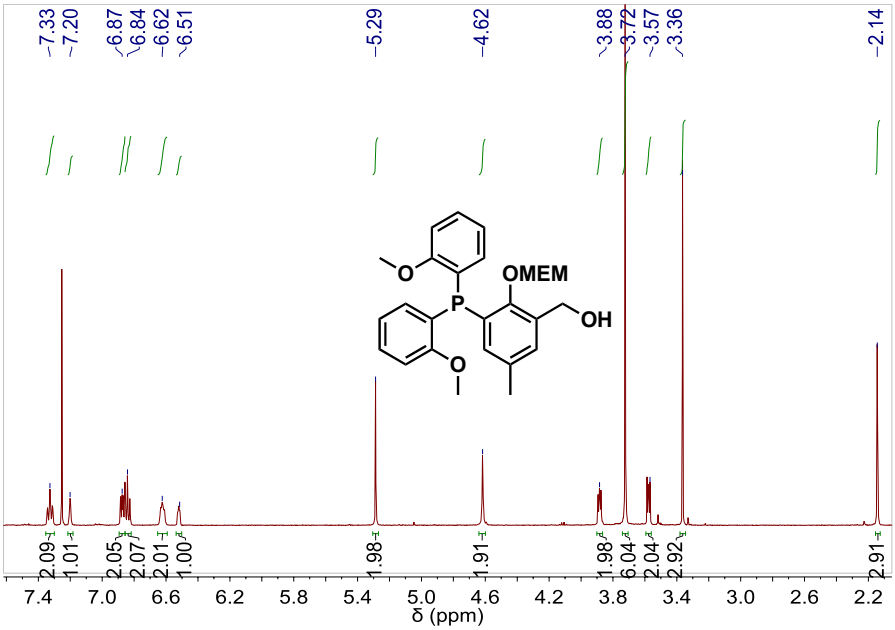

Figure 2.27. ^{1}H NMR spectrum ($CDCl_3$, 500 MHz) of compound **59**.

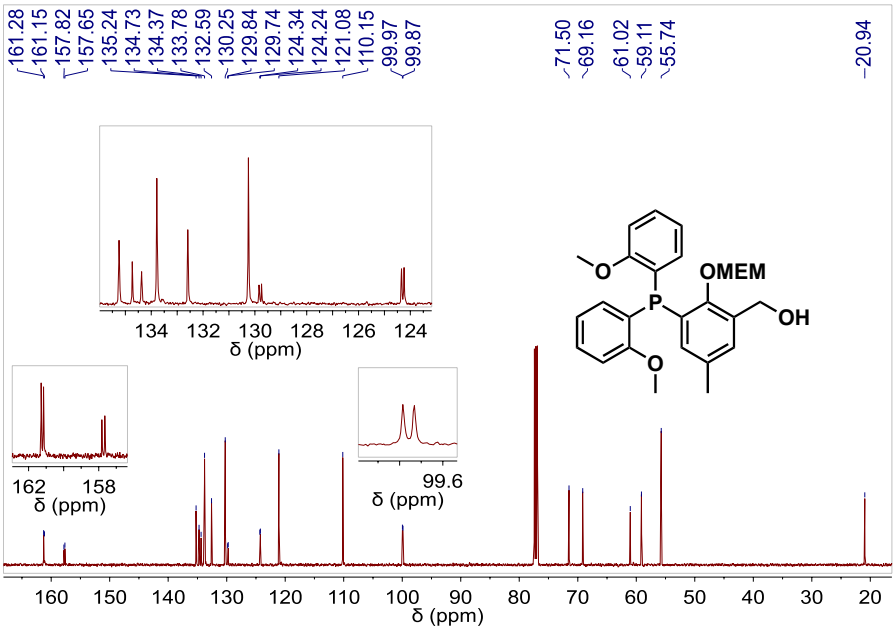

Figure 2.28. ^{13}C NMR spectrum ($CDCl_3$, 126 MHz) of compound **59**.

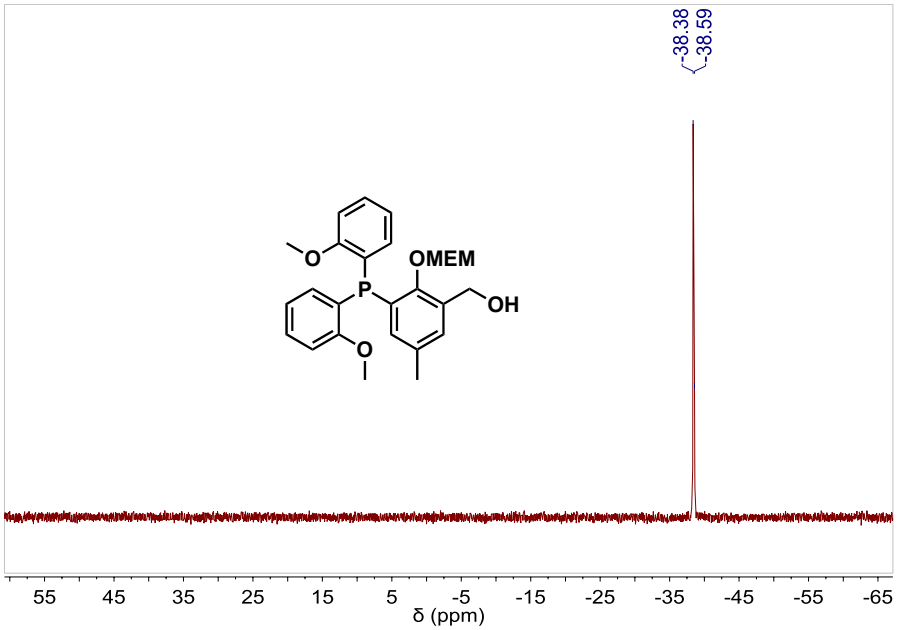

Figure 2.29. ^{31}P NMR spectrum ($CDCl_3$, 202 MHz) of compound **59**.

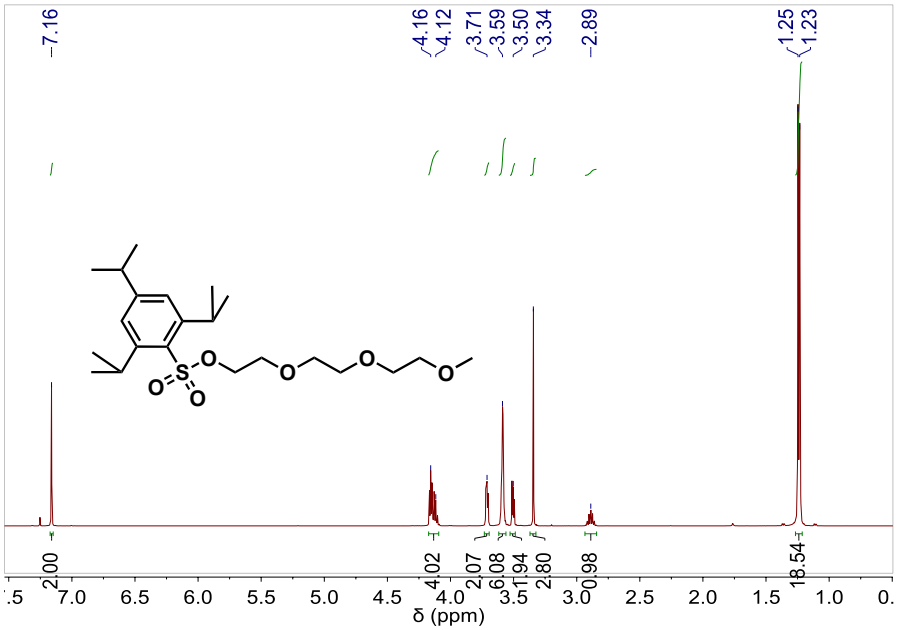

Figure 2.30. ^{1}H NMR spectrum ($CDCl_3$, 500 MHz) of compound **63**

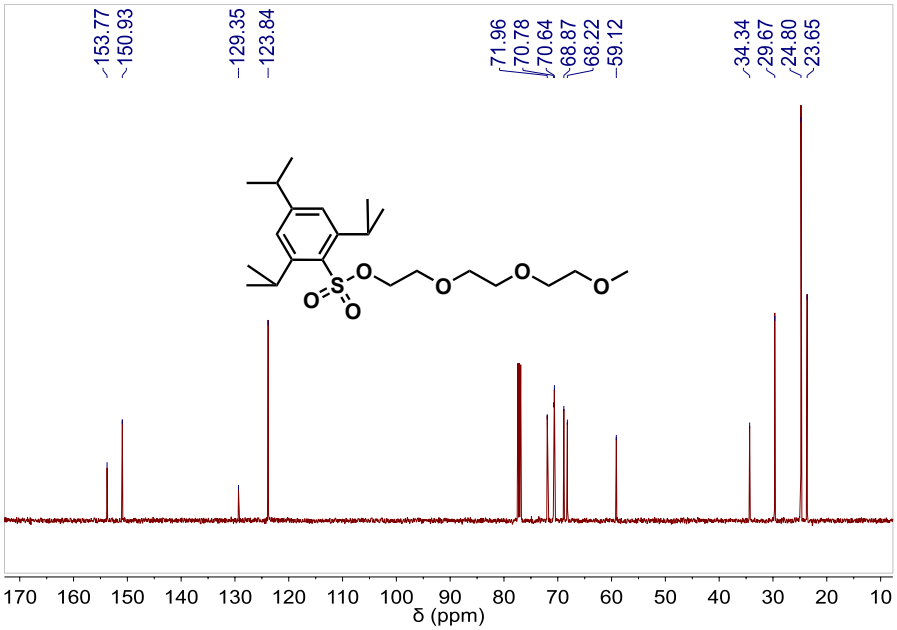

Figure 2.31. ^{13}C NMR spectrum ($CDCl_3$, 126 MHz) of compound **63**.

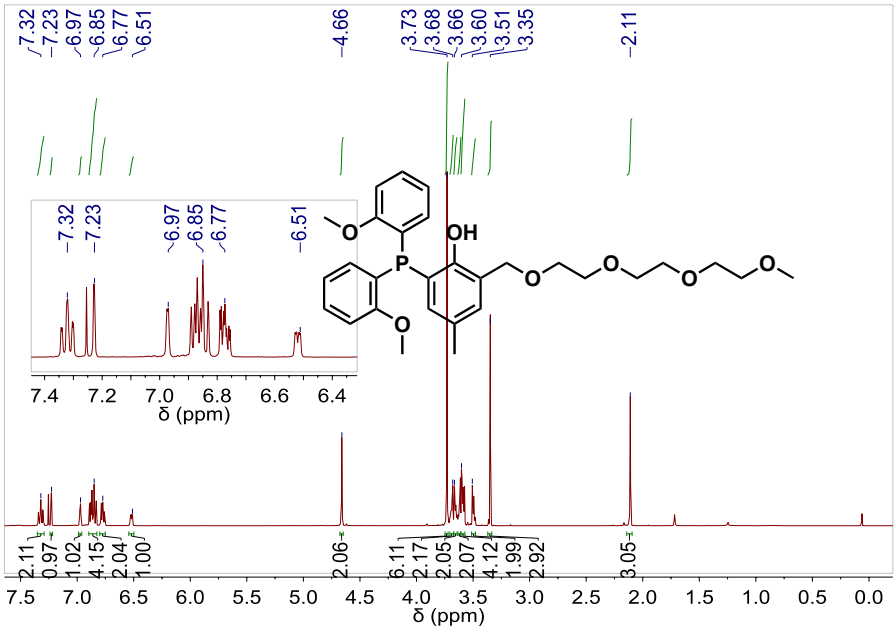

Figure 2.32. ^{1}H NMR spectrum ($CDCl_3$, 126 MHz) of compound **L61**.

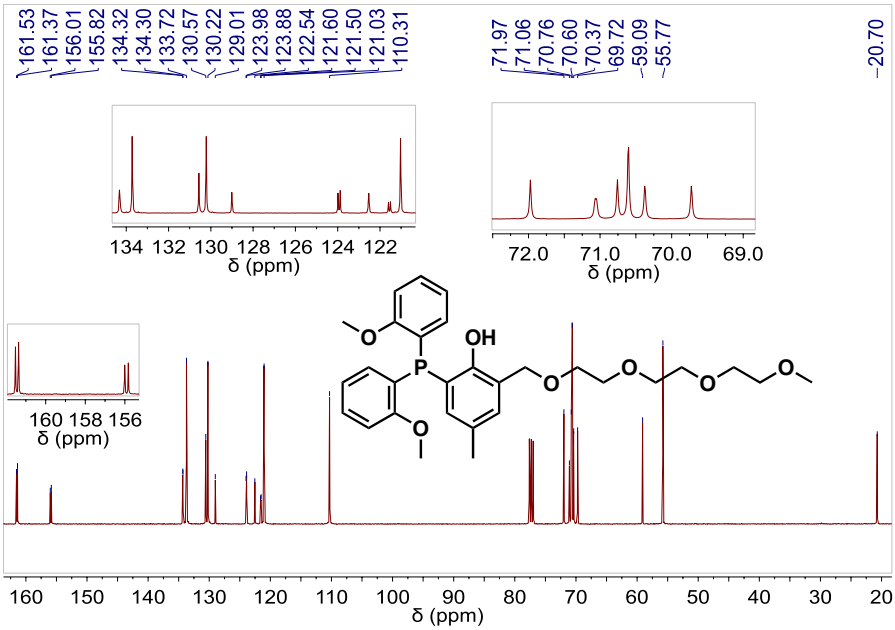

Figure 2.33. ^{13}C NMR spectrum ($CDCl_3$, 126 MHz) of compound **L61**.

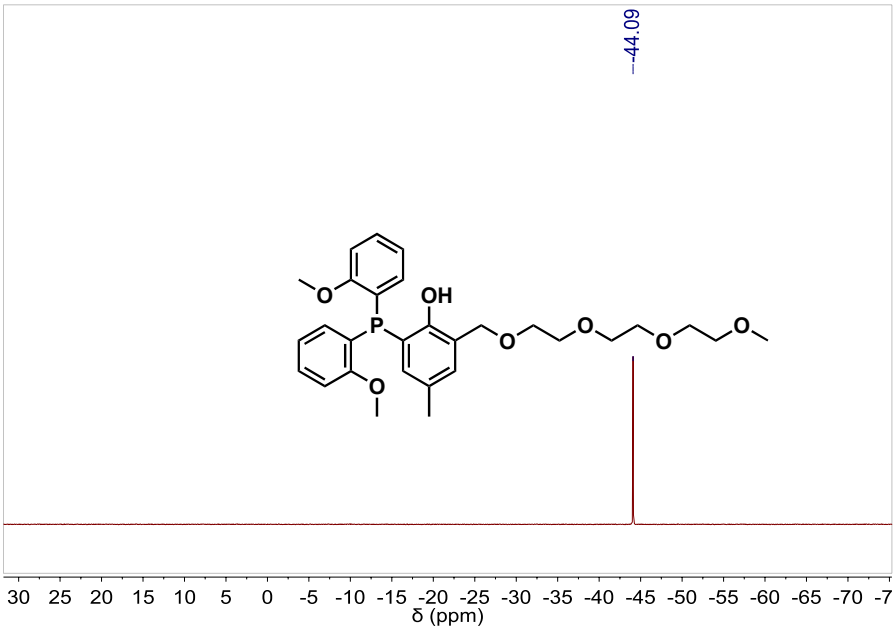

Figure 2.34. ^{31}P NMR spectrum ($CDCl_3$, 162 MHz) of compound **L61**.

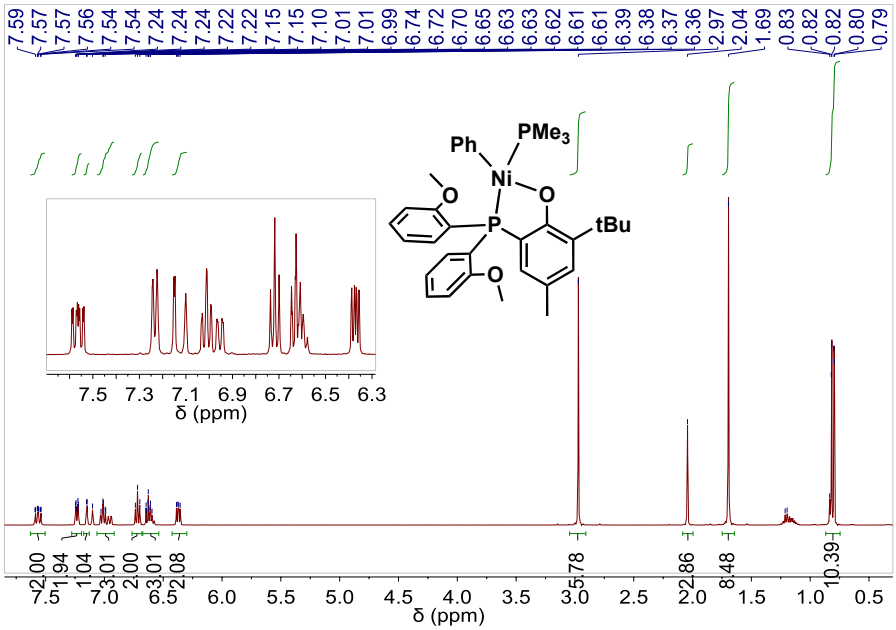

Figure 2.35. ^{1}H NMR spectrum (C_6D_6, 400 MHz) of complex **Ni^{t}Bu**.

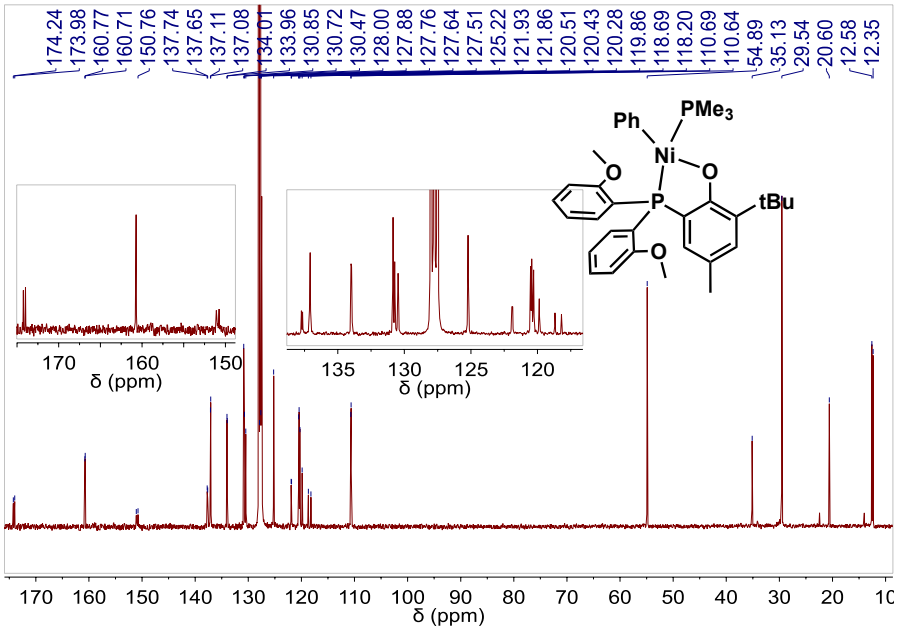

Figure 2.36. ^{13}C NMR spectrum (C_6D_6, 100 MHz) of complex **Ni^{t}Bu**.

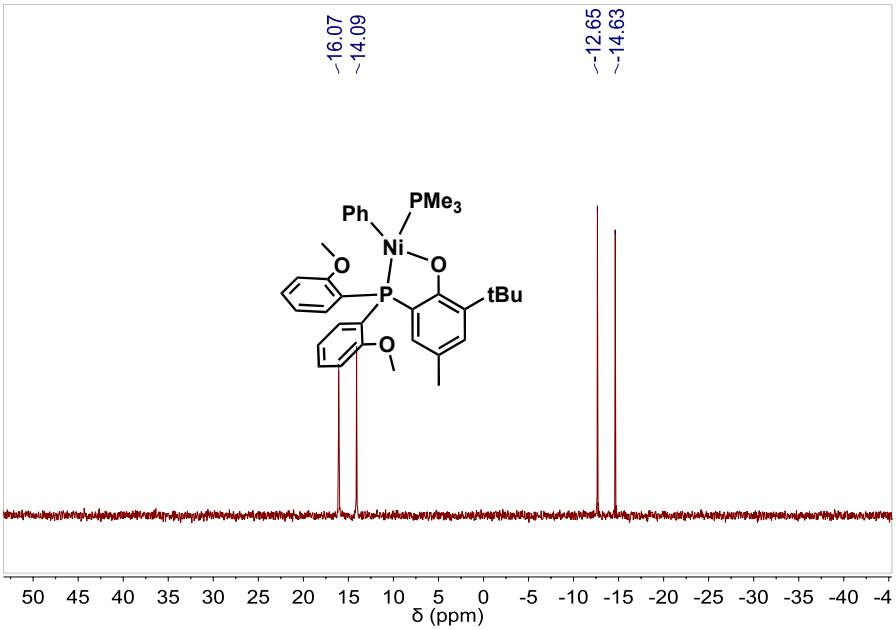

Figure 2.37. ^{31}P NMR spectrum (C_6D_6, 162 MHz) of complex **Ni^{t}Bu**.

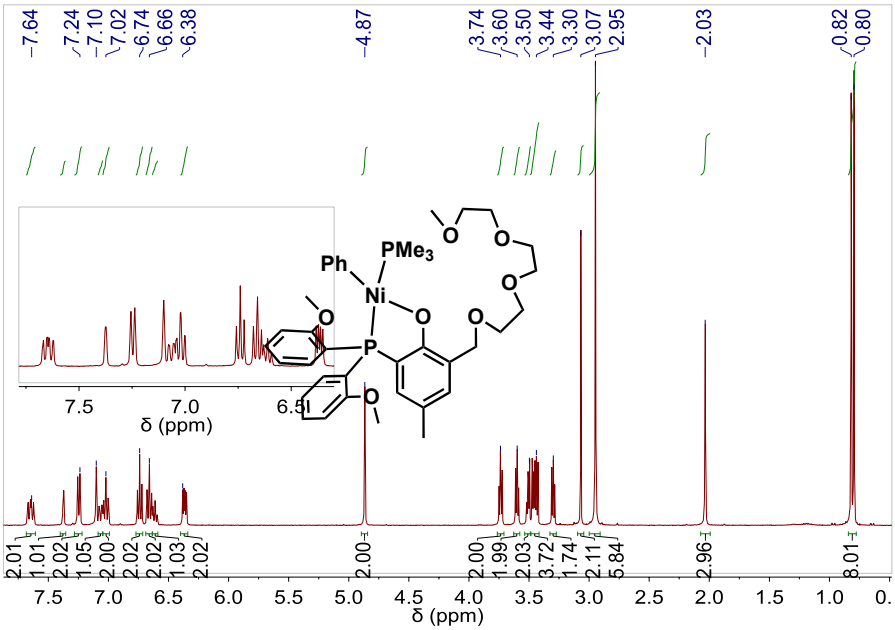

Figure 2.38. ^{1}H NMR spectrum (C_6D_6, 400 MHz) of complex **Ni11**.

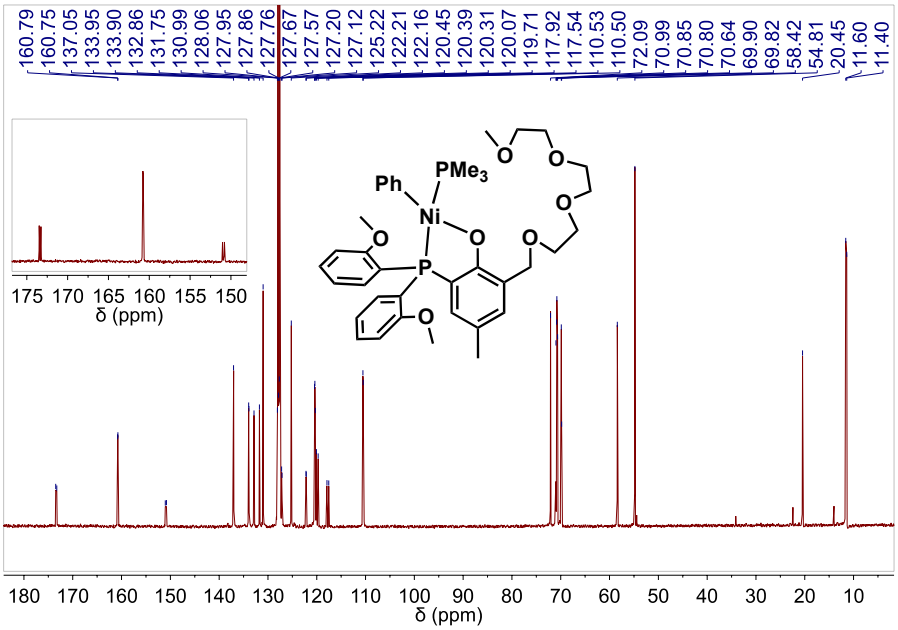

Figure 2.39. ^{13}C NMR spectrum (C_6D_6, 126 MHz) of complex **Ni11**.

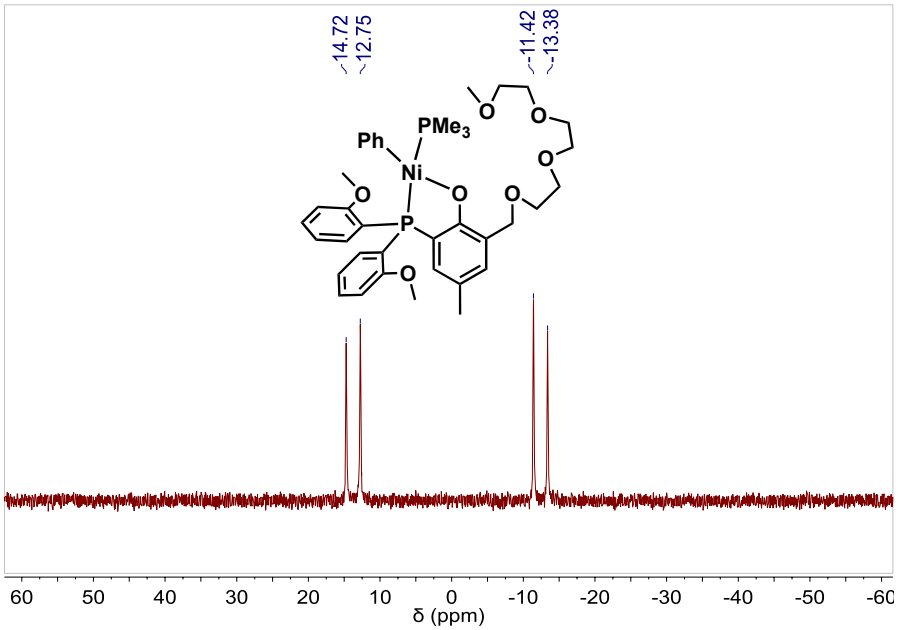

Figure 2.40. ^{31}P NMR spectrum (C_6D_6, 162 MHz) of complex **Ni11**.

Chapter 3. One Catalysts Many Materials: Using Alkali Ions to Control Ethylene Polymerization Catalysts.

3.1. Introduction

In Chapter 2, we showed that chelation of sodium to nickel phenoxyphosphine polyethylene glycol complex **Ni11** led to extraordinary increase in catalytic activity. However, its polymer molecular weight and catalyst thermal stability was limited. In this chapter, we expanded our study of **Ni11** with other alkali metals such as Li, K, and Cs. We performed detailed structural studies of the nickel-alkali resulting bimetallic complexes and mechanistic experiments to investigate the cooperative roles of secondary metals in ethylene polymerization.

3.2. Secondary Alkali Ion Complexation

3.2.1. X-ray Characterization

To obtain structural characterization, we grew single crystals of the nickel-alkali complexes by layering pentane over a toluene/Et_2O, toluene/THF, or benzene/Et_2O solution of **Ni11** and $MBAr^F{}_4$ (M = Li^+, Na^+, K^+, and Cs^+). The **Ni11**-M structures revealed that the nickel centers all adopt square planar arrangements and their phosphine groups are *trans* to each other, except for sodium (Figure 3.1). Each nickel complex is coordinated to an alkali ion, which is ligated by oxygen atoms from PEGs and the bridging phenolate. For potassium and cesium, due to their large cation size, they are found to also coordinate with an extra solvent molecule, THF in **Ni11**-K and benzene in **Ni11**-Cs.

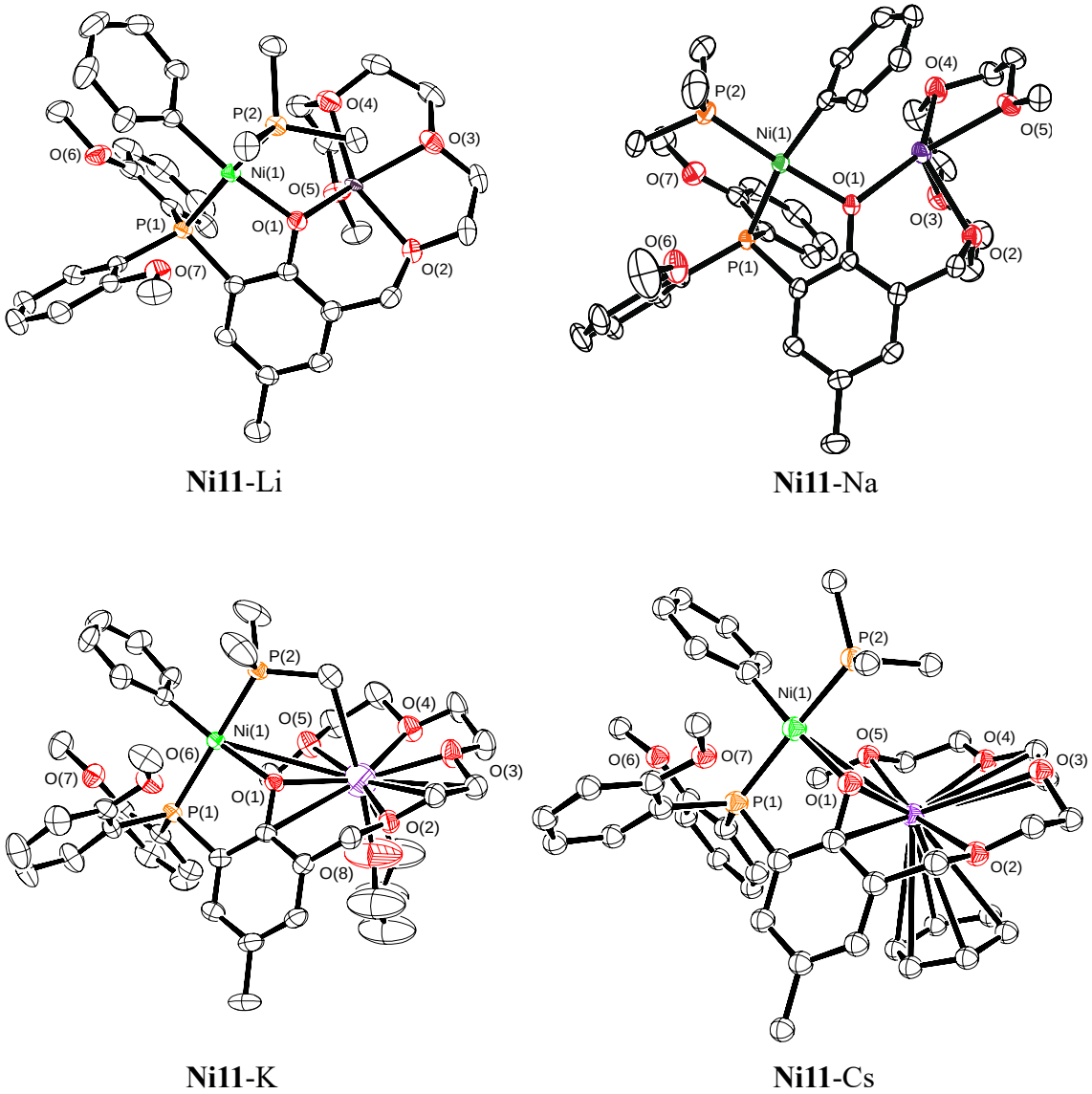

Figure 3.1. X-ray structure of complex **Ni11**-M (ORTEP view, displacement ellipsoids drawn at 50% probability level). Hydrogen atoms have been omitted for clarity.

3.2.2. Metal Binding Study by UV-Vis Absorption Spectroscopy

Even though their solid-state structures showed 1:1 Ni:M binding, additional studies of **Ni11**-M were carried out to confirm this stoichiometry in solution. Our experiments were conducted in a mixture of Et_2O and toluene due to the low solubility of the alkali $BAr^F{}_4$ salts in non-polar solvents. However, we hypothesized that in neat toluene, which is the solvent used in our

polymerization studies, the nickel-alkali binding stoichiometry does not change. Being able to form discrete 1:1 nickel-alkali species in solution is important to having single site catalysts that could produce narrowly dispersed polymers. Polydispersity is a crucial material characteristic because it contributes to its physical and mechanical properties.

3.2.2.1 Job Plots

To establish the binding stoichiometry of **Ni11** and alkali ions, we employed the method of continuous variation. For these studies, stock solution of **Ni11** (500 μM) and $MBAr^F_4$ (500 μM) (M = Li^+, Na^+, K^+, and Cs^+) were prepared separately in a mixture of toluene/Et_2O (1:1). Eleven samples with different ratios of **Ni11:M** in a total volume of 3.5 mL were prepared UV-Vis cuvettes and their UV-vis spectra were recorded at room temperature. The full data and calculations are shown in Tables 3.5-3.8. Our results showed that the peak maxima all occur at X_{Ni} = 0.5, which means that the optimal binding of **Ni11** with M^+ is 1:1 (Figure 3.2). The slopes of the four plots suggest that the alkali ion affinity of **Ni11** follows the order $Li^+ > Na^+ \approx K^+ > Cs^+$. This trend is most likely due to the size matching of the alkali ion with the binding pocket provided by the PEG chain and phenolate donor. Similar observations have been reported in the literature.[86-89]

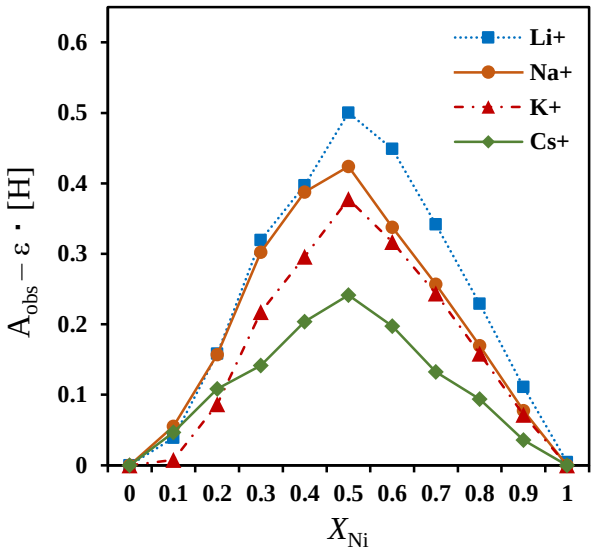

Figure 3.2. Job plots for complex **Ni11** with $MBAr^F{}_4$, M = Li^+ (blue squares), Na^+ (orange circles), K^+ (red triangles), Cs^+ (green rhombus) in a mixture of Et_2O and toluene (1:1) at 25 ºC.

3.2.2.2 Metal Titration

Next, we performed metal ion titration studies to probe the coordination chemistry of **Ni11** in more detail. To carry out these experiments, solutions containing 100 µM **Ni11** in Et_2O/toluene (1:1) were treated with aliquots of 0.1 equiv of $MBAr^F{}_4$ salts (M^+ = Li^+, Na^+, K^+, and Cs^+) and then allowed to equilibrate for ~20−30 min before recording the spectral changes. The $MBAr^F{}_4$ was added up to 1 equiv relative to the nickel complex. Upon addition of the alkali salts, we observed clear isosbestic points that suggest simple A→B transformations (Figure 3.3), the starting trace of **Ni11** is shown in black and the final trace (after 1.0 equiv of M^+ was added) is shown in red.

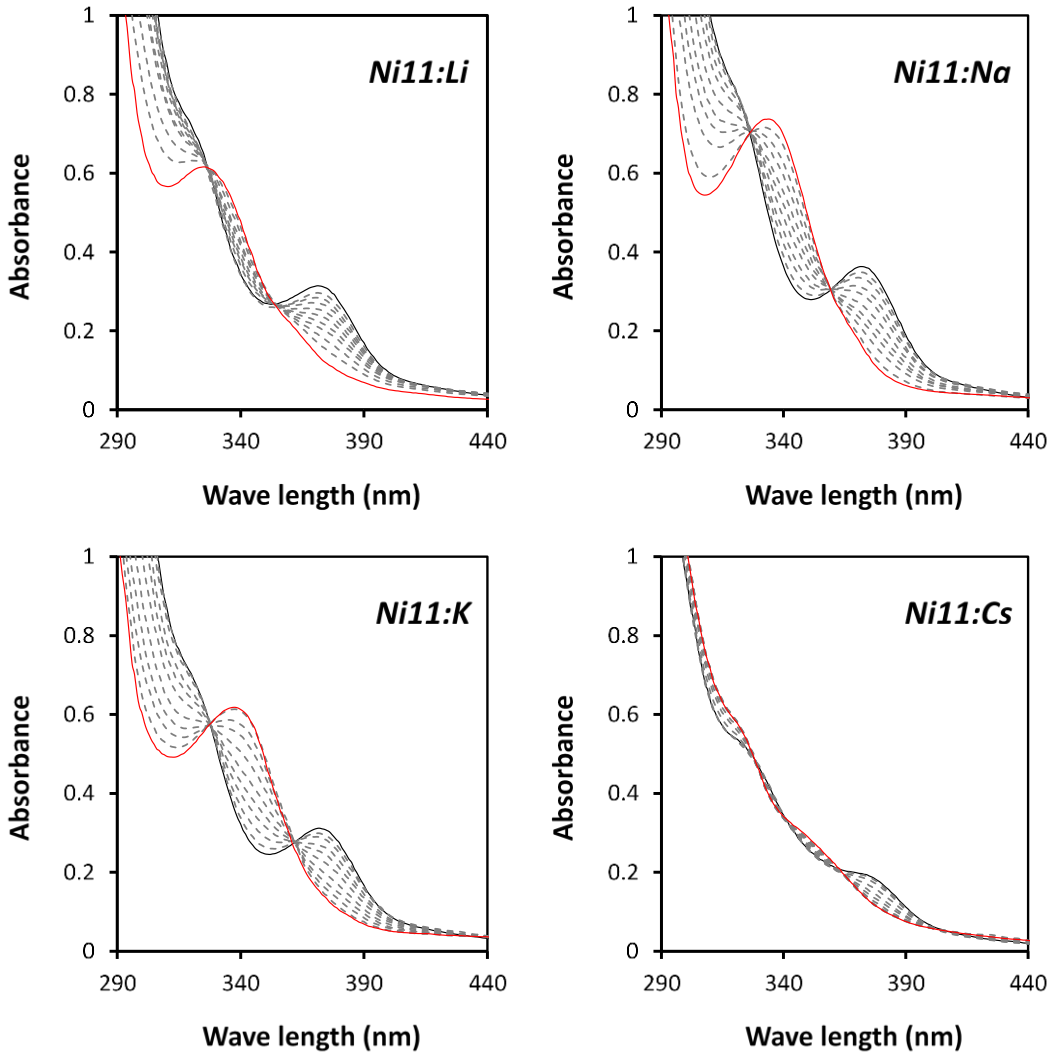

Figure 3.3. UV-vis absorbance spectra of complex **Ni11** after the addition of various aliquots of $MBAr^{F}_{4}$.

3.3. Ethylene Polymerization

We first screened **Ni11** for ethylene homopolymerization activity in the presence of different alkali cations (Table 3.1). We compared our heterobimetallic complexes with monometallic **Ni^{t}Bu** and **NiC$_6$F$_5$**, which possess different electronic and steric properties and do not have secondary coordination sites (Figure 3.4).

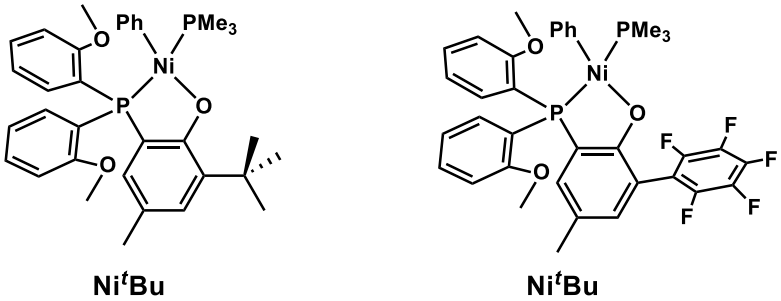

Figure 3.4. Ni^{t}Bu and **NiC$_6$F$_5$** complexes used as standards in this study for comparison.

Interestingly, we observed that the polymerization behavior of **Ni11** is dramatically altered in the presence of cations. Complex **Ni11** itself was catalytically inactive, affording a trace amount of polymer after 1 h (Table 3.1, entry 1). We surmised that its free PEG chain can self-inhibit by occupying open coordination sites at the nickel center. However, in our previous studies on a family of nickel phenoxyimine-polyethylene glycol complexes, the pendent PEG chains neither promote nor inhibit polymerization.[46] As expected, recruitment of alkali cations by **Ni11** led to formation of highly active single-site catalysts for olefin polymerization. At 30 ^{o}C in toluene under 450 psi of ethylene, we found that **Ni11**-Li was the most productive catalyst, affording a TOF of up to 35.3×10^3 kg/(mol Ni·h) and highly linear polyethylene with an average M_n of ~40.1×10^3 g/mol and M_w/M_n of ~1.3. The second most active catalyst was **Ni11**-Na, which afforded a TOF of about 18.14×10^3 g/mol. In comparison to the standard catalysts **Ni^{t}Bu** and **NiC$_6$F$_5$**, our **Ni11**-Li and **Ni11**-Na bimetallic complexes are far more active (Figure 3.5). To understand the effects of

alkali ions, we compared their physical properties such as atomic size (r_{Li+} = 76 pm, r_{Na+} = 102 pm, r_{K+} = 138 pm¸ and r_{Cs+} = 167 pm) and ionic potential (Φ_{Li+} = 1.66, Φ_{Na+} = 1.04, Φ_{K+} = 0.76, and Φ_{Cs+} = 0.55).[90-91] We found that the high activity of **Ni11**-Li complex correlates well with the high binding affinity of **Ni11** for Li^+ and ionic potential of Li^+. Our results are consistent with literature reports that showed electron-deficient nickel catalysts tend to give higher activity and polymer molecular weight in ethylene polymerization than their electron-rich counterparts.[92-95] The TOF decrease in the other **Ni11**-Li > **Ni11**-Na > **Ni11**-K > **Ni11**-Cs is in agreement with their Lewis acid strengths and **Ni11** binding affinities order Li^+ > Na^+ > K^+ > Cs^+. However, the polymer molecular weight followed a different trend **Ni11**-Li > **Ni11**-Cs > **Ni11**-K > **Ni11**-Na (Table 1, entries 2, 3, 4, and 5). Because molecular weight is influenced by both electronic (Lewis acid strength of the alkali cations) and steric (cation size) effects, the observed catalyst behavior reflects a combination of these factors. Branching analysis revealed that all of the polymers produced by **Ni11**-M are highly linear, which is typical for this class of catalysts.[96-97] However, it is interesting to note that **Ni11**-Na and **Ni11**-K produced polyethylene with branching density of ∼26/ 1000 C, whereas **Ni11**-Li and **Ni11**-Cs gave branching density of ∼10/1000 C (Figure 3.6).

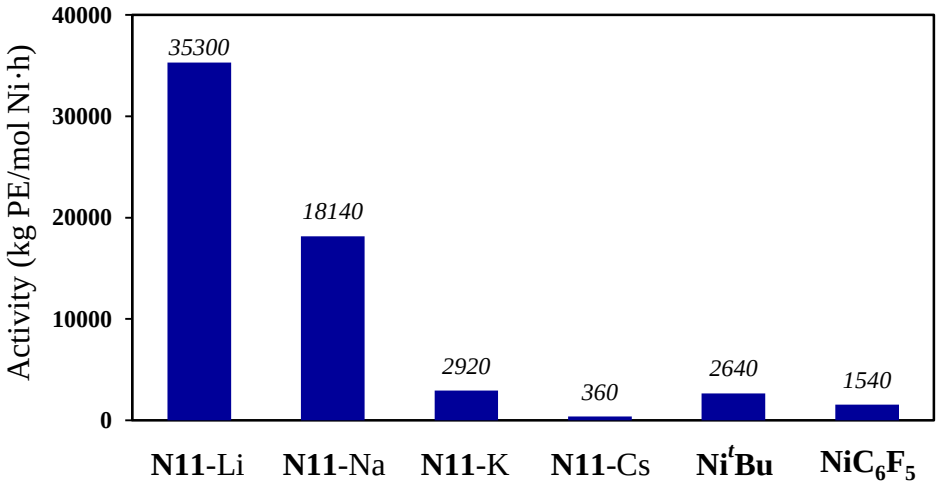

Figure 3.5. Ethylene polymerization using **Ni11**-alkali metals bimetallic complexes and monometallic nickel complexes at 30 ^{o}C.

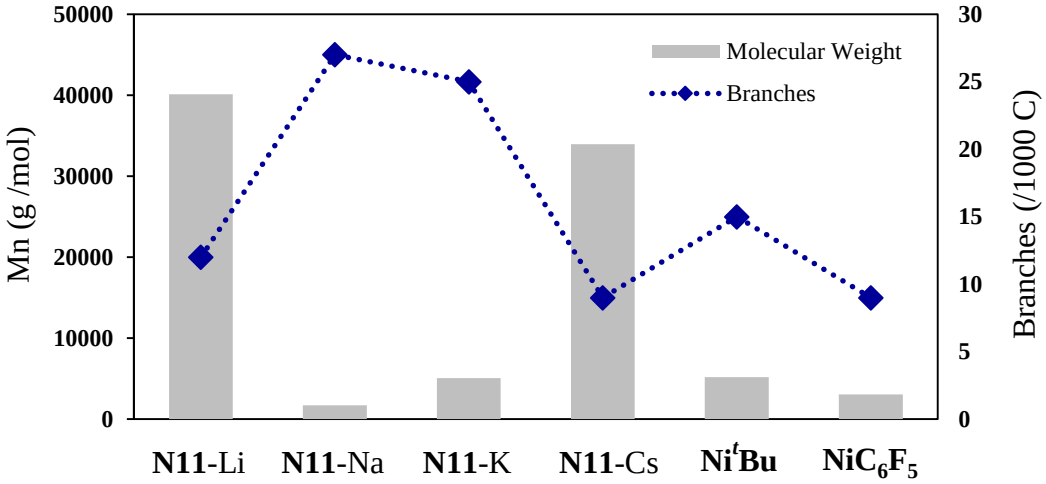

Figure 3.6. Molecular weight and branching density of polyethylenes produced by **Ni11**-alkali metals bimetallic complexes and monometallic nickel complexes at 30 ^{o}C.

To study temperature effects, we screened our catalysts from 30 ^{o}C to 90 ^{o}C. In general, increasing reaction temperature increased catalyst activity and decreased polyethylene molecular weight, but branching density was unaffected (Table 3.1).

Table 3.1. Polymerization Screening for **Ni11** with Different Alkali Metals at Various Temperatures[a]

Entry	Cat.	Salt	Temp. (^{O}C)	Polymer Yield (g)	Activity $(\frac{kg}{mol \cdot h})$	Branches[b] (/1000 C)	M_n[c] ($\times 10^3$)	$\frac{M_n}{M_w}$
1	**Ni11**	none	30	trace	0	–	–	–
2[d]	**Ni11**	Li^+	30	3.53	35300	12	40.1	1.3
3	**Ni11**	Na^+	30	9.07	18140	27	1.72	1.4
4	**Ni11**	K^+	30	1.46	2920	25	4.53	1.6
5	**Ni11**	Cs^+	30	0.18	360	9	33.93	1.5
6	**Ni^{t}Bu**	none	30	1.32	2640	15	5.2	1.9
7	**NiC$_6$F$_5$**	none	30	0.77	1540	9	3.06	2.1
8[d]	**Ni11**	Li^+	50	3.84	38400	7	12.1	1.3
9	**Ni11**	Na^+	50	6.52	13040	30	1.6	1.2
10	**Ni11**	K^+	50	2.73	5460	9	11.5	1.5
11	**Ni11**	Cs^+	50	0.72	1440	8	34.98	1.3
12[d]	**Ni11**	Li^+	70	1.82	18200	10	6.2	1.3
13	**Ni11**	Na^+	70	4.61	9220	27	1.03	1.4
14[e]	**Ni11**	K^+	70	2.89	11560	27	1.39	1.3
15[e]	**Ni11**	Cs^+	70	9.12	36480	9	15.12	1.7
16[d]	**Ni11**	Li^+	90	1.31	13100	17	2.09	2.2
17	**Ni11**	Na^+	90	2.41	4820	30	0.86	1.5
18[e]	**Ni11**	K^+	90	2.49	9960	29	1.06	1.6
19[e]	**Ni11**	Cs^+	90	5.73	22920	10	15.74	1.4
20	**Ni^{t}Bu**	none	90	12.8	25600	12	1.46	3.4
21	**NiC$_6$F$_5$**	none	90	10.3	20600	15	0.97	3.7

[a]Polymerization conditions: catalyst (0.5 μmol), $MBAr^F_4$ (1 μmol, if any), $Ni(COD)_2$ (4 μmol), ethylene (450 psi), 100 mL toluene, 1h. Temperature was controlled by manual external cooling when necessary to ensure that the reaction temperature does not exceed greater than 5°C from the starting temperature. [b]The total number of branches per 1000 carbons was determined by ^{1}H NMR spectroscopy. [c]Determined by GPC in trichlorobenzene at 140 ^{o}C. [d]**Ni11** (0.1 μmol), $MBAr^F_4$ (0.2 μmol, if any), $Ni(COD)_2$ (0.8 μmol). [e]Reaction was run for 30 min. ***Ni^{t}Bu** and **NiC$_6$F$_5$** were tested as standards for comparison.

It is interesting to note that each complex has different optimal working temperatures. **Ni11**-Li was most active at 50 ^{o}C¸ **Ni11**-Na at 30 ^{o}C, and **Ni11**-K and **Ni11**-Cs at 70 ^{o}C, affording TOFs

of about 38.4×10^3, 18.14×10^3, 11.56×10^3, and 36.48×10^3 kg/(mol Ni·h), respectively. For complexes **Ni11**-Li, **Ni11**-Na and **Ni11**-K, they were highly sensitive to elevated reaction temperatures. At 70 ºC, their polymer products displayed significant reduction in molecular weight of about 6.5×, 1.7×, and 3.7× for Li^+ (entry 12), Na^+ (entry 13) and K^+ (entry 14) respectively, in comparison to those obtained at 30 ºC. At 90 ºC, the molecular weight decreased further, M_n ~2.09×10^3 g/mol for **Ni11**-Li (entry 16), ~0.86×10^3 g/mol for **Ni11**-Na (entry 17), and ~1.06×10^3 g/mol for **Ni11**-K (entry 18). The broad polydispersity of **Ni11**-Li (M_w/M_n ~2.2) at this high temperature suggested that more than two active species were present in the reaction mixture that might result from the slow decomposition of bimetallic structure. These observations were matched closely with many previous reports on the temperature sensitivity of Ni(II) systems in olefin polymerization.

Surprisingly, our **Ni11**-Cs complex demonstrated extraordinary thermal stability. At 70 ºC, the catalytic rate enhanced about 101× (TOF = 36.48×10^3 kg/(mol Ni·h)), in comparison to that at 30 ºC (TOF = 0.6×10^3 kg/(mol Ni·h)), but the resulting polyethylene molecular weight was reduced by half (M_n ~33.93×10^3 g/mol at 30 ºC, M_n ~15.12×10^3 g/mol at 70ºC) (entries 5 and 15). Further increasing reaction temperature to 90 ºC led to a slight decrease in catalytic activity but polymer molecular weight and polydispersity were maintained. Although **Ni^{t}Bu** and **NiC$_6$F$_5$** complexes also displayed high activities at 90 ºC, their resulting polymers' molecular weight decreased significantly (M_n = ~$0.97\text{-}1.46\times10^3$) and the corresponding polydispersity increased, up to 3.7, indicating partial decomposition of the catalysts. Our **Ni11**-Cs complex is among one of a few Ni systems that can produce polyethylene with moderate molecular weight and extremely high activity at temperature as high as 90 ºC (entry 19). In comparison with other thermally robust Ni

systems, including those based on the well-established α-diimine platforms, **Ni11**-Cs complex is more active and productive (higher TOF and TON) (Table 3.18).

Next, we proceeded to evaluate the effects of solvents on the reactivity of **Ni11**-M toward ethylene polymerization. We performed reactions in benzene and dichloromethane at 30 ^{o}C. Generally, the nickel-alkali complexes showed similar productivity in benzene and toluene, which have similar chemical properties and polarity. However, **Ni11**-K's activity was found to increase ~4.9×, giving a TOF of 14.4×10^3 kg/(mol Ni·h), which was similar to that of **Ni11**-Na (Figure 3.7).

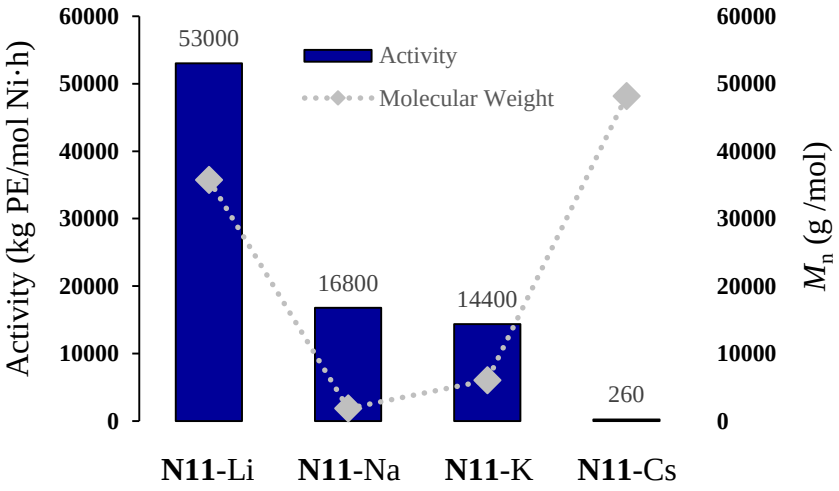

Figure 3.7. Ethylene polymerization study for bimetallic complexes in benzene.

In dichloromethane, the catalytic activities decreased several folds compared to in toluene. In general, the polymerization processes are commonly inhibited in halogenated solvents due to interaction of halogen atoms with metal catalysts. In our study, **Ni11**-Li in CH_2Cl_2 was still the most productive catalyst, yielding polymer with medium molecular weight and high activity. Interestingly, the activity of **Ni11**-Cs increased about 2×, while the resulting polymer molecular weight decreased 3× compared to those recorded in toluene (Figure 3.8). Since the interaction of

solvents with the metal centers is complicated, it is difficult to draw any conclusions without further experimental studies.

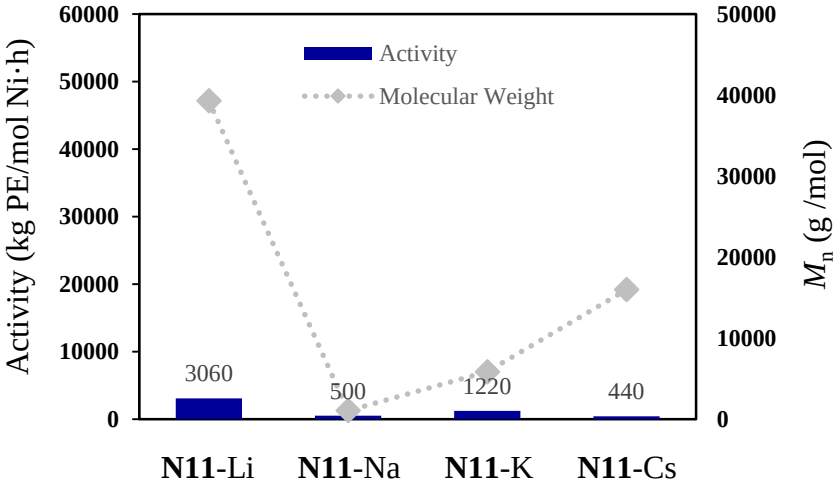

Figure 3.8. Ethylene polymerization study for bimetallic complexes in dichloromethane.

Due to the extremely high catalytic rate of the **Ni11**-Li complex in ethylene polymerization at 30 ^{o}C, we hypothesized that, similar to many common systems, its catalytic activity will get benefits from high temperature, thus we anticipated that the maximum TOF may be much greater at the optimal working condition. Screening the **Ni11**-Li in ethylene polymerization from 30 to 90 ^{o}C, we observed that the optimal temperature was 40 ^{o}C (TOF = 51.8×10^{3} kg/(mol Ni·h), M_n ~25.8×10^{3} g/mol) (Figure 3.9). Its activity decreased gradually at higher temperature, which is most likely due to either catalyst decomposition or change in cation binding affinity. In the former case, the formation of nickel-bis(ligand) species or reprotonation of the ligand could be a possible off-cycle pathway.[98] In the latter case, we have observed similar phenomenon as with the palladium phosphine phosphonate ester complexes.[59] These results further confirm the importance of having suitably strong secondary metal chelators to prevent dissociation of the heterobimetallic structures.

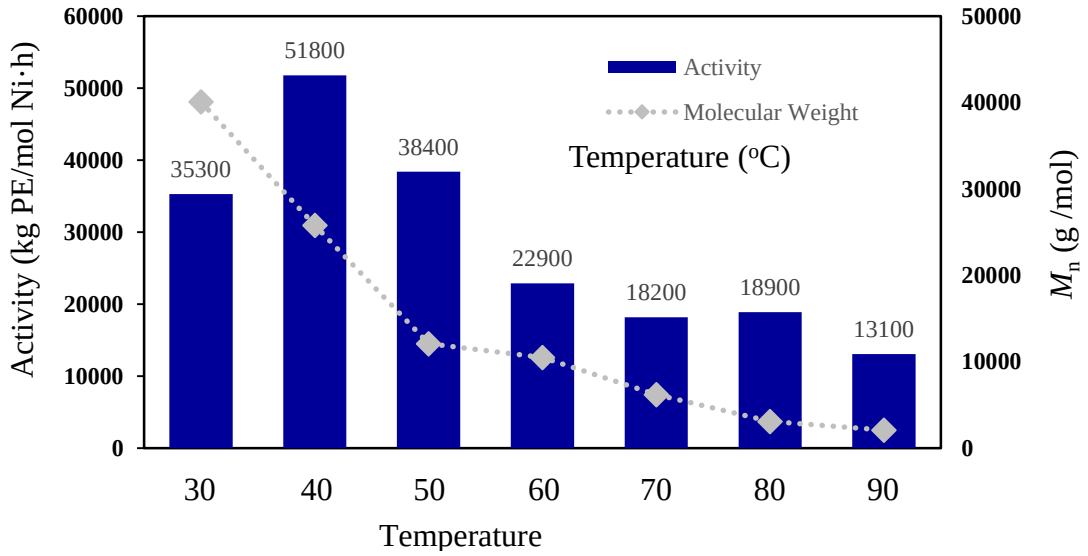

Figure 3.9. Temperature study of **Ni11**-Li in ethylene polymerization.

We further optimized the reaction conditions for **Ni11**-Li at 40 °C. We hypothesized that because mass transport could be a limiting factor due to its extremely high activity, we tested **Ni11**-Li with shorter reaction time and under more dilute catalyst concentration. In both cases, our results showed that the catalytic activity increased, suggesting that the productivity of **Ni11**-Li complex was most likely limited because of precipitation of insoluble polymer rather than decomposition of the active species (Figure 3.10). Under diluted catalyst condition, our **Ni11**-Li complex polymerized ethylene with extraordinary activity (TOF = 89.4×10^3 kg/(mol Ni·h)), affording polyethylenes with an M_n ~21.7×10^3 g/mol. To the best of our knowledge, this heterobimetallic complex could rival some of the best transition-metal catalysts reported to date in ethylene polymerization (Table 3.17).

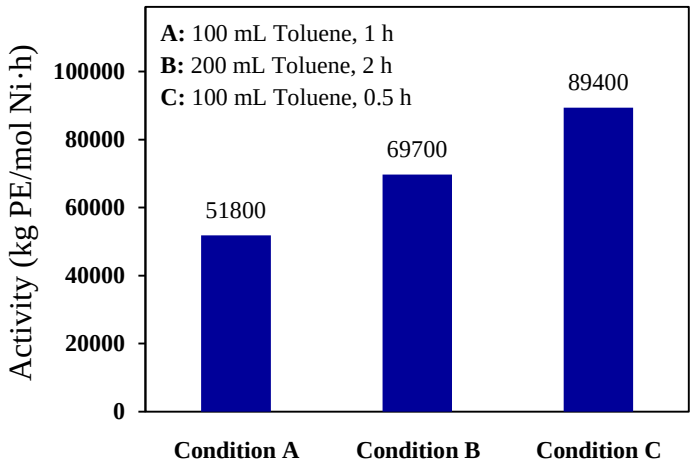

Figure 3.10. Optimizing study for **Ni11**-Li complex in ethylene polymerization at 40 ^{o}C.

We next investigated the catalytic behavior of **Ni11**-Li in a wide range of solvents. In non-polar solvents such as pentane, hexane, benzene, and toluene, **Ni11**-Li complex gave similar results. However, we found that hexane was the best solvent, giving a ~1.5× increase in activity and ~2.0× increase in polymer molecular weight, in comparison to those performed in toluene (Figure 3.11). We hypothesized that hexane solubilized the catalyst/polymer best and enabled tighter metal binding. The catalyst also showed greater tolerance towards diethyl ether than dichloromethane. In acetonitrile, polymerization was completely shut down, which was consistent with our NMR titration studies, showing that heterobimetallic species do not form in CH_3CN (Figure 3.35). The correlation between the stability of bimetallic species and polymerization activity is supported experimentally.

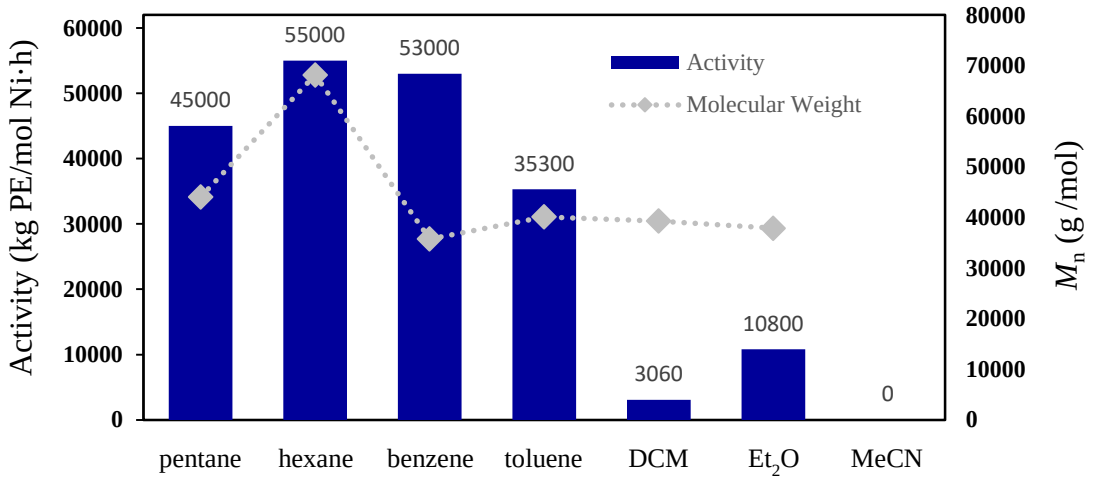

Figure 3.11. Ethylene polymerization study for **Ni11**-Li in different solvents.

To examine the effect of counteranions on catalyst performance, we tested **Ni11** in combination with various lithium salts: $LiBAr^F{}_4$, LiTPFB, $LiBPh_4$, and LiOTf. First, we performed polymerization reactions in neat toluene without temperature control. Our results showed that the $BAr^F{}_4^-$ anion was the most suitable. In the presence of $LiBAr^F{}_4$, **Ni11** polymerized ethylene at the fastest rate, in comparison with the other Li salts (Figure 3.12). Second, to determine whether counteranions are directly involved in polymerization or just influence the salt's solubility, we conducted these reactions in a mixture of toluene/diethyl ether (1:1). Under these conditions, the polymerization rates were slower but still in the same order $LiBAr^F{}_4$ > LiTPFB > $LiBPh_4$, >> LiOTf ~0 (Figure 3.13). We further proposed that the inactivity of **Ni11** with LiOTf salt may result from the chelation of the sp^2-oxygens (S=O) to the nickel centre.[47] Therefore, having weakly coordinating counteranions such as $BAr^F{}_4^-$ or $TPFB^-$ is important to ensure catalyst high productivity.

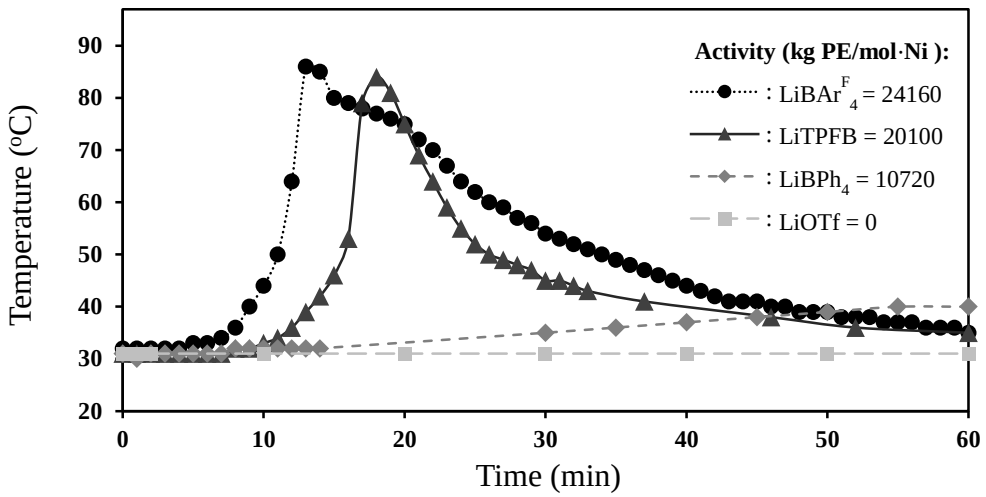

Figure 3.12. Counteranion effect study for **Ni11**-Li in ethylene polymerization in toluene without temperature control.

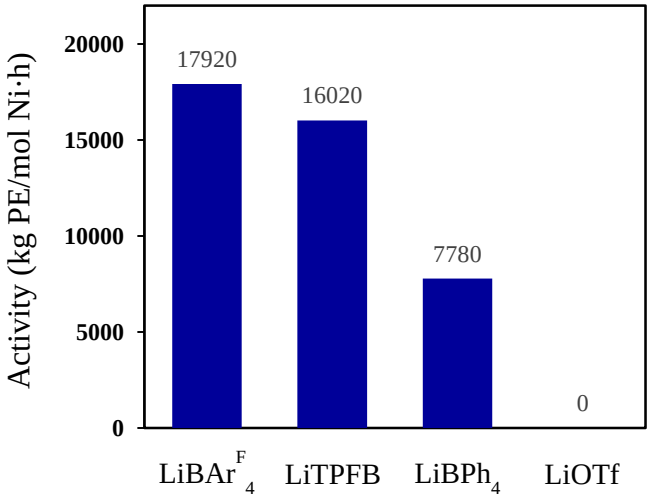

Figure 3.13. Counteranion effect study for **Ni11**-Li in ethylene polymerization in a mixture of toluene and Et_2O (1:1).

Finally, to evaluate the thermal stability of the **Ni11**-Li complex, we measured the reaction temperature and polymer yield as a function of time. When a 5 μM toluene solution of the nickel-lithium catalyst was treated with $Ni[COD]_2$ followed by exposure to 450 psi of ethylene, the reaction temperature slowly increased from 31 to 34 °C after the first 7 min, then quickly rose to

86 °C for another 7 min concomitant with a rapid increase in polymerization rate. Once the exotherm reached a maximum, the solution gradually cooled back down to ~35 °C after 60 min (Figure 3.14). During the first 36 min, an appreciable amount of polymer formed, which suggested the presence of active catalyst. These results indicated that our most active **Ni11**-Li catalyst is quite thermally robust. A pre-activation phase was also observed for several electron-poor nickel complexes.[94]

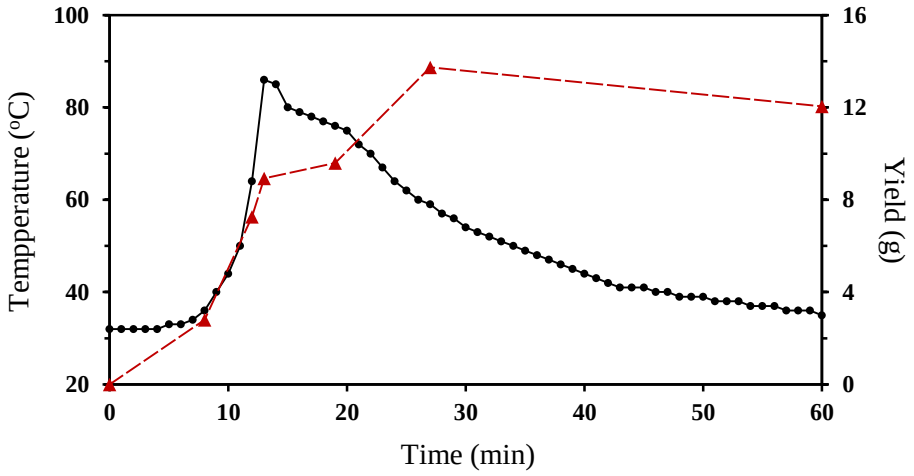

Figure 3.14. Time-Dependent catalyst activity of **Ni11**-Li (5 μM). The temperature values represent the internal reactor temperatures and were recorded manually by reading the digital temperature gauge.

3.4. Structure-Activity Correlation

3.4.1. Steric Influence

The steric environment of a catalysts primary coordination sphere is known to directly impacts its catalytic performance. Steric effects could lead to changes in polymer molecular weight, microstructure, catalyst activity, and catalyst thermal stability. To investigate the steric influence of secondary metals on **Ni11**, we have calculated the percentage buried volume (%V_{bur}) in the nickel-alkali structures using the program SambVca 2.1. We assessed the possible correlation

between $\%V_{bur}$ and catalyst reactivity.[99-100] The structures of our bimetallic catalysts were also compared with monometallic complexes **Ni^{t}Bu** and **NiC$_6$F$_5$**. The X-ray structure of a nickel complex similar to **NiC$_6$F$_5$** was used in our $\%V_{bur}$ calculations.[97]

By comparing the mononickel versus nickel-alkali structures, we found that the alkali-PEG units are positioned above the d_z orbital of the nickel centers, which provides steric protection of the axial sites (Figure 3.16). In contrast, the *t*-butyl substituent of **Ni^{t}Bu** and the C_6F_5 substituent of **NiC$_6$F$_5$** do not provide the same d_z orbital protection (Figure 3.15). It is difficult to synthetic asymmetric ligands like phenoxyphosphines, that can efficiently shield the axial position of square planar nickel and palladium complexes. However, installing pendent chelators to recruit secondary metals can be a useful strategy to achieve efficient steric protection.

On the basic of their topographical steric maps (Figure 3.17) and X-ray structures, we found that the steric bulk of **Ni11**-M followed the order **Ni11**-Na < **Ni11**-Li < **Ni11**-K < **Ni11**-Cs (Figure 3.16). The $\%V_{bur}$ of the bimetallic complexes were higher than those of the monometallic complexes, which further suggested that they have more steric hindrance than their mononuclear counterparts. It has typically been observed that bulkier catalysts tend to produce higher polymer molecular weight, while less bulky catalysts tend to be more active. At low temperature, the activity trend followed the order **Ni11**-Cs < **Ni11**-K < **Ni11**-Na < ***Ni11***-*Li*, whereas molecular weight followed a different order **Ni11**-Na < **Ni11**-K < **Ni11**-Cs < ***Ni11***-*Li*. At elevated temperature, the trends could change, because more stable catalysts tend to give higher activity and molecular weight.[100] Our polymerization results at 90 ^oC showed that the activity and molecular weight both followed the order **Ni11**-Na < **Ni11**-K < ***Ni11***-*Li* < **Ni11**-Cs. Overall, for **Ni11**-Na, **Ni11**-K, and **Ni11**-Cs, we found that their catalytic performance correlated well with their steric congestion. The extraordinary stability of **Ni11**-Cs, which is quite rare for nickel-based

systems, is most likely due to the efficient shielding of the PEG/Cs^+ substituent towards the nickel center. Similarly, the poor steric shielding of the nickel center in **Ni11**-Na, particularly at the top hemisphere (O side), may account for its low stability at elevated temperature. Interestingly, **Ni11**-Li complex did not follow the steric trend, and displayed highest productivity at low temperature, yielding polymer with highest molecular weight and activity. Since the reactivity of polymerization catalysts are affected by both steric and electronic, we propose that the electronic effect of Li^+ has a greater influence on **Ni11**-Li, which might have overridden steric effects.

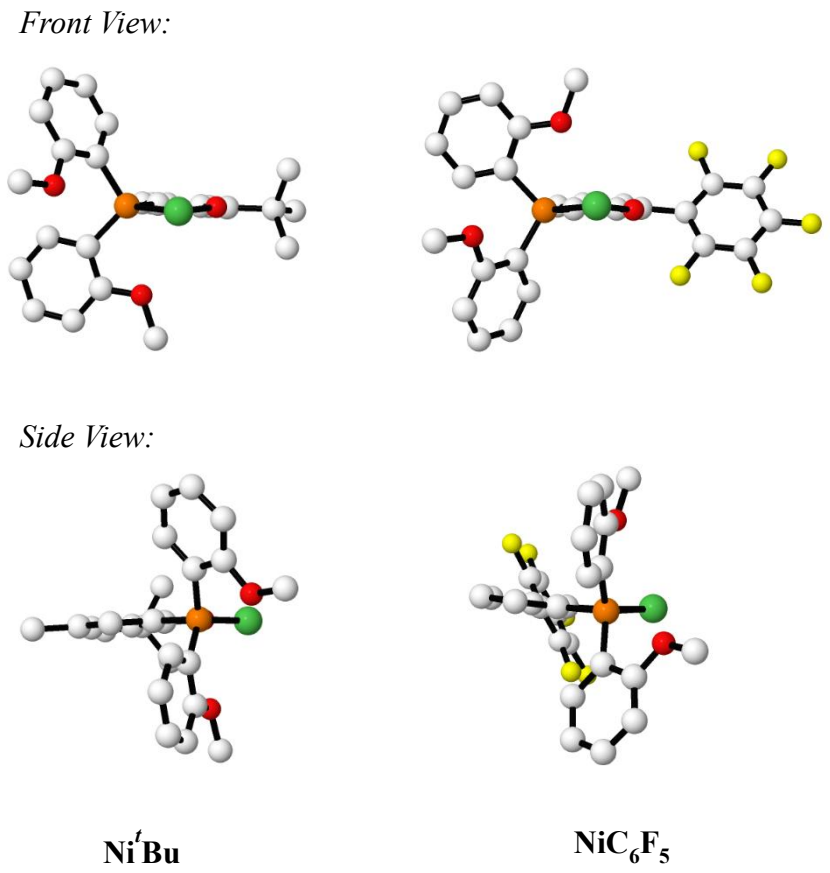

Figure 3.15. Front view and side view of **Ni^{t}Bu** and **NiC$_6$F$_5$**. Atom colors: green = nickel, orange = phosphorus, purple = alkali metal, red = oxygen, white = carbon, yellow = fluorine. The alkyl group and labile ligands were omitted for clarity.

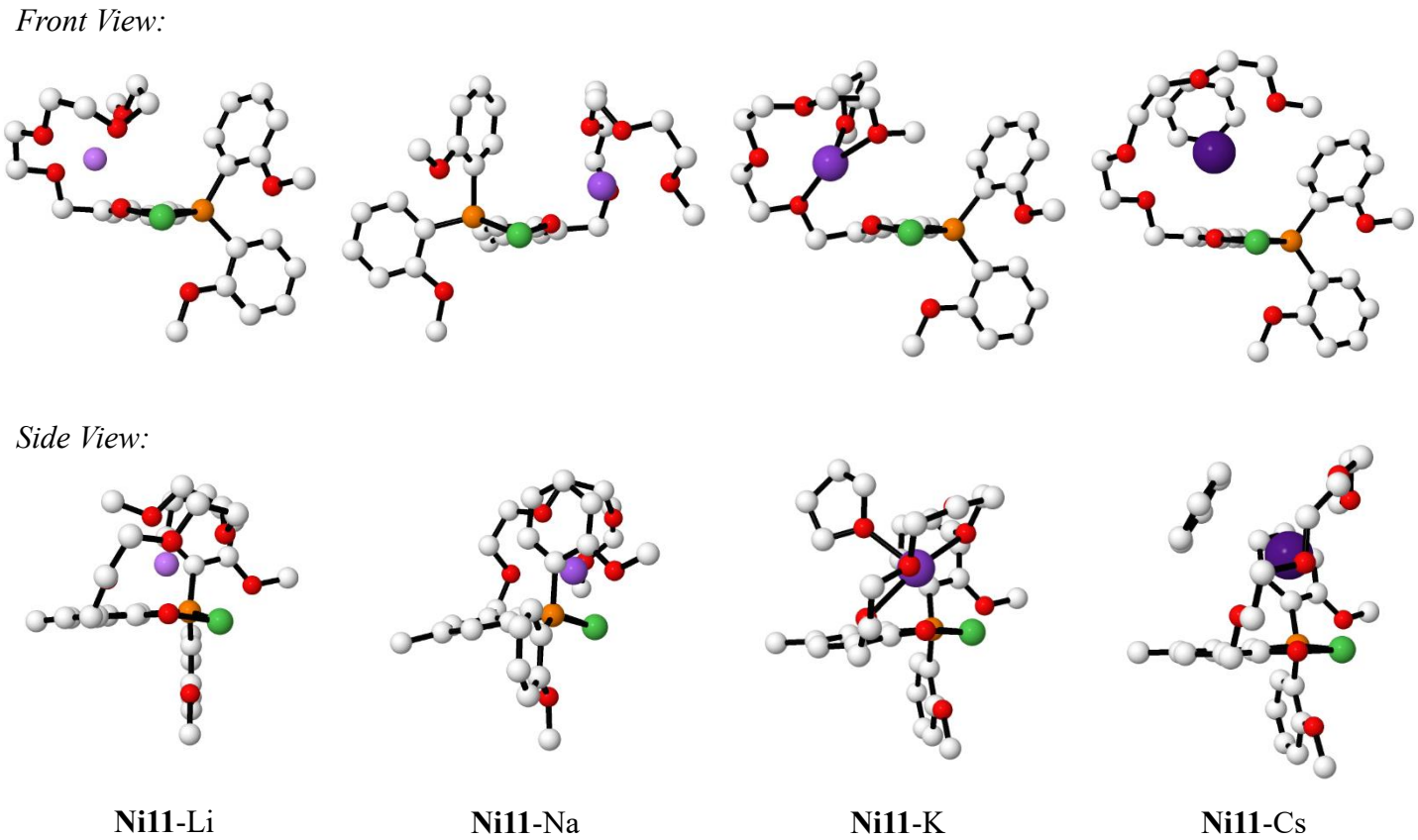

Figure 3.16. Front view and side view of X-ray structures of bimetallic nickel complexes. Atom colors: green = nickel, orange = phosphorus, purple = alkali metal, red = oxygen, white = carbon. The phenyl group and the labile ligand PMe_3 were omitted for clarity.

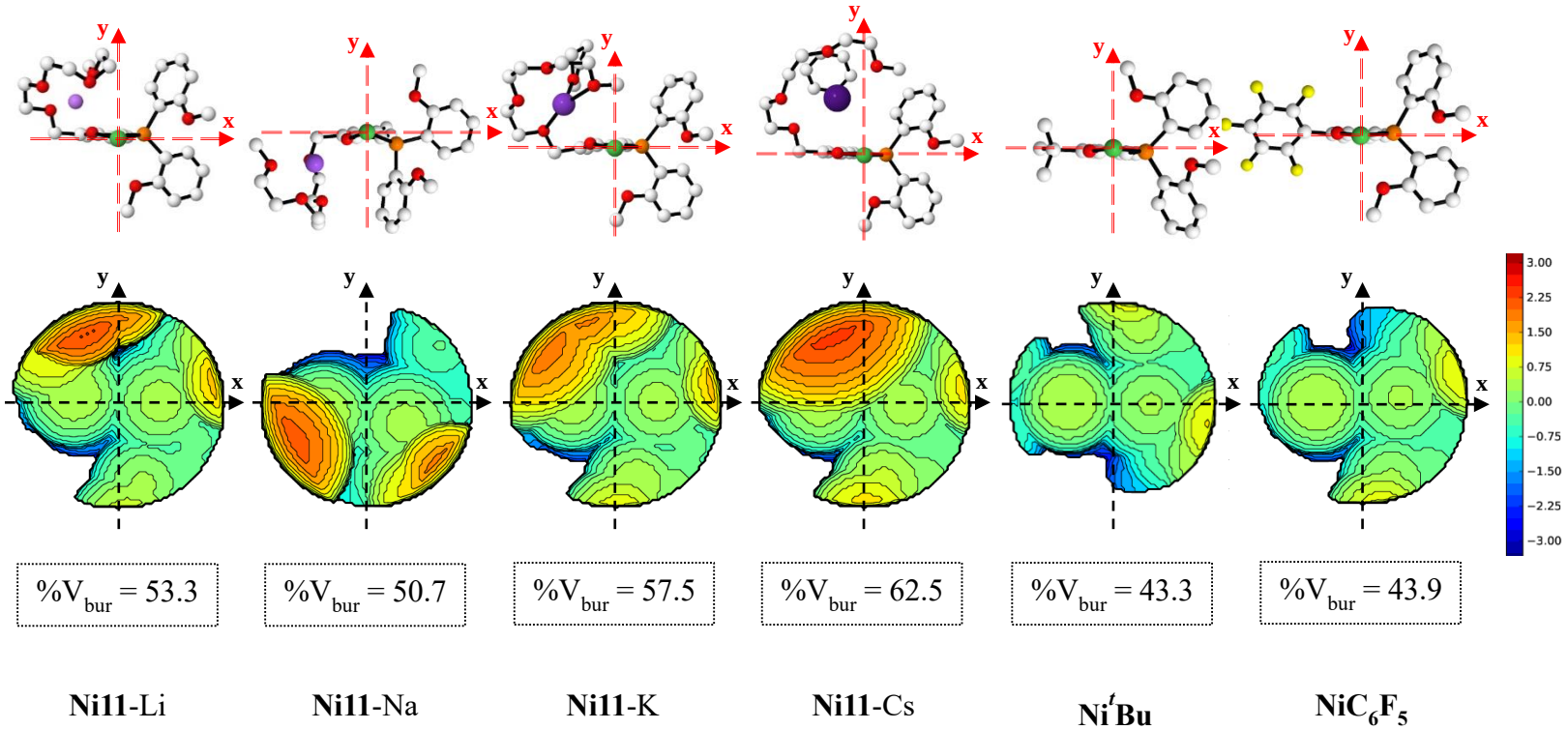

Figure 3.17. Steric map and $\%V_{bur}$ of **Ni^{t}Bu** and **NiC$_6$F$_5$** complexes calculated based on their respective X-ray structures using *SambVca 2.1* software program.[101-103] The Ni-atom is placed at the center of the xyz coordinate system. The P−Ni−O plane is placed in the xz-plane with the z-axis bisecting the P−Ni−O angle. The y-axis represents the axial position of the xz-plane containing the Pd center. The phenyl and trimethylphosphine groups were omitted for the analysis of the steric maps. Atom colors: green = nickel, orange = phosphorous, purple = alkali metal, red = oxygen, yellow = fluorine, black = carbon. *X-ray data of **Ni^{t}Bu** complex was adopted from our previous publication.[58] **For **NiC$_6$F$_5$** complex calculation, a similar X-ray structure was utilized.[66]

3.4.2. Electronic Influence

To probe the electronic effect of M^+ on the nickel complexes, we conducted electrochemical measurements using cyclic voltammetry (CV). Due to solubility reasons, THF was used as the electrochemical solvent. To prevent the interactions of external anions with alkali metals, we chose nBu$_4$NBPh$_4$ as a supporting electrolyte. The CV spectrum are shown in Figure 3.18 and summarized data are shown in Table 3.2. In the absence of M^+, **Ni11** displayed an anodic peak at -0.049 V (vs ferrocene/ferrocenium), which we have tentatively assigned to oxidation of the Ni(II) center. The **Ni^{t}Bu** complex also displayed a peak at -0.051 V, which is close to that of **Ni11**. This result suggested that the nickel centers of these two complexes have similar electron density. The cyclic voltammograms of **Ni11**-Li, **Ni11**-Na, **Ni11**-K, and **Ni11**-Cs showed irreversible peaks at approximately +0.055, –0.014, –0.016, and –0.024, respectively, and were ascribed to Ni-centered reduction processes in the heterobimetallic species. This trend is consistent with the electrophilicity of the alkali ions,[104] which would be expected to cause a decrease in the electron density at the nickel core through electronic induction.[105] The oxidation peak for **NiC$_6$F$_5$** occurred at +0.026, indicating that its nickel core is less susceptible to oxidation than that of **Ni^{t}Bu**, which is expected for an electron poor complex. Generally, for Ni-[P,O] systems, electron-withdrawing substituents at the *ortho* position of the phenolate ring give catalysts with enhanced activity. In our bimetallic systems, the activity trend and the electronic trend followed same other **Ni11**-Li > **Ni11**-Na > **Ni11**-K > **Ni11**-Cs, which was in accordance with many reported literatures.[106] Interestingly, the monometallic complex **NiC$_6$F$_5$**, which was more electron deficient than the **Ni11**-Na, gave an activity of about 8-times lower than that of the **Ni11**-Na. We do not fully understand the origins of the electronic effect induced by a highly electronegative substituent versus an alkali cation,

however, we suggested that in the latter case, there could be several cooperative interactions occurred during the polymerization process.

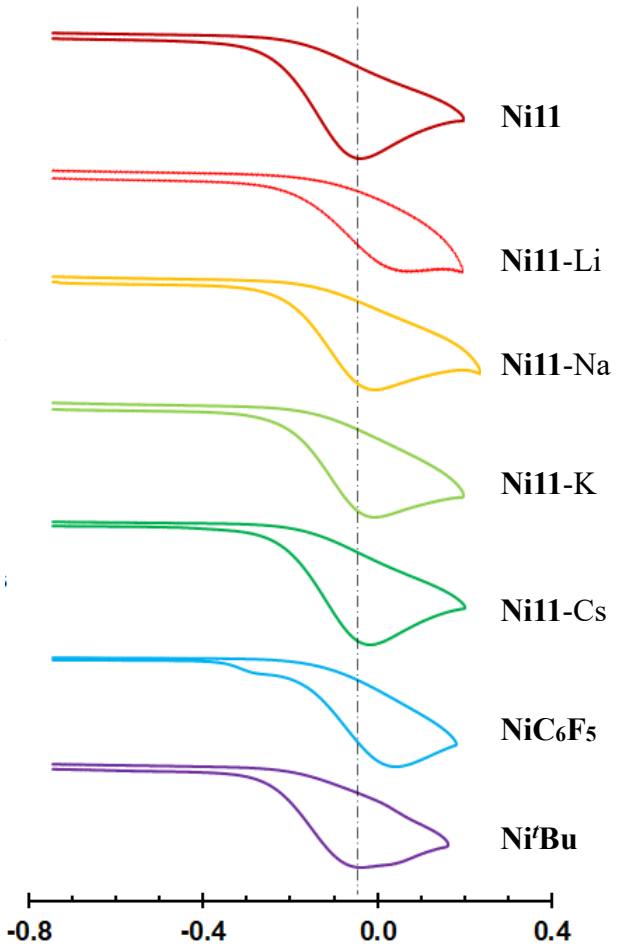

Figure 3.18. Cyclic voltammograms of a nickel complexes, recorded at 0.2 V/s in acetonitrile with 0.09 M nBu$_4$NBPh$_4$ supporting electrolyte, a glassy carbon working electrode, a platinum wire counter electrode, and a silver wire pseudoreference. Potentials are referenced to an internal standard of ferrocene, and currents are normalized to bring all of the traces onto the same scale.

Table 3.2. Summary of oxidation potential for seven nickel complexes

	(E vs. Fc^+/Fc)/V	(E vs. **Ni11**)/V
Ni11	-0.049	0
Ni11-Li	0.055	+0.104
Ni11-Na	-0.014	+0.035
Ni11-K	-0.016	+0.033
Ni11-Cs	-0.024	+0.025
NiC_6F_5	0.026	+0.075
Ni^tBu	-0.051	-0.002

3.5. Catalyst Stability

3.5.1. Post-Activation Study

As mentioned above, for many highly active catalysts, they could be deactivated due to decomposition or precipitation of insoluble polymer. To clarify these two possibilities, we carried out stability studies. Our experiment was performed in a mixture of toluene/ether (8:2) to ensure complete solubility of the reactants. After combining the catalyst, $MBAr^F_4$ salt, and borane activator $B(C_6F_5)_3$, the solution was kept for variable amounts of time (off-time) under a low pressure of ethylene (~3 psi) at 50 ^oC. Subsequently, the reactor was pressurized with 450 psi ethylene and run for 1 h. The polymer yields were then used for calculation of percentage catalyst active. Our results showed that the stability trend followed the order: **Ni11**-Cs > **Ni11**-K ~ **Ni11**-Li > **Ni11**-Na (Figure 3.19), which is in accordance with the steric trend.

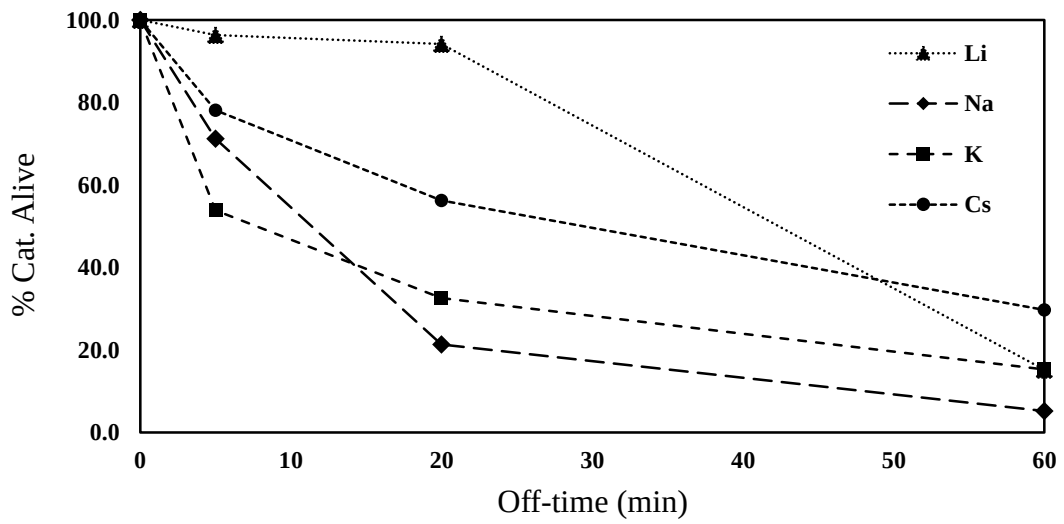

Figure 3.19. Comparison of Ni complexes in decomposition study.

For **Ni11**-Li, we noticed that, in the first 20 min, its activity decreased only slightly, which correlated with more than 90% catalyst active. Since our temperature profile study above showed that **Ni11**-Li has an activation period, we proposed that during the first 20 min the amount of active species decomposed was compensated by formation of new active species; thus, the overall activity remained constant. Long induction periods for nickel catalysts have been observed previously. For example, Grubbs and coworkers reported that when they combined their salicylaldiiminato Ni(II) complex **Nia3** with a phosphine scavenger, a 5-8 min induction period was required before rapid ethylene uptake and temperature increase was observed. When an electron deficient complex such as **Nib3** was used, the induction period was found to increase to be ~20 min (Figure 3.20).[94] The activity of **Nib3** was about 9× greater than that of **Nia3**. They proposed that their observations were consistent with a mechanism in which phosphine dissociation is the rate-limiting step, since electron-withdrawing ligands strengthen the Ni-PPh_3 bond.

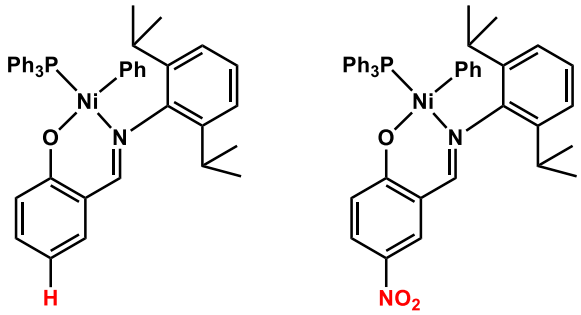

Nia3 **Nib3**

Figure 3.20. Salicylaldiimino nickel complexes studied by Grubbs et. at.

3.5.2. UV-Vis Absorption Spectroscopy

To further understand the stability of the active species, we attempted to monitor their decomposition rate by UV-Vis absorption spectroscopy. To carry out these experiments, 3.0 mL solutions containing 100 µM **Ni11** in toluene/Et_2O (8:2) and 5 equiv of $MBAr^F{}_4$ salts (if any) were placed in a 1 cm quartz cuvette. Next, aliquots containing 3.0 equiv of $B(C_6F_5)_3$ was added, followed by vigorously mixng and then the mixture was allowed to equilibrate for ~3 min before recording the spectral changes at 50 ^oC under nitrogen. The kinetic scan was set for every 3-minute interval and the experiments was monitored up to 6 h. After treating with $B(C_6F_5)_3$, the activated nickel species would be susceptible to thermal decomposition and thus, changes in absorbance over time was expected. The slopes of the single wave plots suggest that the decomposition rates followed the order: **Ni11**-Cs < **Ni11**-K < **Ni11**-Li ~ **Ni11**-Na (Figure 3.21). This outcome was consistent with the off-time polymerization studied above. Full kinetic scans were showed in Figure 3.36-3.43.

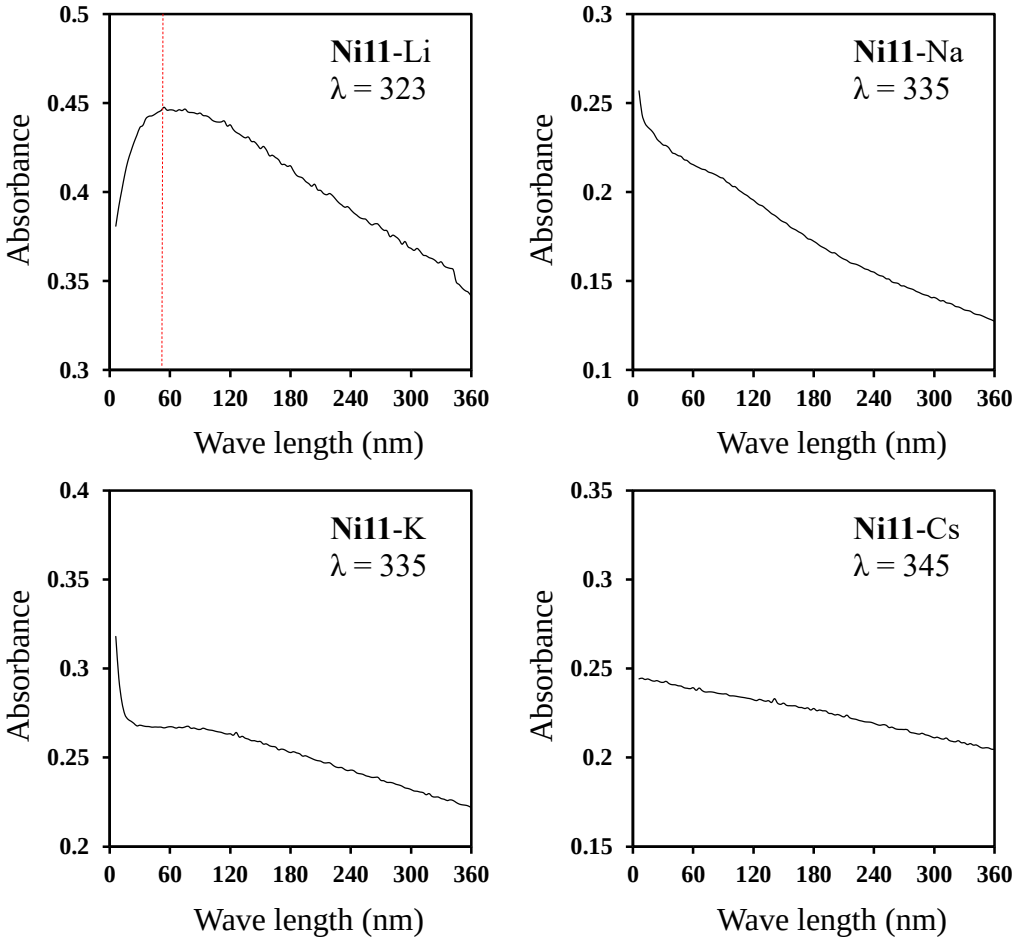

Figure 3.21. UV-Vis absorption data for nickel bimetallic complexes after addition of phosphine scavenger $B(C_6F_5)_3$ at the single wave-length that gave the most change in absorbance.

Moreover, the abruptly decomposition of **Ni11**-K within the first few minutes observed in the off-time polymerization studies was also in agreement with the absorbance change of **Ni11**-K at 335 nm. Interestingly, the slow activation of **Ni11**-Li, which was observed in the off-time polymerization and reaction temperature profile studies above, was clearly indicated in this study. The change in absorbance of **Ni11**-Li at 323 nm could be considered in two stages: the first 50 minutes, involved activation of the nickel complexes, followed by catalyst decomposition

3.5.3. Activation Study

To obtain addition data on the activation step, we used NMR spectroscopy to investigate the reaction of $B(C_6F_5)_3$ with **Ni11**-M. As shown in Table 3.3, our results demonstrated that the $B(C_6F_5)_3$ has a strong affinity for trimethylphosphine, giving complete reactions within several minutes. The facile abstraction of trialkyl- or triaryl-phosphine by boranes has been reported previously.[107] The exceptional stability of **Ni11**-Li at 30 ^{o}C further confirmed since the activation of **Ni11**-Li took about 2 h to complete. However, at 50 ^{o}C, the reaction time was reduced to 30 min. These observations were in agreement with our UV-Vis and off-time polymerization studies above, indicating that the **Ni11**-Li complex was exceptionally more stable than the other complexes. To demonstrate further that the stability of **Ni11** was enhanced by chelation of $LiBAr^F{}_4$, we repeated the reaction of **Ni11**-Li with borane. However, instead of premixing **Ni11** with $LiBAr^F{}_4$, we added a mixture of $LiBAr^F{}_4$ and borane to a solution of **Ni11** complex. Our result showed that without coordination of Li, **Ni11** react with $B(C_6F_5)_3$ within 5 minutes, indicating that chelation of Li was crucial to enhance the stability of the Ni-PMe_3 bonds.

Table 3.3. Summarized data for activation study of nickel complexes

Entry	Complex	Temp. (°C)	Time Needed for Complete Activation
1	**Ni11**	30	less than 5 min
2	**Ni11**-Li	30	up to 2h
3[b]	**Ni11** + $LiBAr^F{}_4$	30	less than 5 min
4	**Ni11**-Li	50	less than 30 min
5	**Ni11**-Na	30	less than 5 min
6	**Ni11**-K	30	less than 5 min
7	**Ni11**-Cs	30	less than 5 min

[a]Activation study: nickel complex **Ni11** and alkali salts were premixed in a mixture of toluene-d_8/Et_2O in a NMR tube, followed by addition of borane activator (if any). Then the NMR tube was sealed and shaken vigorously before analysis by NMR (^1H & ^{31}P). [b]This experiment was conduct without premixing of **Ni11** and $LiBAr^F{}_4$.

3.6. Mechanistic Implications

3.6.1. *cis/trans* Isomerization

Because the bidentate [P,O] ligands are asymmetric, in theory, the nickel square plane of **Ni11** could exist in two isomeric forms (Figure 3.22). The energy difference between the *cis* and *trans* isomers will determine their relative ratios in solution. Cis/trans isomerization of square planar palladium [P,O] complexes has been studied using DFT calculations by Nozaki and coworkers.[108] Later, Jordan's group demonstrated that the *cis/trans* ratio of palladium [P,O] complexes could be quantified by ^1H NMR spectroscopy, using excess P(O-*o*-tolyl)$_3$ to promote isomerization (Figure 3.23). They also found that substituting alkyl or aryl moieties with chlorine also helped facilitate isomerization because the *trans*-influence of chlorine is much weaker than that of aryl- and alkyl-

moieties.[109] Observations of *cis* and *trans* isomers have also been reported for Pd(II) [N,O] "sandwich" complexes by Daugulis/Brookhart and co-workers.[110]

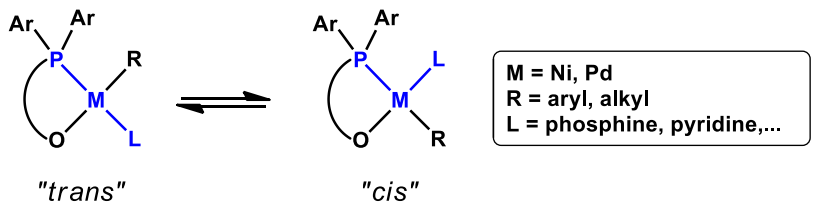

Figure 3.22. Proposed *cis/trans* isomerization of square planar nickel and palladium complexes.

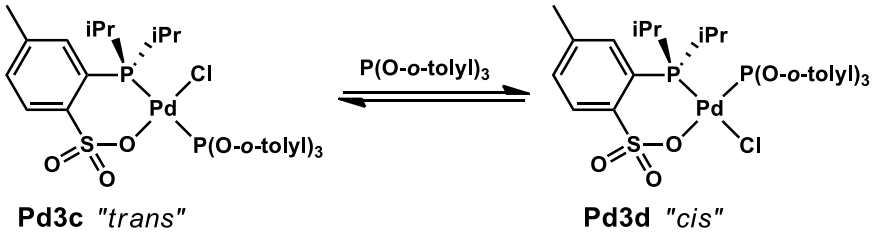

Figure 3.23. *cis/trans* isomerization of palladium complexes studied by Jordan's group.

Our nickel complex **Ni11** showed only one conformation by ^{1}H and ^{31}P NMR spectroscopy. Interestingly, upon addition of secondary alkali metals, we detected two species. We assigned the isomer with a smaller J_{PP} coupling constant as the *"cis*-isomer*"* since the two phosphine groups are *cis* relatively to each other. The species with the larger J_{PP} coupling constant was assigned as the *"trans*-isomer*"* (Figure 3.24). The J_{PP} coupling constants of "*cis*" and "*trans*" square planar metal complexes have been reported in the literature.[111] **Ni^{t}Bu** and **NiC$_6$F$_5$** also showed only trans isomers in solution, which was in agreement with DFT calculations performed in collaboration with the Wu group showing that the *cis* isomers had a ground state energy of at least 6.2 kcal/mol higher than that of the *trans* isomers. The *trans* configuration is more thermodynamically favored because it avoids d orbital sharing between the strong σ-donors phosphine and alkyl/aryl groups.[80, 96-97, 112-113] The *trans* conformation are also dominant in most complexes based on [N,O] or [C,O]

ligands.[17, 85, 114] Suprisingly, the *cis* isomer of **Ni11**-Li complex was only 2.0 kcal/mol higher than its *trans* isomer, which is consistent with the 8:92 *cis/tran*s ratio observed by NMR. Interestingly, for **Ni11**-Na and **Ni11**-K, the *cis* conformations were more favorable than the *trans* with the *cis/trans* ratio of about 90:10 and 88:12, respectively. These ratios correspond to their calculated values of 2.8 kcal/mol and 1.3 kcal/mol lower in energy for *cis* than for *trans*, respectively. Good correlations were obtained for the experimentally determined *cis/trans* ratio and ground state energy calculations for **Ni11**-Cs complex. Because solvent interaction was omitted in our DFT calculations and the electron density of Cs was approximated, calculated energies for **Ni11**-Cs may not be accurate. However, based on the consistency of our NMR spectroscopic data with DFT calculations, we have concluded that interactions of secondary metals with **Ni11** significantly changed the electronic and steric properties of the resulting nickel complexes. For the first time the existence of *cis* for nickel phenoxyphosphine complexes were observed experimentally.

Table 3.4. Summarized data for *cis/trans* isomerization study.

Entry	**Complex**	***cis/trans* ratio** (determined by ^{31}P NMR)	**Ground State Energy** (kcal/mol) (determined by DFT Calculation)	
			cis	***trans***
1	**Ni11**	0:100	6.2	0.0
2	**Ni11**-Li	8:92	2.0	0.0
3[b]	**Ni11**-Na	90:10	0.0	2.8
4	**Ni11**-K	88:12	0.0	1.3
5	**Ni11**-Cs	35:65	3.3	0.0
6	**Ni^{t}Bu**	0:100	6.6	0.0
7	**NiC$_6$F$_5$**	0:100	9.3	0.0

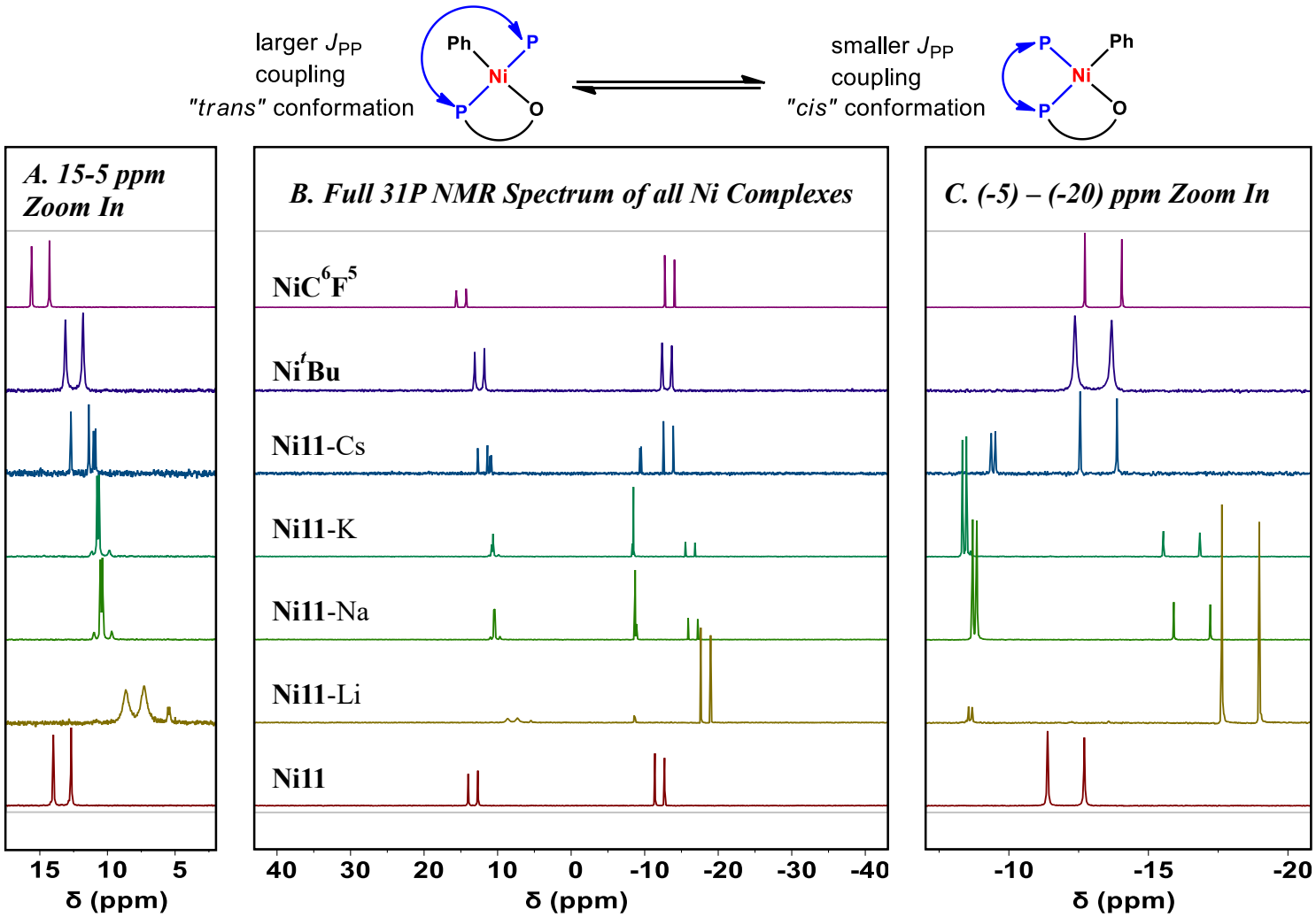

Figure 3.24. ^{31}P NMR spectrum of nickel complexes.

3.6.2. Ethylene Insertion Energy Barrier

We conducted further DFT calculations to probe the effect of secondary metals on the coordination/insertion process. To be consistent with the *cis/trans* isomerization nomenclature used above, we have assigned the conformation having the alkyl group *trans* to the oxygen donor as *trans* isomer and the other is *cis*. Our result showed that **Ni11**-Li favored a different reaction pathway than the other nickel complexes (Figure 3.25), which might account for its unusually high activity. As described in the previous section, the **Et-*trans*** intermediates, which have the alkyl groups *trans* to the oxygen donors instead of the phosphines, tends to have lower energy than their *cis* counterparts. However, the transition state **TS-*trans*** for ethylene insertion is higher than **TS-*cis*** by at least ~5 kcal/mol for **Ni11**-Na complex (Figure 3.26) and up to ~12 kcal/mol for **Ni^{t}Bu** complex (Figure 3.27). Because ethylene insertion involves migration of the alkyl group to ethylene, the strong *trans* effect of the phosphorus atom could enhanced the migrating ability of the alkyl group resulting in a lower reaction barrier. Our DFT calculations showed that after coordination of ethylene, the resulting intermediate **Et-*trans*** would be formed more favorably than **Et-*cis***. Insertion then occurs through higher energy transition state **TS-*trans***, which was also the rate-determining step. This trend has been observed for all monometallic and bimetallic complexes except for **Ni11**-Li, which showed that the **Et-*trans*** and **Et-*cis*** isomers were nearly equal in energy, indicating that these isomers could readily interconvert between each other. Therefore, after **Et-*trans*** forms, it could isomerize to **Et-*cis***, which would undergo the lower energy transition state **TS-*cis*** to insert ethylene. Hence, the overall catalytic rate of **Ni11**-Li would be must faster than the other nickel complexes, which is in agreement with our experimental.

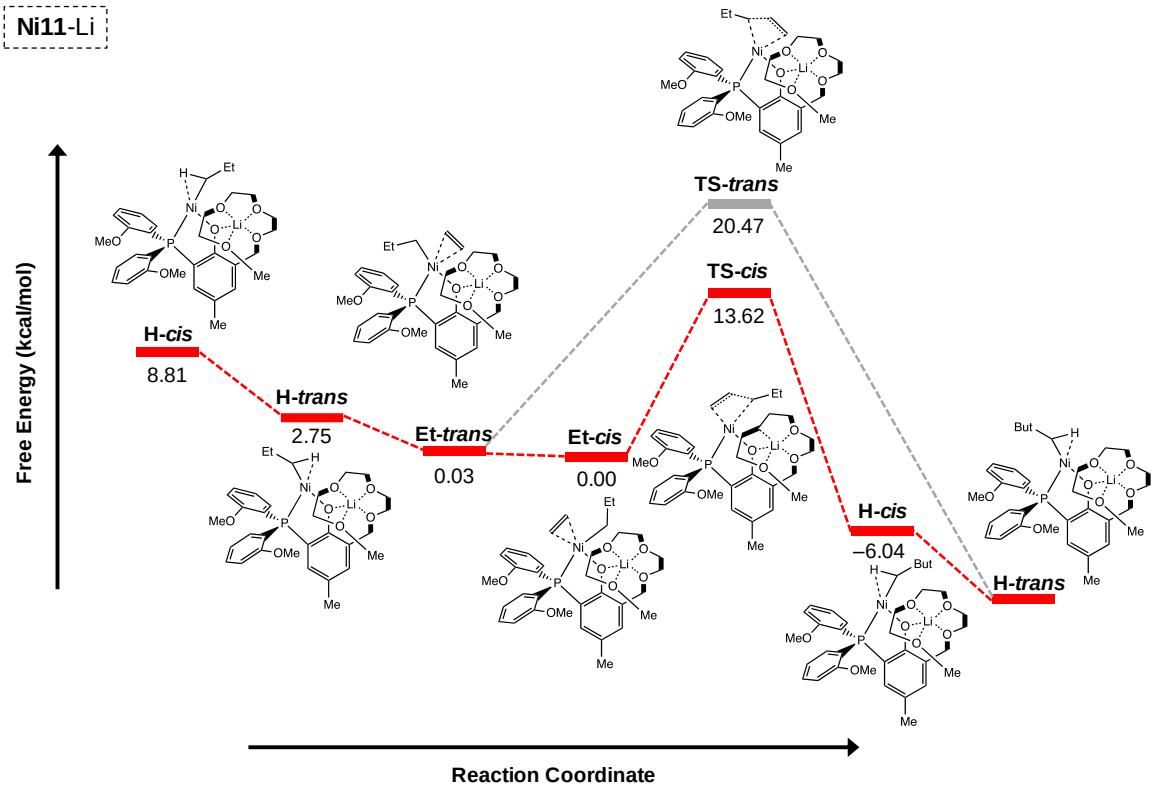

Figure 3.25. Free energy profile of **Ni11**-Li in ethylene coordination/insertion polymerization.

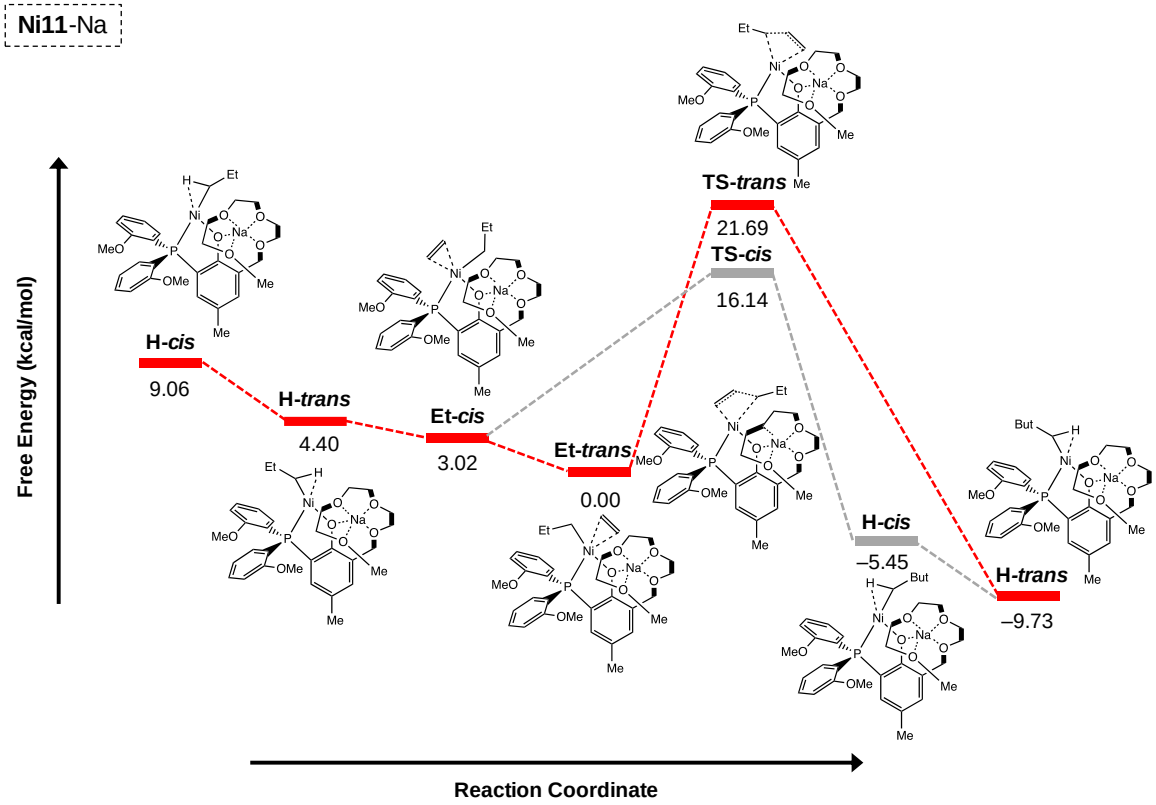

Figure 3.26. Free energy profile of **Ni11**-Na in ethylene coordination/insertion polymerization.

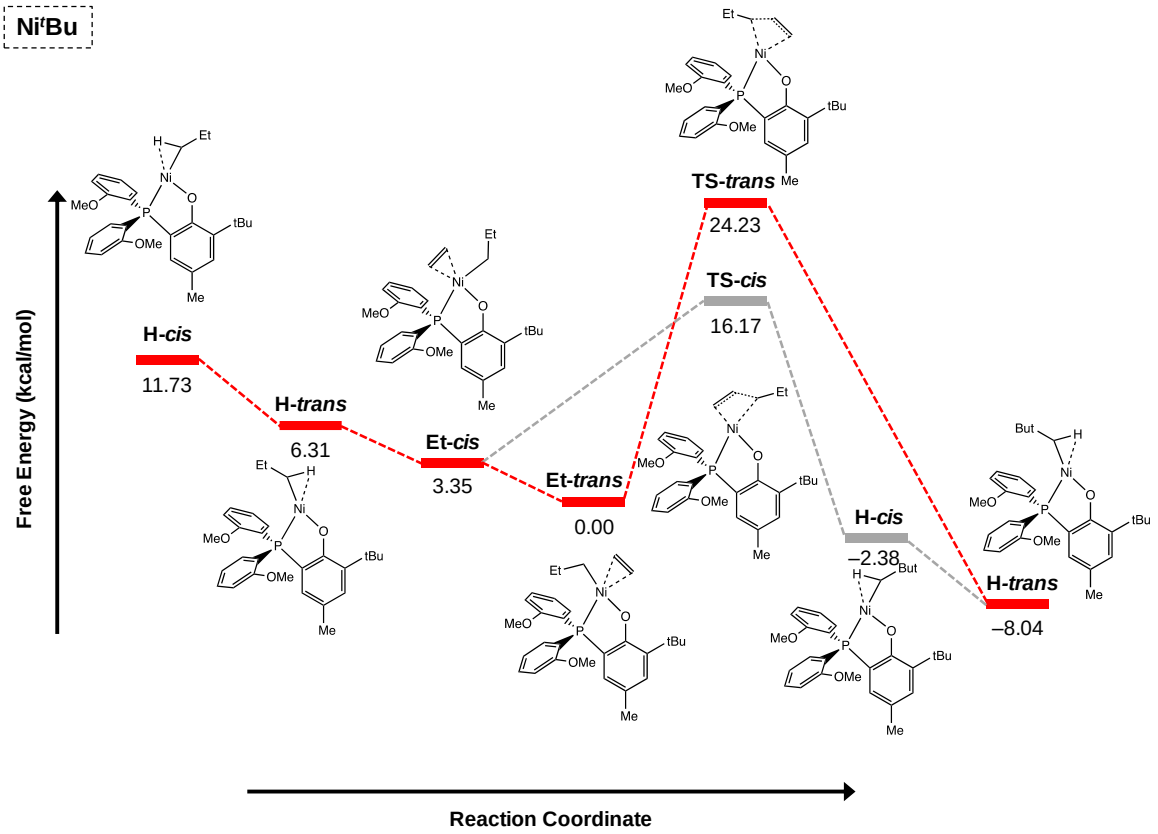

Figure 3.27. Free energy profile of **Ni^{t}Bu** in ethylene coordination/insertion polymerization.

3.7. Conclusion

In summary, we have demonstrated that diverse group of functionally distinct catalysts could easily be accessed form a common parent nickel complex. The catalyst's activity, thermal stability, and polymer molecular weight can be fine-tuned by pairing it with a suitable secondary alkali metal. This work illustrates the importance of using weakly coordinating counteranions to enable high catalytic activity by avoiding coordination inhibition. To maximize electronic effects, the two metals should be positioned in close proximity to each other. The ultra-high activity of the **Ni11**-Li complex and thermal stability of the **Ni11**-Cs complex demonstrate the usefulness of our "mix-and-match" polymerization strategy. Furthermore, the detailed temperature studies should be taken into serious consideration when optimizing polymerization processes to achieve the best results.

We also conducted experimental studies and DFT calculations to probe the cooperative role of secondary metals, which revealed that chelation of Li^+ to nickel altered the thermodynamics of key reaction intermediates and opened up lower energy pathways for polymerization. In the presence of alkali metals, we were able to observe *cis/trans* isomers in solution by ^1H and ^{31}P NMR spectroscopy, which has not been demonstrated for their monometallic complexes.

3.8. Experimetal

General Procedures

Commercial reagents were used as received. All air- and water-sensitive manipulations were performed using standard Schlenk techniques or under a nitrogen atmosphere using a drybox. Anhydrous solvents were obtained from an Innovative Technology solvent drying system saturated with argon. High-purity polymer grade ethylene was obtained from Matheson TriGas without further purification. The $LiBAr^F_4$, $NaBAr^F_4$, $KBAr^F_4$ and $CsBAr^F_4$ salts were prepared according to literature procedures.[67, 115]

NMR spectra were acquired using JEOL spectrometers (ECA-400, -500, and -600) and referenced using residual solvent peaks. All ^{13}C NMR spectra were proton decoupled. ^{31}P NMR spectra were referenced to phosphoric acid. ^1H NMR spectroscopic characterization of polymers: each NMR sample contained ~20 mg of polymer in 0.5 mL of 1,1,2,2-tetrachloroethane-d_2 (TCE-d_2) and was recorded on a 500 MHz spectrometer using standard acquisition parameters at 120 °C.

Gel permeation chromatography (GPC) data were obtained using a Malvern high temperature GPC instrument equipped with refractive index, viscometer, and light scattering detectors at 150 °C with 1,2,4-trichlorobenzene (stabilized with 125 ppm BHT) as the mobile phase. A calibration

curve was established using polystyrene standards in triple detection mode. All molecular weights reported are based on the triple detection method.

Synthesis and Characterization

Nickel **NiC$_6$F$_5$** was synthesized as depicted in Scheme 3.1 below:

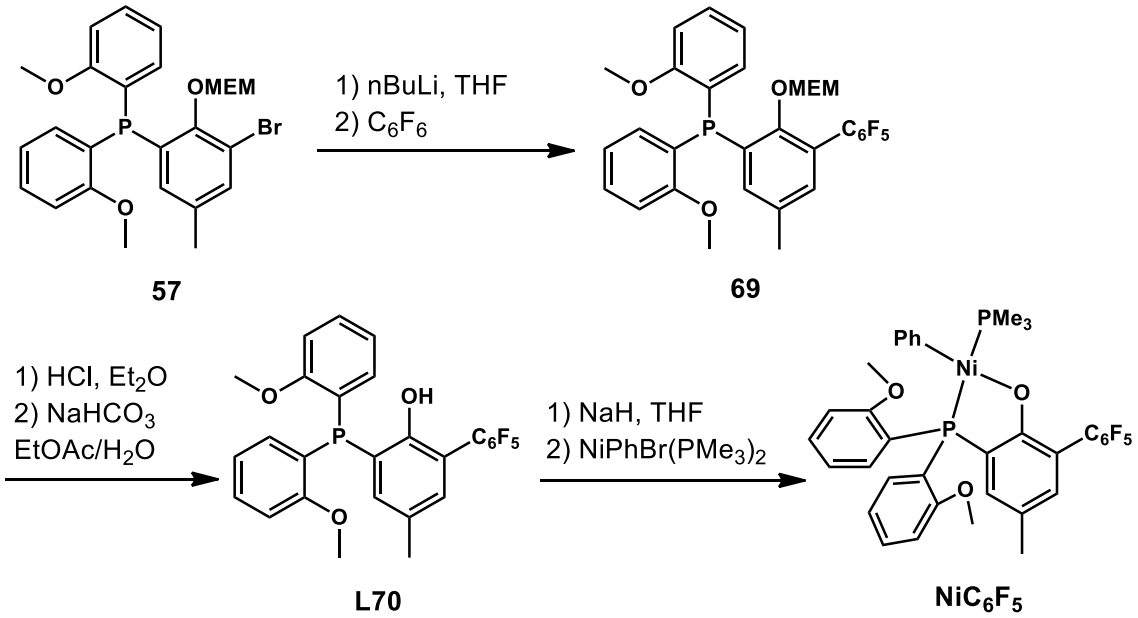

Scheme 3.1. Synthesis of **NiC$_6$F$_5$** complex.

Preparation of Compound 69. This synthesis was modified from a literature procedure.[116] To a solution of compound **57** (4.64 g, 8.92 mmol, 1.0 equiv) in 100 mL of dry THF in a 200 mL Schlenk flask under nitrogen at -78 ^{o}C, *n*BuLi (1.6M in hexanes, 6.67 mL, 10.7 mmol, 1.2 equiv) was added dropwise using a syringe pump. The reaction mixture was stirred at -78 ^{o}C for 40 min. Then C_6F_6 (3.32 g, 2.1 mL, 17.87 mmol, 2.0 equiv) was added dropwise via syringe. The resulting mixture was naturally warmed to room temperature and stirred overnight. The reaction was quenched by the slow

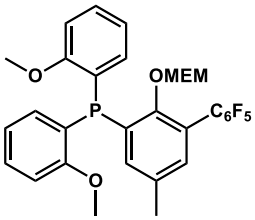

addition of H_2O and the products were extracted into Et_2O (3×100 mL). The organic layers were combined, washed with H_2O (2×100 mL), dried over Na_2SO_4, filtered, and evaporated to dryness. The crude material was purified by silica gel column chromatography (3:1 hexane: ethyl acetate), followed by washing with pentane (2×10 mL) to afford a white solid (3.1 g, 5.11 mmol, 57%). This compound was used directly in the next step without further purification.

Preparation of Compound L70. This synthesis was modified from a literature procedure.[116]

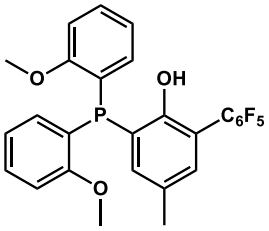

Compound **69** (3.1 g, 5.11 mol, 1.0 equiv) was dissolved in 50 mL of MeOH and then 50 mL solution of 2M HCl in Et_2O was added. The reaction mixture was stirred at room temperature overnight and then dried to remove solvent. The product was dissolved in 200 mL of EtOAc along and then combined with 50 mL of 1M aqueous $NaHCO_3$. The mixture was stirred at room temperature for 30 min and the product was extracted into Et_2O (3×100 mL). The organic layers were combined, washed with H_2O (2×100 mL), dried over Na_2SO_4, filtered, and evaporated to dryness. The crude material was purified by silica gel column chromatography (3:1 hexane:ethyl acetate). The resulting product was further recrystallized using a mixture of pentane and dichloromethane to afford a white solid (1.9 g, 3.66 mmol, 72%). ^{1}H NMR (500 MHz, Benzene-d_6): δ 7.27 – 7.17 (m, 3H), 7.07 – 6.99 (m, 3H), 6.80 (s, 1H), 6.70 (t, J = 7.4 Hz, 2H), 6.36 (dd, J = 8.1, 5.0 Hz, 2H), 3.09 (s, 6H), 1.82 (s, 3H). ^{13}C NMR (126 MHz, Benzene-d_6): δ 161.35, 161.23, 155.93, 137.96, 137.87, 133.98, 133.28, 130.64, 122.72, 121.48, 121.23, 113.17, 110.42, 54.88, 19.95. ^{19}F NMR (470 MHz, Benzene-d_6): δ -140.43 (dd, J = 24.7, 6.9 Hz), -156.43 (t, J = 21.5 Hz), -163.32 – -163.53 (m). ^{31}P NMR (202 MHz, Benzene-d_6) δ -47.26.

Preparation of Complex NiC$_6$F$_5$. Inside the glovebox, ligand **L67** (0.193 g, 0.37 mmol, 1 equiv) was dissolved in 10 mL of THF. Small aliquots of NaH (60%, 0.3 g, 0.74, 2.0 equiv) were added and the mixture was stirred at room temperature for 2h. The solution was filtered to remove excess NaH and then combined with a solution of NiPhBr(PMe$_3$)$_2$ (0.121 g, 0.33 mmol, 0.9 equiv) in 5 mL of benzene. The resulting mixture was stirred at room temperature overnight. The precipitate formed was removed by filtration and the filtrate was dried under vacuum. The crude material was dissolved in a mixture of 5 mL of pentane and 5 mL of toluene and the solution was filtered once again before evaporating dryness. Finally, the resulting solid was washed with pentane (5×3 mL) and dried under vacuum to afford a yellow powder (0.153 g, 0.21 mmol, 64%). ^{1}H NMR (500 MHz, Benzene-d_6) δ 7.53 – 7.44 (m, 2H), 7.14 (d, J = 7.4 Hz, 2H), 7.09 (d, J = 11.1 Hz, 2H), 7.02 (t, J = 7.8 Hz, 2H), 6.90 (s, 1H), 6.68 (t, J = 7.4 Hz, 2H), 6.62 (t, J = 7.4 Hz, 2H), 6.57 (t, J = 7.1 Hz, 1H), 6.36 (dd, J = 8.0, 4.6 Hz, 2H), 3.01 (s, 6H), 1.91 (s, 3H), 0.55 (d, J = 9.3 Hz, 9H). ^{13}C NMR (101 MHz, Benzene-d_6) δ 170.72, 170.45, 158.58, 158.53, 134.79, 131.74, 129.16, 123.22, 120.18, 120.12, 118.46, 118.38, 112.76, 108.48, 108.45, 52.69, 17.86, 8.94, 8.69. ^{19}F NMR (470 MHz, Benzene-d_6) δ -138.98 (dd, J = 24.8, 6.3 Hz), -159.39 (t, J = 21.5 Hz), -165.02 (td, J = 22.3, 6.5 Hz). ^{31}P NMR (202 MHz, Benzene-d_6) δ 10.57 (d, J = 288 Hz), -15.12 (d, J = 288 Hz).

Metal-Binding Studies

***UV-Vis Absorption Spectroscopy: Metal Titration*.** Stock solutions of **Ni11** and MBAr$^F_4$ were prepared inside an inert nitrogen-filled glovebox. A 500 μM stock solution of **Ni11** were obtained by dissolving 25 μmol of **Ni11** in 50 mL of Et$_2$O. A 10 mL aliquot of this 500 μM solution was diluted to 50 mL using a volumetric flask to give a final concentration of 100 μM. The 3.0 mM

stock solution of $MBAr^F_4$ was obtained by dissolving 30 μmol of $MBAr^F_4$ in 10 mL of Et_2O using a volumetric flask. A 3.0 mL solution of **Ni11** was transferred to a 1 cm quartz cuvette and then sealed with a septum screw cap. A 100 μL airtight syringe was loaded with the 3.0 mM solution of $MBAr^F_4$. The cuvette was placed inside a UV-vis spectrophotometer and the spectrum of the **Ni11** solution was recorded. Aliquots containing 0.1 equiv of $MBAr^F_4$ (10 μL), relative to the nickel complex, were added and the solution was allowed to reach equilibrium before the spectra were measured (about 20−30 min). The titration experiments were stopped after the addition of up to 1.0 equiv of $MBAr^F_4$.

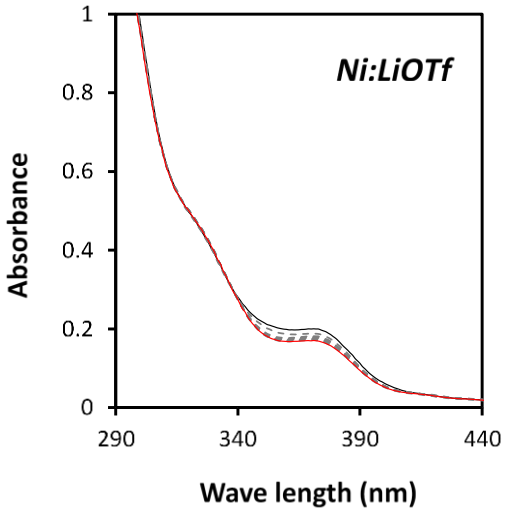

Figure 3.28. UV-vis absorbance spectra of complex **Ni11 (**100 μM in Et_2O) after the addition of various aliquots of LiOTf. The starting trace of **Ni11** is shown in black and the final trace (+ 1.0 equiv of Li^+ relative to Ni) is shown in red.

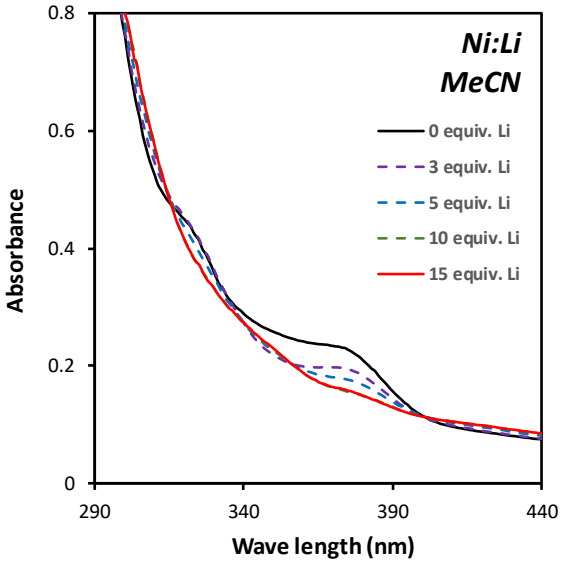

Figure 3.29. UV-vis absorbance spectra of complex **Ni11 (**100 μM in MeCN) after the addition of various aliquots of $LiBAr^F{}_4$. The starting trace of **Ni11** is shown in black and the final trace (+ 15.0 equiv of Cs^+ relative to Ni) is shown in red.

UV-Vis Absorption Spectroscopy: Job Plot Studies.

Stock solutions of **Ni11** (500 µM) and $MBAr^F{}_4$ (500 µM) (M = Li, Na, K and Cs) in Et_2O were prepared in separate volumetric flasks inside the drybox. Stock solutions of **Ni11** and $MBAr^F{}_4$ were combined in different ratios to give 10 different samples, each having a final volume of 3.0 mL. The samples were recorded by UV-vis absorption spectroscopy at RT.

The UV-vis spectral data were analyzed according to the method reported by Hirose.[68] In our case, the host (H) is **Ni11**, the guest (g) is M^+, and the complex (C) is **Ni11**-M. Since the alkali salt has no absorption in the 300-500 nm range, we used this simplified expression to analyze the data: $A_{obs} - \varepsilon_h \cdot [H]_t = (\varepsilon_C - a \cdot \varepsilon_h) \cdot [C]$, where A_{obs} = observed absorbance, a = constant, ε_h = molar absorptivity of host **Ni11**, ε_C = molar absorptivity of **Ni11**-M, $[H]_t$ = starting concentration of host **Ni11**, and [C] = observed concentration of **Ni11**-M. Since [C] is proportional to $A_{obs} - \varepsilon_h \cdot [H]_t$, a Job Plot was constructed by plotting $A_{obs} - \varepsilon_h \cdot [H]_t$ vs. χ_{Ni} (the mole ratio of **Ni11** = [**Ni11**]/([**Ni11**]+[Na^+])).

Table 3.5. Job Plot Data and Calculations Used for **NiL**-Li[a]

χ_{Ni}	**Volume of Stock Soln of H** (mL)	**Amount of H Added** (mol)	**Final Conc. of H** (M)	A_h (calculated)	A_{obs} (@379 nm)	A_{obs}-A_h
1.0	3.000E-03	1.500E-06	5.000E-04	1.482E+00	1.482E+00	0.000E+00
0.9	2.700E-03	1.350E-06	4.500E-04	1.334E+00	1.295E+00	3.873E-02
0.8	2.400E-03	1.200E-06	4.000E-04	1.186E+00	1.028E+00	1.582E-01
0.7	2.100E-03	1.050E-06	3.500E-04	1.038E+00	7.182E-01	3.195E-01
0.6	1.800E-03	9.000E-07	3.000E-04	8.894E-01	4.922E-01	3.972E-01
0.5	1.500E-03	7.500E-07	2.500E-04	7.412E-01	2.411E-01	5.001E-01
0.4	1.200E-03	6.000E-07	2.000E-04	5.929E-01	1.442E-01	4.488E-01
0.3	9.000E-04	4.500E-07	1.500E-04	4.447E-01	1.031E-01	3.416E-01
0.2	6.000E-04	3.000E-07	1.000E-04	2.965E-01	6.749E-02	2.290E-01
0.1	3.000E-04	1.500E-07	5.000E-05	1.482E-01	3.717E-02	1.111E-01

[a]The molar absorptivity of H (ε_h) at 379 nm = 2965 $M^{-1}cm^{-1}$. Stock solution of H is 500 µM.

Table 3.6. Job Plot Data and Calculations Used for **NiL**-Na[a]

χ_{Ni}	**Volume of Stock Soln of H** (mL)	**Amount of H Added** (mol)	**Final Conc. of H** (M)	A_h (calculated)	A_{obs} (@379 nm)	A_{obs}-A_h
1.0	3.000E-03	1.500E-06	5.000E-04	1.238E+00	1.238E+00	0.000E+00
0.9	2.700E-03	1.350E-06	4.500E-04	1.115E+00	1.059E+00	5.543E-02
0.8	2.400E-03	1.200E-06	4.000E-04	9.908E-01	8.340E-01	1.568E-01
0.7	2.100E-03	1.050E-06	3.500E-04	8.669E-01	5.645E-01	3.024E-01
0.6	1.800E-03	9.000E-07	3.000E-04	7.431E-01	3.553E-01	3.877E-01
0.5	1.500E-03	7.500E-07	2.500E-04	6.192E-01	1.951E-01	4.241E-01
0.4	1.200E-03	6.000E-07	2.000E-04	4.954E-01	1.578E-01	3.376E-01
0.3	9.000E-04	4.500E-07	1.500E-04	3.715E-01	1.149E-01	2.567E-01
0.2	6.000E-04	3.000E-07	1.000E-04	2.477E-01	7.796E-02	1.697E-01
0.1	3.000E-04	1.500E-07	5.000E-05	1.238E-01	4.617E-02	7.768E-02

[a]The molar absorptivity of H (ε_h) at 379 nm = 2477 $M^{-1}cm^{-1}$. Stock solution of H is 500 µM.

Table 3.7. Job Plot Data and Calculations Used for **NiL**-K[a]

χ_{Ni}	**Volume of Stock Soln of H** (mL)	**Amount of H Added** (mol)	**Final Conc. of H** (M)	A_h (calculated)	A_{obs} (@379 nm)	A_{obs}-A_h
1.0	3.000E-03	1.500E-06	5.000E-04	1.201E+00	1.201E+00	0.000E+00
0.9	2.700E-03	1.350E-06	4.500E-04	1.081E+00	1.073E+00	7.443E-03
0.8	2.400E-03	1.200E-06	4.000E-04	9.606E-01	8.741E-01	8.649E-02
0.7	2.100E-03	1.050E-06	3.500E-04	8.406E-01	6.233E-01	2.172E-01
0.6	1.800E-03	9.000E-07	3.000E-04	7.205E-01	4.245E-01	2.959E-01
0.5	1.500E-03	7.500E-07	2.500E-04	6.004E-01	2.225E-01	3.779E-01
0.4	1.200E-03	6.000E-07	2.000E-04	4.803E-01	1.635E-01	3.168E-01
0.3	9.000E-04	4.500E-07	1.500E-04	3.602E-01	1.167E-01	2.435E-01
0.2	6.000E-04	3.000E-07	1.000E-04	2.402E-01	8.181E-02	1.583E-01
0.1	3.000E-04	1.500E-07	5.000E-05	1.201E-01	4.852E-02	7.156E-02

[a]The molar absorptivity of H (ε_h) at 379 nm = 2402 $M^{-1}cm^{-1}$. Stock solution of H is 500 µM

Table 3.8. Job Plot Data and Calculations Used for **NiL**-Cs[a]

χ_{Ni}	**Volume of Stock Soln of H** (mL)	**Amount of H Added** (mol)	**Final Conc. of H** (M)	A_h (calculated)	A_{obs} (@379 nm)	A_{obs}-A_h
1.0	3.000E-03	1.500E-06	5.000E-04	1.248E+00	1.25E+00	0.00E+00
0.9	2.700E-03	1.350E-06	4.500E-04	1.123E+00	1.077E+00	4.655-02
0.8	2.400E-03	1.200E-06	4.000E-04	9.986E-01	8.902-01	1.083-01
0.7	2.100E-03	1.050E-06	3.500E-04	8.738E-01	7.320-01	1.417-01
0.6	1.800E-03	9.000E-07	3.000E-04	7.489E-01	5.451-01	2.038-01
0.5	1.500E-03	7.500E-07	2.500E-04	6.241E-01	3.829-01	2.412-01
0.4	1.200E-03	6.000E-07	2.000E-04	4.993E-01	3.0169-01	1.976-01
0.3	9.000E-04	4.500E-07	1.500E-04	3.745E-01	2.421-01	1.323-01
0.2	6.000E-04	3.000E-07	1.000E-04	2.496E-01	1.557-01	9.391-02
0.1	3.000E-04	1.500E-07	5.000E-05	1.248E-01	8.926-02	3.556-02

[a]The molar absorptivity of H (ε_h) at 379 nm = 2500 $M^{-1}cm^{-1}$. Stock solution of H is 500 µM.

Polymerization Studies

General Procedure for Ethylene Polymerization.

Inside the drybox, the nickel complex **Ni11** and $MBAr^F{}_4$ (if any) were dissolved in a mixture of 8 mL of toluene and 2 mL of Et_2O (if any) in a 20 mL vial and stirred for 10 min. Solid $Ni(COD)_2$ (8 equiv relative to nickel) was added and stirred until a clear solution was obtained (4−5 min). The mixture was loaded into a 10 mL syringe equipped with an 8-inch stainless steel needle. The loaded syringe was sealed by sticking the needle tip into a rubber septum and brought outside of the drybox. To prepare the polymerization reactor, 90 mL of dry toluene was placed in an empty autoclave. The autoclave was pressurized with ethylene to 80 psi, stirred for 5 min, and then the reactor pressure was reduced to 5 psi. This process was repeated three times to remove trace amounts of oxygen inside the reaction vessel. The reactor was then heated to the desired temperature and the catalyst solution was injected into the autoclave through a side arm. The autoclave was sealed and purged with ethylene at 40 psi (no stirring) three times. Finally, the reactor pressure was increased to the desired pressure, and the contents were stirred vigorously. To stop the polymerization, the autoclave was vented and cooled in an ice bath. A solution of MeOH (700 mL) was added to precipitate the polymer. The polymer was collected by vacuum filtration, rinsed with MeOH, and dried under vacuum at 80 °C overnight. The reported yields are average values obtained from duplicate or triplicate runs.

Special Notes:

- To obtain consistent polymer yields from run to run, the amount of catalyst used in each run must be kept as consistent as possible. Since 0.5 μmol of the **Ni11** catalyst weighs only 0.37 mg, it is extremely difficult to weigh out exactly this amount using a standard analytical balance.

To minimize errors due to weighing inconsistencies, we used a batch catalyst preparation method. First, we weighed out 37 mg (50 μmol) of the catalyst and then dissolved it into 50 mL of toluene. This solution was divided equally into 10 vials so that each vial contained 5 μmol of catalyst. Next, we combined each 5 μmol of catalyst with 20 mL of toluene and partitioned this 25 mL mixture into 10 vials so that each vial contained 0.5 μmol of catalyst. Finally, each vial was dried completely under vacuum and stored in a refrigerator inside the drybox until ready for use.

- For reactions using 0.1 μmol of the **Ni11** catalyst, the catalyst preparation was similar to the procedure mentioned above.
- For all polymerization reactions, except ones that were performed to determine the temperature profiles, the reaction temperature was controlled by manual cooling of the reactor with an air stream when the reactor increases more than 5 °C above the starting temperature.
- To clean the Parr reactor, the vessel was washed with hot toluene (80 ^{o}C) to remove the polymer sample from the previous run and rinsed with acetone before drying under vacuum for at least 1 h to remove trace amounts of water.

Table 3.9. Ethylene Polymerization Study of **Ni11**-M Bimetallic Complexes in Benzene and DCM[a]

Entry	Complex	solvent		polymer yield (g)	activity (kg/mol·h)	M_n[b] (× 10^3)	M_w/M_n[b]
		benzene (mL)	DCM (mL)				
1	**Ni11**-Li	100	–	4.3	43000	35.76	1.3
2	**Ni11**-Na	100	–	8.4	16800	1.9	1.4
3	**Ni11**-K	100	–	7.2	14400	6.06	1.6
4	**Ni11**-Cs	100	–	0.13	260	48.17	1.3
5	**Ni11**-Li	–	100	1.53	3060	39.3	1.3
6	**Ni11**-Na	–	100	0.25	500	1.06	1.4
7	**Ni11**-K	–	100	0.61	1220	5.86	1.3
8	**Ni11**-Cs	–	100	0.22	440	15.99	1.3

[a]Polymerization conditions: **Ni11** (0.5 μmol), $MBAr^F_4$ (1 μmol, if any), $Ni(COD)_2$ (4 μmol), ethylene (450 psi), 100 mL toluene, 30 °C, 1h. Temperature was controlled by manual external cooling when necessary to ensure that the reaction temperature does not exceed greater than 5 °C from the starting temperature. [b]Determined by GPC in trichlorobenzene at 140 °C. [c]**Ni11** (0.1 μmol), $MBAr^F_4$ (0.2 μmol, if any), $Ni(COD)_2$ (0.8 μmol). [d]2 mL of Et_2O was added to help dissolving the alkali salts.

Table 3.10. Temperature Study for **Ni11-**Li Complex in Ethylene Polymerization[a]

Entry	**Temp.** (°C)	**Polymer yield** (g)	**Activity** (kg/mol·h)	M_n[b] (× 10^3)	M_w/M_n[b]
1	30	3.53	35300	40.1	1.3
2	40	5.18	51800	25.8	1.3
3[c]	40	6.97	69700	25.0	1.4
4[d]	40	4.47	89400	21.7	1.2
5	50	3.84	38400	12.1	1.3
6	60	2.29	22900	10.5	1.3
7	70	1.82	18200	6.2	1.3
8	80	1.89	18900	3.1	2
9	90	1.31	13100	2.09	2.2

[a]Polymerization conditions: **Ni11** (0.1 μmol), $LiBAr^F{}_4$ (0.2 μmol), $Ni(COD)_2$ (0.4 μmol), ethylene (450 psi), 100 mL toluene, 1h. Temperature was controlled by manual external cooling when necessary to ensure that the reaction temperature does not exceed greater than 5 °C from the starting temperature. [b]Determined by GPC in trichlorobenzene at 140 °C. [c]200 mL of toluene solvent was used. [d]Reaction was run for 0.5 h.

Table 3.11. Solvent Study for **Ni11**-Li in Ethylene Polymerization[a]

Entry	Solvent	Polymer yield (g)	Activity (kg/mol·h)	Branches[b] (/1000 C)	M_n[c] (× 10^3)	M_w/M_n[c]
1	**Pentane**	4.5	45000	4	44.02	1.4
2	**Hexane**	5.5	55000	4	68.15	1.4
3	**Benzene**	5.3	53000	6	35.76	1.3
4	**Toluene**	3.53	35300	12	33.93	1.5
5[d]	**DCM**	1.53	3060	7	39.3	1.3
6[e]	**Et_2O**	10.8	10800	6	37.86	1.6
7[e]	**MeCN**	trace	0	–	–	–

[a]Polymerization conditions: **Ni11** (0.1 μmol), $LiBAr^F{}_4$ (0.2 μmol), $Ni(COD)_2$ (0.8 μmol), ethylene (450 psi), 100 mL solvent, 1h. Temperature was controlled by manual external cooling when necessary to ensure that the reaction temperature does not exceed greater than 5 °C from the starting temperature. [b]The total number of branches per 1000 carbons was determined by ^{1}H NMR spectroscopy. [c]Determined by GPC in trichlorobenzene at 140 °C. [d] **Ni11** (0.5 μmol), $LiBAr^F{}_4$ (1 μmol), $Ni(COD)_2$ (4 μmol). [e] **Ni11** (1 μmol), $LiBAr^F{}_4$ (2 μmol), $Ni(COD)_2$ (8 μmol).

Table 3.12. Salt/Catalyst Ratio Screening for **Ni11** in Ethylene Polymerization[a]

Entry	**Catalyst amount** (μmol)	**Ni[COD]$_2$** (μmol)	**Salt**	**Salt equiv**	**Polymer yield** (g)	**Activity** (kg/mol·h)
1	0.5	4	$LiBAr^F{}_4$	2	2.03	12180
2	0.5	4	$LiBAr^F{}_4$	10	3.38	20280
3	0.5	4	$LiBAr^F{}_4$	20	3.54	21240
4	5	20	$NaBAr^F{}_4$	2	2.1	1260
5	5	20	$NaBAr^F{}_4$	10	4.53	2718
6	5	20	$NaBAr^F{}_4$	20	6.6	3960
7	5	20	$KBAr^F{}_4$	2	0.49	294
8	5	20	$KBAr^F{}_4$	10	2.62	1572
9	5	20	$KBAr^F{}_4$	20	3.05	1830

[a]Polymerization conditions: ethylene (450 psi), 50 mL toluene/50 mL Et_2O, 20 min, 30 ºC. Temperature was controlled by manual external cooling when necessary to ensure that the reaction temperature does not exceed greater than 5 °C from the starting temperature.

Table 3.13. Counteranion Effect Study of **Ni11**-Li in Ethylene Polymerization in Toluene Without Temperature Control[a]

Entry	**Salt** (2 equiv)	**Polymer yield** (g)	**Activity** (kg/mol·h)	M_n^c ($\times 10^3$)	M_w/M_n^c	**Branches**[b] (/1000 C)
1	$LiBAr^F{}_4$	12.08	24160	13.3	1.7	–
2	LiTPFB	10.05	20100	11.6	1.4	–
3	$LiBPh_4$	5.36	10720	15.6	1.3	–
4	LiOTf	trace	0	–	–	–

[a]Polymerization conditions: **Ni11** (0.5 µmol), $Ni[COD]_2$ (4 µmol), ethylene (450 psi), 100 mL toluene, 1 h, start reaction at 30 °C. Temperature *was not* controlled by manual external cooling.

Table 3.14. Counteranion Effect Study for **Ni11**-Li in Ethylene Polymerization in a Mixture of Toluene and Et_2O (1:1) With Temperature Control[a]

Entry	**Salt** (2 equiv)	**Polymer yield** (g)	**Activity** (kg/mol·h)	M_n[c] (× 10^3)	M_w/M_n[c]	**Branches**[b] (/1000 C)
1	$LiBAr^F{}_4$	8.96	17920	27.2	1.4	10
2	LiTPFB	8.01	16020	29.2	1.4	8
3	$LiBPh_4$	3.89	7780	32.19	1.3	4
4	LiOTf	trace	0	–	–	–

[a]Polymerization conditions: **Ni11** (0.5 µmol), $Ni[COD]_2$ (4 µmol), ethylene (450 psi), 50 mL toluene/50 mL Et_2O, 1 h, 30 ºC. Temperature was controlled by manual external cooling when necessary to ensure that the reaction temperature does not exceed greater than *10°C* from the starting temperature.

Table 3.15. Time-Dependent Catalyst Activity of Ni11-Li (5 μM)[a]

Entry	Time (min)	Polymer yield (g)	Activity (kg/mol·h)	M_n[c] (× 10^3)	M_w/M_n[c]	Branches[b] (/1000 C)
1	8	2.8	42000	–	–	–
2	13	7.26	67015	–	–	–
3	14	8.93	76543	–	–	–
4	19	9.59	60568	–	–	–
5	27	13.74	61067	–	–	–
6	60	12.08	24160	–	–	–

[a]Polymerization conditions: **Ni11** (0.5 μmol), $Ni[COD]_2$ (4 μmol), ethylene (450 psi), 100 mL toluene, 1 h, start reaction at 30 ºC. Temperature *was not* controlled by manual external cooling.

Table 3.16. Additional Study of **Ni11** in Ethylene Polymerization[a]

Entry	Solvent			Salt (equiv)	Polymer yield (g)	Activity (kg/mol·h)	M_n^c ($\times 10^3$)	$\frac{M_n^c}{M_w}$
	Tol. (mL)	Et_2O (mL)	THF (mL)					
1	90	10	–	$KBAr^F{}_4$ (2)	8.1	3240	16.7	1.5
2	90	10	–	$KBAr^F{}_4$ (8)	26.76	10704	5.6	1.6
3	90	–	10	$KBAr^F{}_4$ (8)	1.55	620	13.6	1.3
4	90	–	10	$NaBAr^F{}_4$ (8)	6.44	2576	2.4	1.4
5	90	–	10	$NaBAr^F{}_4$ (30)	13.22	5288	1.57	1.3
6	80	–	20	$NaBAr^F{}_4$ (30)	0.32	128	5.1	1.4
7	80	–	20	$LiBAr^F{}_4$ (30)	1.2	480	11.1	1.4

[a]Polymerization conditions: **Ni11** (5 µmol), $Ni[COD]_2$ (20 µmol), ethylene (150 psi), 100 mL solvent, 1 h, 50 °C. Temperature *was not* controlled by manual external cooling.

Table 3.17. Comparison of Nickel Catalysts Reported in the Literature

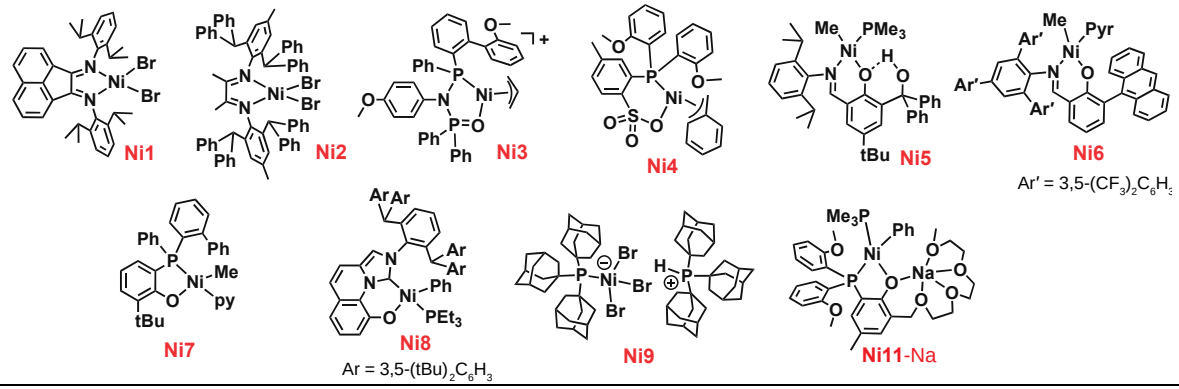

Complex (conc.)	C_2H_4 Pressure (psi)	Temp. (°C)	Time (min)	Activity (kg PE/mol Ni · h)	TON ($\times 10^3$ mol ethylene/ mol Ni)	M_n	$\frac{M_n^c}{M_w}$	Reference (Compound name in original reference)
Ni1 (0.83 μmol in 200 mL)	200	35	10	67200	400	337000	1.8	Brookhart (**4g**)[70]
Ni2 (1.57 μmol in 100 mL)	100	100	10	2856	17	422000	1.2	Long (**2b**)[71]
Ni3 (5.00 μmol in 20 mL)	118	25	60	260	9	188900	2.5	Chen (**Ni4**)[72]
Ni4 (20.0 μmol in 30 mL)	300	25	120	163	12	1500	–	Jordan (**4a**)[73]
Ni5 (10.0 μmol in 25 mL)	118	25	40	1184	28	6700	1.8	Marks (**1b**)[74]
Ni6 (5.00 μmol in 100 mL)	580	30	40	1218	29	466100	1.6	Mecking (**2-CF3/Py**)[84]
Ni7 (5.00 μmol in 100 mL)	145	30	20	2100	25	398000	1.5	Li (**2c**)[100]
Ni8 (2.50 μmol in 8.5 mL)	580	30	30	1000	18	84000	2.0	Nozaki (**7c**)[85]
Ni9 (0.50 μmol in 150 mL)	400	10	3.5	103600	216	1390000	1.4	Daugulis/Brookhart (**6**)[77]
NiL-Na (0.50 μmol in 100 mL)	450	30	60	18100	646	1710	1.5	Do (**Ni11**-Na)
NiL-Li (0.10 μmol in 200 mL)	450	40	60	69700	2484	25000	1.4	This work
NiL-Cs (0.50 μmol in 100 mL)	450	70	30	36480	650	15120	1.7	This work

Table 3.18. Comparison of **Ni11**-Cs Complex and Selected Highly Active Nickel Ethylene Polymerization Catalysts Reported in the Literature at High Temperature.

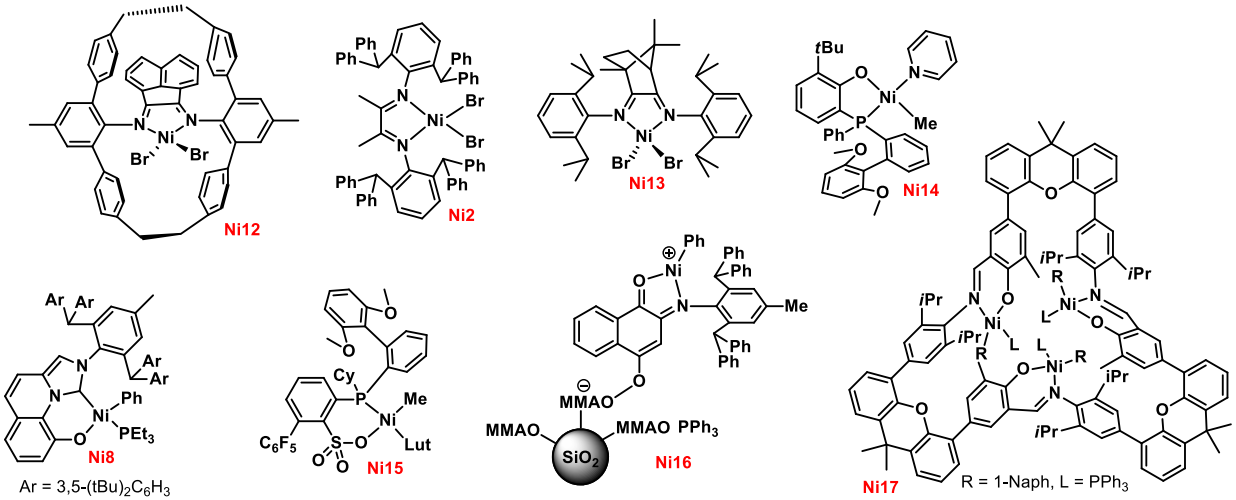

Complex (conc.)	**C_2H_4 Pressure** (psi)	**Temp.** (°C)	**Time** (min)	**Activity** (kg PE/mol Ni· h)	**TON** ($\times 10^3$ mol ethylene/ mol Ni)	M_n	$\frac{M_n^c}{M_w}$	**Reference** (Compound name in original reference)
Ni12 (1.00 μmol in 100 mL)	200	90	15	18513	165	292000	1.4	Guan (**1**)[117]
Ni2 (1.57 μmol in 100 mL)	100	100	10	2856	17	422000	1.2	Long (**2b**)[71]
Ni13 (5.00 μmol in 20 mL)	7.3	80	30	2516	49	233200	2.7	Wu (**4b**)[118]
Ni14 (5.00 μmol in 100 mL)	145	90	20	10020	119	9500	2.7	Li (**2b**)[100]
Ni15 (2.00 μmol in 50 mL)	118	100	30	4000	71	3800	3.49	Chen (**4**)[119]
Ni8 (2.50 μmol in 8.5 mL)	580	100	30	720	13	16000	2.3	Nozaki (**7c**)[85]
Ni16 (5.00 μmol in 30 mL)	145	80	5	2000	6	16800	2.13	Cai (**1**)[120]
Ni17 (40.0 μmol in 20 mL)	90	100	10	27	0.2	9880	3.4	Ma (**3-Ni3**)[121]
NiL-Cs (0.5 μmol in 100 mL)	450	70	30	36480	650	15120	1.7	This work
NiL-Cs (0.5 μmol in 100 mL)	450	90	30	22920	408	15740	1.6	This work

3.9. X-ray Data Collection and Refinement

Single crystals suitable for X-ray diffraction studies were picked out of the crystallization vials and mounted onto Mitogen loops using Paratone oil. The crystals were collected at a 6.0 cm detector distance at –150°C on a Brucker Apex II diffractometer using Mo Kα radiation (λ = 0.71073 Å). The structures were solved by direct methods using the program SHELXT and refined by SHELXLE. Hydrogen atoms connected to carbon were placed at idealized positions using standard riding models and refined isotropically. All non-hydrogen atoms were refined anisoptriocally.

Crystals of complex **Ni11**-Li, **Ni11**-Na, **Ni11**-K, and **Ni11**-Cs were grown by layering of pentane into a solution of the complex and $LiBAr^F_4$, $NaBAr^F_4$, $KBAr^F_4$ and $NaBAr^F_4$, respectively, in a mixture of toluene and Et_2O at -30 ºC. The fluorine atoms of the $MBAr^F_4$ were refined using positional disorder due to free rotation of the CF_3 groups. X-ray data for **NiL**-Na complex was obtained from our previous publication.[58]

Table 3.19. Crystal Data and Structure Refinement for **NiL**-Li, **NiL**-Na, **NiL**-K and **NiL**-Cs.

	NiL-Li	**NiL**-Na	**NiL**-K	**NiL**-Cs
Empirical Formula	$NiLiC_{50}H_{70}O_7P_2$ ($BC_{32}H_{12}F_{24}$)	$NiNaC_{38}H_{30}O_7P_2$ ($BC_{32}H_{12}F_{24}$)	$NiKC_{47}H_{70}O_8P_2$ ($BC_{32}H_{12}F_{24}$)	$NiCsC_{44}H_{56}O_7P_2$ ($BC_{32}H_{12}F_{24}$)
Formula Weight	1773.87	1625.64	1860.00	1813.67
Temperature (°C)	-150	-150	-150	-150
Wavelength (Å)	0.71073	0.71073	0.71073	0.71073
Crystal System	Triclinic	Monoclinic	Triclinic	Monoclinic
Space Group	$P\bar{1}$	$P2_1/c$	$P\bar{1}$	P2(1)/n
Unit Cell Dimensions				
a (Å)	14.2489(12)	21.7805(17)	13.151(3)	17.3656(15)
b (Å)	14.2542(12)	17.3222(14)	13.356(3)	23.606(2)
c (Å)	20.5358(18)	19.7901(16)	24.585(6)	20.3261(18)
α (°)	84.3560(10)	90	86.239(2)	90
β (°)	86.9020(10)	102.5400(10)	81.170(3)	103.6820(10)
γ (°)	86.2420(10)	90	87.895(3)	90
Volume ($Å^3$)	4137.1(6)	7288.4(10)	4256.1(17)	8095.9(12)
Z, Calculated Density (Mg/m^3)	2, 1.424	4, 1.481	2, 1.394	4, 1.488
Absorption Coefficient (mm^{-1})	0.38	0.429	0.418	0.828
F(000)	1820	3312	1836	3656
Theta Range for Data Collection (°)	1.671 to 24.713	1.516 to 27.554	0.840 to 25.350	1.344 to 24.711
Limiting Indices	$-15 \le h \le 16$	$-23 \le h \le 28$	$-15 \le h \le 15$	$-20 \le h \le 20$
	$-15 \le k \le 16$	$-24 \le k \le 22$	$-16 \le k \le 16$	$-24 \le k \le 27$
	$-14 \le l \le 24$	$-25 \le l \le 25$	$-29 \le l \le 29$	$-19 \le l \le 23$
Reflections Collected/ Unique	20662/13855	43028/16670	50354/15533	40225/13791
	[R(int) = 0.0177]	[R(int) = 0.0181]	[R(int) = 0.0429]	[R(int) = 0.0259]
Data/ Restraints/ Parameters	13855 / 203 / 1005	16670 / 57 / 944	15533 / 213 / 998	13791 / 2257 / 962
Goodness of Fit on F^2	1.030	1.053	1.038	1.035
Final R Indices	R_1= 0.0706	R_1= 0.0666	R_1= 0.0985	R_1= 0.1011
[I > 2σ(I)]	wR_2 = 0.1979	wR_2 = 0.1861	wR_2 = 0.2889	wR_2 = 0.2712
R Indices (All Data)*	R_1 = 0.0809	R_1 = 0.0779	R_1 = 0.1301	R_1 = 0.1203
	wR_2 = 0.2086	wR_2 = 0.2007	wR_2 = 0.3224	wR_2 = 0.2907
Largest Diff. Peak and Hole (e $Å^{-3}$)	1.483 and -0.975	1.893 and -1.533	2.294 and -2.017	2.761 and -1.275

*$R_1 = \Sigma\, ||F_o|-|F_o||/\Sigma|F_o|$; $wR_2 = [\Sigma[w(F_o^2 - F_c^2)^2]/\Sigma[w(F_o^2)_2]]^{1/2}$; GOF = $[\Sigma[w(F_o^2 - F_c^2)_2]/(n-p)]^{1/2}$, where *n* is the number of reflections and *p* is the total number of parameters refine

3.10. Decomposition study by UV-Vis

Ni11 complex (1 equiv) and $MBAr^F{}_4$ alkali salt (5 equiv, if any) was dissolved in a mixture of toluene/diethyl ether (80:20) inside an inert nitrogen-filled glovebox. Next, a 3.0 mL of the resulting solution was transferred to a 1 cm quartz cuvette and then sealed with a septum screw cap. The cuvette was then placed inside a UV-Vis spectrophotometer and heated up to 50 ^oC with stirring. The spectrum of the solution was recorded. Aliquots containing 3 equiv of $B(C_6F_5)_3$ were added and the spectra were measured every three minutes. The experiment was stopped after 3 hours. The spectra were compared to evaluate the stability of the Ni complexes.

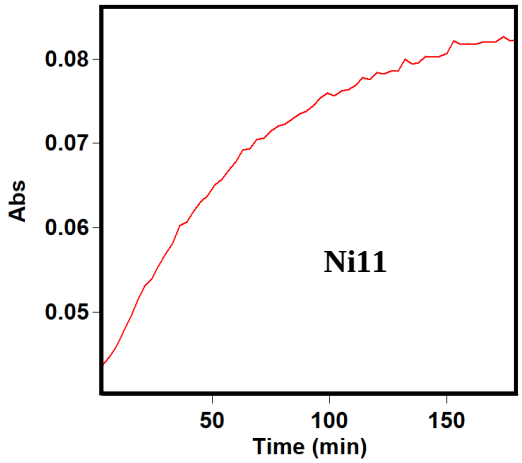

Figure 3.30. UV-vis absorbance spectra at the wavelength of 340 nm of complex **Ni11** after activating by $B(C_6F_5)_3$.

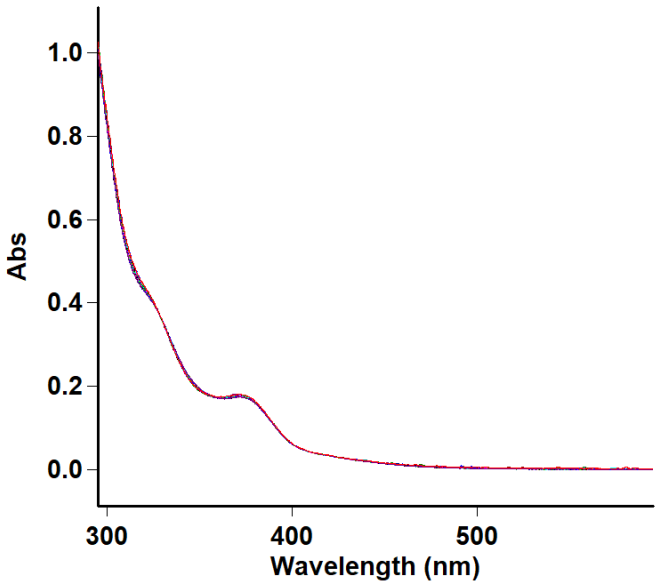

Figure 3.31. UV-vis absorption spectra of **Ni11** at 50 ^{o}C. Kinetic scan was run for 3 h.

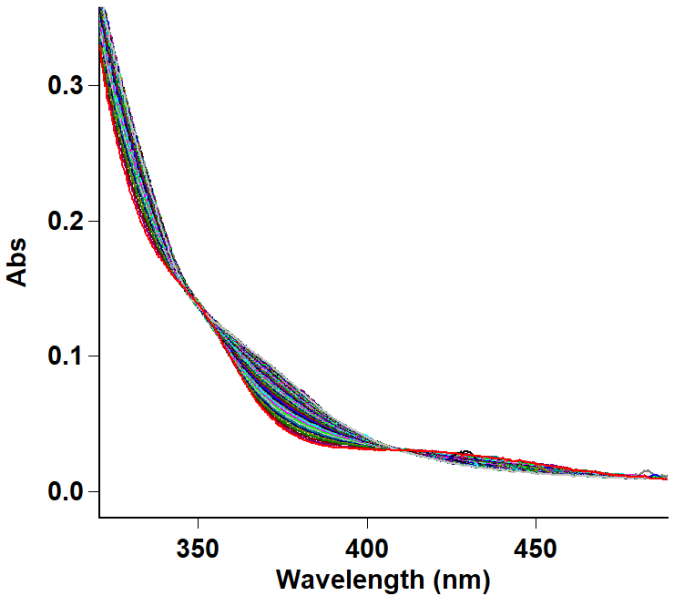

Figure 3.32. UV-vis absorption spectra of **Ni11** after activating with $B(C_6F_5)_3$ at 50 ^{o}C. Kinetic scan was run for 3 h.

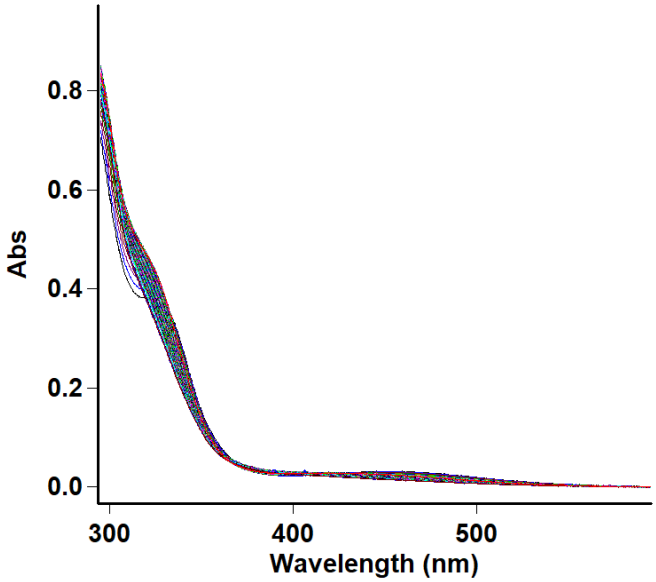

Figure 3.33. UV-vis absorption spectra of **Ni11**-Li after activating with $B(C_6F_5)_3$ at 50 ^oC. Kinetic scan was run for 6 h.

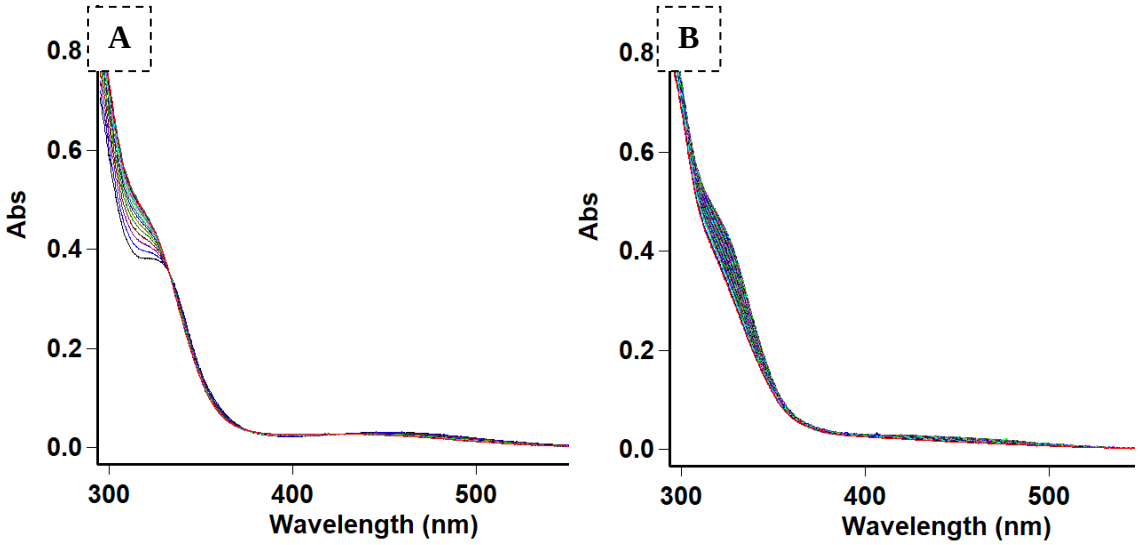

Figure 3.34. Kinetic traces of **Ni11**-Li: A) within 51 min and B) after 51 min. Data obtained from Figure 3.39.

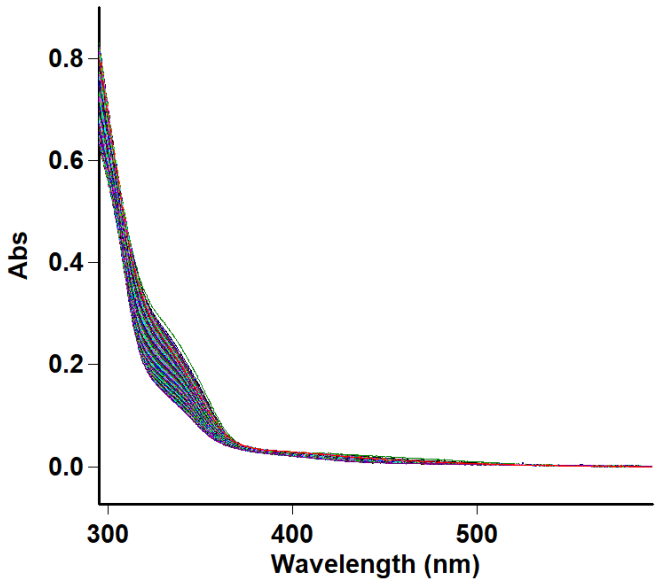

Figure 3.35. UV-vis absorption spectra of **Ni11**-Na after activating with $B(C_6F_5)_3$ at 50 ºC. Kinetic scan was run for 6 h.

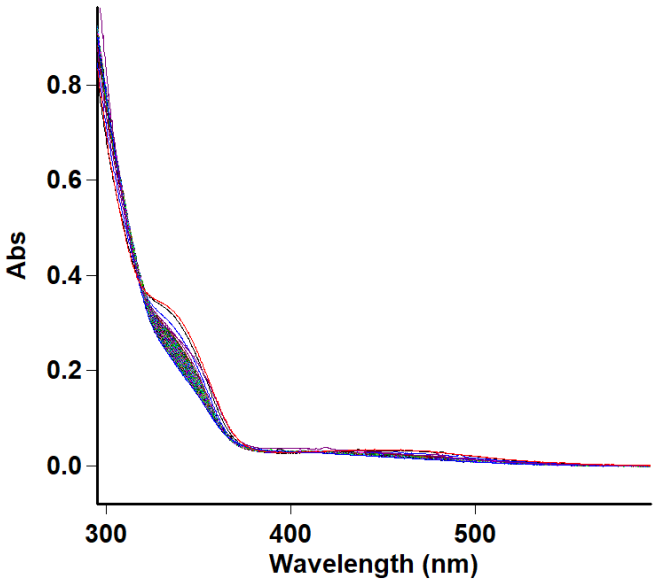

Figure 3.36. UV-vis absorption spectra of **Ni11**-K after activating with $B(C_6F_5)_3$ at 50 ºC. Kinetic scan was run for 6 h.

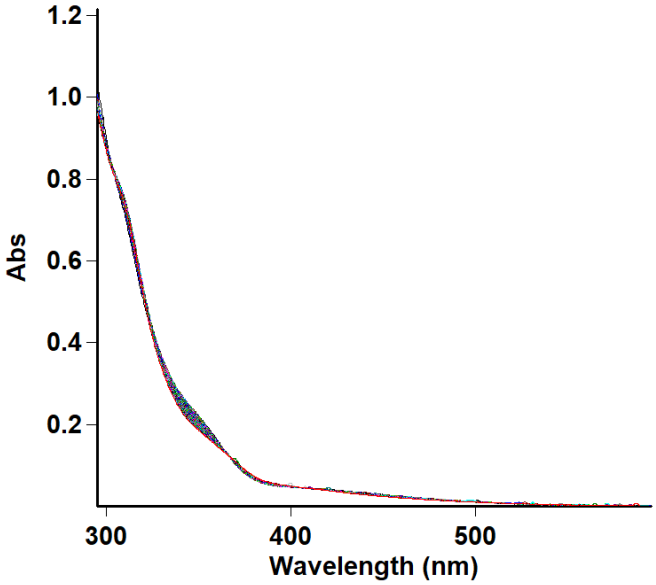

Figure 3.37. UV-vis absorption spectra of **Ni11**-Cs after activating with $B(C_6F_5)_3$ at 50 ºC. Kinetic scan was run for 6 h.

3.11. DFT Calculation Data

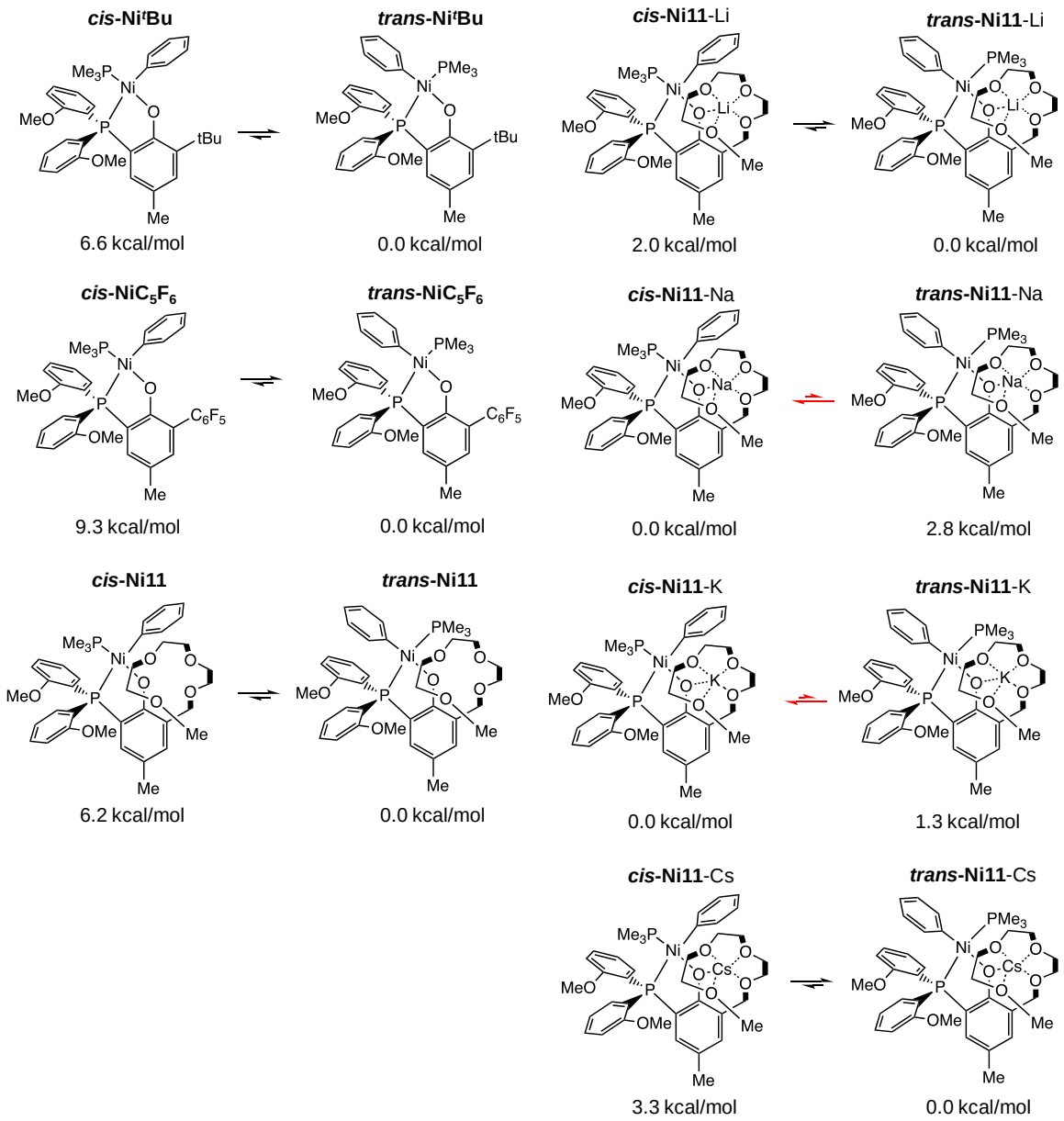

Figure 3.38. Ground state energy for *cis/trans* isomers of nickel complexes.

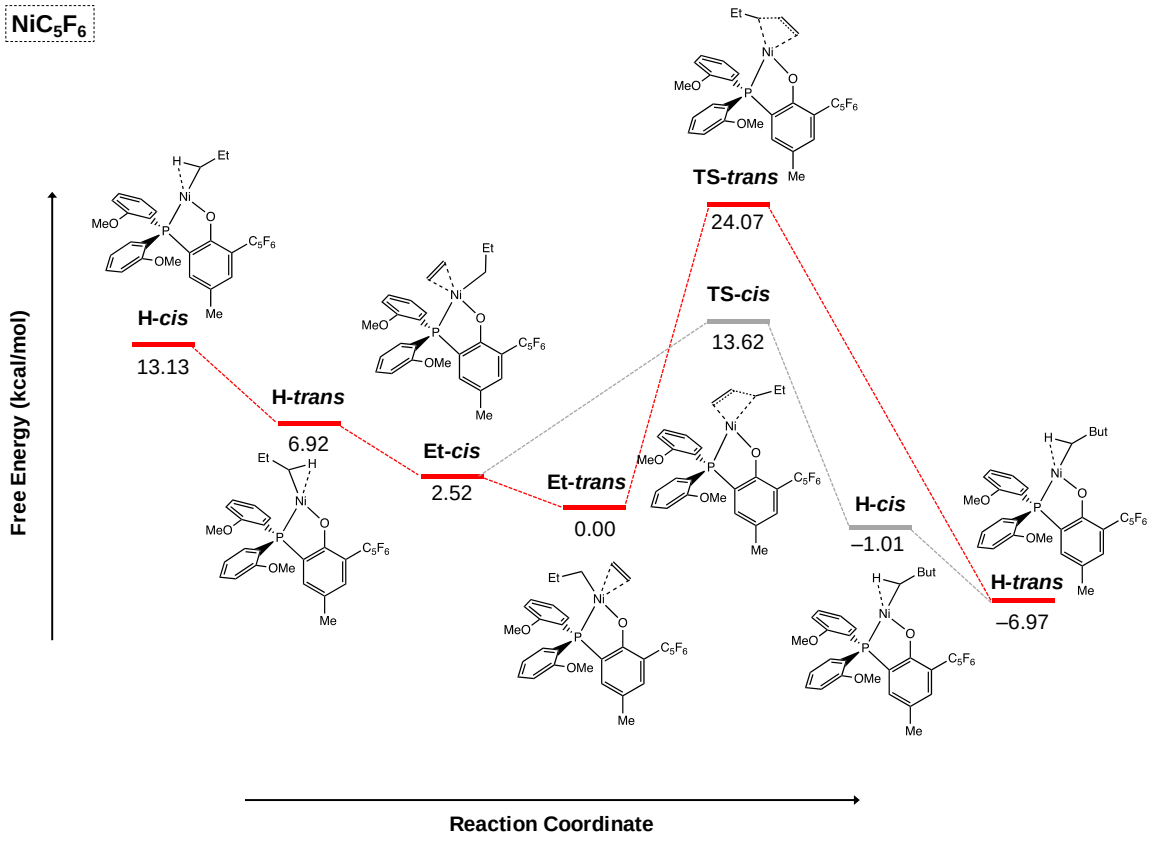

Figure 3.39. Free energy profile of **NiC$_6$F$_5$** in ethylene coordination/insertion polymerization.

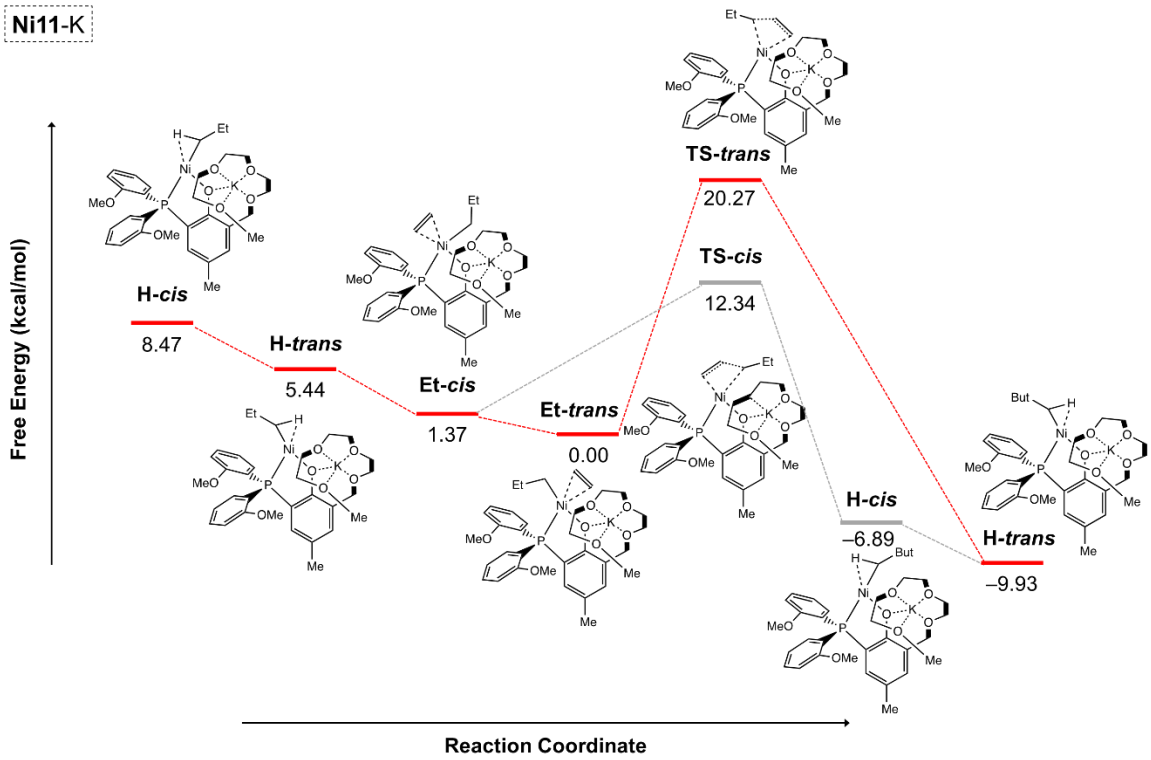

Figure 3.40. Free energy profile of **Ni11**-K in ethylene coordination/insertion polymerization.

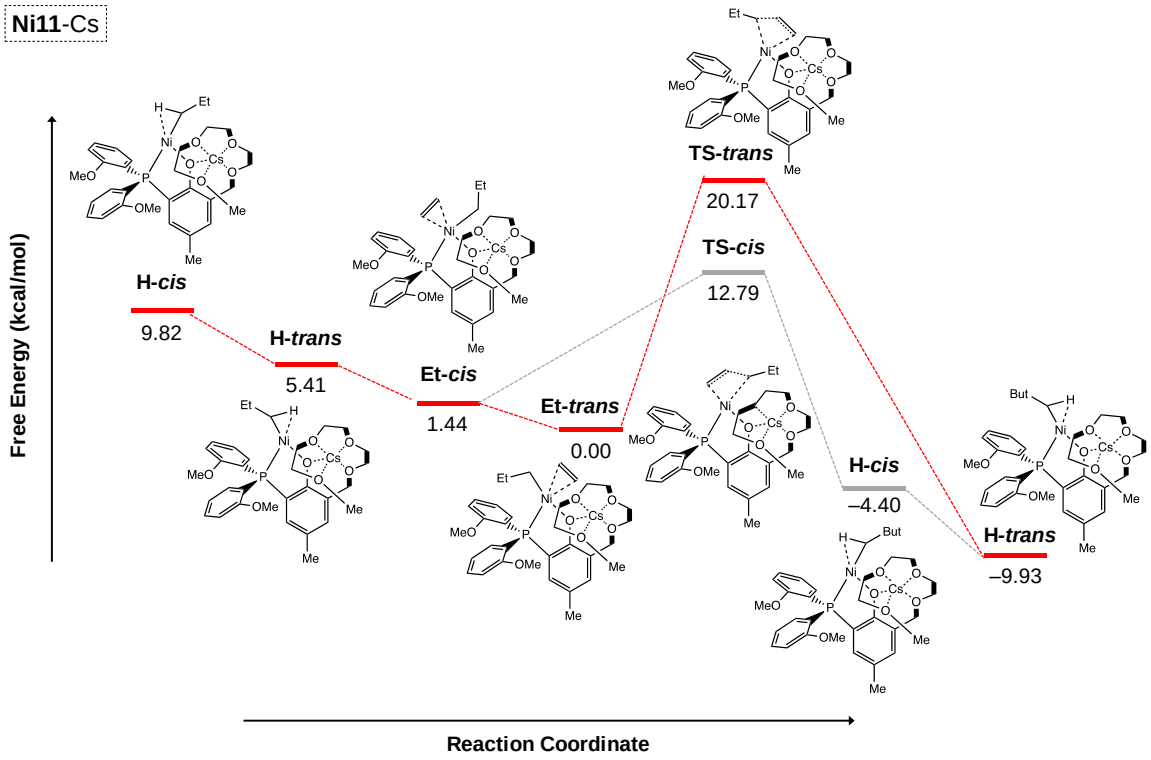

Figure 3.41. Free energy profile of **Ni11**-Cs in ethylene coordination/insertion polymerization.

3.12. Spectral Characterization

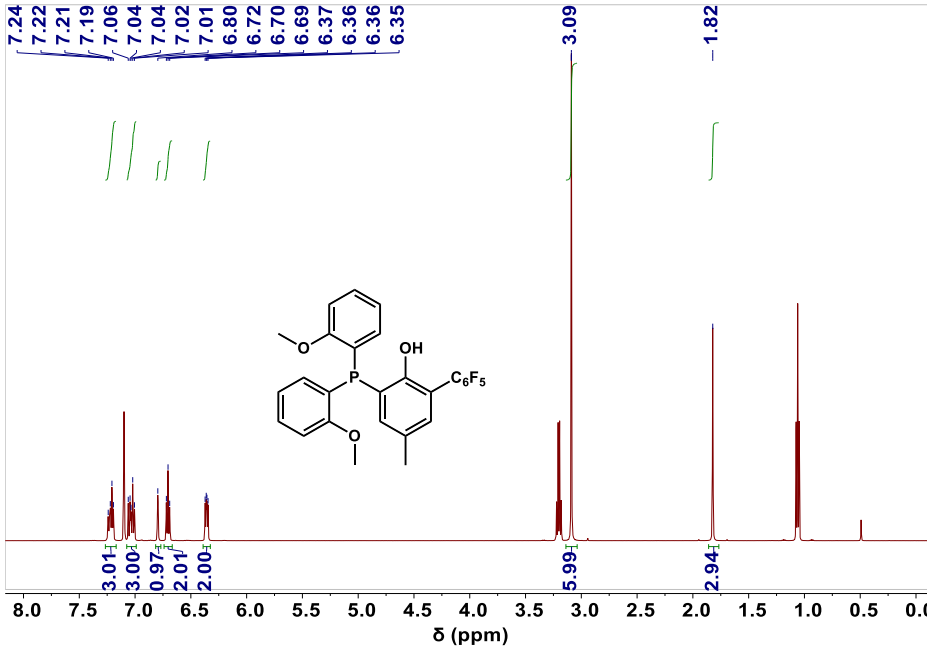

Figure 3.42. ^{1}H NMR spectrum (C_6D_6, 500 MHz) of compound **L70**.

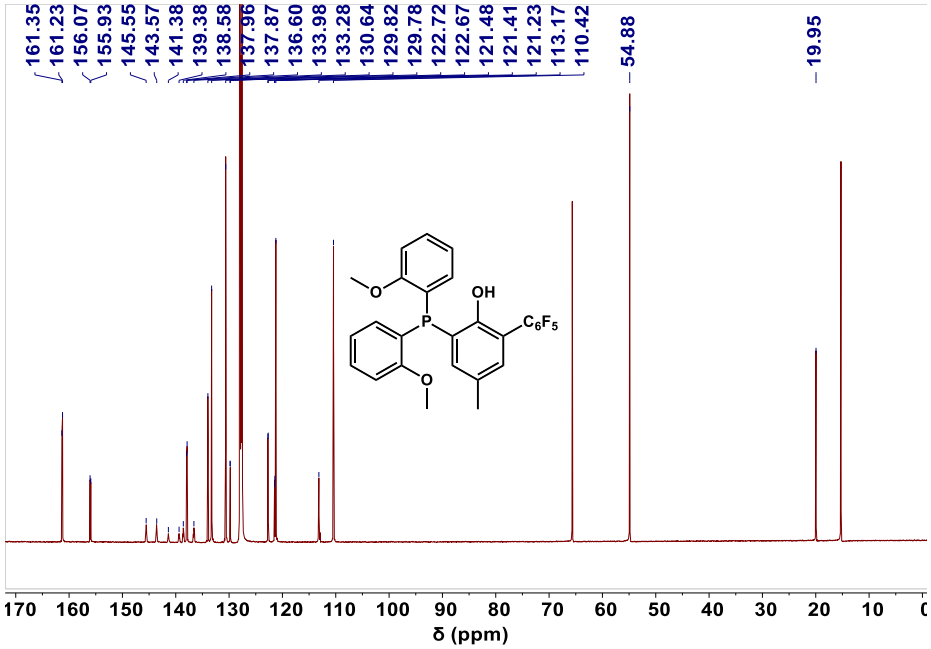

Figure 3.43. ^{13}C NMR spectrum (C_6D_6, 125 MHz) of compound **L70**.

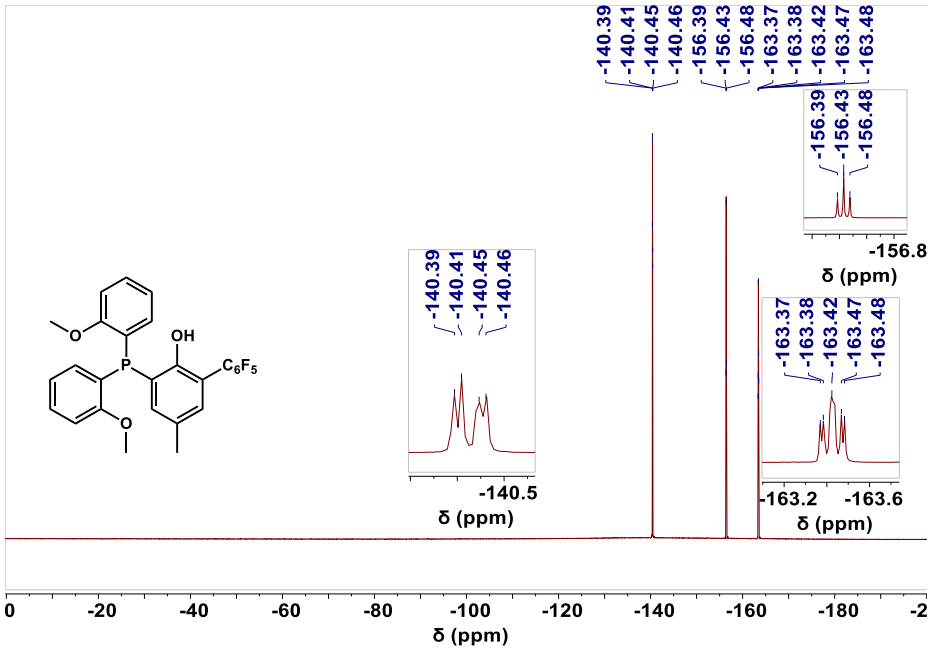

Figure 3.44. ^{19}F NMR spectrum (C_6D_6, 470 MHz) of compound **L70**.

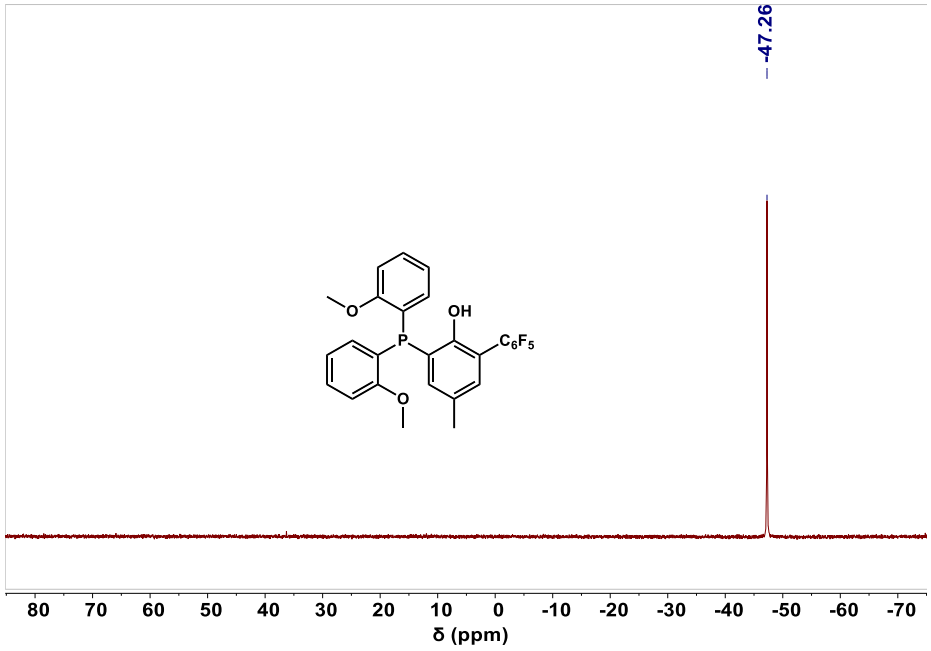

Figure 3.45. ^{31}P NMR spectrum (C_6D_6, 202 MHz) of compound **L70**.

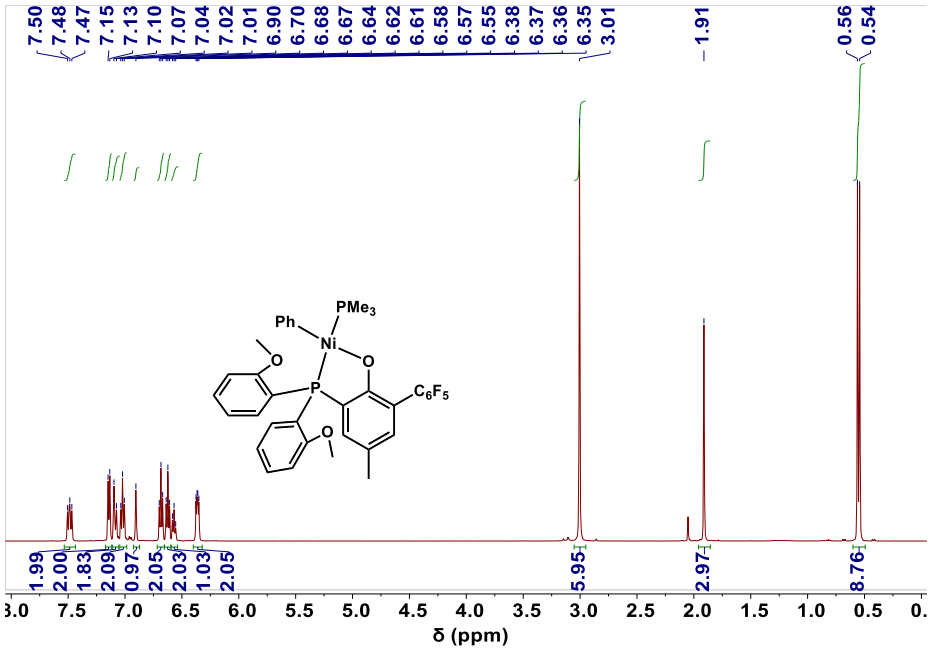

Figure 3.46. ^{1}H NMR spectrum (C_6D_6, 500 MHz) of complex **NiC$_6$F$_5$**.

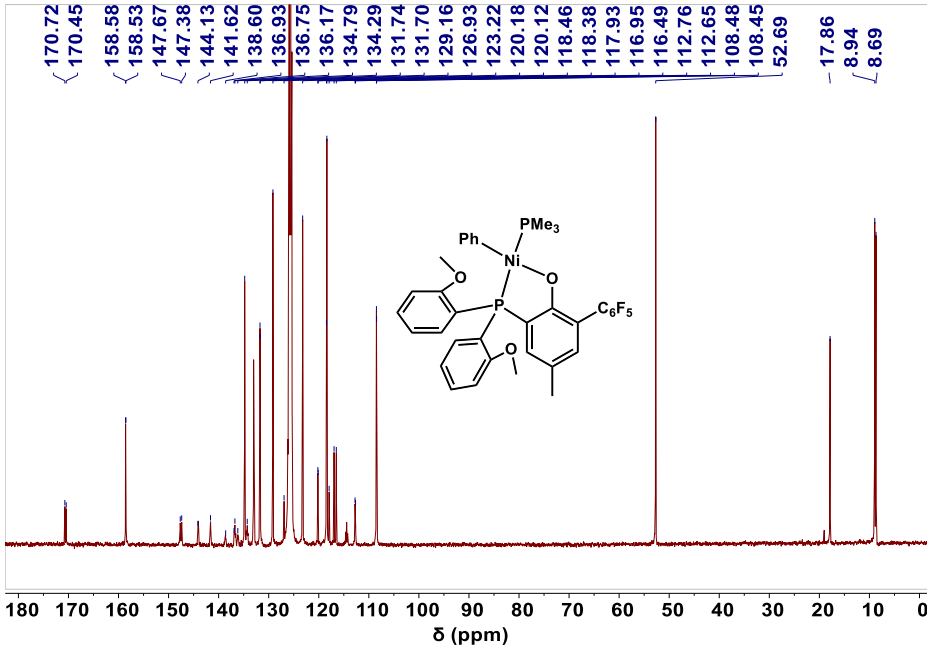

Figure 3.47. ^{13}C NMR spectrum (C_6D_6, 100 MHz) of complex **NiC$_6$F$_5$**.

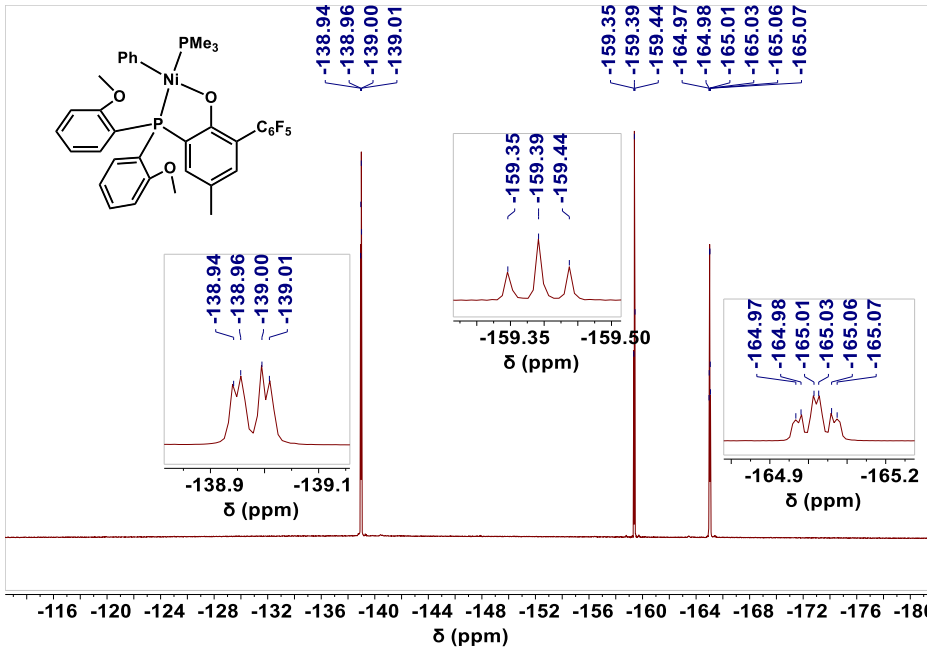

Figure 3.48. ^{19}F NMR spectrum (C_6D_6, 470 MHz) of complex **NiC$_6$F$_5$**.

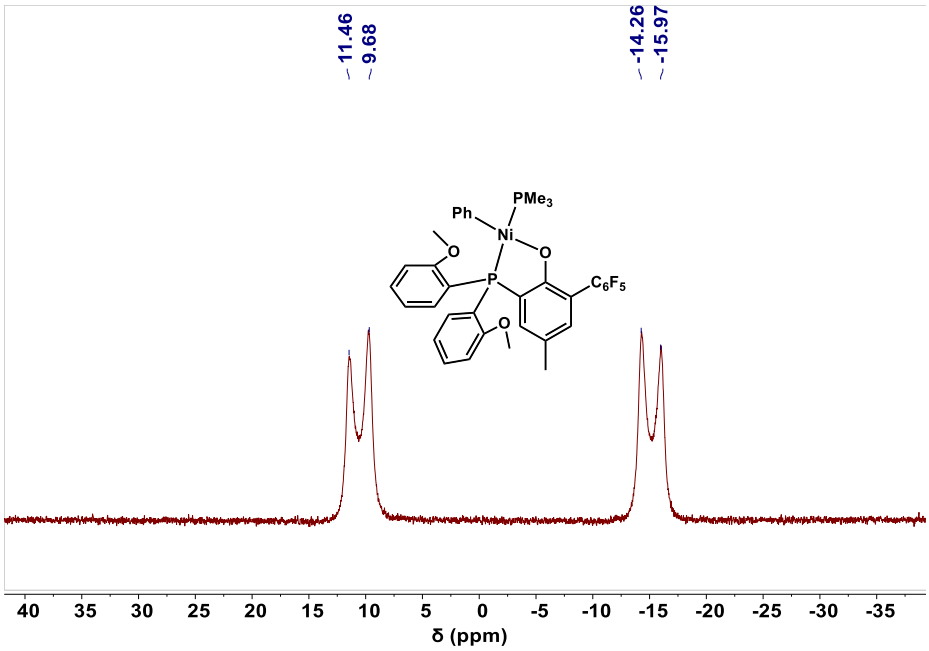

Figure 3.49. ^{31}P NMR spectrum (C_6D_6, 202 MHz) of **NiC$_6$F$_5$** complex.

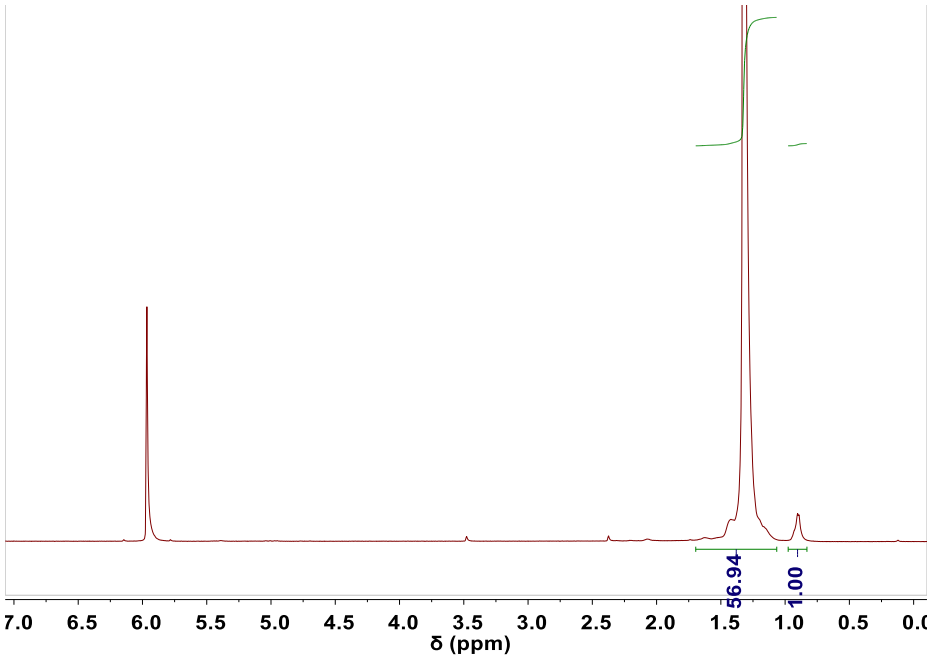

Figure 3.50. ^{1}H NMR spectrum ($C_2D_2Cl_4$, 500 MHz, 120 ^{o}C) of polyethylene produced by **Ni11**-Li at 30 ^{o}C (Table 3.1, entry 2).

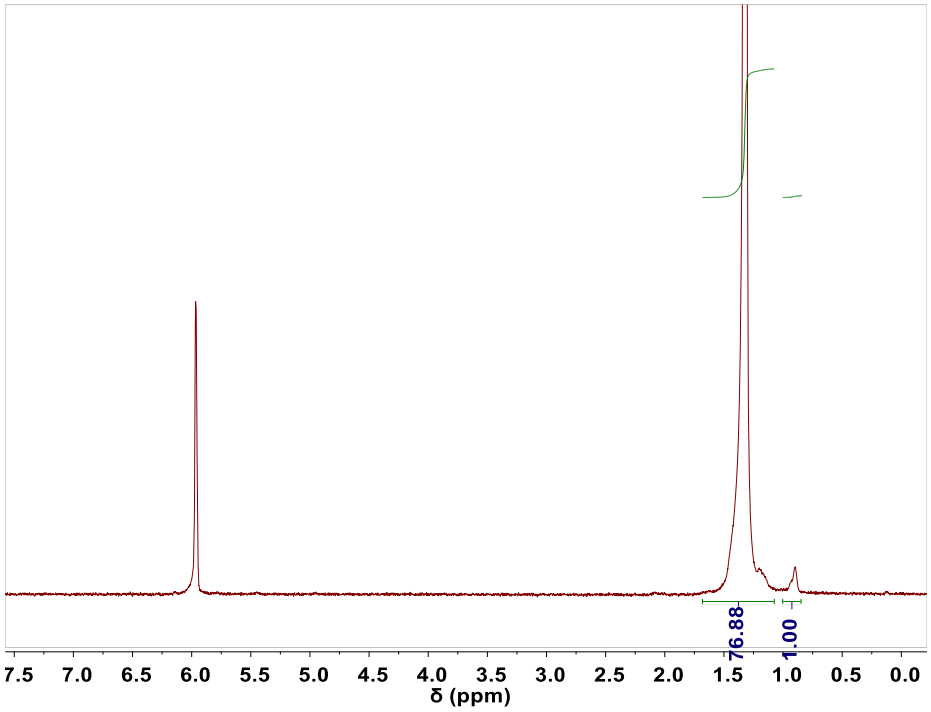

Figure 3.51. ^{1}H NMR spectrum ($C_2D_2Cl_4$, 500 MHz, 120 ^{o}C) of polyethylene produced by **Ni11**-Cs at 30 ^{o}C (Table 3.1, entry 5).

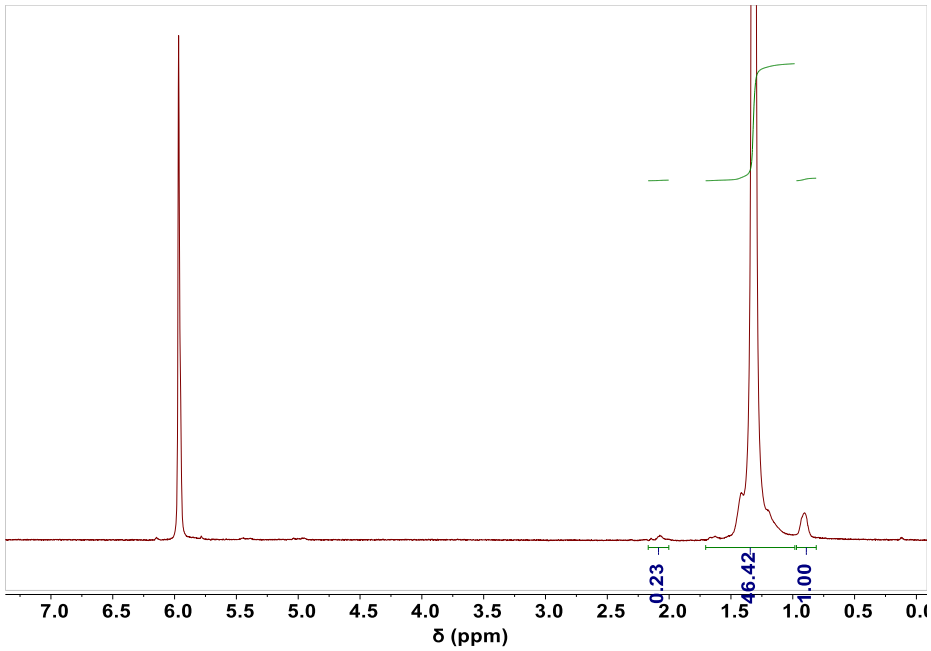

Figure 3.52. ^{1}H NMR spectrum ($C_2D_2Cl_4$, 500 MHz, 120 ^{o}C) of polyethylene produced by **Ni^{t}Bu** at 30 ^{o}C (Table 3.1, entry 6).

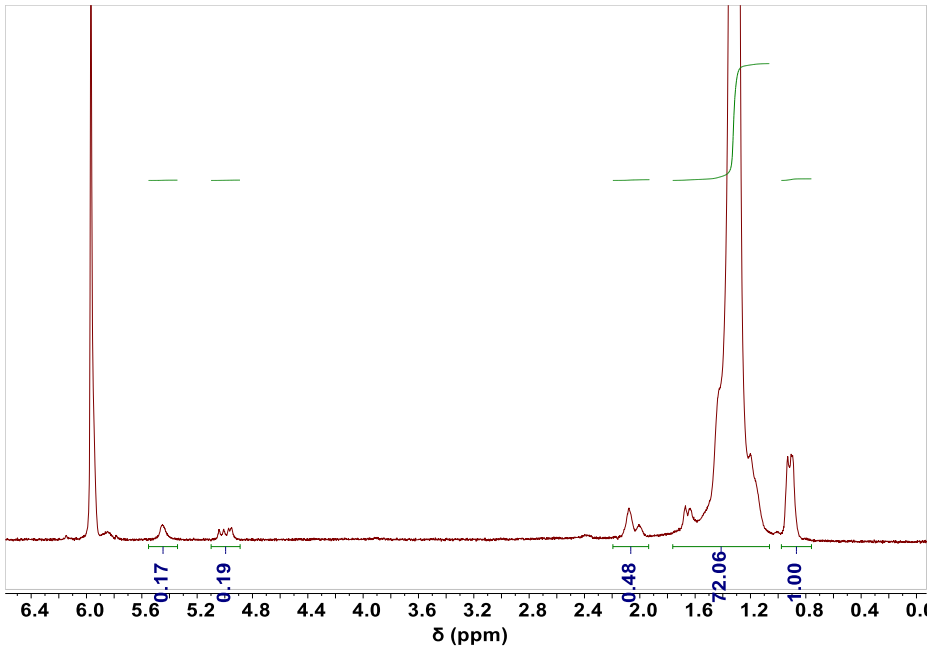

Figure 3.53. ^{1}H NMR spectrum ($C_2D_2Cl_4$, 500 MHz, 120 ^{o}C) of polyethylene produced by **NiC_6F_5** at 30 ^{o}C (Table 3.1, entry 7).

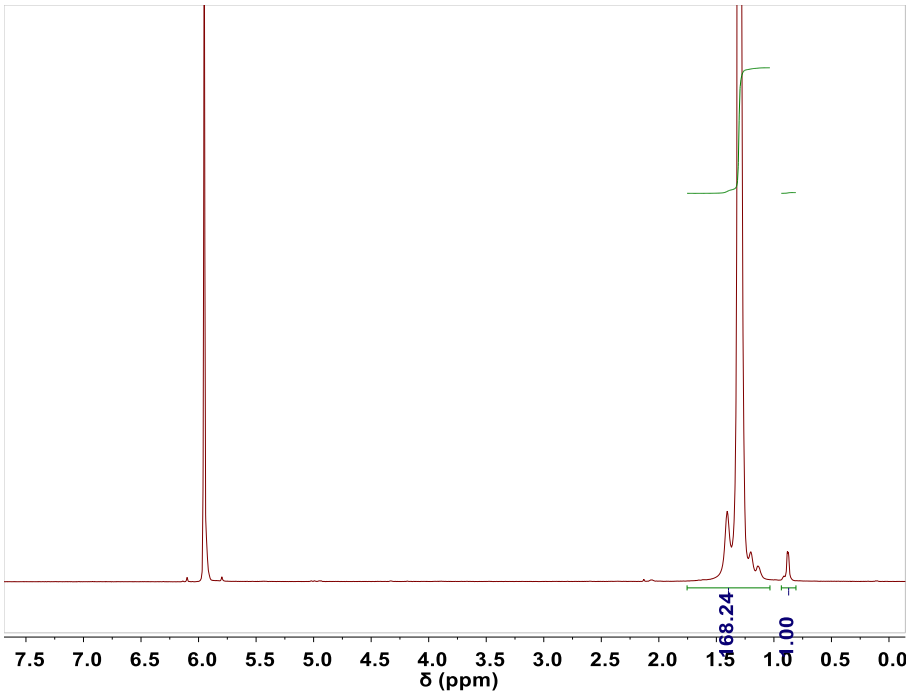

Figure 3.54. ^{1}H NMR spectrum ($C_2D_2Cl_4$, 600 MHz, 120 ^{o}C) of polyethylene produced by **Ni11-**Li in pentane (Table 3.11, entry 1).

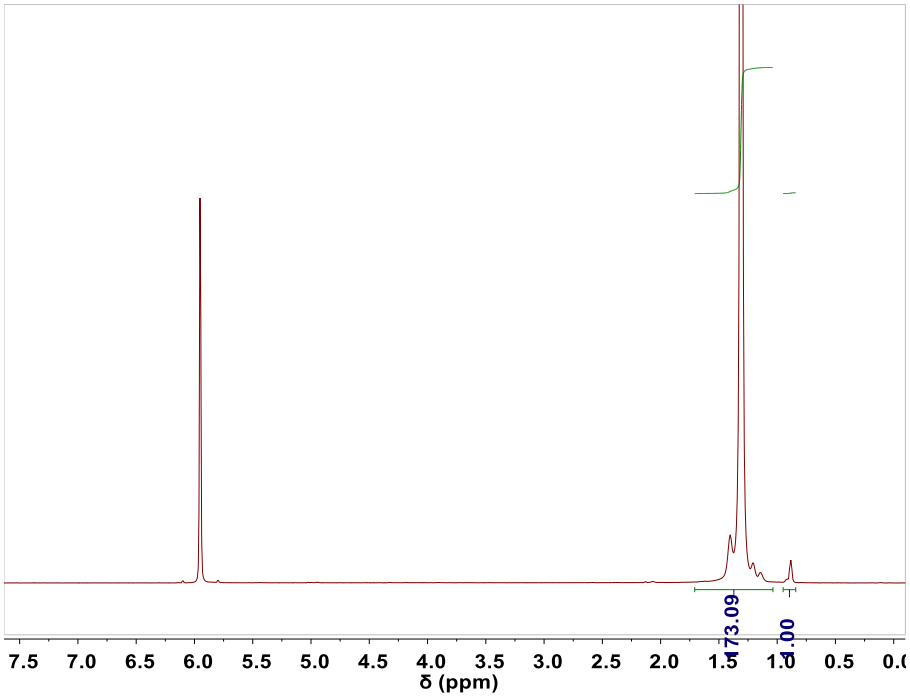

Figure 3.55. ^{1}H NMR spectrum ($C_2D_2Cl_4$, 600 MHz, 120 ^{o}C) of polyethylene produced by **Ni11-**Li in hexane (Table 3.11, entry 2).

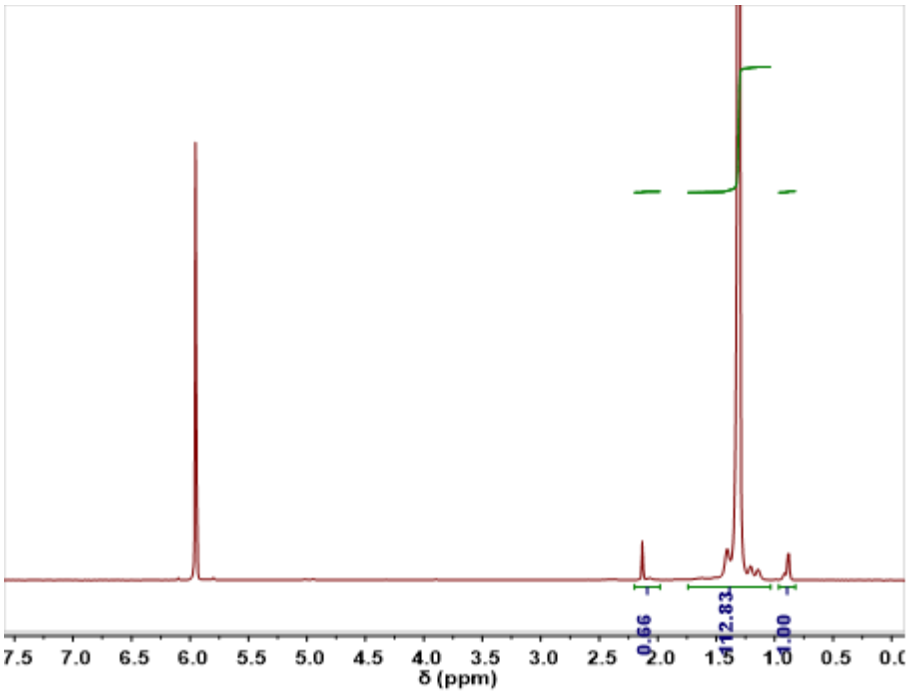

Figure 3.56. ^{1}H NMR spectrum ($C_2D_2Cl_4$, 600 MHz, 120 ºC) of polyethylene produced by **Ni11-Li** in benzene (Table 3.11, entry 3).

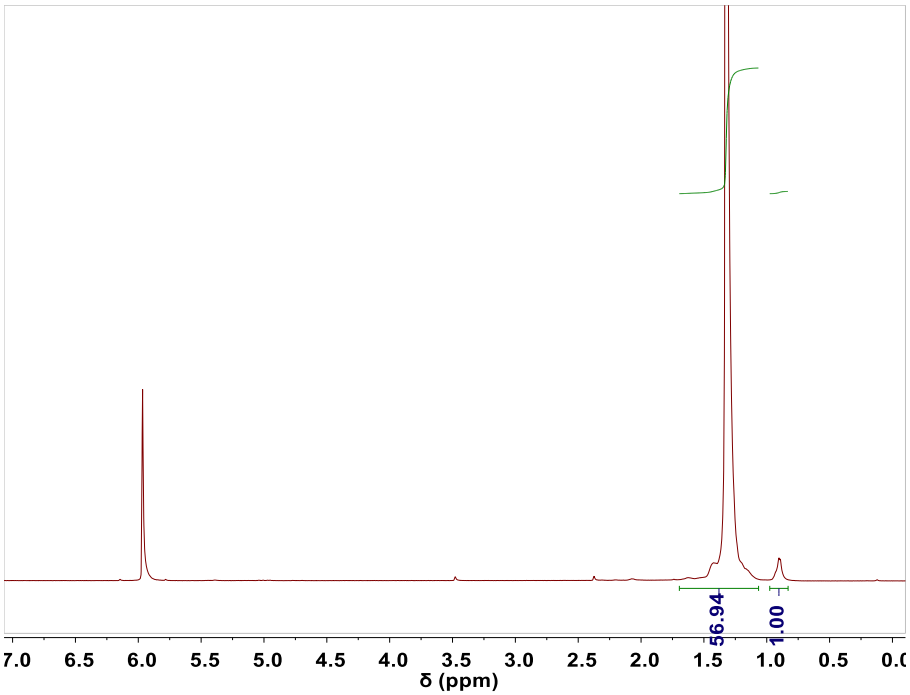

Figure 3.57. ^{1}H NMR spectrum ($C_2D_2Cl_4$, 500 MHz, 120 ºC) of polyethylene produced by **Ni11-Li** in toluene (Table 3.11, entry 4).

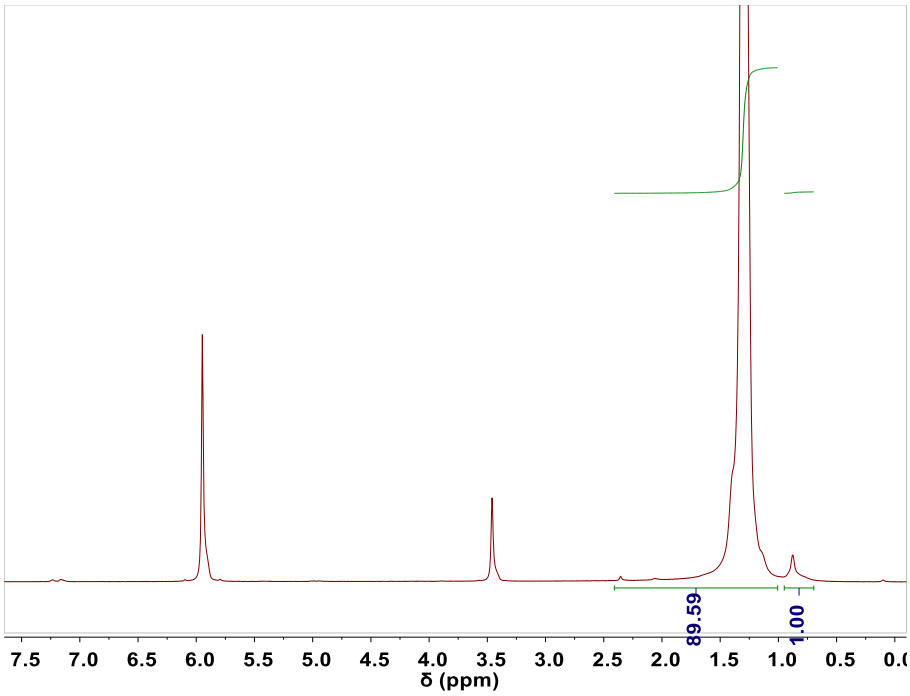

Figure 3.58. ^{1}H NMR spectrum ($C_2D_2Cl_4$, 600 MHz, 120 ^{o}C) of polyethylene produced by **Ni11-**Li in DCM (Table 3.11, entry 5).

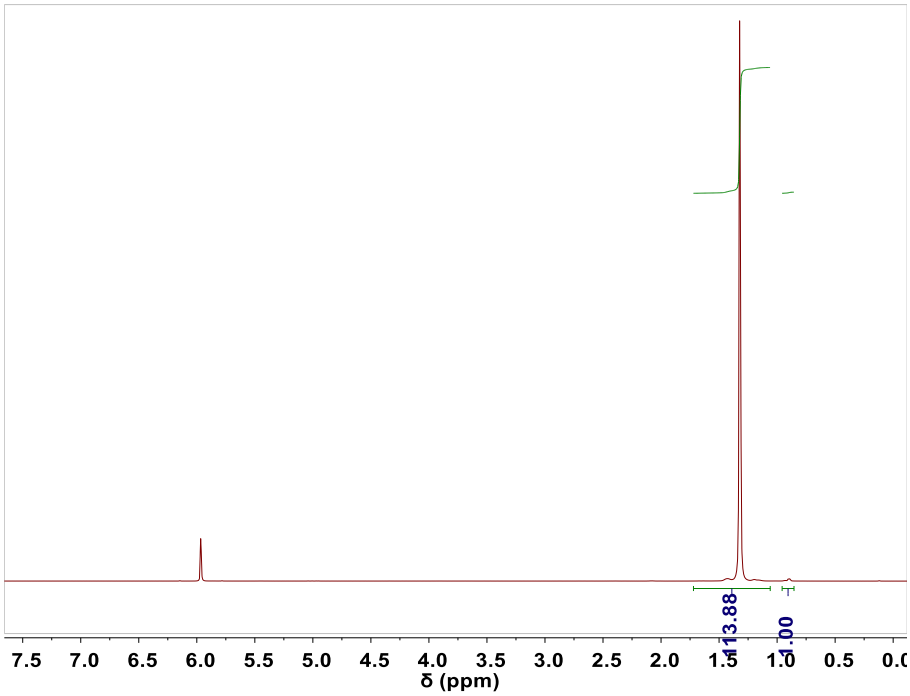

Figure 3.59. ^{1}H NMR spectrum ($C_2D_2Cl_4$, 600 MHz, 120 ^{o}C) of polyethylene produced by **Ni11-**Li in diethyl ether (Table 3.11, entry 6).

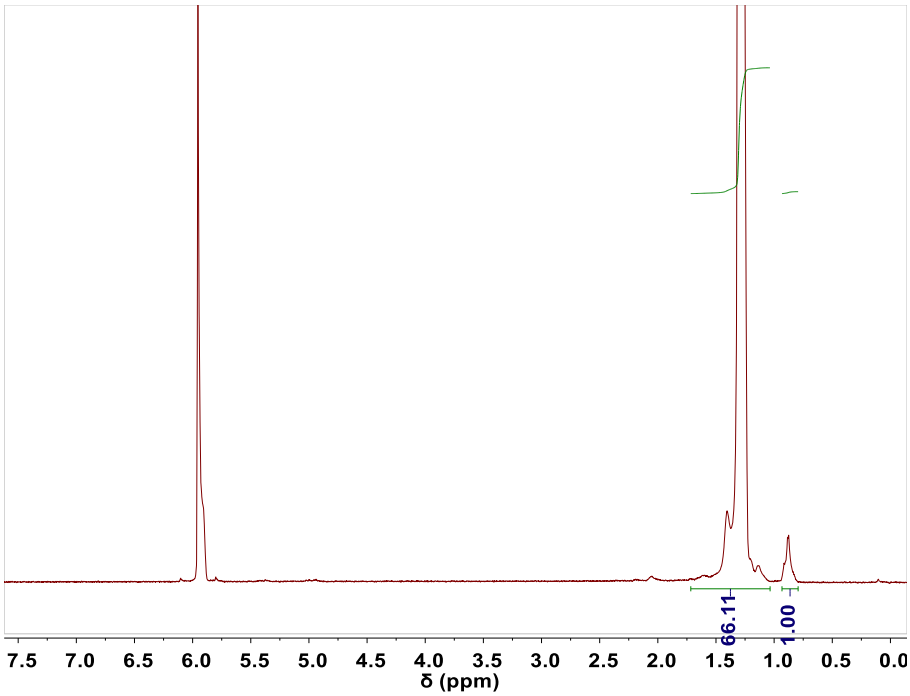

Figure 3.60. ^{1}H NMR spectrum ($C_2D_2Cl_4$, 600 MHz, 120 ºC) of polyethylene produced by **Ni11**-Li(BARF) (Table 3.14, entry 1).

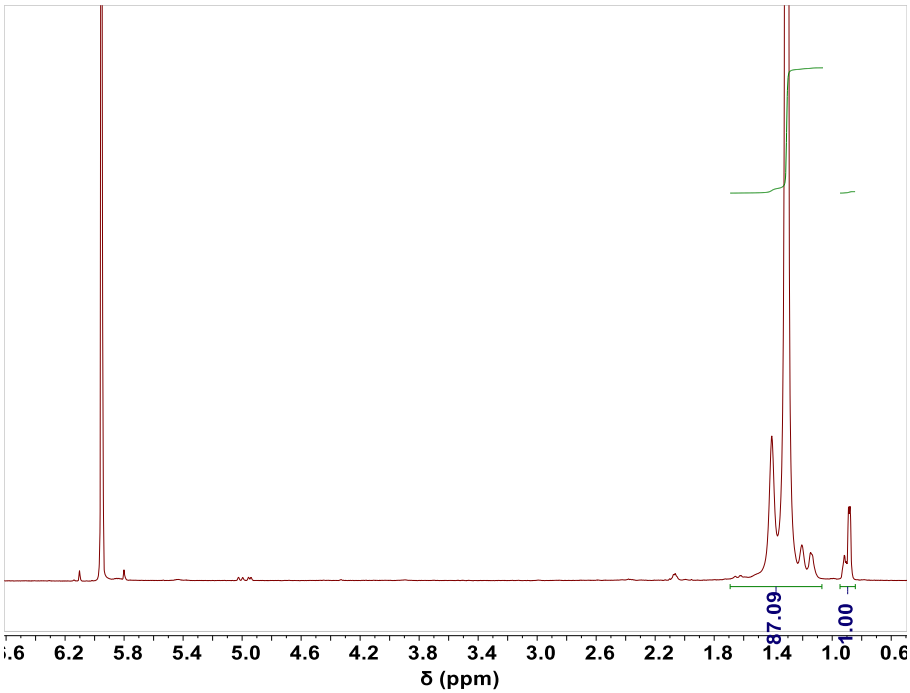

Figure 3.61. ^{1}H NMR spectrum ($C_2D_2Cl_4$, 600 MHz, 120 ºC) of polyethylene produced by **NiL**-Li(TPFB) (Table 3.14, entry 2).

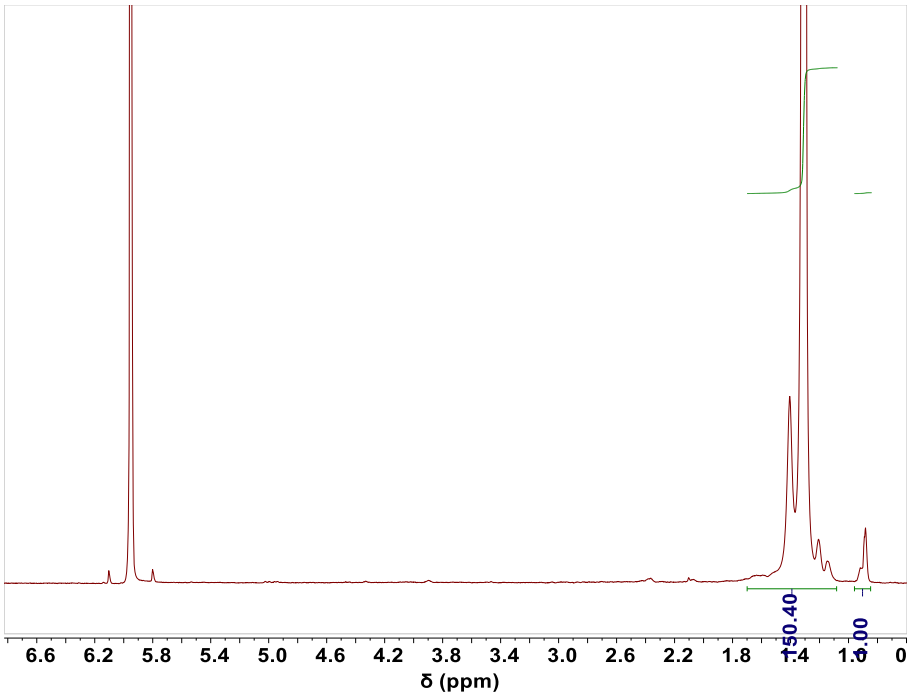

Figure 3.62. ^{1}H NMR spectrum ($C_2D_2Cl_4$, 600 MHz, 120 ^{o}C) of polyethylene produced by **NiL**-Li(BPh_4) (Table 3.14, entry 3).

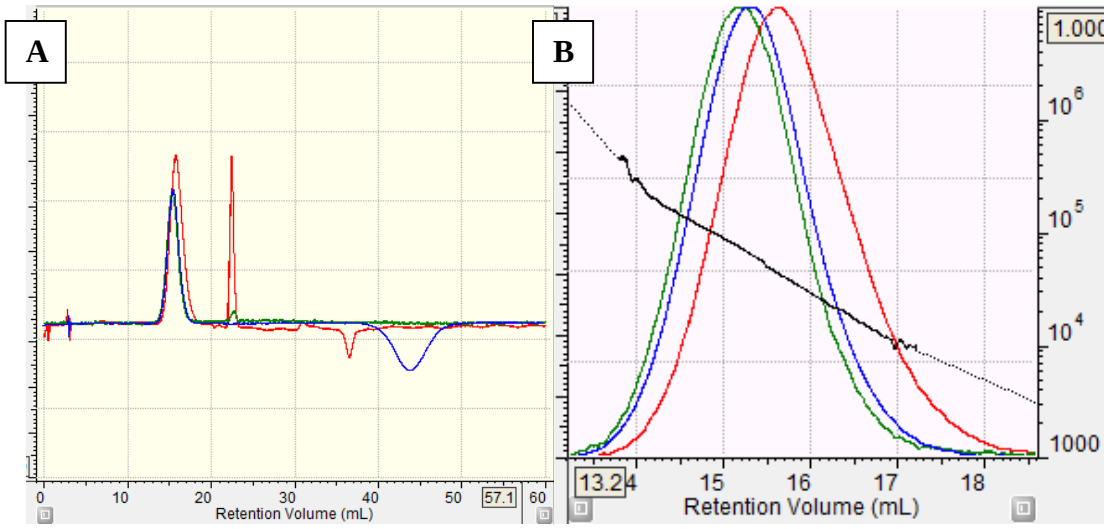

Figure 3.63. A) GPC chromatograms of the polyethylene obtained in Table 3.1, Entry 2. B) Normalized chromatograms showing the peaks corresponding to the polyethylene product and the molecular weight range (black line). The data were acquired using a triple detector system: red = refractive index, green = right angle light scattering, blue = viscometer. The peak at ~31 mL retention volume marked with an asterisk (*) is derived from a contaminant in the GPC column, not the sample itself.

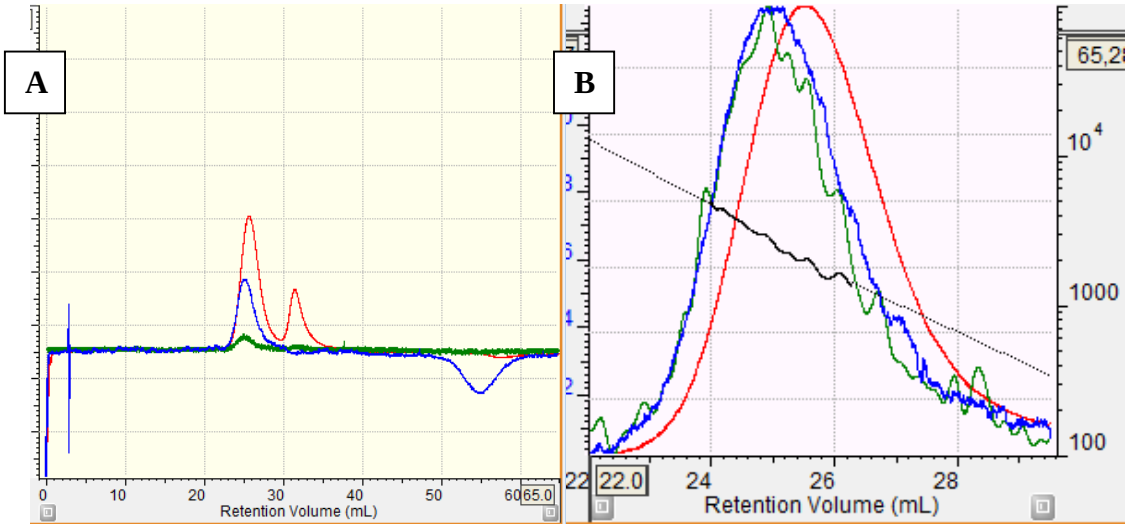

Figure 3.64. A) GPC chromatograms of the polyethylene obtained in Table 3.1, Entry 3. B) Normalized chromatograms showing the peaks corresponding to the polyethylene product and the molecular weight range (black line). The data were acquired using a triple detector system: red = refractive index, green = right angle light scattering, blue = viscometer. The peak at ~31 mL retention volume marked with an asterisk (*) is derived from a contaminant in the GPC column, not the sample itself.

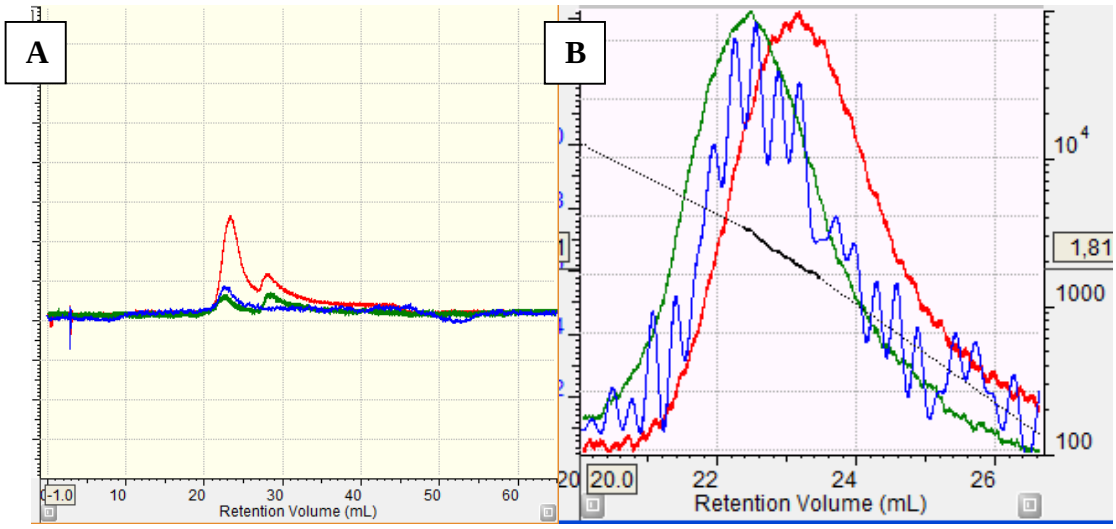

Figure 3.65. A) GPC chromatograms of the polyethylene obtained in Table 3.1, Entry 4. B) Normalized chromatograms showing the peaks corresponding to the polyethylene product and the molecular weight range (black line). The data were acquired using a triple detector system: red = refractive index, green = right angle light scattering, blue = viscometer. The peak at ~31 mL retention volume marked with an asterisk (*) is derived from a contaminant in the GPC column, not the sample itself.

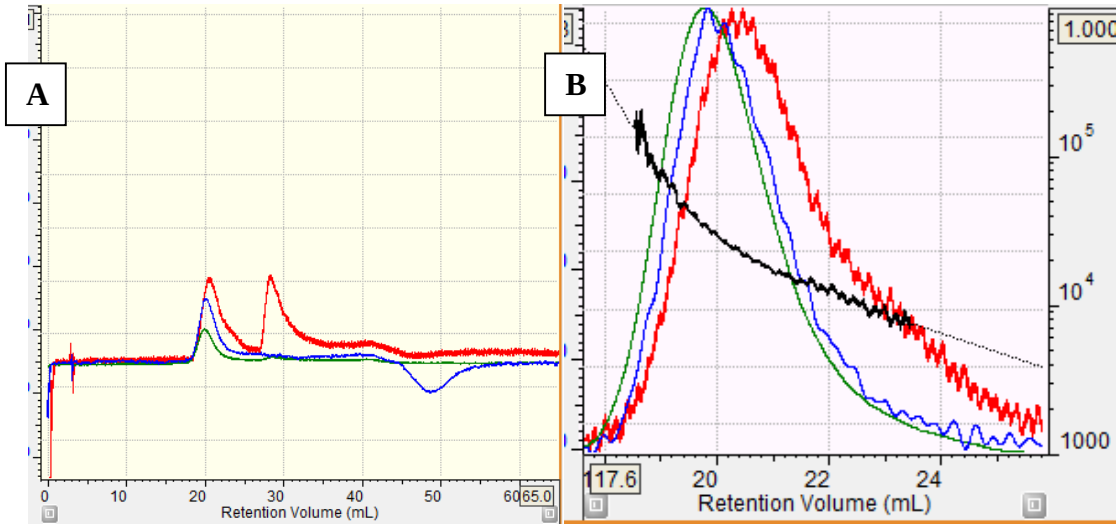

Figure 3.66. A) GPC chromatograms of the polyethylene obtained in Table 3.1, Entry 5. B) Normalized chromatograms showing the peaks corresponding to the polyethylene product and the molecular weight range (black line). The data were acquired using a triple detector system: red = refractive index, green = right angle light scattering, blue = viscometer. The peak at ~31 mL retention volume marked with an asterisk (*) is derived from a contaminant in the GPC column, not the sample itself.

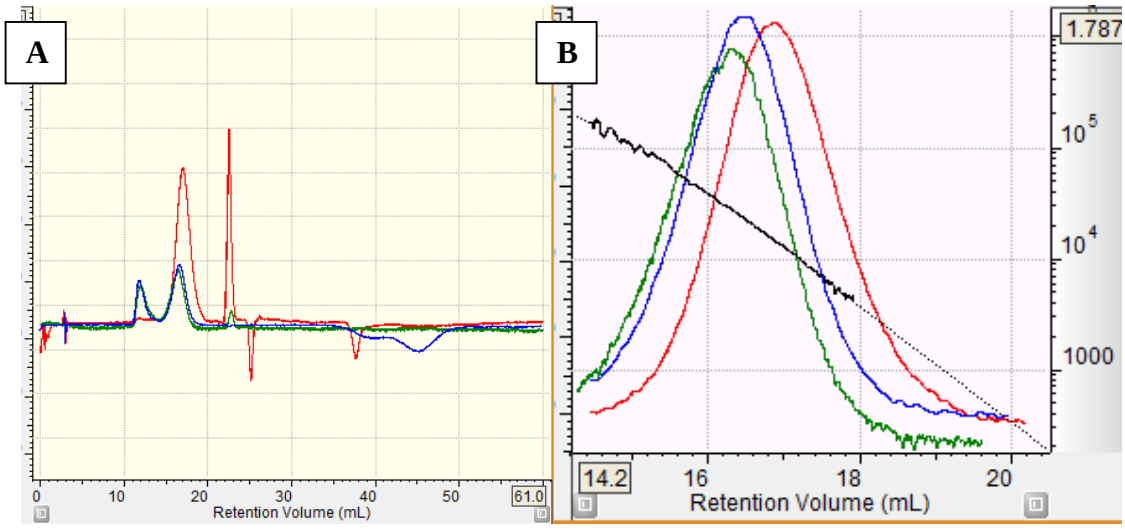

Figure 3.67. A) GPC chromatograms of the polyethylene obtained in Table 3.1, Entry 6. B) Normalized chromatograms showing the peaks corresponding to the polyethylene product and the molecular weight range (black line). The data were acquired using a triple detector system: red = refractive index, green = right angle light scattering, blue = viscometer. The peak at ~31 mL retention volume marked with an asterisk (*) is derived from a contaminant in the GPC column, not the sample itself.

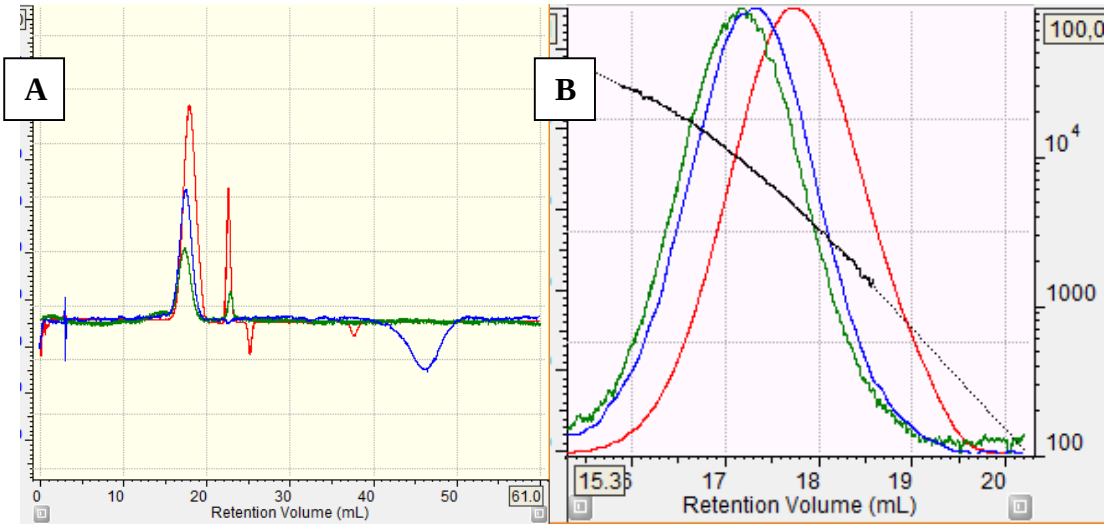

Figure 3.68. A) GPC chromatograms of the polyethylene obtained in Table 3.1, Entry 7. B) Normalized chromatograms showing the peaks corresponding to the polyethylene product and the molecular weight range (black line). The data were acquired using a triple detector system: red = refractive index, green = right angle light scattering, blue = viscometer. The peak at ~31 mL retention volume marked with an asterisk (*) is derived from a contaminant in the GPC column, not the sample itself.

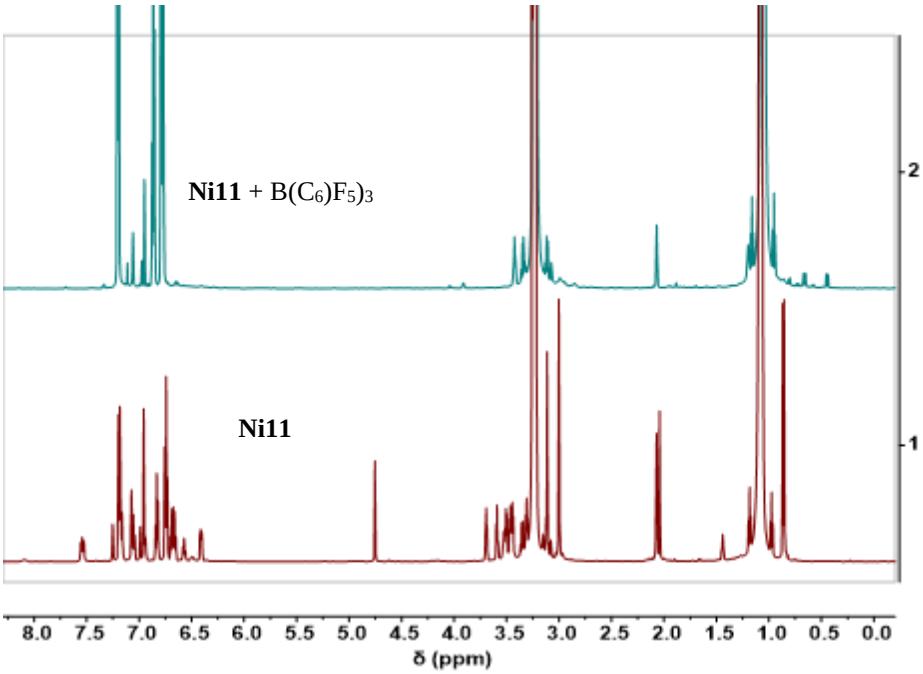

Figure 3.69. ^{1}H NMR of **Ni11** complex before and after adding $B(C_6F_5)_3$ at 30 ºC.

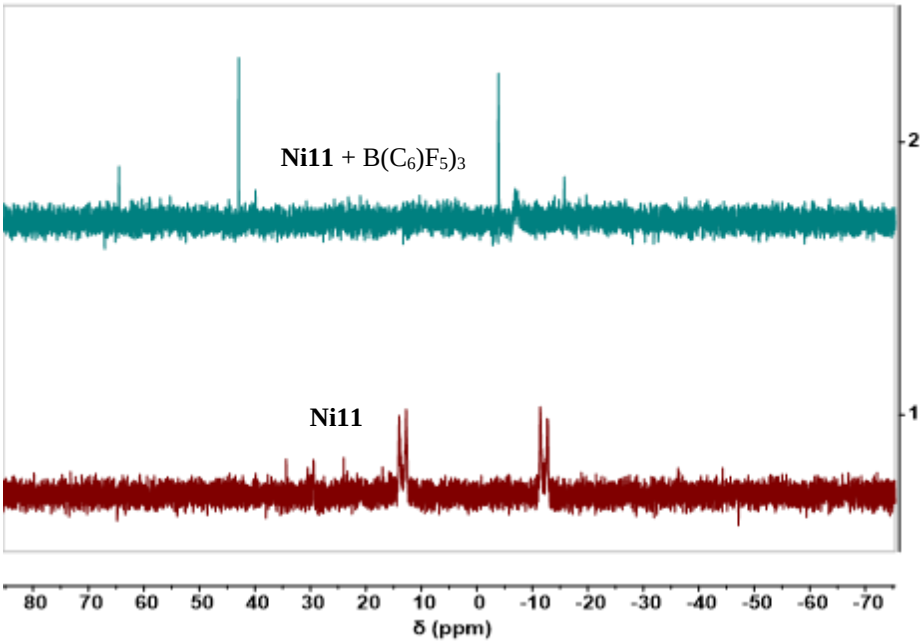

Figure 3.70. ^{31}P NMR of **Ni11** complex before and after adding $B(C_6F_5)_3$ at 30 ºC.

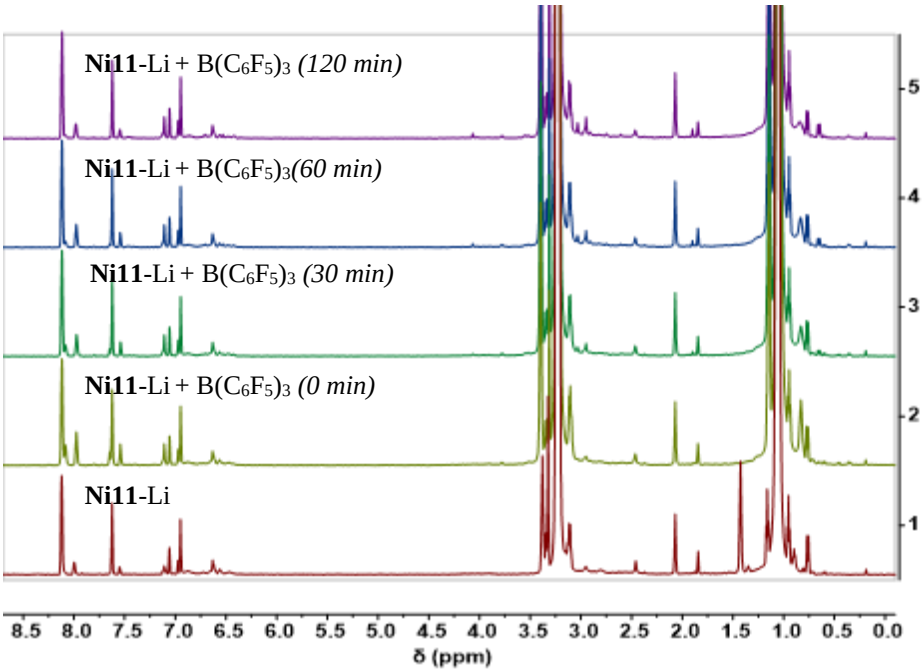

Figure 3.71. ^{1}H NMR of **Ni11**-Li complex before and after adding $B(C_6F_5)_3$ at 30 ºC.

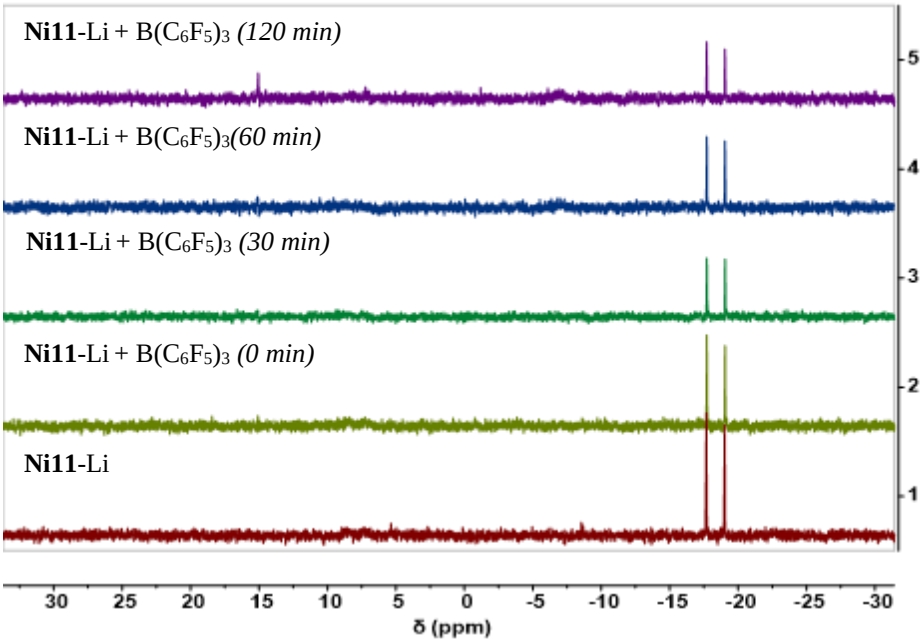

Figure 3.72. ^{31}P NMR of **Ni11**-Li complex before and after adding $B(C_6F_5)_3$ at 30 ºC.

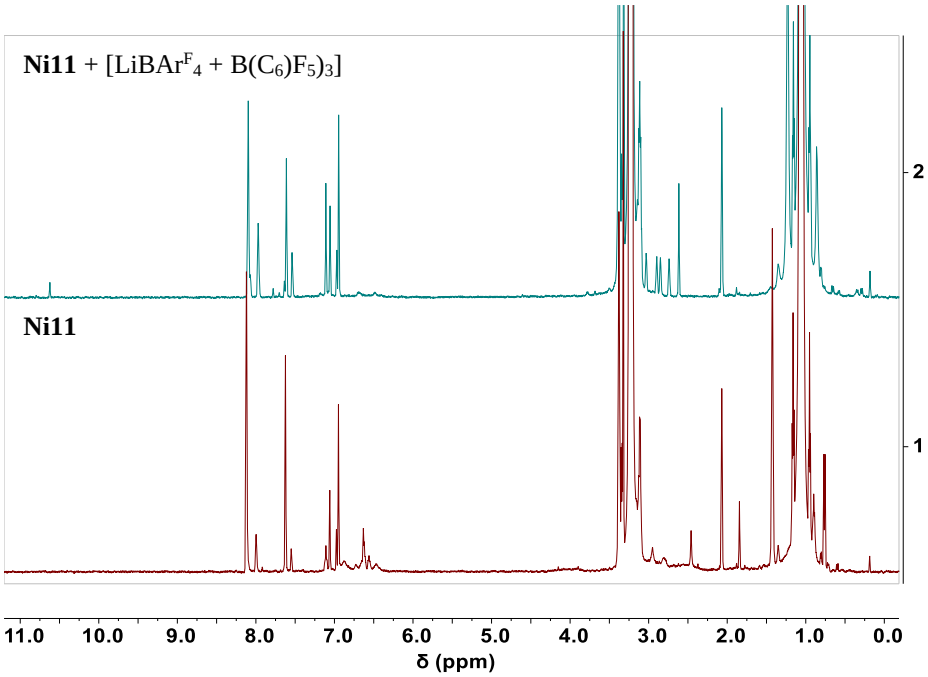

Figure 3.73. ^{1}H NMR of **Ni11** complex before and after adding [LiBAr$^{F}_{4}$ + B(C_6F_5)$_3$] at 30 ºC.

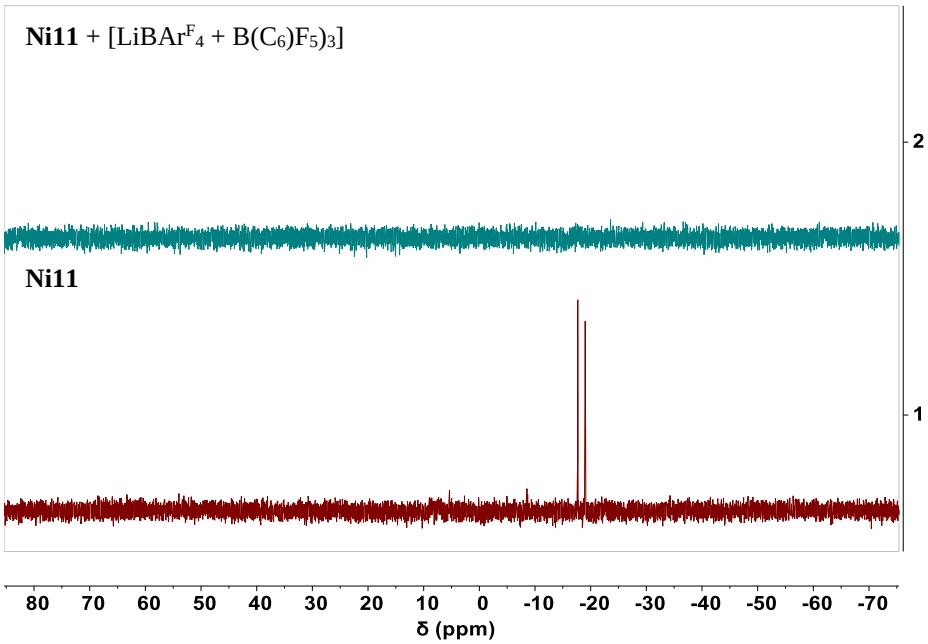

Figure 3.74. ^{31}P NMR of **Ni11** complex before and after adding [LiBAr$^{F}_{4}$ + B(C_6F_5)$_3$] at 30 ºC.

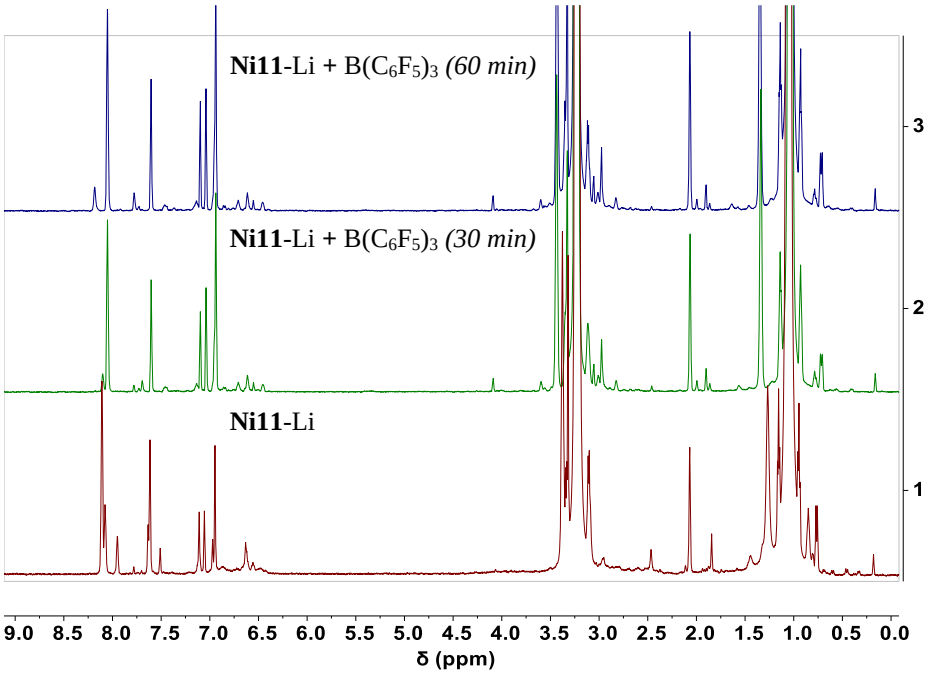

Figure 3.75. ^{1}H NMR of **Ni11**-Li before and after adding $B(C_6F_5)_3$ at 50 ºC.

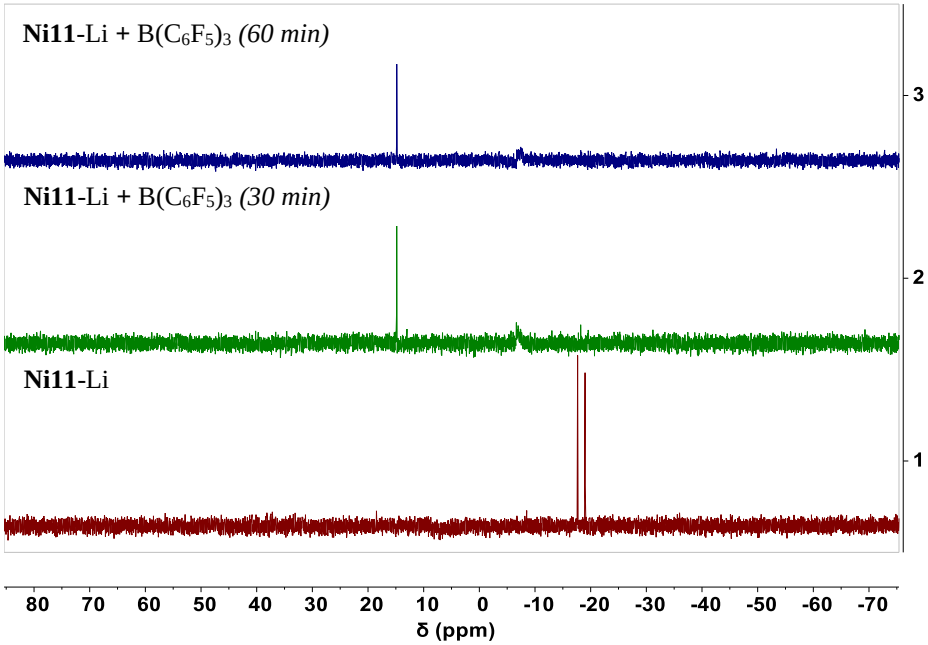

Figure 3.76. ^{31}P NMR of **Ni11**-Li before and after adding $B(C_6F_5)_3$ at 50 ºC.

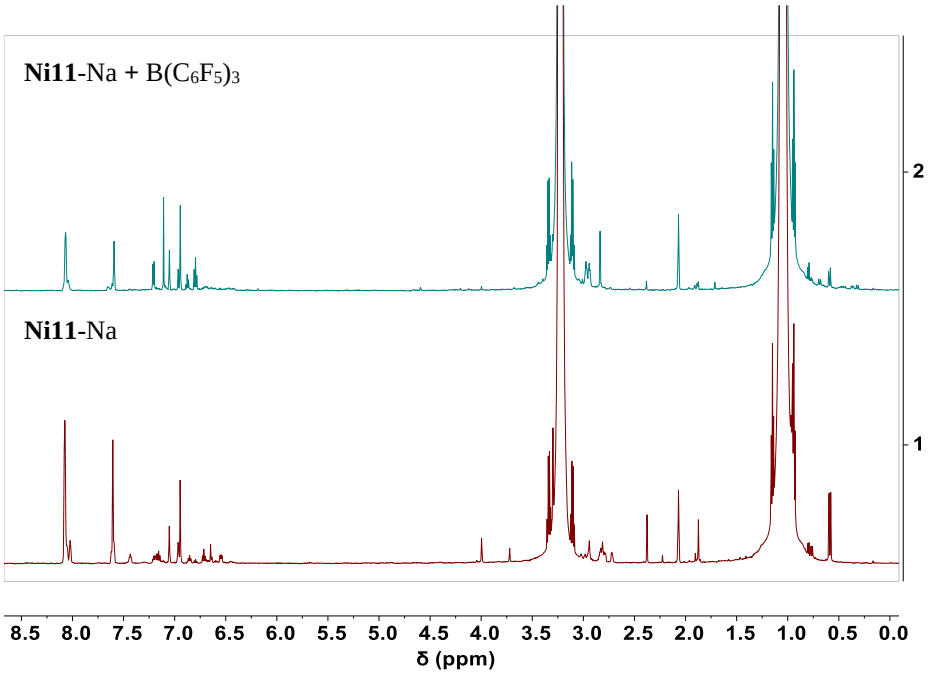

Figure 3.77. ^{1}H NMR of **Ni11**-Na before and after adding $B(C_6F_5)_3$ at 30 ºC.

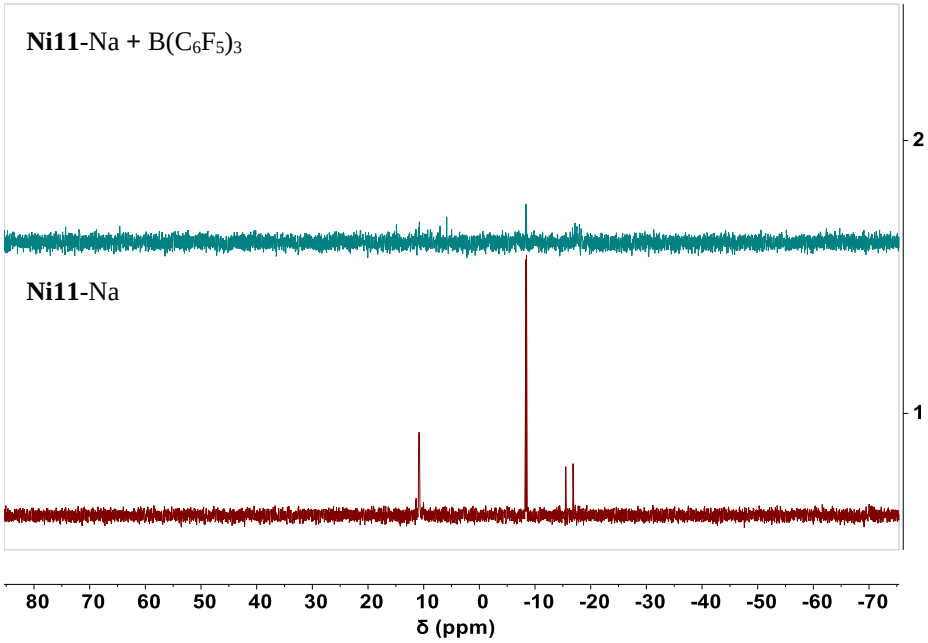

Figure 3.78. ^{31}P NMR of **Ni11**-Na before and after adding $B(C_6F_5)_3$ at 30 ºC.

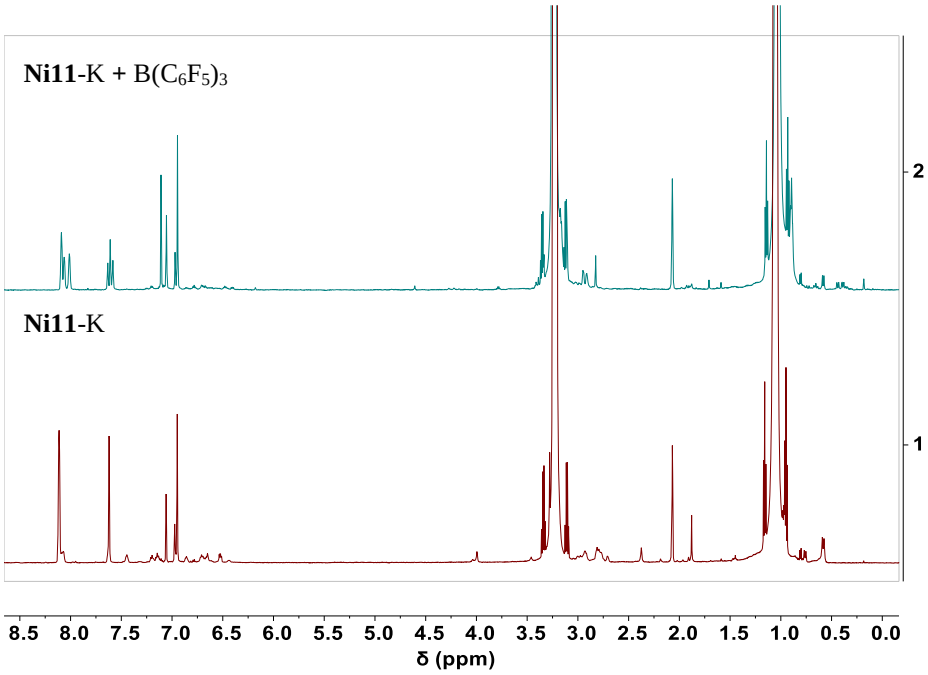

Figure 3.79. ^{1}H NMR of **Ni11**-K before and after adding $B(C_6F_5)_3$ at 30 ºC.

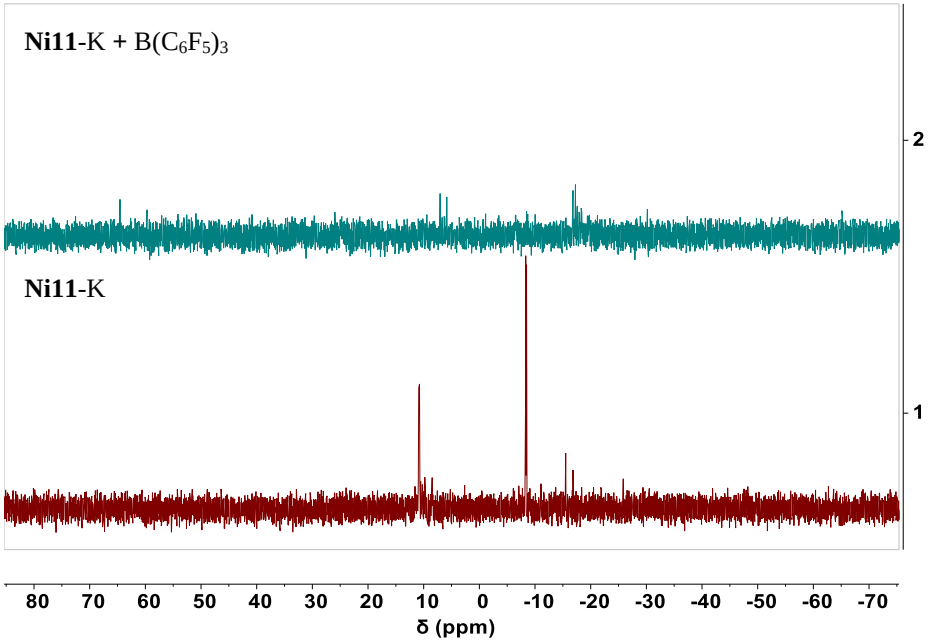

Figure 3.80. ^{1}H NMR of **Ni11**-K before and after adding $B(C_6F_5)_3$ at 30 ºC.

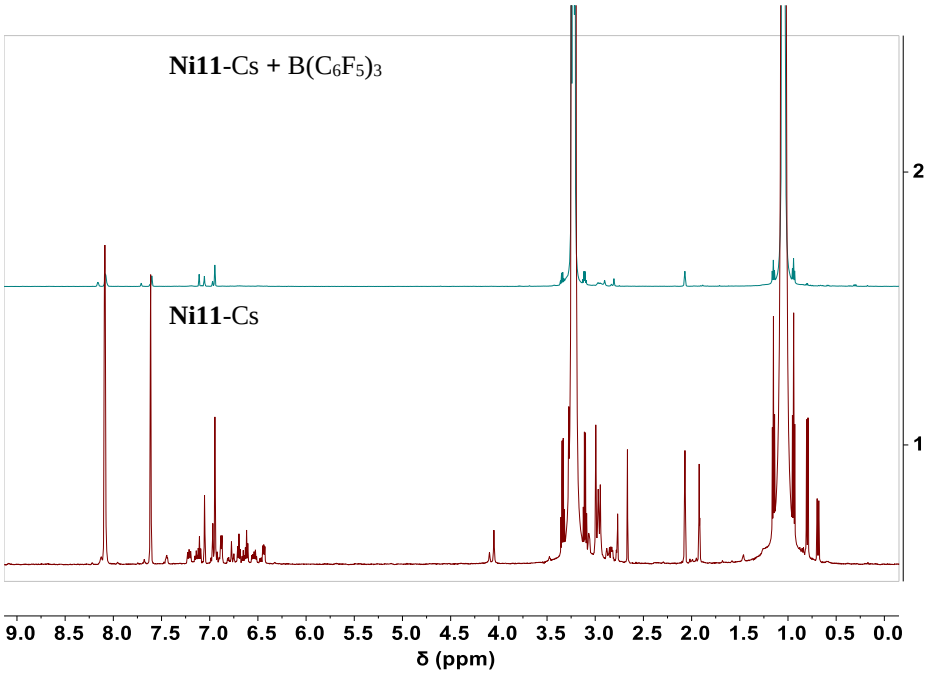

Figure 3.81. ^{1}H NMR of **Ni11**-Cs before and after adding $B(C_6F_5)_3$ at 30 ºC.

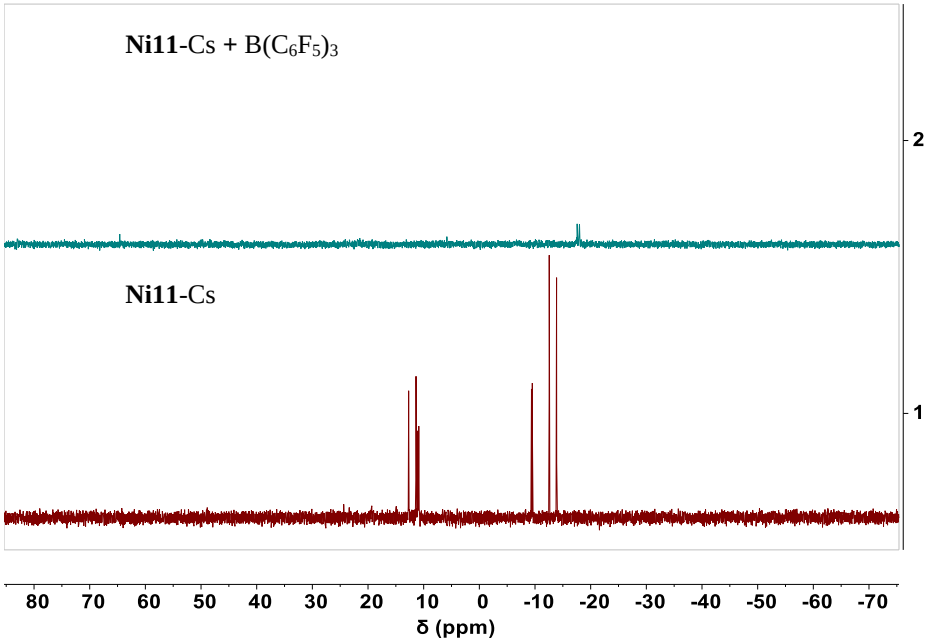

Figure 3.82. ^{31}P NMR of **Ni11**-Cs before and after adding $B(C_6F_5)_3$ at 30 ºC.

Chapter 4. Nickel-Alkali Catalysts for Controlled Synthesis of Bimodal Polyethylenes

4.1. Introduction

In Chapter 3, we showed that **Ni11** paired with different secondary cations gave functionally distinct catalysts. In this chapter, we have created a bulkier variant of **Ni11** and developed a "mix" metal strategy to synthesize polymers with bimodal molecular weight distribution in one-pot reactions.

Increasing steric hindrance around nickel catalysts is known to increase their catalyst thermal stability and polymer molecular weight. Inspired by Shimizu and coworkers' results, which showed that 2,6-dimethoxyphenyl attached to phosphine could significant enhance the steric congestion of SHOP-type nickel catalysts,[66] we have incorporated this substituent into our catalyst to create **Ni21**.

Polyethylene with bimodal molecular weight distribution is of interest to material scientists because they possess combined advantages of two types of different polyethylene, which are necessary for specific application.[122] For example, high density polyethylene (HDPE) resins possess high strength and stiffness, however, those properties result in poor stress crack resistance and difficult process ability, while medium density polyethylene (MDPE) resins are softer but possess better shock and drop resistance properties and are much easier to process than HDPE. The combination of these two polyethylene resins benefit from their bimodality by having the strength and stiffness of HDPE, while incorporating the high stress resistance and processability

of MDPE. This class of bimodal polyethylene resins is ideally fitted with the application demands of pipes for gas and water distribution.[123-125] Blending with other low MW polyethylene has also been widely used to improve the processability of ultra-high molecular weight polyethylene (UHMWPE).[126] UHMWPE has been known for its predominant mechanical properties compared to many conventional polyolefins such as extremely high impact strength and crack resistance.[127-128] However, their ultra-high molecular weight results in ultrahigh melt viscosity and high degree of chain entanglements, which prohibit them from being processed via conventional melt extrusion of injection molding.[129-130] Similar to HDPE case, to overcome this issue, scientists have blended UHMWPE with another low molecular weight polyethylene (PE) to improve it processability.[126,131-133]

Several methods for synthesizing bimodal polyethylenes have been developed, including physical blending of two polyethylene resins with different molecular weight,[134] using cascade reactor processes,[135-136] and mixing different catalysts in one-pot.[137-141] Some of the drawbacks of these methods include gelation, high cost, and complex manipulation. Since **Ni11** is capable of binding different cations, we took advantage of this property to use two different metals in various ratios in a single pot to control the molecular weight distribution.

4.2. Synthesis of Bulky Catalyst

Ligand **L75** was synthesized using a procedure similar to that described in Scheme 2.1 with an overall yield of about 9% (Scheme 4.1). To obtain nickel complex **Ni21**, **L75** was deprotonated by sodium hydride in THF, followed by treatment with $NiPhBr(PMe_3)_2$ to furnish the desired product as a yellow solid in moderate yield (0.35 g, 45 %) (Scheme 4.1).

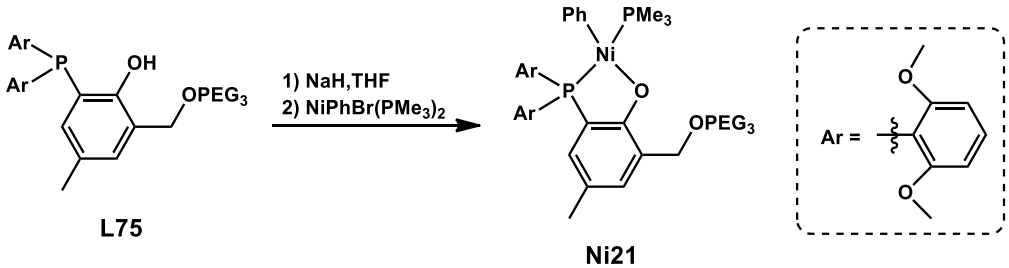

Scheme 4.1. Synthesis of nickel phenoxyphosphine complexes.

4.3. Ethylene Polymerization

We first screened our nickel **Ni21** complexes from 30 ^{o}C to 90 ^{o}C to study temperature effects (Table 4.1). At 30 ^{o}C, **Ni21** displayed moderate activity (entry 1, activity = 279 kg/(mol·h)), affording polymer with molecular weight of ~270 kg/mol. Upon addition of secondary cations, the activity and molecular weight both increased, while polydispersity decreased. Similar to **Ni11**-M, the activity of **Ni21**-M decrease in the other **Ni21**-Li > **Ni21**-Na > **Ni21**-K > **Ni21**-Cs, which is in agreement with the Lewis acid strengths of their alkali ions, while the polymer molecular weight followed a different trend **Ni21**-Cs > **Ni21**-Na > **Ni21**-K > **Ni21**-Li. It is interesting to note that both **Ni21** and **Ni21**-Cs produced about one polymer chain per nickel center. This result suggests that chelation of Cs only speeds up insertion rate (~ 5.3×) and does not affect chain transfer rate. **Ni21**-Na and **Ni21**-K afforded similar results, giving around two polymer chain per nickel center. However, the polymer molecular weight and catalyst activity of **Ni21**-Na are higher than that of **Ni21**-K, which means that Na^+ enhanced insertion rate to a large degree than K^+. This effect could be attributed to the stronger Lewis acid strength of Na^+ compared to K^+. Because the catalyst productivity (polymer molecular weight, activity) is influenced by both steric and

electronic effects, our polymerization results suggests that chelation of secondary metals to **Ni21** simultaneously altered its steric and electronic properties.

We observed that increasing reaction temperature decreased polymer molecular weight but increased catalytic activity. At 50 ^{o}C, **Ni21**-Li, **Ni21**-Na, and **Ni**-K produced polythylenes with similar molecular weight, but their activity trend (**Ni21**-Li > **Ni21**-K > **Ni21**-Na) is slightly different than that observed at 30 ^{o}C. Surprisingly, **Ni21** and **Ni21**-Cs still afforded similar numbers of polymer chain per nickel center (4.5 chains/nickel). Increase the temperature further to 90 ^{o}C, we found that the activity significantly increased while polymer molecular weight decreased. However, **Ni11**-Cs still produced polymer with relatively high molecular weight (entry 15). We observed that when 0.2 μmol of **Ni11**-Cs was used, the polymerization was highly exothermic with a reaction temperature increase up to 114 ^{o}C within several minutes after injection into the reaction. Because the nickel catalysts are sensitive to elevated temperatures, we hypothesize that if the reaction exotherm is too large, the catalyst could decompose due to the heat generated. Thus, the corresponding results may not reflect accurately the catalytic behavior.

When the amount of **Ni11**-Cs was reduced to 0.1 μmol, the reaction temperature was able to be controlled within 5 ^{o}C deviation. At this lower catalyst loading, the activity of **Ni11**-Cs was found to have an activity of 33000 kg/(mol·h) and the polymer molecular weight was 185.2 kg/mol, while the polydispersity are still narrow (M_n/M_w = 1.5). This result is exciting because most nickel complexes decompose at elevated temperatures, resulting in significant reduction in both activity and molecular weight and broad PDI.

Table 4.1. Polymerization Study for **Ni41**-M at Different Temperature[a]

Entry	Cat.	Salt	Temp. (^{O}C)	Polymer Yield (g)	Activity ($\frac{kg}{mol \cdot h}$)	M_n^b ($\times 10^3$)	$\frac{M_n^b}{M_w}$	$\frac{\text{PE Chain}}{\text{Ni Center}}$
1	**Ni21**	none	30	0.279	279	270.7	2.0	1.0
2	**Ni21**	Li^+	30	2.94	2940	684.9	1.5	4.3
3	**Ni21**	Na^+	30	2.43	2400	1234	1.3	1.9
4	**Ni21**	K^+	30	1.88	1880	948.5	1.4	2.0
5	**Ni21**	Cs^+	30	1.26	1260	1415	1.6	0.9
6[c]	**Ni21**	none	50	0.105	525	115.5	2.2	4.5
7[c]	**Ni21**	Li^+	50	6.2	31000	181.6	1.6	170.7
8[c]	**Ni21**	Na^+	50	1.13	5650	198.7	1.6	28.4
9[c]	**Ni21**	K^+	50	1.7	8500	196.4	1.6	43.3
10[c]	**Ni21**	Cs^+	50	0.64	3200	707.9	1.4	4.5
11[c]	**Ni21**	none	90	4.6	23000	40.6	2.0	566.5
12[c]	**Ni21**	Li^+	90	9.9	49500	15.2	2.6	3256.6
13[c]	**Ni21**	Na^+	90	11.7	58500	30.7	1.8	1905.5
14[c]	**Ni21**	K^+	90	3.7	18500	49.8	1.6	371.5
15[c]	**Ni21**	Cs^+	90	4.7	23500	117.3	1.7	200.3
16[d]	**Ni21**	Cs^+	90	3.3	33000	185.2	1.5	178.2

[a]Polymerization conditions: catalyst (1.0 µmol), $MBAr^F_4$ (5.0 µmol, if any), $Ni(COD)_2$ (8 µmol), ethylene (450 psi), 98 mL toluene/2 mL Et_2O, 1h. Temperature was controlled by manual external cooling when necessary to ensure that the reaction temperature does not exceed greater than 5 °C from the starting temperature. [b]Determined by GPC in trichlorobenzene at 140 °C. [c]**Ni21** (0.2 µmol), $MBAr^F_4$ (1 µmol, if any), $Ni(COD)_2$ (1.6 µmol), temperature quickly increased to 114 °C after addition of catalyst mixture. [d]**Ni21** (0.1 µmol), $MBAr^F_4$ (0.5 µmol, if any), $Ni(COD)_2$ (0.8 µmol).

Because our nickel-alkali complexes provided different types of polymer under the same reaction condition, we took advantage of this property to produce polyethylene with bimodal molecular weight distributions. We hypothesize that upon mixing our nickel complex with a mixture of two alkali metals, we will obtain two types of bimetallic complexes, which will polymerize ethylene at different rates and produce different types of polymer products. Our study was conducted with **Ni11** and mixtures of Na and Li because **Ni11**-Na and **Ni11**-Li displayed much different in productivity (activity, polymer molecular weight, branching density), which will be facile for data characterization and analysis. Furthermore, these two catalysts are highly active so they can perform at low reaction temperature that will make polymerization process easy to control.

Upon testing **Ni11** for ethylene polymerization in the presence of various ratios of Na/Li mixtures, we obtained polyethylenes with broad polydispersity. Characterization of these polymers by gel permeation chromatography showed two distinct peaks (Figure 4.17), indicating that two types of polyethylene were produced. The high-MW fraction with less branches was most likely formed by **Ni11**-Li and the low-MW fraction with more branches was most likely formed by **Ni11**-Na. As shown in Table 4.2, the relative ratios of the polymer peaks correlated well with the Na^+/Li^+ ratios used. Increasing amount of Li^+ over Na^+ gave increased polymer yield, greater fractions of high molecular weight polymer and lower branching density. Our results showed that when the Na^+/Li^+ ratio was 5:1, the amount of polymer generated by **Ni11**-Na was equal to that produced by **Ni11**-Li, which is consistent with the relative reactivity of the **Ni11**-M species and the binding affinity of **Ni11** for Li^+ versus Na^+.

Our results suggest that because two distinct PEs were formed, the interconversion rate between the wo active species **Ni11**-Li and **Ni11**-Na is relatively slow compared to their chain

propagation rates. If the interconversion rate was faster than that of chain growth, a monomodal MW distribution would be expected.

Table 4.2. Ethylene Polymerization Study for **Ni11** in the presence of a mixture of Li/Na.

Entry	**Na/Li ratio**	**Polymer Yield** (g)	**Activity** $(\frac{kg}{mol \cdot \mathrm{h}})$	$M_n{}^b$ ($\times 10^3$)	$\frac{M_n^b}{M_w}$	**Branches**[c] (/1000C)
1	100:0	0.83	16600	1.54	1.73	27
2	20:1	0.85	17000	2.19	3.94	25
3	10:1	0.91	18200	2.99	4.88	17
4	5:1	1.14	22800	4.62	5.13	15
5	2:1	1.26	25200	10.29	3.65	10
6	1:1	1.33	26600	14.02	2.55	9
7	0.5:1	1.65	33000	18.59	2.28	8
8	0.25:1	1.95	39000	21.17	1.97	7
9	0:100	2.14	42800	31.13	1.65	11

[a]Polymerization conditions: catalyst (0.1 μmol), $LiBAr^F{}_4$ (0.2 μmol), $NaBAr^F{}_4$ (varied), $Ni(COD)_2$ (0.8 μmol), ethylene (450 psi), 100 mL toluene, 0.5 h. Stock solutions of Na/Li mixture were prepared in Et_2O, in which the concentration of Li was kept at 1 M. Temperature was controlled by manual external cooling when necessary to ensure that the reaction temperature does not exceed greater than 5°C from the starting temperature. [b]Determined by GPC in trichlorobenzene at 140 °C. [c]Determined by ^{1}H NMR in trichlorobenzene at 120 °C.

4.4. Conclusion

In summary, we have successfully expanded our study of nickel phenoxyphosphine-PEG complexes to include structurally bulky derivatives, which showed significant improvement in catalyst thermal stability and polymer molecular weight. Complex **Ni21**-Cs is among rare examples of nickel based systems that can perform well at temperatures as high as 90 °C. We also took advantage of the switchable capability of our nickel catalysts to synthesize polyethylene with bimodal molecular distribution in one-pot reactions.

In summary, we have demonstrated that heterobimetallic complexes are excellent catalysts for olefin polymerization. In future work, we can replace the PEG chelator with other metal binding groups to expand the range of secondary metals that are compatible with our catalyst. It is also possible to apply similar design strategies to other well-established ligand platforms. Furthermore, the mix metal polymerization method can be applied to produce polymer blends or polymer with novel morphologies depending on the secondary metal exchange dynamics and living versus non-living catalyst behavior. We anticipate that this work will open up new opportunities in catalyst design and provide novel method to access new type of polyolefins.

4.5. Experimental

General Procedures

Commercial reagents were used as received. All air- and water-sensitive manipulations were performed using standard Schlenk techniques or under a nitrogen atmosphere using a drybox. Anhydrous solvents were obtained from an Innovative Technology solvent drying system saturated with argon. High-purity polymer grade ethylene was obtained from Matheson TriGas without further purification. The $LiBAr^F_4$, $NaBAr^F_4$, $KBAr^F_4$ and $CsBAr^F_4$ salts were prepared according to literature procedures.[67, 115]

NMR spectra were acquired using JEOL spectrometers (ECA-400, -500, and -600) and referenced using residual solvent peaks. All ^{13}C NMR spectra were proton decoupled. ^{31}P NMR spectra were referenced to phosphoric acid. ^{1}H NMR spectroscopic characterization of polymers: each NMR sample contained ~20 mg of polymer in 0.5 mL of 1,1,2,2-tetrachloroethane-d_2 (TCE-d_2) and was recorded on a 500 MHz spectrometer using standard acquisition parameters at 120 °C.

Gel permeation chromatography (GPC) data were obtained using a Malvern high temperature GPC instrument equipped with refractive index, viscometer, and light scattering detectors at 150 °C with 1,2,4-trichlorobenzene (stabilized with 125 ppm BHT) as the mobile phase. A calibration curve was established using polystyrene standards in triple detection mode. All molecular weights reported are based on the triple detection method.

Synthesis and Characterization

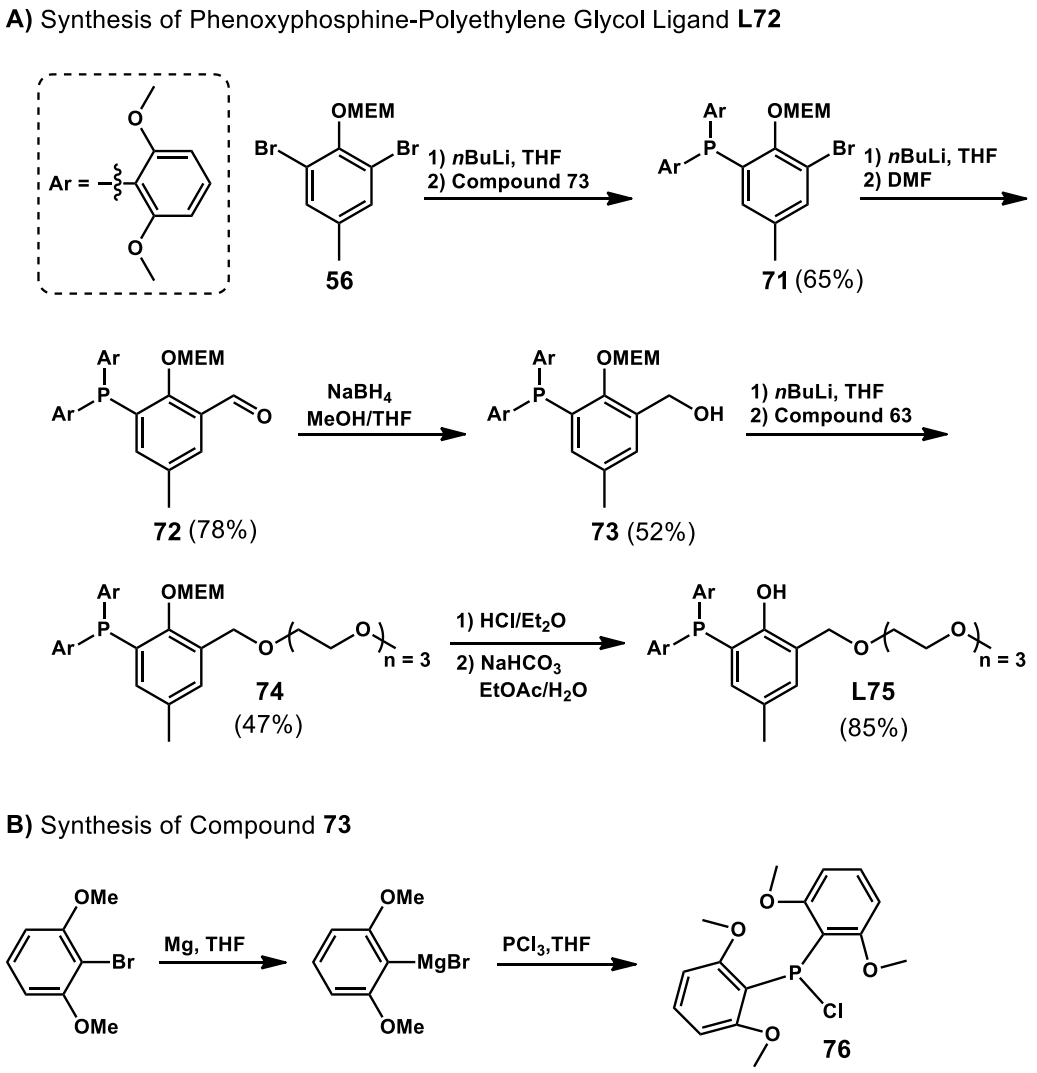

Scheme 4.2. Synthesis of ligand **L72** and compound **73**.

Preparation of Compound 71. To a solution of **56** (7.08 g, 20 mmol, 1.0 equiv) in 70 mL of dry THF in a Schlenk flask under nitrogen at -78 ^{o}C, *n*BuLi (1.6 M in hexanes, 12.8 mL, 20.5 mmol, 1.02 equiv) was added dropwise using a syringe pump. The reaction mixture was then stirred at -78 ^{o}C for 40 min. A solution of **73**

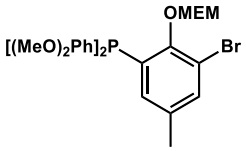

(6.13 g, 18 mmol, 0.9 equiv) in 50 mL of dry THF was cannula transferred to the reaction mixture and stirred for another 40 min at -78 ^{o}C, followed by warming naturally to RT. The reaction was quenched by the slow addition of H_2O and the products were extracted into Et_2O (3×75 mL). The organic layers were combined, washed with H_2O (2×50 mL), dried over Na_2SO_4, filtered, and evaporated to dryness. The crude material was purified by silica gel column chromatography (1:1 hexane: ethyl acetate) to afford a colorless oil (6.78 g, 11.7 mmol, 65%). ^{1}H NMR ($CDCl_3$, 400 MHz) δ 7.21 (d, *J* = 9.1 Hz, 3H), 6.72 (s, 1H), 6.48 (d, *J* = 8.2 Hz, 4H), 5.24 (s, 2H), 3.84 (t, *J* = 4.8 Hz, 2H), 3.49 (d, *J* = 4.1 Hz, 14H), 3.33 (s, 3H), 2.13 (s, 3H). ^{13}C NMR ($CDCl_3$, 101 MHz) δ 162.77, 162.68, 134.00, 132.46, 132.41, 130.12, 115.81, 113.19, 112.97, 104.64, 97.25, 97.17, 71.90, 69.04, 69.01, 59.03, 56.02, 20.78. ^{31}P NMR ($CDCl_3$, 162 MHz) δ -49.99.

Preparation of Compound 72. To a solution of **71** (6.78 g, 11.7 mmol, 1.0 equiv) in 70 mL of dry THF in a Schlenk flask under nitrogen at -78 ^{o}C, *n*BuLi (1.6 M in hexanes, 7.7 mL, 12.29 mmol, 1.05 equiv) was added dropwise using a syringe pump. The reaction mixture was stirred at -78 ^{o}C for 40 min. Dry DMF (5 mL, 65 mmol, 5.6 equiv) was added to the reaction mixture and stirred for another 40 min at -78 ^{o}C, followed by naturally warming to RT. The reaction was quenched by the slow addition of H_2O and the product was extracted into Et_2O (3×75 mL). The organic layers were combined, washed with H_2O (2×50 mL), dried over Na_2SO_4, filtered, and evaporated to dryness to afford a light yellow oil (4.83 g, 9.13 mmol, 78%). This compound was used directly in the next step without further purification.

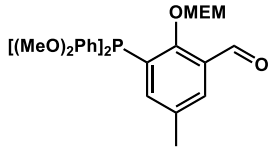

Preparation of Compound 73. Compound **72** (4.83 g, 9.13 mmol, 1.0 equiv) was dissolved in

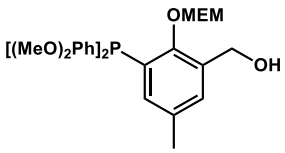

400 mL of MeOH and 80 mL of THF. Small aliquots of $NaBH_4$ (1.04 g, 27.4 mmol, 3 equiv) were added and the mixture was stirred at RT overnight. The reaction solvent was removed under vacuum and the residue was redissolved in Et_2O (100 mL). The ether layer was washed with H_2O (2×100 mL), dried over Na_2SO_4, filtered, and evaporated to dryness. The crude material was purified by silica gel column chromatography (2:3 hexane: ethyl acetate) to afford a white solid (2.52 g, 4.75 mmol, 52%). ^{1}H NMR ($CDCl_3$, 500 MHz) δ 7.21 (t, *J* = 8.3 Hz, 2H), 7.01 (d, *J* = 2.2 Hz, 1H), 6.85 – 6.81 (m, 1H), 6.47 (dd, *J* = 8.2, 2.8 Hz, 4H), 5.16 (s, 2H), 4.55 (d, *J* = 7.1 Hz, 2H), 3.86 – 3.80 (m, 2H), 3.72 (t, *J* = 7.1 Hz, 1H), 3.58 – 3.53 (m, 2H), 3.46 (s, 12H), 3.35 (s, 3H), 2.15 (s, 3H). ^{13}C NMR ($CDCl_3$, 126 MHz) δ 162.71, 162.64, 133.92, 133.13, 132.75, 130.64, 129.96, 104.47, 99.02, 98.93, 71.49, 68.76, 61.35, 59.10, 55.90, 21.02. ^{31}P NMR ($CDCl_3$, 202 MHz) δ -52.61.

Preparation of Compound 74. To a mixture of **73** (2.52 g, 4.75 mmol, 1 equiv) in 100 mL of dry

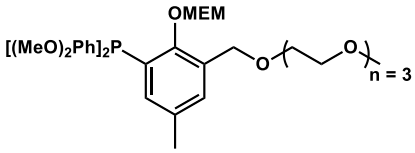

THF in a Schlenk flask under nitrogen at -0 ^oC, small aliquots of NaH (60%, 0.76 g, 19 mmol, 4 equiv) was added. The reaction mixture was stirred at RT for 1 h. A solution of compound **63** (4.9 g, 11.4 mmol, 2.0 equiv) in 50 mL of THF was cannula transferred into the reaction mixture and then stirred at RT for two day. The reaction was quenched by the slow addition of cold H_2O and the product was extracted into Et_2O (3×100 mL). The organic layers were combined, washed with H_2O (2×75 mL), dried over Na_2SO_4, filtered, and evaporated to dryness. The crude material was purified by silica gel column chromatography (1:4 hexane: ethyl acetate to 97:3 ethylacetate: methanol) to afford a

colorless oil (1.51 g, 2.23 mmol, 47%). This compound was used directly in the next step without further purification.

Preparation of Compound L75. Compound **74** (1.51 g, 2.23 mmol, 1 equiv) was dissolved in 100 mL of MeOH and then treated with 10 mL of 2 M HCl in Et_2O. The reaction mixture was stirred at RT overnight. The solvent was removed under vacuum and the product was dissolved in 200 mL of EtOAc. A 50 mL solution of 1 M $NaHCO_3$ in H_2O was then added. The mixture was stirred at RT for 30 min and the product was extracted into Et_2O (2×100 mL). The organic layers were combined, washed with H_2O (2×100 mL), dried over Na_2SO_4, filtered, and evaporated to dryness. The crude material was washed with hexane to afford a white waxy solid (1.12 g, 1.9 mmol, 85%). ^{1}H NMR (C_6D_6, 500 MHz) δ 7.63 (d, *J* = 2.3 Hz, 1H), 7.60 (d, *J* = 2.4 Hz, 1H), 7.53 (d, *J* = 2.1 Hz, 2H), 7.18 (d, *J* = 2.2 Hz, 2H), 6.99 (t, *J* = 8.2 Hz, 4H), 6.21 (dd, *J* = 8.1, 2.8 Hz, 9H), 4.62 (s, 3H), 3.46 (dd, *J* = 5.9, 3.9 Hz, 5H), 3.43 – 3.36 (m, 18H), 3.29 (dd, *J* = 5.8, 4.0 Hz, 4H), 3.13 (s, 25H), 3.07 (s, 5H), 2.09 (s, 6H). ^{13}C NMR (C_6D_6, 101 MHz) δ 162.00, 161.91, 154.86 (d, *J* = 8.2 Hz), 135.10, 134.79, 129.78, 127.49, 127.38, 122.51, 112.97, 112.78, 104.33, 72.01, 70.72, 70.69, 70.61, 69.55, 59.14, 55.85, 20.73. ^{31}P NMR (C_6D_6, 162 MHz) δ -59.76.

Preparation of Complex Ni21. Inside the glovebox, ligand **L72** (0.62 g, 1.05 mmol, 1.0 equiv) was dissolved in 50 mL of dry THF. Small aliquots of NaH (60%, 0.08 g, 2.10 mmol, 2.0 equiv) were added and the mixture was stirred at RT for 2 h. The mixture was filtered to remove excess NaH and then a solution of $NiPhBr(PMe_3)_2$ (0.3 g, 0.95 mmol, 0.9 equiv) in 20 mL of benzene was added. The resulting mixture was stirred at RT overnight. The next day, the solution was filtered to remove the precipitate and the filtrate was dried completely under vacuum. The crude material was dissolved in a mixture of 10 mL of pentane and 5 mL of benzene. Another filtration was performed to remove the precipitate and the filtrate was dried once again. Finally, the resulting solid was washed with pentane (3×5 mL) and dried to under vacuum to afford a yellow powder (0.35 g, 0.43 mmol, 45%).

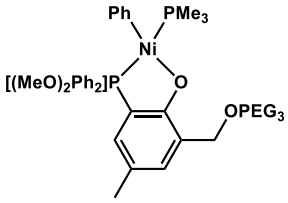

^{1}H NMR (C_6D_6, 500 MHz) δ 7.54 (d, *J* = 10.0 Hz, 1H), 7.30 (s, 1H), 7.20 (d, *J* = 7.3 Hz, 2H), 6.97 (t, *J* = 8.2 Hz, 2H), 6.72 (t, *J* = 7.4 Hz, 2H), 6.61 (t, *J* = 7.2 Hz, 1H), 6.15 (dd, *J* = 8.4, 3.5 Hz, 4H), 4.90 (s, 2H), 3.77 (t, *J* = 5.3 Hz, 2H), 3.62 (t, *J* = 5.3 Hz, 2H), 3.48 – 3.43 (m, 4H), 3.30 (dd, *J* = 12.0, 7.3 Hz, 4H), 3.08 (s, 13H), 2.15 (s, 3H), 0.87 (d, *J* = 8.8 Hz, 9H).

^{31}P NMR (C_6D_6, 162 MHz) δ -3.97 (d, *J* = 317.0 Hz), -15.24 (d, *J* = 317.0 Hz).

Preparation of Compound 75. This synthesis was modified from a reported procedure. A 200 mL Schlenk flask was charged with magnesium turnings (1.2 g, 50 mmol, 2.5 equiv) under nitrogen in 50 mL of dry THF. The compound **2-bromo-3-methoxyanisole** (8.68 g, 40 mmol, 2.0 equiv) was added to the reaction mixture and then stirred at RT for 3 h until the solution turned dark gray. The resulting Grignard reagent was slowly cannula transferred over a period of 45 min to a solution of PCl_3 (1.6 mL, 20 mmol,

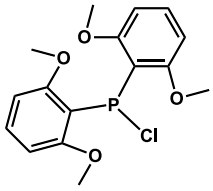

1.0 equiv) in 100 mL of dry THF at -78 ^{o}C. After the addition was complete, the heterogeneous mixture was continued stirring and allowed to warm up to RT overnight. Finally, the solvent was removed under vacuum and the crude product was used in the next step without further purification.

Polymerization Studies

General Procedure for Ethylene Polymerization.

Inside the drybox, the nickel complex (**Ni11** or **Ni21**) and $MBAr^{F}_{4}$ (if any) were dissolved in a mixture of 8 mL of toluene and 2 mL of Et_2O (if any) in a 20 mL vial and stirred for 10 min. Solid $Ni(COD)_2$ (8 equiv relative to nickel) was added and stirred until a clear solution was obtained (4–5 min). The mixture was loaded into a 10 mL syringe equipped with an 8-inch stainless steel needle. The loaded syringe was sealed by sticking the needle tip into a rubber septum and brought outside of the drybox. To prepare the polymerization reactor, 90 mL of dry toluene was placed in an empty autoclave. The autoclave was pressurized with ethylene to 80 psi, stirred for 5 min, and then the reactor pressure was reduced to 5 psi. This process was repeated three times to remove trace amounts of oxygen inside the reaction vessel. The reactor was then heated to the desired temperature and the catalyst solution was injected into the autoclave through a side arm. The autoclave was sealed and purged with ethylene at 40 psi (no stirring) three times. Finally, the reactor pressure was increased to the desired pressure, and the contents were stirred vigorously. To stop the polymerization, the autoclave was vented and cooled in an ice bath. A solution of MeOH (700 mL) was added to precipitate the polymer. The polymer was collected by vacuum filtration, rinsed with MeOH, and dried under vacuum at 80 °C overnight. The reported yields are average values obtained from duplicate or triplicate runs.

Special Notes:

- To obtain consistent polymer yields from run to run, the amount of catalyst used in each run must be kept as consistent as possible. To minimize errors due to weighing inconsistencies, we used a batch catalyst preparation method. First, we weighed out 50 µmol of the catalyst and then dissolved it into 50 mL of toluene. This solution was divided equally into 10 vials so that each vial contained 5 µmol of catalyst. Next, we combined each 5 µmol of catalyst with 20 mL of toluene and partitioned this 25 mL mixture into 10 vials so that each vial contained 0.5 µmol of catalyst. Finally, each vial was dried completely under vacuum and stored in a refrigerator inside the drybox until ready for use.
- For all polymerization reactions, except ones that were performed to determine the temperature profiles, the reaction temperature was controlled by manual cooling of the reactor with an air stream when the reactor increases more than 5°C above the starting temperature.
- To clean the Parr reactor, the vessel was washed with hot toluene (80 ^{o}C) to remove the polymer sample from the previous run and rinsed with acetone before drying under vacuum for at least 1 h to remove trace amounts of water.

4.6. Spectra Charaterization

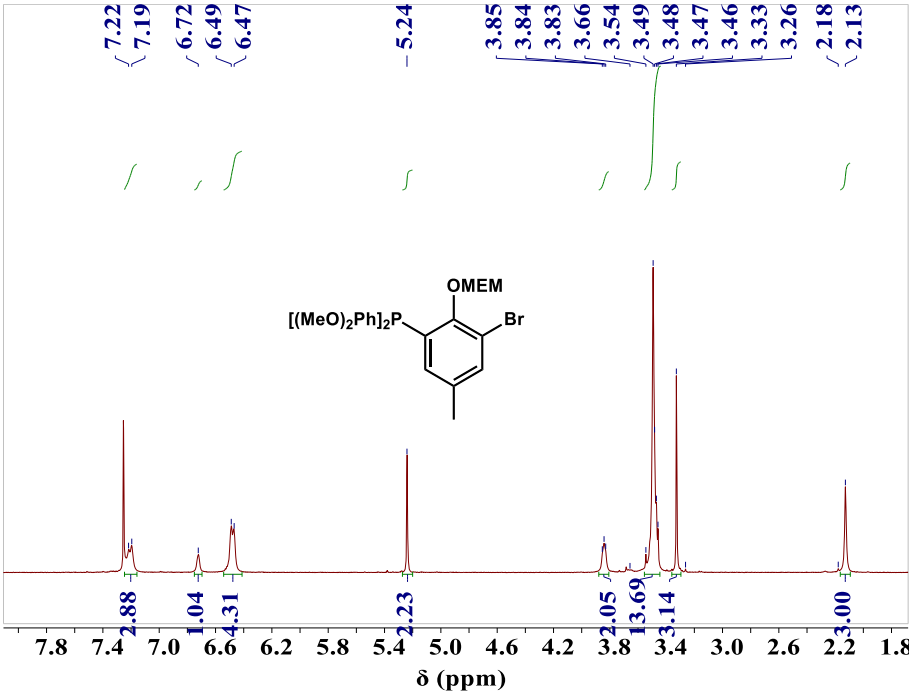

Figure 4.1. ^{1}H NMR spectrum ($CDCl_3$, 400 MHz) of compound **71**.

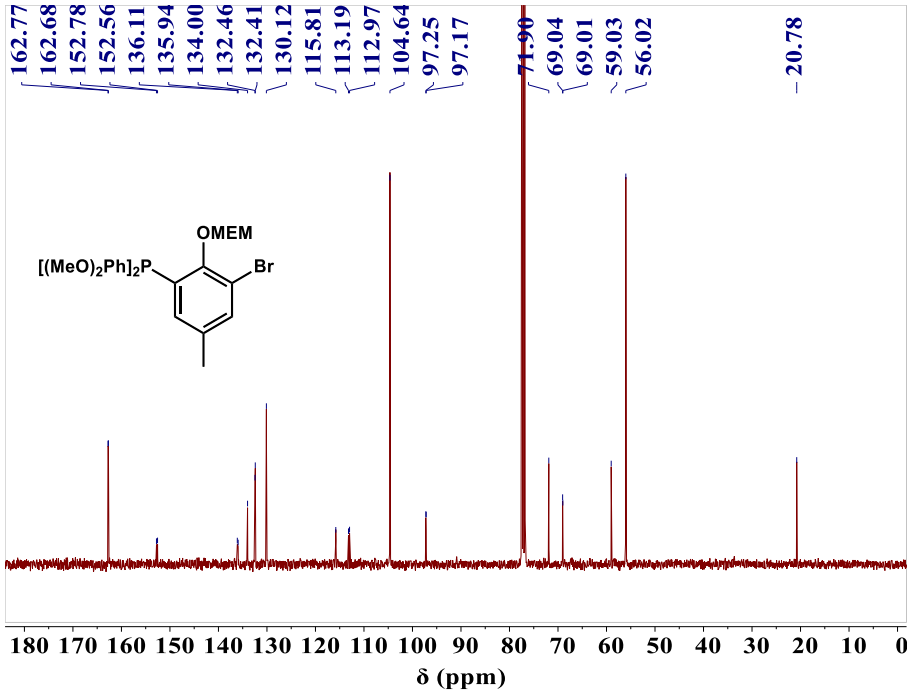

Figure 4.2. ^{13}C NMR spectrum ($CDCl_3$, 101 MHz) of compound **71**.

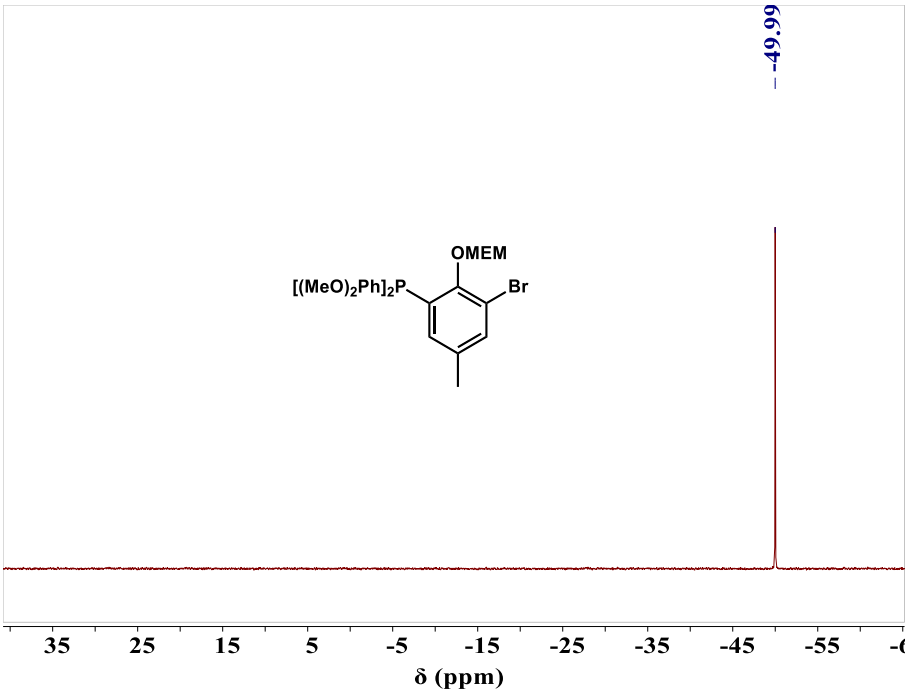

Figure 4.3. ^{31}P NMR spectrum ($CDCl_3$, 162 MHz) of compound **71**.

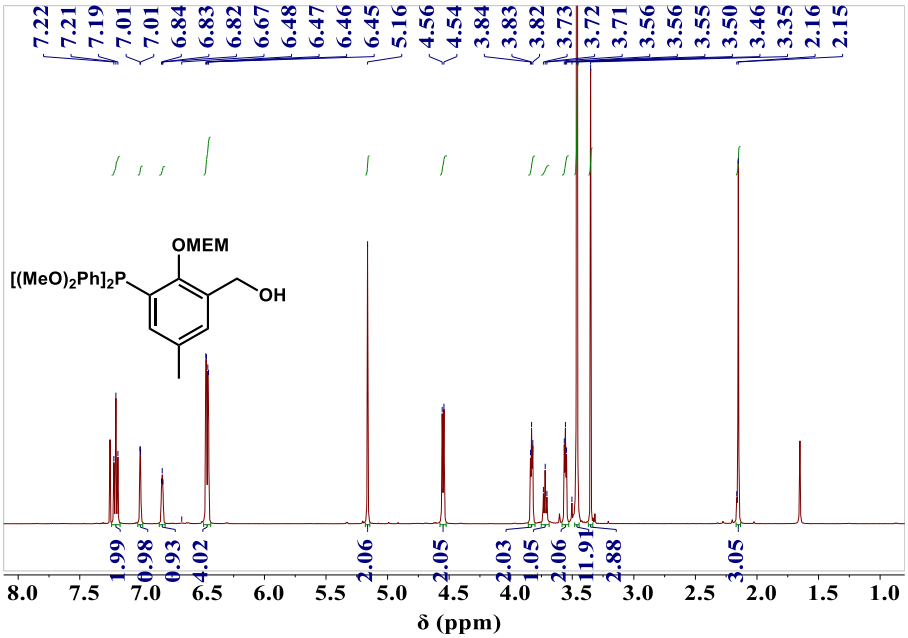

Figure 4.4. ^{1}H NMR spectrum ($CDCl_3$, 500 MHz) of compound **73**.

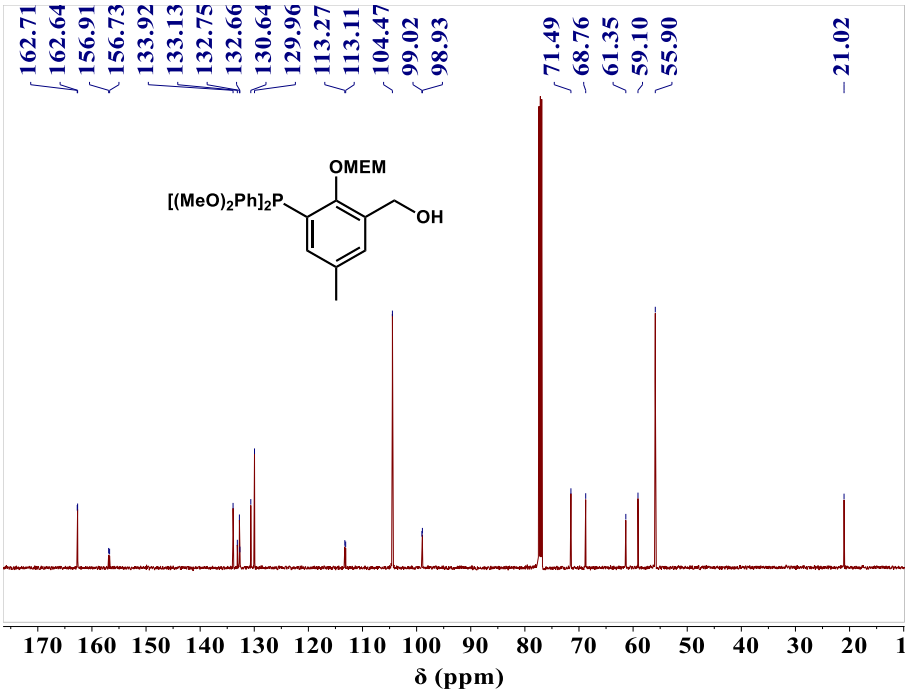

Figure 4.5. ^{13}C NMR spectrum ($CDCl_3$, 126 MHz) of compound **73**.

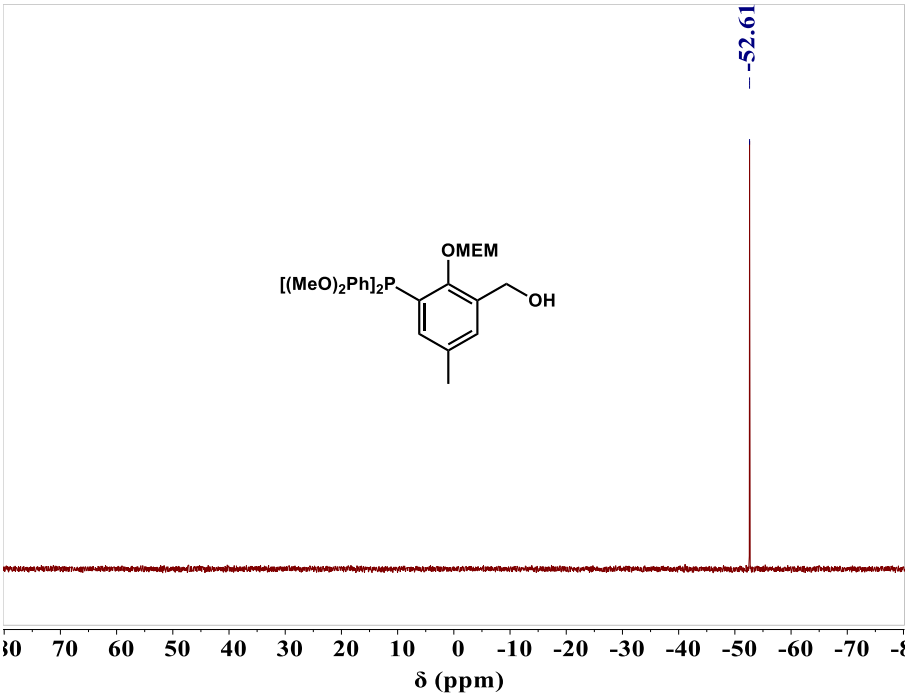

Figure 4.6. ^{31}P NMR spectrum ($CDCl_3$, 202 MHz) of compound **73**.

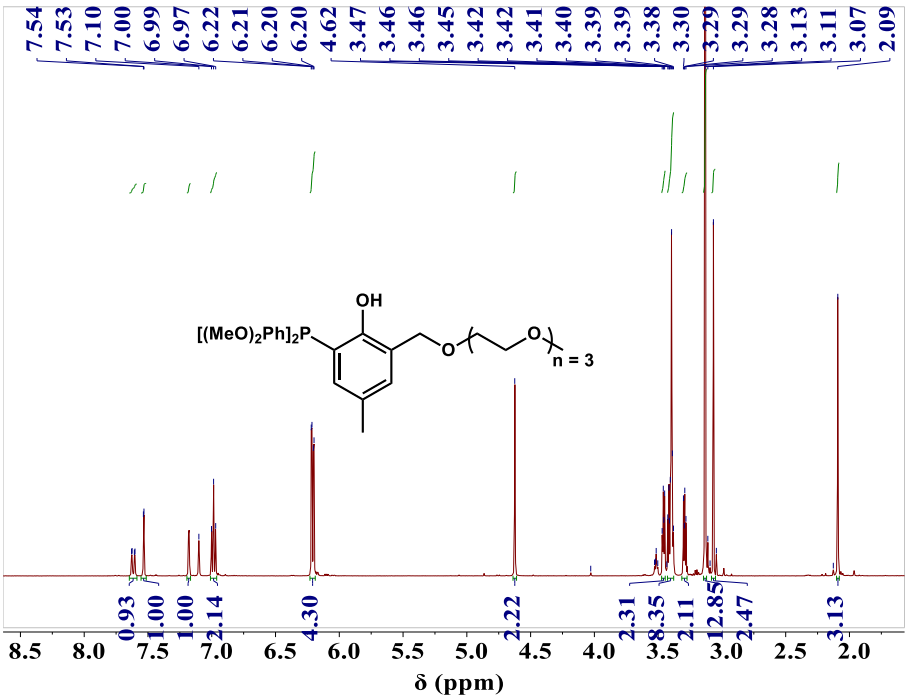

Figure 4.7. ^{1}H NMR spectrum (C_6D_6, 500 MHz) of compound **L75**.

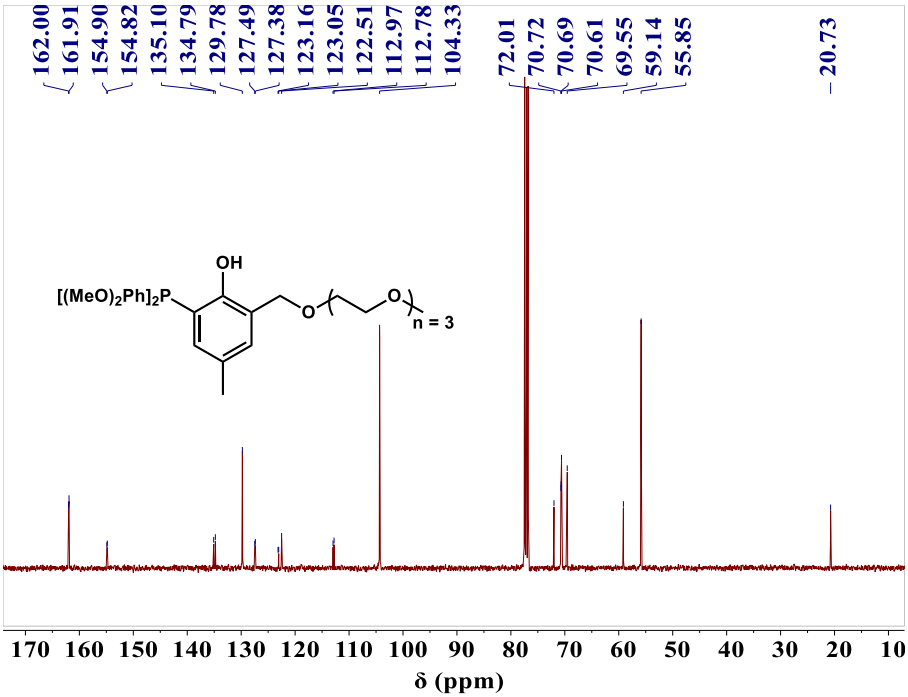

Figure 4.8. ^{13}H NMR spectrum (C_6D_6, 101 MHz) of compound **L75**.

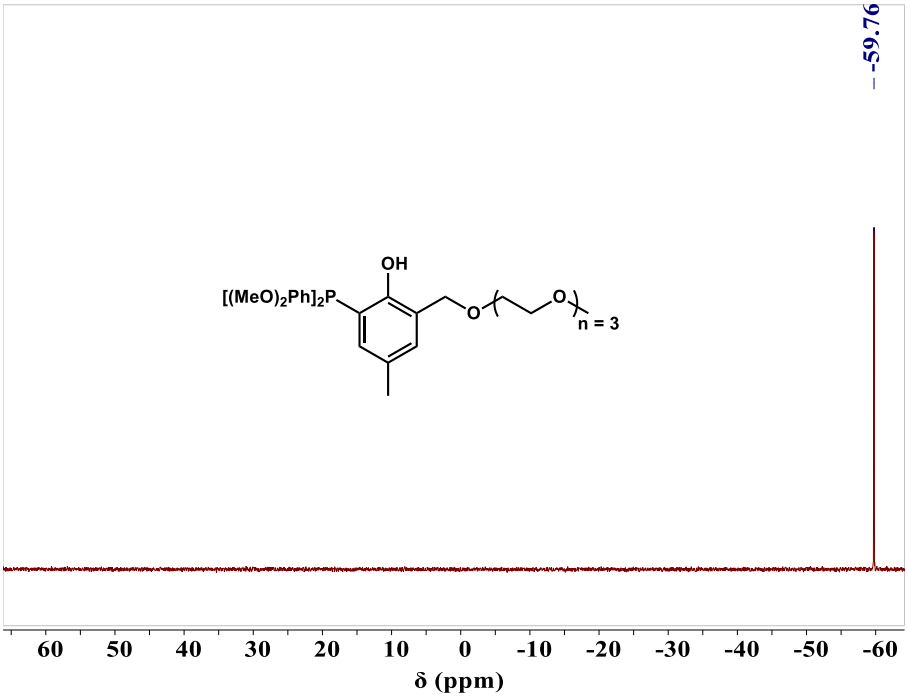

Figure 4.9. ^{31}P NMR spectrum (C_6D_6, 162 MHz) of compound **L75**.

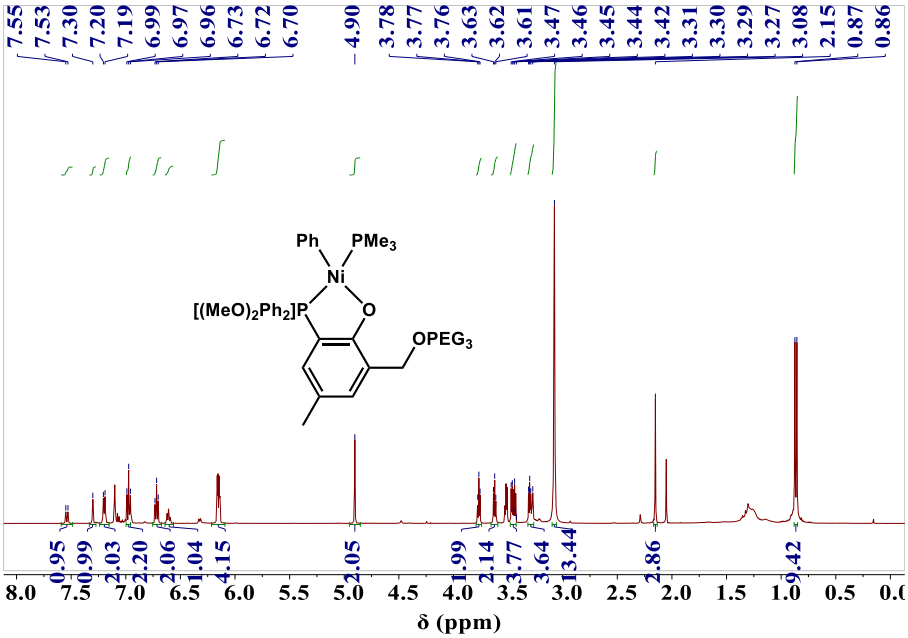

Figure 4.10. ^{1}H NMR spectrum (C_6D_6, 500 MHz) of complex **Ni21**.

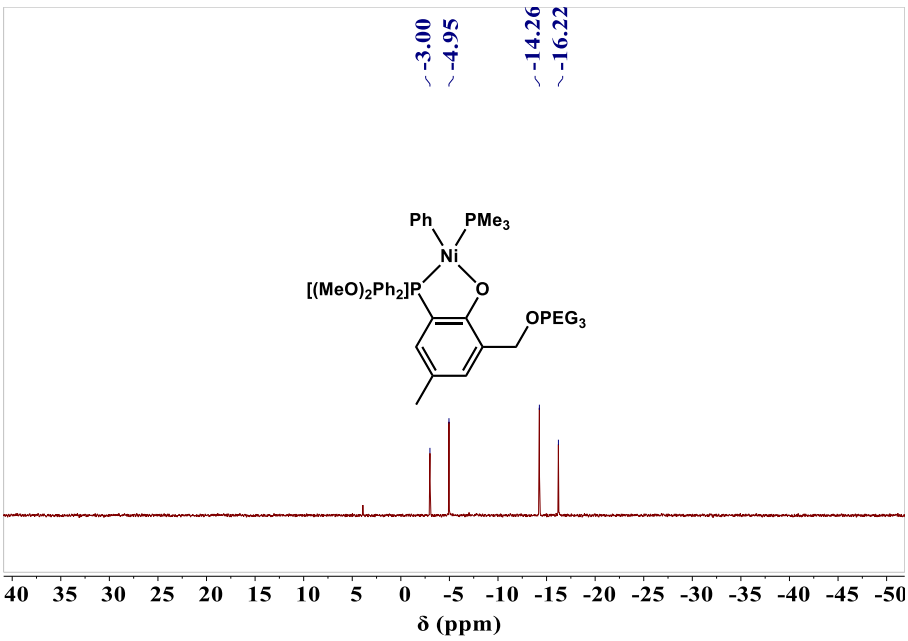

Figure 4.11. ^{31}P NMR spectrum (C_6D_6, 162 MHz) of complex **Ni21**.

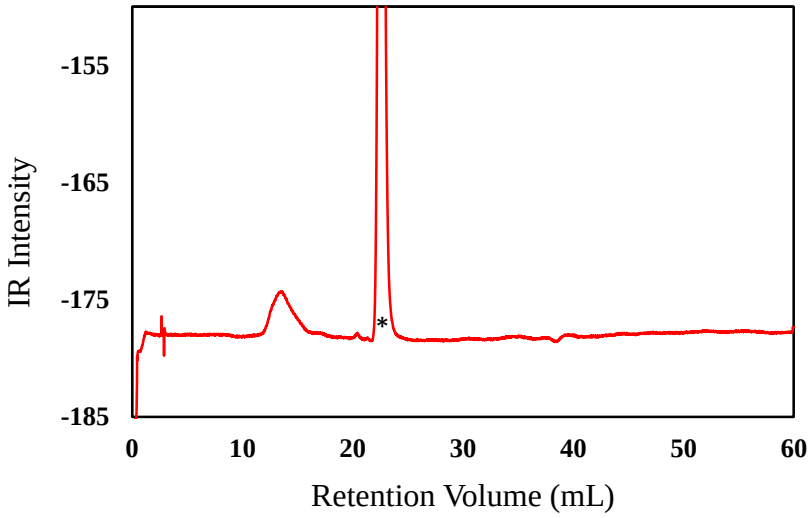

Figure 4.12. GPC chromatograms of the polyethylene obtained in Table 4.1, Entry 1. The peak at ~22 mL retention volume marker with an asterisk (*) is derived from a contaminant in the GPC column, not the sample itself.

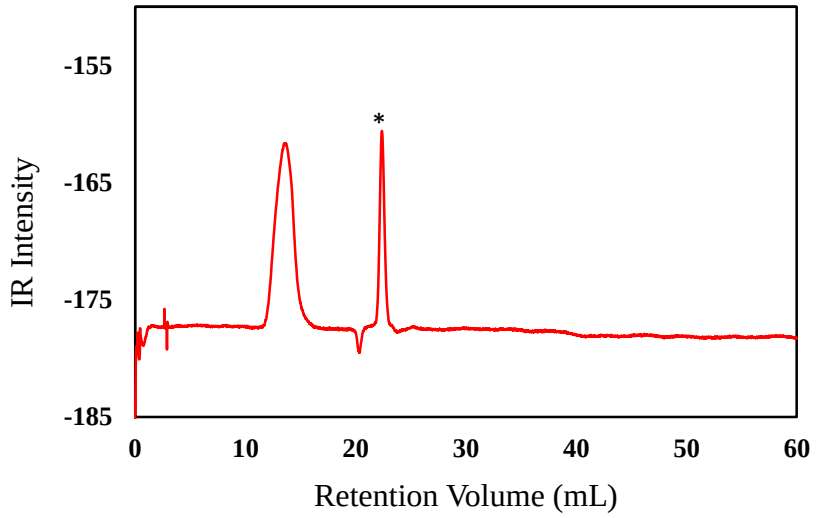

Figure 4.13. GPC chromatograms of the polyethylene obtained in Table 4.1, Entry 2. The peak at ~22 mL retention volume marker with an asterisk (*) is derived from a contaminant in the GPC column, not the sample itself.

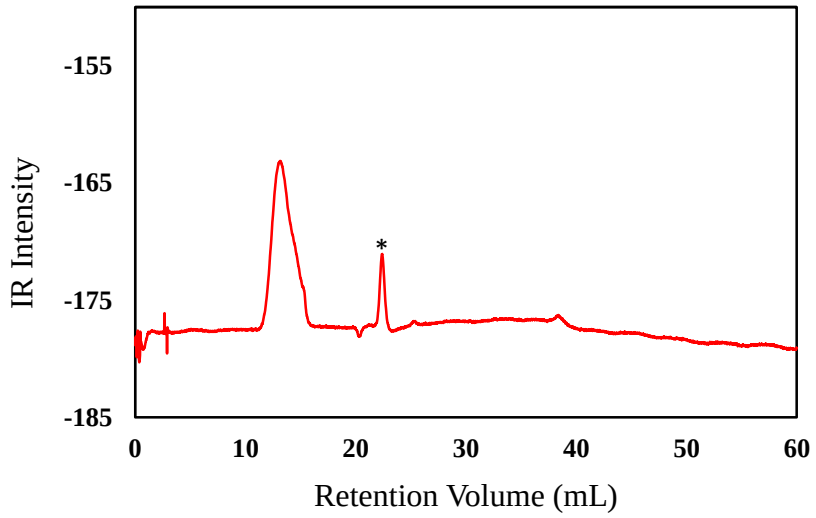

Figure 4.14. GPC chromatograms of the polyethylene obtained in Table 4.1, Entry 3. The peak at ~22 mL retention volume marker with an asterisk (*) is derived from a contaminant in the GPC column, not the sample itself.

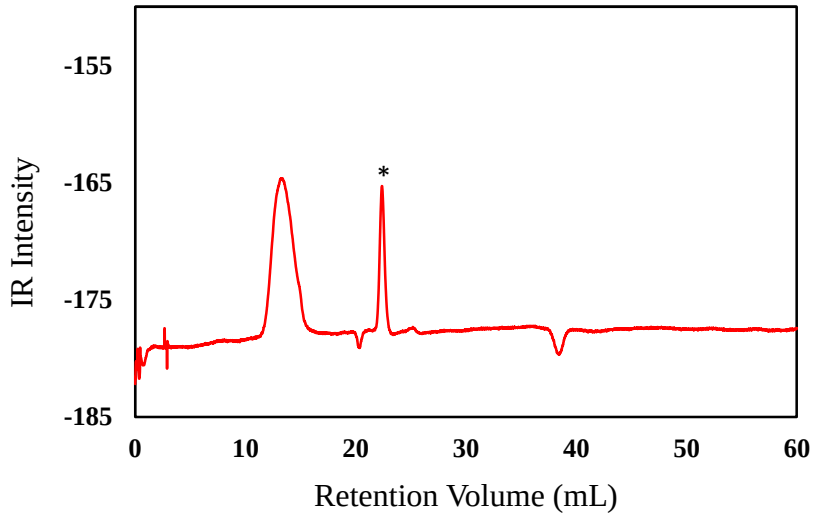

Figure 4.15. GPC chromatograms of the polyethylene obtained in Table 4.1, Entry 4. The peak at ~22 mL retention volume marker with an asterisk (*) is derived from a contaminant in the GPC column, not the sample itself.

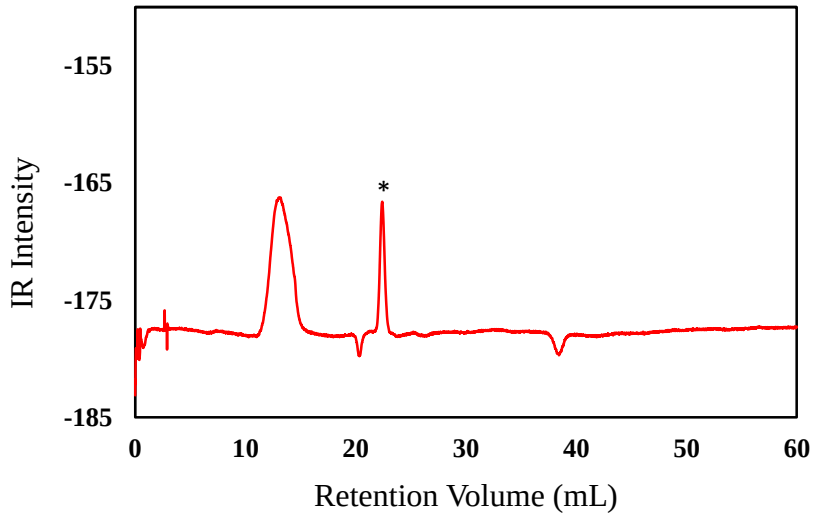

Figure 4.16. GPC chromatograms of the polyethylene obtained in Table 4.1, Entry 5. The peak at ~22 mL retention volume marker with an asterisk (*) is derived from a contaminant in the GPC column, not the sample itself.

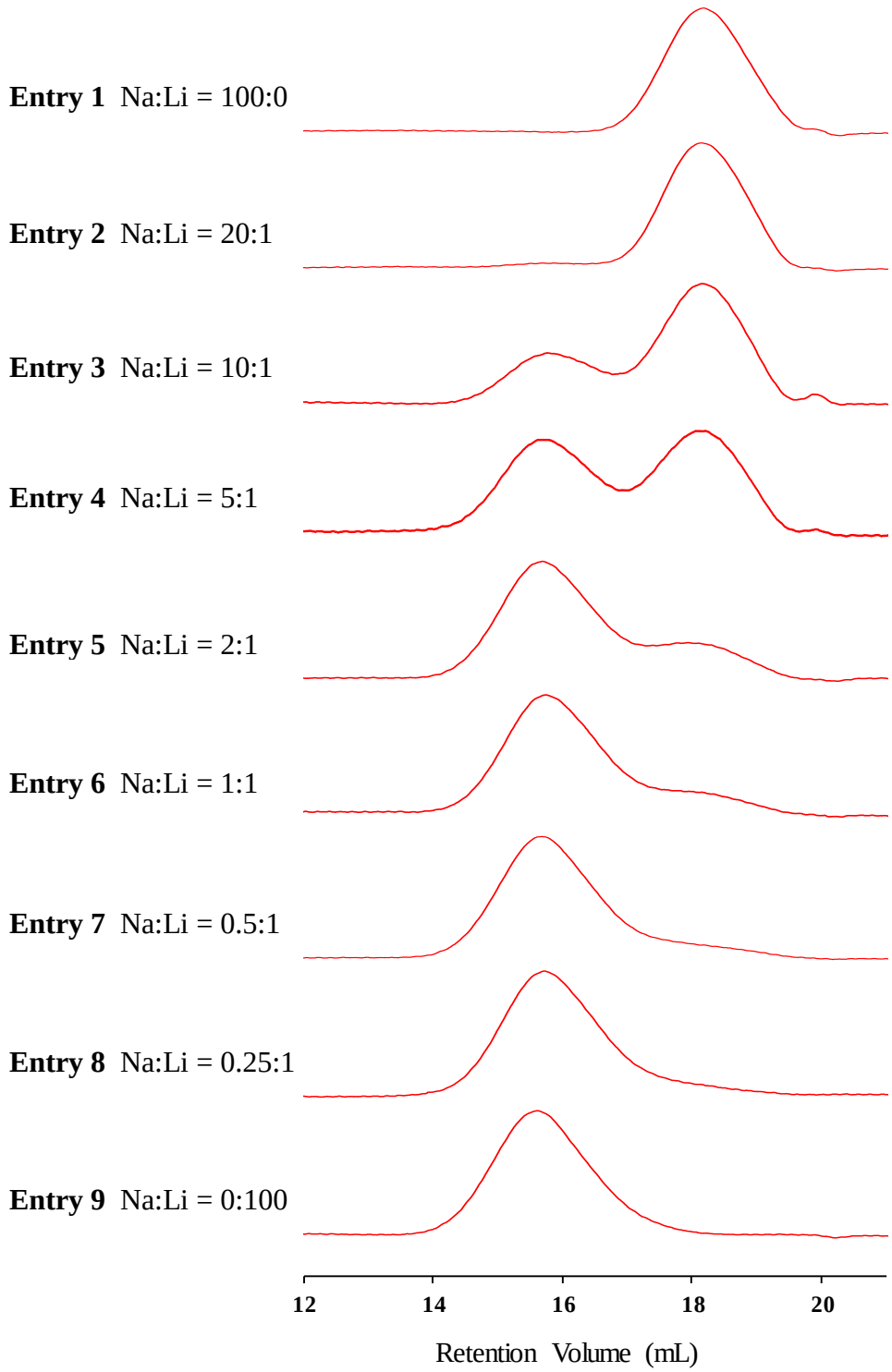

Figure 4.17. GPC chromatograms of the polyethylene obtained in Table 4.2.

Chapter 5. Evaluation of Dicopper Azacryptand Complexes in Aqueous CuAAC Reactions and Their Tolerance Toward Biological Thiols

This work has been previously published.

Reproduced with permission from Tran, T. V.; Couture, G.; Do, L. H. *Dalton Trans.*, **2019**, *48*, 9751-9758. DOI:10.1039/C9DT00724E.

5.1. Introduction

Copper-catalysed azide-alkyne cycloaddition (CuAAC)[142-143] is undoubtedly one of the most versatile reactions in the bioorthogonal chemistry toolbox (Scheme 5.1A).[144-146] It has been used extensively in chemical biology research, ranging from the conjugation of biomolecules with fluorescent tags[147] to the study of biomolecule-drug interactions.[148] Although the application of copper complexes for CuAAC reactions inside living cells has also been achieved,[149-152] their catalytic efficiency in vivo is extremely low.[153] It is believed that the copper complexes are prone to catalyst inhibition via coordination by endogenous nucleophiles (Scheme 5.1B, left). More recently, there have been exciting advances in *copper-free* azide-alkyne cycloaddition reactions.[154] However, these methods typically require the use of specialized strained alkynes as coupling partners, which can add to the cost and labour required to prepare the desired reaction substrates.

Inspired by Nature's strategy of using substrate gating in metalloenzymes to prevent active site deactivation by intracellular species,[155-156] we sought to mimic this capability in small-molecule complexes. We were fascinated by examples in the literature in which molecular cages were used successfully to carryout metal-catalysed processes in environments that are typically unfavourable for such reactions.[157-160] Presumably, such complexes can provide a confined space that promotes selective bimolecular reactions[161] and shield their metal centres from undergoing deactivation pathways.

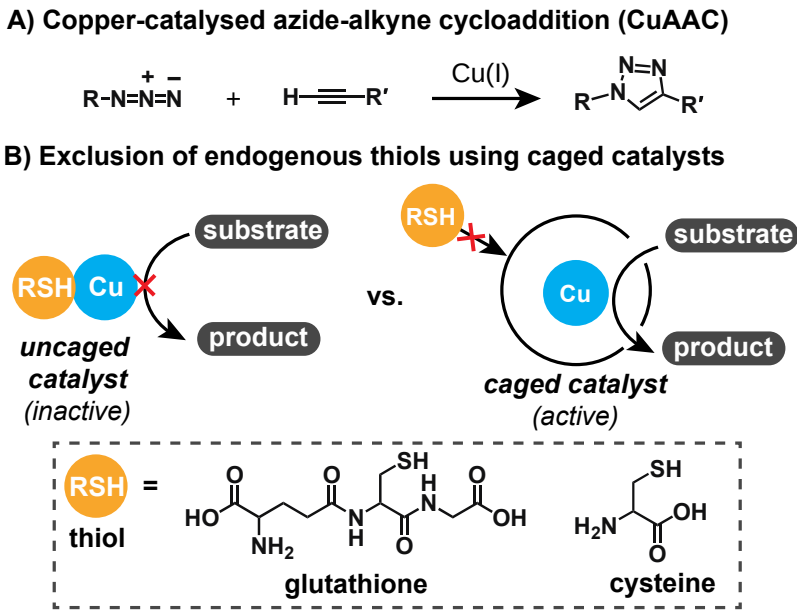

Scheme 5.1. A) General reaction scheme for copper-catalysed azide-alkyne cycloaddition (CuAAC); and B) proposed application of caged catalysts to prevent inhibition by biological thiols.

To determine whether molecular caging could be a viable approach toward more biocompatible CuAAC catalysts, we sought to explore the reactivity of dicopper azacryptand complexes in water.[162-164] We hypothesized that the sterically protecting azacryptand structure might allow passage of small neutral substrates into the catalyst interior but could exclude larger

molecular species from entry (Scheme 5.1B). Using benzyl azide and phenylacetylene as model substrates,[165] we compared the performance of various copper catalysts in the presence and absence of biological thiols.[166] Although these studies were carried out in the reaction flask rather than inside living cells, our results will help to inform ongoing efforts to design better catalysts for in vivo applications.[167]

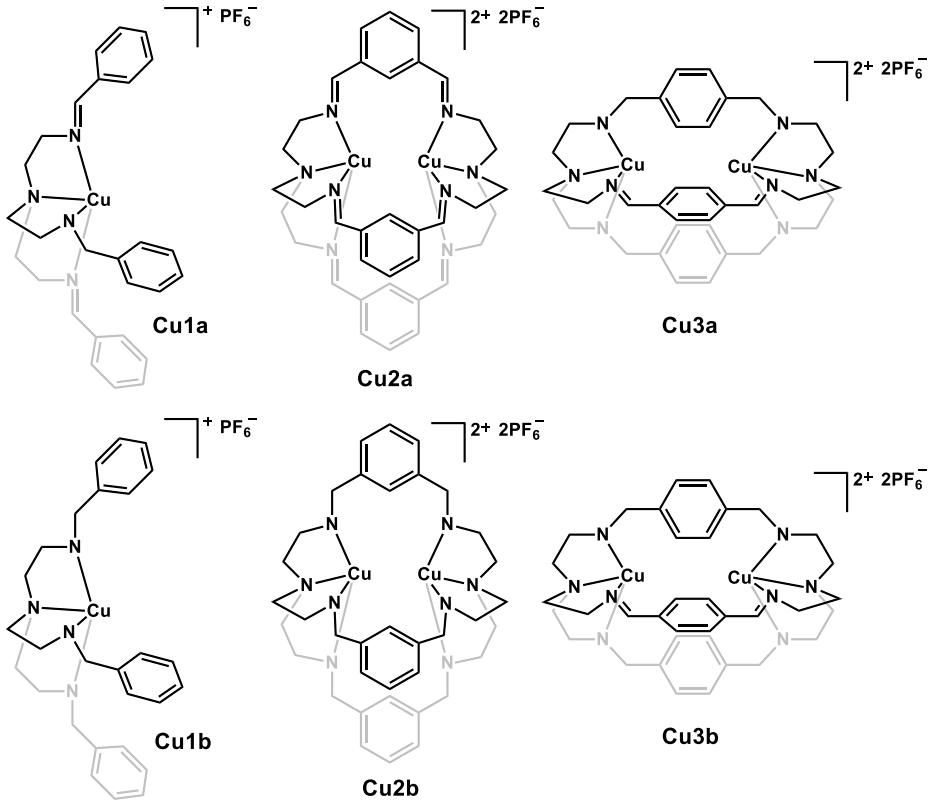

Chart 5.1. Structures of monocopper (**Cu1**) and dicopper complexes (**Cu2-3**) used in this study.

5.2. Copper Catalyst Selection and Synthesis

A variety of copper complexes have been tested previously for aqueous CuAAC reactions,[168-169] including those containing dendrimers[170] and organic nanoparticles.[171-172] The criteria we used for selecting possible CuAAC catalysts were that the metal centres must be encapsulated within a

caged structure and the supporting ligands should be easy to synthesize. In this regard, the dicopper(I) azacryptand complexes seemed to satisfy these requirements (Chart 5.1).[164, 173] The azacryptand ligands can have either tris(imino)amine (**Cu2a**/**Cu3a**) or tris(amino)amine chelators (**Cu2b**/**Cu3b**) for copper, which provide different electronic donor abilities and ligand flexibility. The benzene spacers in the azacryptands could be attached to the tetradentate chelators via either 1,3- or 1,4-linkages, which leads to differences in the Cu–Cu distance and active site accessibility of the corresponding metal complexes.

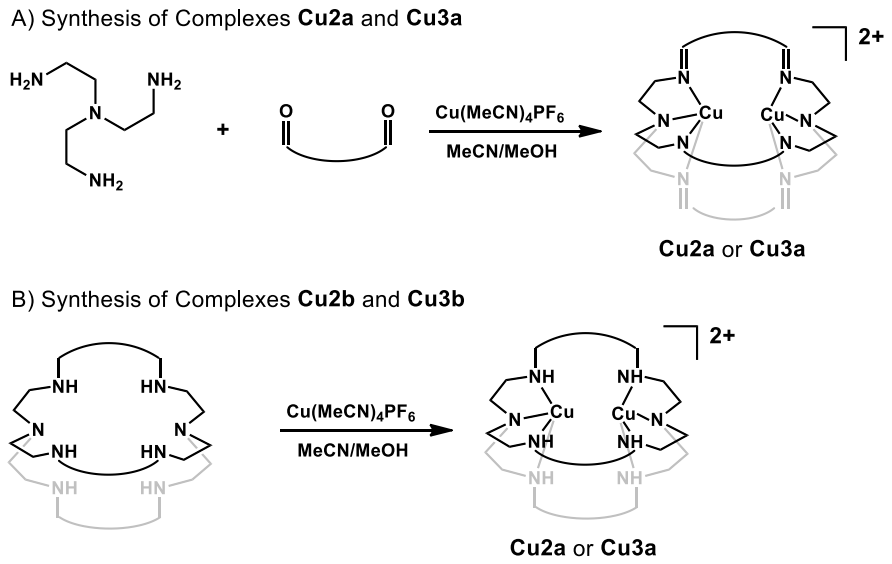

Scheme 5.2. Synthesis of the copper azacryptand complexes. The curved lines between the aldehyde group represent either the 1,3- or 1,4- benzene spacers.

Rather than generating the copper(I) catalysts in situ for reaction studies, we first prepared the metal complexes using one of the procedures outlined in Scheme 2.[164] For the Schiff base complexes, a one pot synthesis procedure was carried out by combining tris(2-aminoethyl)amine, isophthalaldehyde (for **Cu2a**) or terephthalaldehyde (for **Cu3a**), and

$Cu(MeCN)_4PF_6$ in MeCN/MeOH. To synthesize complexes **Cu2b** and **Cu3b**, the corresponding apo azacryptand ligands were treated with 2.0 equiv of $Cu(MeCN)_4PF_6$ to provide the desired products. The dicopper(I) complexes **Cu2a** and **Cu3a** are much less sensitive toward air oxidation than **Cu2b** and **Cu3b**,[174] respectively, presumably because their more rigid structures prevent reaction of the copper(I) ions with dioxygen.[173] Several dicopper(I) tris(imino)amine[175-177] and dicopper(II) tris(amino)amine[163, 178] cryptand complexes have been characterized structurally by X-ray crystallography.

As mononuclear analogues of the azacryptand complexes, we also prepared Cu(I) species using tripodal tetradentate ligands (**Cu1a**/**Cu1b**, Chart 5.1).[179-180] The synthesis of these compounds is described in Schemes 5.4 and Schemes 5.5. Complex **Cu1b** was found to spontaneously disproportionate in solution, however, as indicated by the gradual formation of a red precipitate over time.[165, 179]

5.3. CuAAC Reaction

5.3.1. Comparison of Catalyst Activity

To evaluate their catalytic performance, we tested complexes **Cu1-3** in the reaction between benzyl azide and phenylacetylene in water at 37 °C for 24 h (Table 5.1). A slight excess of phenylacetylene was used to promote the formation of Cu(I)-acetylide σ complexes.[181] Sodium ascorbate was also added to prevent oxidation of Cu(I) to Cu(II) since the reactions were performed in air.[182] At a catalyst concentration of 50 μM, which is approximately 0.05 mol% catalyst loading relative to benzyl azide, all of the copper complexes gave quantitative yields. When the catalyst concentration was lowered to 5 μM

(0.005 mol% catalyst loading relative to benzyl azide), complexes **Cu1b** (77%, entry 2), **Cu2a** (87%, entry 3), and **Cu2b** (94%, entry 4) gave good yields. However, complexes **Cu1a** (entry 1), **Cu3a** (entry 5), and **Cu3b** (entry 6) only provided moderate amounts (~50%) of 1-benzyl-4-phenyltriazole (**P4**). In comparison, the reaction of benzyl azide and phenylacetylene under similar conditions using $CuSO_4$ salt gave only 29% yield at 50 μM of copper and <5% yield at 5 μM of copper (entry 7). It has been reported that in the absence of supporting ligands, Cu(I) is prone to be oxidized to Cu(II) and to form catalytically inactive metal-acetylide clusters. The addition of *β*-cyclodextrin (*β*-CD), which has been shown to improve aqueous CuAAC reactions,[183] did not appear to help at 5 μM copper salt concentration (entry 8).

Several interesting observations were made in the experiments above. First, all of the copper complexes tested showed excellent to moderate activity in water and under air using relatively low catalyst loading. We found that no special additives or "catalyst enhancements" were needed to achieve high catalytic activity. Second, it appears that dicopper azacryptand complexes **Cu2a** and **Cu2b** are slightly more active than their monocopper counterparts **Cu1a** and **Cu1b**, respectively. Although the dicopper complexes have twice as many equivalences of copper atoms as that of the monocopper complexes, it is not clear whether both copper sites in the dicopper systems are involved in catalysis. Different mechanistic pathways have been proposed for CuAAC reactions,[184] including those based on monometallic,[185] bimetallic,[186] and polymetallic[187-188] active species. Without conducting further mechanistic studies, we are uncertain which is the preferred mechanism for dicopper azacryptands. Third, our results suggest that the dicopper

complexes with 1,3-benzene linkers (**Cu2a**/**Cu2b**) are more efficient catalysts than those with 1,4-benzene linkers (**Cu3a**/**Cu3b**). Perhaps the more open catalyst structures in **Cu3a** and **Cu3b** provide less steric protection of the copper ions compared to those in **Cu2a** and **Cu2b**, respectively.

Table 5.1. Comparison of Copper Catalysts[a]

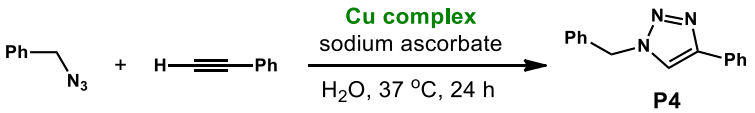

Entry	Complex	GC Yield (%)[b]	
		50 µM Complex	5 µM Complex
1	**Cu1a**	99	50
2	**Cu1b**	99	77
3	**Cu2a**	99	87
4	**Cu2b**	99	94
5	**Cu3a**	99	54
6	**Cu3b**	99	51
7	$CuSO_4$	29	<5
8	$CuSO_4$/ β-CD[c]	40	<5

[a]Reaction conditions: benzyl azide (1.00 mmol), phenylacetylene (1.37 mmol), Cu (0.5 or 0.05 µmol), sodium ascorbate (0.15 mmol) in H_2O (10 mL) at 37 °C for 24 h. [b]Average GC yields from duplicate runs. [c]Abbreviation: β-CD = β-cyclodextrin.

5.3.2. Comparison of Thiol Tolerance

Given the favourable results in Table 5.1, we next examined whether the copper complexes are inhibited by biological thiols (Table 5.2).[189-190] We found that in the presence of 100 µM of glutathione, all of the copper complexes (50 µM) afforded quantitative yields of the CuAAC product **P4**. In contrast, the addition of 100 µM of cysteine to the benzyl azide, phenylacetylene, and copper mixture, led to significant decrease in yields. For

complexes **Cu1a** (entry 1), **Cu 3a** (entry 6), and **Cu 3b** (entry 7), the yields were observed to be <20%. For the more active catalysts, **Cu 1b** (entry 2), **Cu 2a** (entry 3), and **Cu 2b** (entry 4), about ~30-40% yields of **P4** were obtained. To evaluate the effects of pH, we carried out CuAAC using benzyl azide, phenylacetylene, and complex **Cu 2b** in phosphate buffered saline (PBS, pH = 7.4). We observed that in the presence of 100 μM of glutathione, quantitative amounts of **P4** were obtained. However, once again, the addition of cysteine instead of glutathione afforded a lower yield (79%), albeit higher than that obtained when the reaction was performed in pure water (cf. entry 4 vs. 5). Interestingly, our results suggest that the caged complexes **Cu2a** and **Cu2b** *do not* provide greater protection of the catalyst than the tripodal complex **Cu1b** since all three catalysts performed similarly in the presence of the sulphur-containing amino acid. However, it is worth noting that in the biological milieu, the concentration of glutathione can be as high as 10 mM[191] whereas that of free cysteine is several orders of magnitude lower.[192] Thus, CuAAC catalysts that are not inhibited by glutathione could be useful for intracellular applications.

Table 5.2. Comparison of Copper Catalysts in the Presence of Biological Thiols[a]

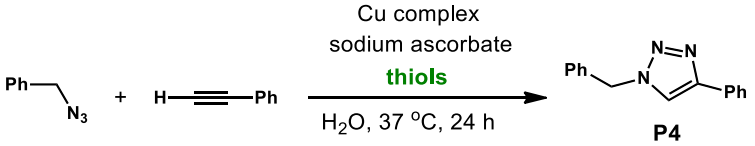

Entry	Complex (50 μM)	GC Yield (%)[b]	
		Glutathione (100 μM)	Cysteine (100 μM)
1	**Cu1a**	99	18
2	**Cu1b**	99	37
3	**Cu2a**	99	30
4	**Cu2b**	99	41
5[c]	**Cu2b**	99	79
6	**Cu3a**	99	18
7	**Cu3b**	99	13

[a]Reaction conditions: benzyl azide (1.00 mmol), phenylacetylene (1.37 mmol), Cu (0.5 μmol), sodium ascorbate (0.15 mmol), thiol (1.0 μmol) in H_2O (10 mL) at 37°C for 24 h. [b]Average GC yields from duplicate runs. [c]This reaction was performed in PBS buffer (pH = 7.4) rather than in pure water.

Our surprising observation that the copper complexes are more tolerant of glutathione than cysteine warranted further investigations. To determine whether the thiol additives bind to copper we first carried out metal binding studies by UV-vis absorption spectroscopy (Figures 5.1, Figure 5.2 and Figure 5.3). When a 50 μM aqueous solution of **Cu2a** was treated with 2 equiv of either glutathione (Figure 5.1A) or cysteine (Figure 5.1B), the optical band at ~360 nm decreased instantaneously and continued to diminish over the course of ~1 h. To gain further insights into the interactions between **Cu2a** and thiols, additional studies by ^{1}H NMR spectroscopy were performed. As shown in Figure 1C, the peaks corresponding to the cryptand ligands in **Cu2a**/glutathione and **Cu2a**/cysteine were shifted in comparison to those in **Cu2a**. The NMR spectrum of **Cu2a**/cysteine showed more

peaks than that of **Cu2a**/glutathione, perhaps suggesting that more than one chemical species might be present in the latter.

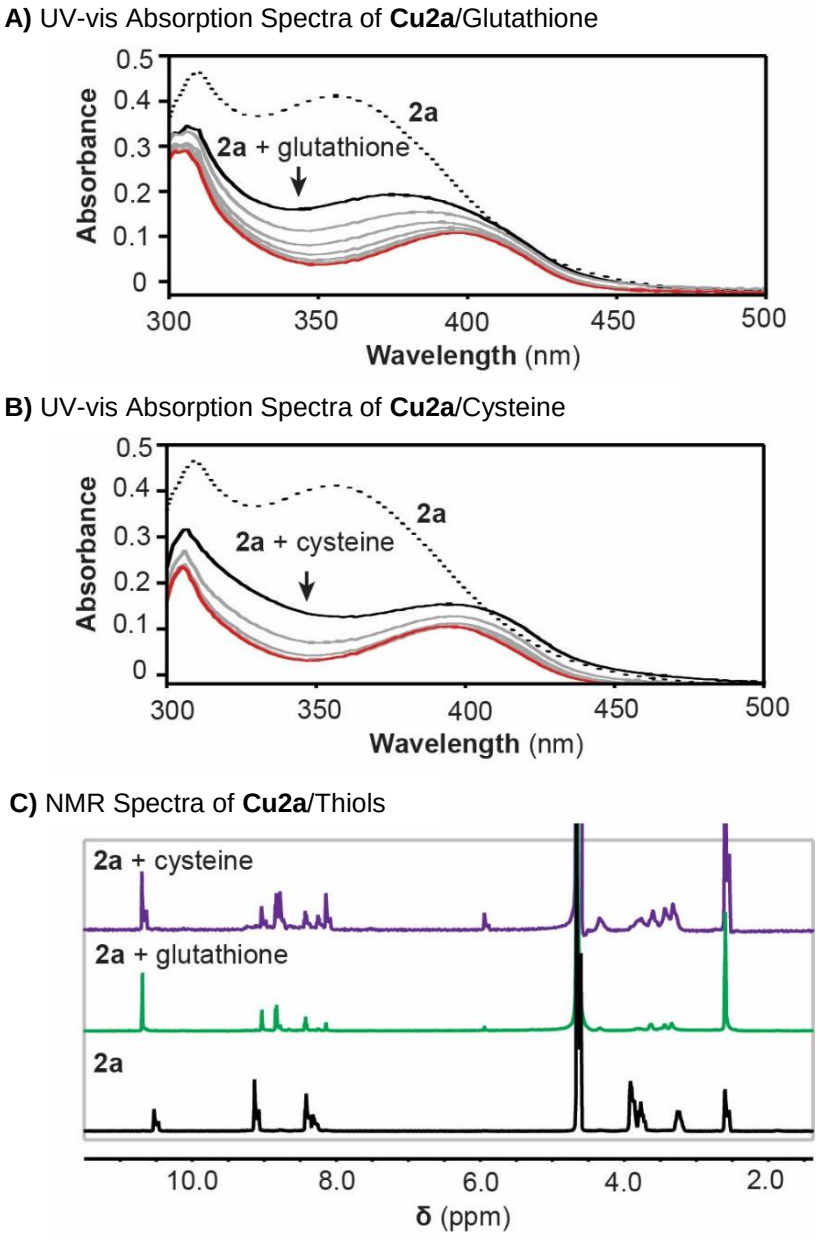

Figure 5.1. Reaction of complex **Cu2a** (50 µM) with biological thiols (100 µM). Plots A and B show the UV-vis absorption spectra (H_2O) of **Cu2a**/glutathione and **Cu2a**/cysteine, respectively. The dotted trace shows the spectrum of **Cu2a** without any additives. The solid black traces were obtained right after mixing **Cu2a** with either glutathione or cysteine and the solid red traces were

obtained after ~60-80 min. Plot C shows the NMR spectra (D_2O/CD3CN:1/2, 600 MHz) of **Cu2a**, **Cu2a**/glutathione and **Cu2a**/cysteine as indicated.

Similar results were obtained in the study of the monocopper **Cu1a** complex (Figure 5.2) and the dicopper **Cu3a** complex (Figure 5.3) with thiols. Taken together, these data clearly indicate that sulfur-containing biomolecules readily coordinate to the copper complexes, regardless of whether they are supported by cryptand or tripodal ligands. However, the exact nature of the copper-thiol interaction cannot be deduced from these spectroscopic data.

In light of the observations above, it is difficult to rationalize why the CuAAC reaction is so much less efficient in the presence of cysteine compared to glutathione since they both bind copper ions. Perhaps an important clue is our observation that metal precipitation might be occurring. For example, we found that when aqueous solutions containing high concentrations (6.7 maM) of **Cu2a** were mixed with 2 equiv of glutathione, a light yellow solid had formed, which could be redissolved with prolonged stirring. Characterization of this yellow material by NMR spectroscopy in DMSO-d_6 revealed that it contained the reaction components. Interestingly, when cysteine was added to **Cu2a** instead of glutathione, a dark colored material quickly precipitated out of solution over the course of several minutes. This precipitate was washed with acetonitrile to remove organic soluble species and then the dark insoluble fraction was dissolved in DMSO-d_6. Analysis by NMR spectroscopy showed that this sample does not give any proton signals, which suggest that it most likely contains copper metal. Under our experimental CuAAC conditions (Table 5.2), the catalyst (50 μM) and thiol (100 μM) concentrations were significantly lower so we would not likely be able to detect any copper-containing precipitates if such species were formed. At this time, we

tentatively attribute the different effects of thiols to their differences in modes of action. However, further evidence must be obtained to support this working hypothesis.

5.3.3. Copper Azacryptand vs. TBTA Complexes

One of the most successful catalysts for aqueous CuAAC are copper tris(benzyltriazolemethyl)amine (Cu-**TBTA**) complexes.[165, 169] The commercially available **TBTA** ligand (Scheme 5.3) was shown to protect Cu(I) from oxidation and disproportionation and at the same time, enhance its catalytic activity. To determine how the dicopper azacryptands measure up to the well-known Cu-**TBTA** complexes, we decided to perform additional reactivity studies.

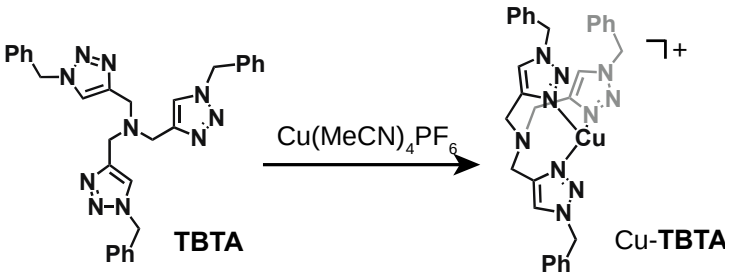

Scheme 5.3. Structure of the tris(benzyltriazolemethyl)amine ligand (TBTA) and its Cu(I) complex.

First, we evaluated the reaction of benzyl azide and phenylacetylene using low catalyst concentrations under our standard conditions. As shown in Table 5.3, decreasing the amount of **Cu2b** from 20 to 5 μM still gave high yields of compound **P4** (>90%, entries 1-3). At 2 μM catalyst loading, however, the yield dropped to about 71% (entry 4). In comparison, when 20 μM of Cu-**TBTA** was generated in situ by combining $Cu(MeCN)_4PF_6$ and **TBTA** (1:1), about 80% yield of **P4** was obtained (entry 5). Decreasing the Cu-**TBTA**

concentration to 2 μM led to an appreciable decrease in yield (~44%, entry 8). Although these results might suggest that dicopper azacryptands are more active than Cu-**TBTA**, it should be noted once again that **Cu2b** has two copper atoms per complex whereas Cu-**TBTA** has only one. Without knowing the nuclearity of the active catalysts, it is not meaningful to make activity comparisons on the basis of copper rather than catalyst concentrations.

Interestingly, we observed that the CuAAC reactions seemed to be significantly faster in pure water compared to in mixtures of aqueous/non-aqueous solvents.[171] For example, Fokin and coworkers reported that Cu-**TBTA** at 1.0 mol% in tBuOH/H_2O (2:1) provided compound **P4** in 84% yield after 24 h.[165] However, when we used pure water as the reaction solvent, we could obtain similar yields by lowering the **Cu-TBTA** catalyst loading down to 0.02 mol% (Table 5.3, entry 5). The effects of solvent were also significant for the azacryptand catalyst **Cu2b**. We found that about 10 mol% of **Cu2b** (10 mM) was needed to obtain complete reaction between benzyl azide and phenylacetylene in acetone/water (2:3) after 24 h (Table 5.5, entry 4), whereas only 0.05 mol% (50 μM) of catalyst was needed in water alone (Table 5.1, entry 4). We postulate that the formation of hydrophobic aggregates between substrates and catalysts is more greatly enhanced in water than in water/organic solvent mixtures. Reaction rate acceleration in water due to the hydrophobic effect has been documented in a variety of chemical processes, such as pericyclic reactions, Claisen rearrangements, and Michael addition.[193]

Table 5.3. Comparison of Copper Catalyst Concentrations[a]

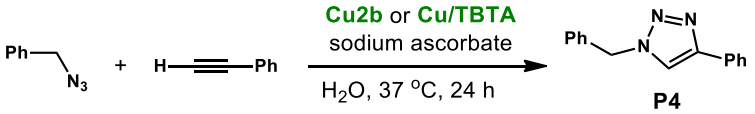

Entry	Complex	Conc. (μM)	GC Yield (%)[b]	Isolated Yield (%)[b]
1	**Cu2b**	20	97	95
2	**Cu2b**	10	93	92
3	**Cu2b**	5	94	90
4	**Cu2b**	2	71	63
5	Cu/**TBTA**[c]	20	80	-
6	Cu/**TBTA**[c]	10	67	-
7	Cu/**TBTA**[c]	5	49	-
8	Cu/**TBTA**[c]	2	44	-

[a]Reaction conditions: benzyl azide (1.00 mmol), phenylacetylene (1.37 mmol), Cu (varies), sodium ascorbate (0.15 mmol) in H_2O (10 mL) at 37°C for 24 h. [b]Average yields from triplicate runs. [c]A 1:1 ratio of $Cu(MeCN)_4PF_6$:**TBTA** was used.

Table 5.4. Comparison of Copper Catalyst Concentrations in the Presence of Thiols[a]

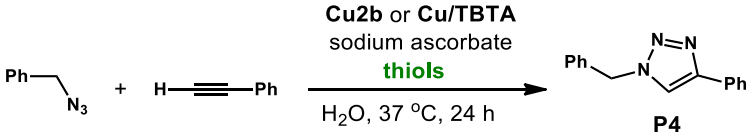

Entry	Complex	Conc. (μM)	GC Yield (%)	
			Glutathione (1.0 mM)	Cysteine (1.0 mM)
1	**Cu2b**	500	97	71
2	**Cu2b**	200	97	46
3	**Cu2b**	100	94	33
4	**Cu2b**	50	86	20
5	Cu/**TBTA**[c]	500	-	99
6	Cu/**TBTA**[c]	200	-	99
7	Cu/**TBTA**[c]	100	-	67
8	Cu/**TBTA**[c]	50	-	11

[a]Reaction conditions: benzyl azide (1.00 mmol), phenylacetylene (1.37 mmol), Cu (varies), sodium ascorbate (0.15 mmol), and thiols (10.0 mmol) in H_2O (10 mL) at 37°C for 24 h. [b]Average yields from triplicate runs. [c]A 1:1 ratio of $Cu(MeCN)_4PF_6$:**TBTA** was used.

Finally, since we are ultimately interested in carrying out CuAAC reactions inside living cells, we wanted to determine what concentrations of copper catalyst are required to achieve high catalytic conversion in the presence of high concentrations of biological thiols (Table 5.4).[166] We found that for **Cu2b**, at least 100 μM of catalyst was necessary to obtain greater than 90% yield of the CuAAC product in the presence of 1.0 mM glutathione (entry 3). When 1.0 mM of cysteine was used instead of glutathione, 500 μM of catalyst was needed to give only a 71% yield (entry 1). Interestingly, the monocopper complex Cu-**TBTA** was more tolerant of cysteine than **Cu2b**. For example, Cu-**TBTA** gave quantitative yields of compound **P4** at 200 μM catalyst in the presence of cysteine (entry 6). However, at lower concentrations of Cu-**TBTA**, the reaction conversions were significantly decreased (entries 7-8). In terms of the biological relevance of these results, the use of >50 μM of catalyst is typically considered quite high. Of course, the acceptable catalyst concentrations for biological studies would depend on the copper complexes' cytotoxicity.[194-195] However, such studies are beyond the scope of this work.

5.4. Conclusions

In summary, we have evaluated the competency of dicopper azacryptand complexes as catalysts for aqueous CuAAC. In the absence of biological nucleophiles, they can exhibit high catalytic activity at concentrations as low as 5 μM. Interestingly, the dicopper catalysts are not as strongly inhibited in the presence of glutathione as compared to in the presence of cysteine (Table 5.2). Control studies using either **Cu1a**/**Cu1b** or Cu-**TBTA** showed that, in many cases, the mononuclear catalysts had similar reactivity in comparison to that of the

dinuclear catalysts. Our general observation that the copper complexes are more susceptible toward inhibition by cysteine rather than glutathione is intriguing and warrants further investigation to elucidate their catalyst deactivation mechanisms. Unfortunately, our results seem to suggest that the azacryptands do not provide any substantial benefits over conventional tripodal ligands in terms of their ability to provide greater active site protection. We believe, however, that because the azacryptands are amendable to further synthetic modifications, it might be possible to develop new caged ligand structures that are more effective at substrate gating than their parent ligands. Furthermore, since metal azacryptands have so far been underexplored as intracellular catalysts, we anticipate that much exciting chemistry is still yet to be discovered.

5.5. Experimental

General Procedures.

Commercial reagents were used as received. All air- and water-sensitive manipulations were performed using standard Schlenk techniques or under a nitrogen atmosphere using a drybox. Anhydrous solvents were obtained from an Innovative Technology solvent drying system saturated with argon. The ligands **Lig2**,[196] **Lig3**,[197-198] **Lig4**,[198] and **Lig6**[199] were synthesized according to literature procedures. The copper catalysts were prepared as described below.[197, 200]

NMR spectra were acquired using JEOL spectrometers (ECA-400, -500, and -600) and referenced using residual solvent peaks. Gas chromatographic (GC) analyses were performing using an Agilent 7820E spectrometer equipped with both a 5977A extractor mass spectral detector (MSD) and a flame ionization detector (FID). All substrate quantification measurements were conducted by integrating peaks in their GC-FID chromatograms and corrected based on their experimental GC response factors. Biphenyl was used as an internal standard in GC studies. ESI-MS analyses were performed using a Thermo Exactive Nano-ESI Mass Spectrometer.

Procedure for CuAAC Reactions.

In a 20 mL disposable scintillation vial, benzyl azide (125 µL, 1 mmol) and phenyl acetylene (150 µL, 1.37 mmol) were added to a 10 mL aqueous mixture containing a copper complex (various amounts), sodium ascorbate (30 mg, 0.15 equiv) and bioadditive (if tested). After the reaction was heated to 37±5°C and stirred for 24 h, water (50 mL) was

added and the resulting mixture was extracted into CH_2Cl_2 (2×50 mL) and dried over Na_2SO_4. *To obtain isolated yield*: the combined organic layers were concentrated in vacuo. The residue was then purified by column chromatography on silica gel column (70-230 mesh) eluted with hexane:ethyl acetate 4:1. *To obtain GC yield:* a known amount of biphenyl was added to an aliquot of the organic layer. This mixture was analyzed by GC-FID. GC yields were calculated based on the integrated area between the internal standard and product peaks, corrected by their corresponding GC response factors. Using excess sodium ascorbate helps to maintain the copper complexes in the +1 oxidation state and improve their products yields. Data for the reactions performed in the absence of sodium ascrobate or copper are provided in Table 5.6.

Table 5.5. Comparison of Cu Catalysts in Water/Acetone[a]

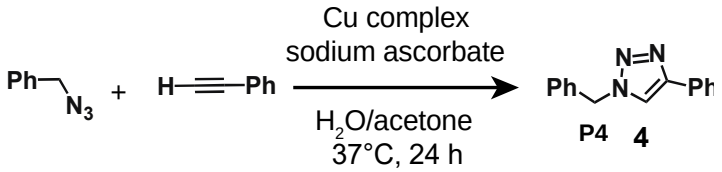

Entry	Cu Complex	GC Yield (%)[b]
1	**Cu1a**	43
2	**Cu1b**	6
3	**Cu2a**	20
4	**Cu2b**	95
5	**Cu3a**	trace
6	**Cu3b**	trace
7	$CuSO_4$	73

[a]Reaction conditions: benzyl azide (1.00 mmol), phenylacetylene (1.37 mmol), Cu (0.10 mmol, 10 mM), sodium ascorbate (1.50 mmol) in H_2O/acetone (3:2, 10 mL) at 37 °C for 24 h. [b]Average yields from duplicate runs.

Table 5.6. Additional CuAAC Reactions[a]

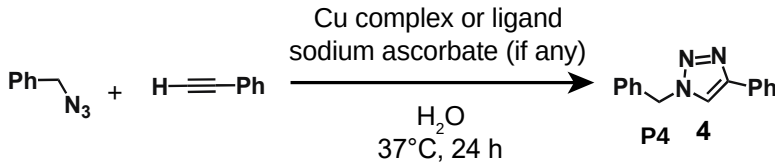

Entry	Compound	Ascrobate	GC Yield (%)
1	**Cu1a**	No	22
2	**Cu1b**	No	99
3	**Cu2a**	No	82
4	**Cu2b**	No	99
5	**Cu3a**	No	34
6	**Cu3b**	No	44
7	Cu-**TBTA**	No	99
8	**Lig3** ligand	Yes	0
9	**TBTA** ligand	Yes	0

[a]Reaction conditions: benzyl azide (1.00 mmol), phenylacetylene (1.37 mmol), Cu (0.5 µmol) or ligand alone (0.5 µmol), sodium ascorbate (0.15 mmol, if any) in H_2O (10 mL) at 37 °C for 24 h.

Synthesis and Characterization

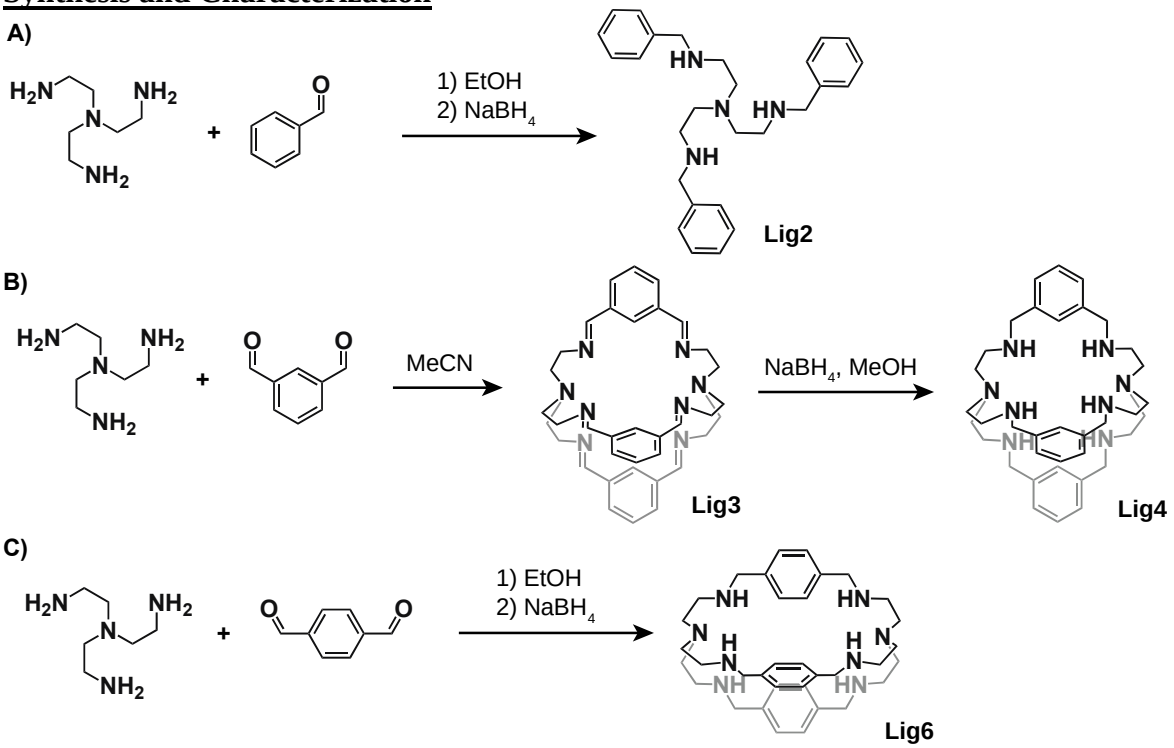

Scheme 5.4. Procedures for the synthesis of ligands **Lig2**, **Lig3**, **Lig4**, and **Lig6**.

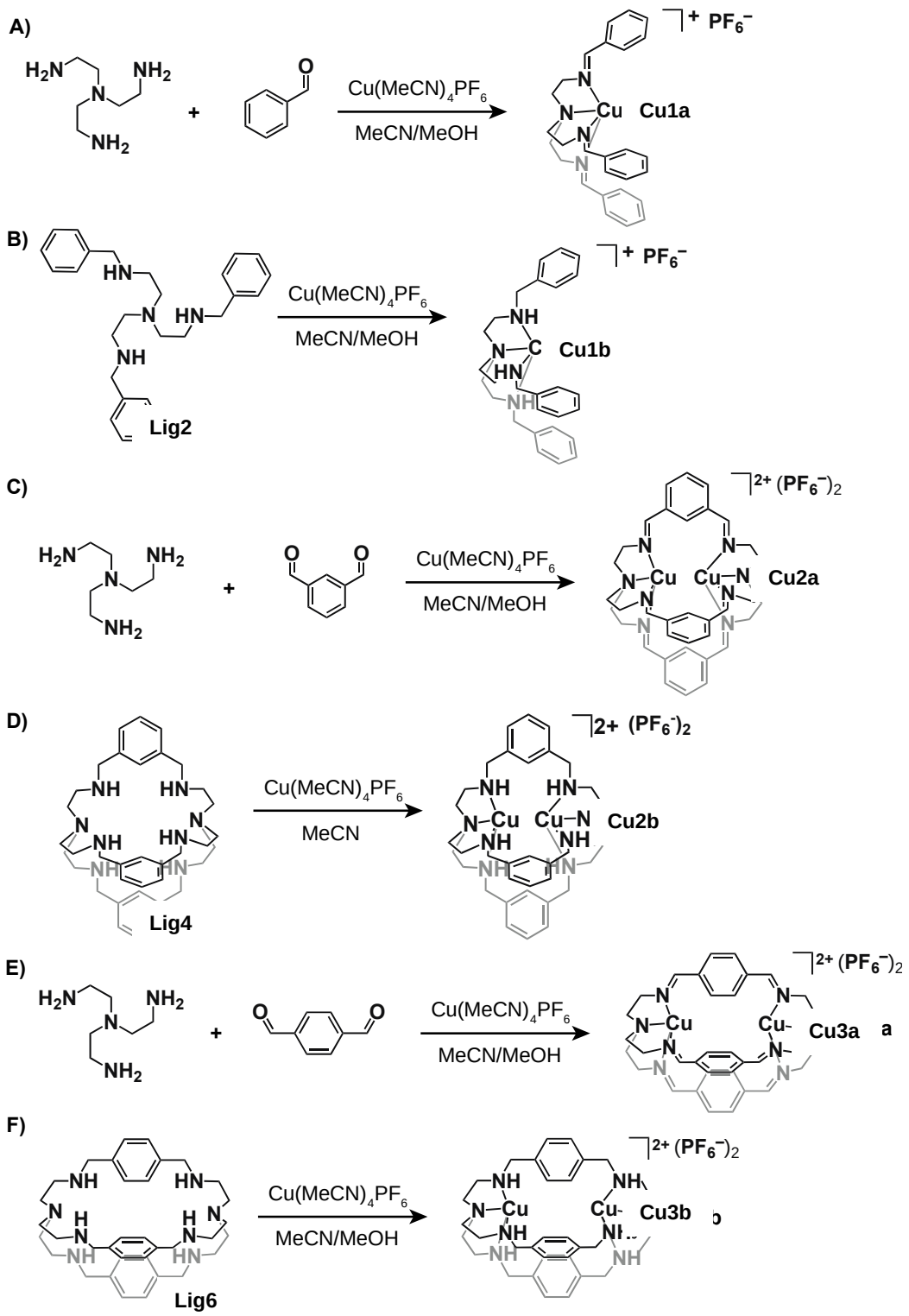

Scheme 5.5. Procedures for the synthesis of copper complexes **Cu1-Cu3**.

Preparation of Cu1a. Inside the glovebox, benzaldehyde (0.318 g, 3 mmol), tris(2-aminoethyl)amine (0.146 g, 1 mmol), and $Cu(MeCN)_4PF_6$ (0.373 g, 1 mmol) were dissolved in 50 mL of MeCN/MeOH (1:1) in a Schlenk flask. The flask was taken outside of the glovebox and the reaction was stirred under reflux overnight to give a yellow precipitate. This material was collected by filtration and then washed with cold methanol to afford the desired product (0.34 g, 0.79 mmol, 79%). ^{1}H NMR (CD_3CN, 400 MHz): δ (ppm) = 8.48 (s, 3H), 8.03 (d, J_{HH} = 8 Hz, 6H), 7.37 (t, J_{HH} = 7.6 Hz, 3H), 6.88 (t, J_{HH} = 7.6 Hz, 6H), 3.82 (t, J_{HH} = 5.2 Hz, 6H), 3.10 (t, J_{HH} = 6 Hz, 6H). ^{13}C NMR (CD_3CN, 126 MHz): δ (ppm) = 163.02, 133.96, 132.12, 128.67, 128.48, 60.29, 52.31. HRMS–ESI(+): Calc. for $C_{27}H_{30}CuN_4$ m/z = 473.1767, Found = 473.1929. FT-IR: 2841 (ν_{CHN}), 1636 (ν_{CN}) cm^{-1}.

Preparation of Cu1b. Inside the glovebox, ligand **Lig2** (0.75 g, 2 mmol) and $Cu(MeCN)_4PF_6$ (0.746 g, 2 mmol) were combined in a 20 mL scintillation vial along with 10 mL of MeCN/MeOH (1:1). The reaction mixture was stirred at RT for 24 h. The solvent was then removed and the resulting green solid was collected and washed with a small amount of methanol (0.39 g, 0.88 mmol, 44%) ^{1}H NMR (CD_3CN, 400 MHz): δ (ppm) = 7.31-7.24 (m, 9H), 7.18-7.16 (m, 6H), 3.63 (m, 6H), 2.70-2.68 (m, 6H), 2.62-2.60 (m, 6H). *Note: This copper(I) species is prone to air oxidation and disproportionation.*[165, 179]

Preparation of Cu2a. Inside the glovebox, isophthalaldehyde (0.40 g, 3.00 mmol), tris(2-aminoethyl)amine (0.29 g, 2.0 mmol), and $Cu(MeCN)_4PF_6$ (0.75 g, 2.00 mmol)

were combined with 50 mL of MeCN/MeOH (1:1) in a Schlenk flask. The flask was taken outside of the glovebox and the reaction was stirred under reflux overnight to give a yellow precipitate. This material was collected by filtration and then washed with cold methanol to afford the desired product (0.54 g, 0.75 mmol, 75%). ^{1}H NMR (CD_3CN, 400 MHz): δ (ppm) = 9.88 (s, 3H), 8.47 (s, 6H), 7.76 (d, J_{HH} = 7.6 Hz, 6H), 7.68 (t, J_{HH} = 7.2 Hz, 3H), 3.27 (d, J_{HH} = 7.2 Hz, 12H), 3.14 (d, J_{HH} = 13.6 Hz, 6H), 2.68-2.60 (m, 6H) . ^{13}C NMR (CD_3CN, 100 MHz); δ (ppm) = 165.22, 136.77, 133.98, 129.82, 117.92, 62.08, 57.90. HRMS–ESI(+): Calc. for $C_{36}H_{41}Cu_2N_8$ m/z = 356.1057, Found = 356.1180. FT-IR: 2870 (ν_{CHN}), 1637 (ν_{CN}) cm^{-1}.

Preparation of Cu2b. Inside the glovebox, ligand **Lig4** (0.24 g, 0.40 mmol) and $Cu(MeCN)_4PF_6$ (0.30 g, 0.80 mmol) were dissolved in 10 mL of MeCN in a scintillation vial and then stirred at RT for 24 h. After removal of solvent, a pale green solid was obtained. The solid was washed with a small amount of MeOH to afford the desired product (0.44 g, 0.60 mmol, 76%) ^{1}H NMR (CD_3CN, 400 MHz): δ (ppm) = 8.10 (s, 3H), 7.36 (t, J_{HH} = 7.4 Hz, 3H), 7.19 (d, J_{HH} = 7.2 Hz, 6H), 3.59 (m, 12H), 2.68 (s, 12H), 2.56 (s, 12H). ^{13}C NMR (CD_3CN, 100 MHz): δ (ppm) = 139.44, 129.98, 127.13, 54.98, 51.57, 49.66. *Note: Because this copper(I) species was very sensitive to air oxidation, it could not be analyzed by ESI-MS.*

Preparation of Cu3a. Inside the glovebox, teraphthalaldehyde (0.40 g, 3.00 mmol), tris(2-aminoethyl)amine (0.29 g, 2.00 mmol), and $Cu(MeCN)_4PF_6$ (0.75 g, 2.00 mmol)

were combined in 50 mL of MeCN/MeOH (1:1). The flask was taken outside of the glovebox and the reaction was stirred under reflux overnight to give a yellow precipitate. This material was collected by filtration and then washed with cold methanol to afford the desired product (0.51 g, 0.71 mmol, 71%).^{1}H NMR (CD_3CN, 400 MHz): δ (ppm) = 8.55 (s, 6H), 7.70 (s, 12H), 3.83 (t, J_{HH} = 5.4 Hz, 12H), 3.12 (m, 12H).^{13}C NMR (CD_3CN, 126 MHz); δ (ppm) = 163.15, 137.11, 128.56, 60.46, 50.83. HRMS–ESI(+): Calc. for $C_{36}H_{41}Cu_2N_8$ m/z = 356.1057, Found = 356.1179. FT-IR: 2901 (ν_{CHN}), 1640 (ν_{CN}) cm^{-1}.

Preparation of Cu3b. Inside the glovebox, ligand **Lig6** (0.12 g, 0.20 mmol) and $Cu(MeCN)_4PF_6$ (0.15 g, 0.40 mmol) were combined in 10 mL of MeCN/MeOH (1:1) and then stirred at RT for 24 h. After removal of solvent, a white solid was obtained. The product was recrystallized by CH_3CN/Et_2O (0.10 g, 0.14 mmol, 35%). ^{1}H NMR (CD_3CN, 400 MHz): δ (ppm) = 6.84 (s, 12H), 3.86-3.56 (br, 12H), 3.19 (m, 6H), 2.87 (s, 12H), 2.76-2.74 (m, 12H). ^{13}C NMR (CD_3CN, 100 MHz); δ (ppm) = 137.26, 127.37, 55.09, 50.78, 49.98. *Note: Because this copper(I) species was very sensitive to air oxidation, it could not be analyzed by ESI-MS.*

Preparation of Lig2. This synthesis was modified from a literature procedure.[201] Benzaldehyde

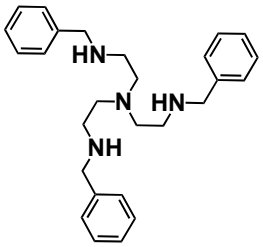

(3.0 g, 28.3 mmol) wad added to a mixture of tris(2-aminoethyl)amine (0.73 g, 5.0 mmol) in 100 mL of ethanol. The mixture was stirred under reflux overnight. It was then cooled to RT, treated with solid $NaBH_4$ (1.0 g, 26.4 mmol), and then continued to reflux for another 24 h. The volatiles were removed by rotary evaporation and the residues were dissolved in CH_2Cl_2 (100 mL). An aqueous solution of $NaHCO_3$ (10%, 50 mL) was added and the mixture was shaken. The organic layer was separated, washed with H_2O (100 mL), dried over Na_2SO_4, filtered, and then evaporated to dryness. The crude product was purified by column chromatography using basic alumina (Act. I, 50-200 mess) and eluted with CH_2Cl_2/MeOH/NEt_3 (95.5/4.0/0.5) to afford a light yellow oil (0.41 g, 1.1 mmol, 22%). The NMR spectra of the product matches those reported previously.[201] ^{1}H NMR ($CDCl_3$, 400 MHz): δ (ppm) = 7.35-7.20 (m, 15H), 3.73 (s, 6H), 2.66 (t, J_{HH} = 6Hz, 6H), 2.56 (t, J_{HH} = 6Hz, 6H).

Preparation of Lig3. This synthesis was modified from a literature procedure.[197-198] To a stirred

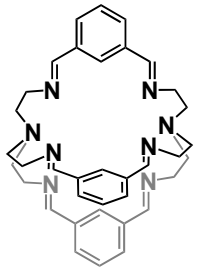

solution of tris(2-aminoethyl)amine (20 mmol, 2.92 g) in MeCN (250 mL) was added dropwise a mixture of isophthalaldehyde (30 mmol, 4.03 g) in MeCN (150 ml) over a period of 1 h at RT. After stirring for additional 24 h, a large amount of a white precipitate had formed. The solid was isolated by filtration and then washed with Et_2O to afford the desired product (5.34 g, 9.1 mmol, 91%). The NMR spectra of the product matches those reported previously.[197-198] ^{1}H NMR ($CDCl_3$, 400 MHz): δ (ppm) = 8.18 (dd, J_{HH} = 7.7, 1.6 Hz, 6H), 7.57 (s, 6H), 7.52 (t, JHH = 8 Hz, 3H), 5.31 (m, 3H), 3.77-2.69 (m, 24H). ^{13}C NMR ($CDCl_3$, 100 MHz): δ (ppm) = 160.81, 136.94, 132.46, 129.10, 127.46, 60.09, 56.07.

Preparation of Lig4. This synthesis was modified from a literature procedure.[198] Solid $NaBH_4$ (1 g, 26.4 mmol) was added slowly portion-wise over 15 min to a stirred solution of **Lig3** (1.1 g, 1.88 mmol) in methanol (100 mL) at RT. The mixture was refluxed under nitrogen overnight. The solution was then cooled to RT and the solvent was removed by rotary evaporation. The residue was dissolved in CH_2Cl_2 (100 mL) and combined with aqueous $NaHCO_3$ (10%, 50 mL). The product was extracted into CH_2Cl_2, washed with H_2O (50 mL), and then dried over Na_2SO_4. Removal of solvent afforded a white sticky solid (0.51 g, 0.85 mmol, 45%). The NMR spectra of the product matches those reported previously.[198] ^{1}H NMR ($CDCl_3$, 500 MHz): δ (ppm) = 7.21-7.13 (m, 9H), 7.07 (s, 3H), 3.60 (m, 12H), 2.62-2.60 (m, 12H), 2.57-2.55 (m, 12H).

Preparation of Lig6. This synthesis was modified from a literature procedure.[199]

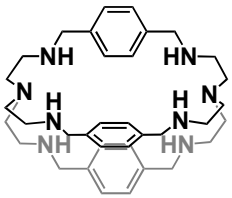

Terephthaldehyde (2.01 g, 15.0 mmol) was dissolved in 150 mL of ethanol in a 500 mL three-neck round bottom flask. The flask was equipped with a reflux condenser on one neck and an addition funnel on another. The solution was heated to 78°C while tris(2-aminoethyl)amine (1.46 g, 10.0 mmol) in 50 mL of ethanol was added slowly dropwise using the addition funnel. The reaction mixture was then refluxed overnight. The next day, the solution was filtered to remove insoluble materials and the filtrate was transferred to another round bottom flask. The mixture was then treated with solid $NaBH_4$ (2 g, 10.5 equiv). The solution was refluxed overnight and cooled to RT. The volatiles were removed by rotary evaporation and the residue was dissolved in CH_2Cl_2 (200 mL). The organic layer was combined with aqueous $NaHCO_3$ (10%, 100 mL) and shaken. The organic layer was separated, washed with H_2O (100 mL), dried with Na_2SO_4, removed solvent and recrystallized with toluene/hexane to afford solid white product (0.42 g, 0.7 mmol, 14%). NMR spectroscopic characterization of the product matches that measured previously.[199] ^{1}H NMR ($CDCl_3$, 400 MHz): δ (ppm) = 6.87 (s, 12H), 3.68 (s, 12H), 2.83-2.81 (m, 12H), 2.67-2.65 (m, 12H).

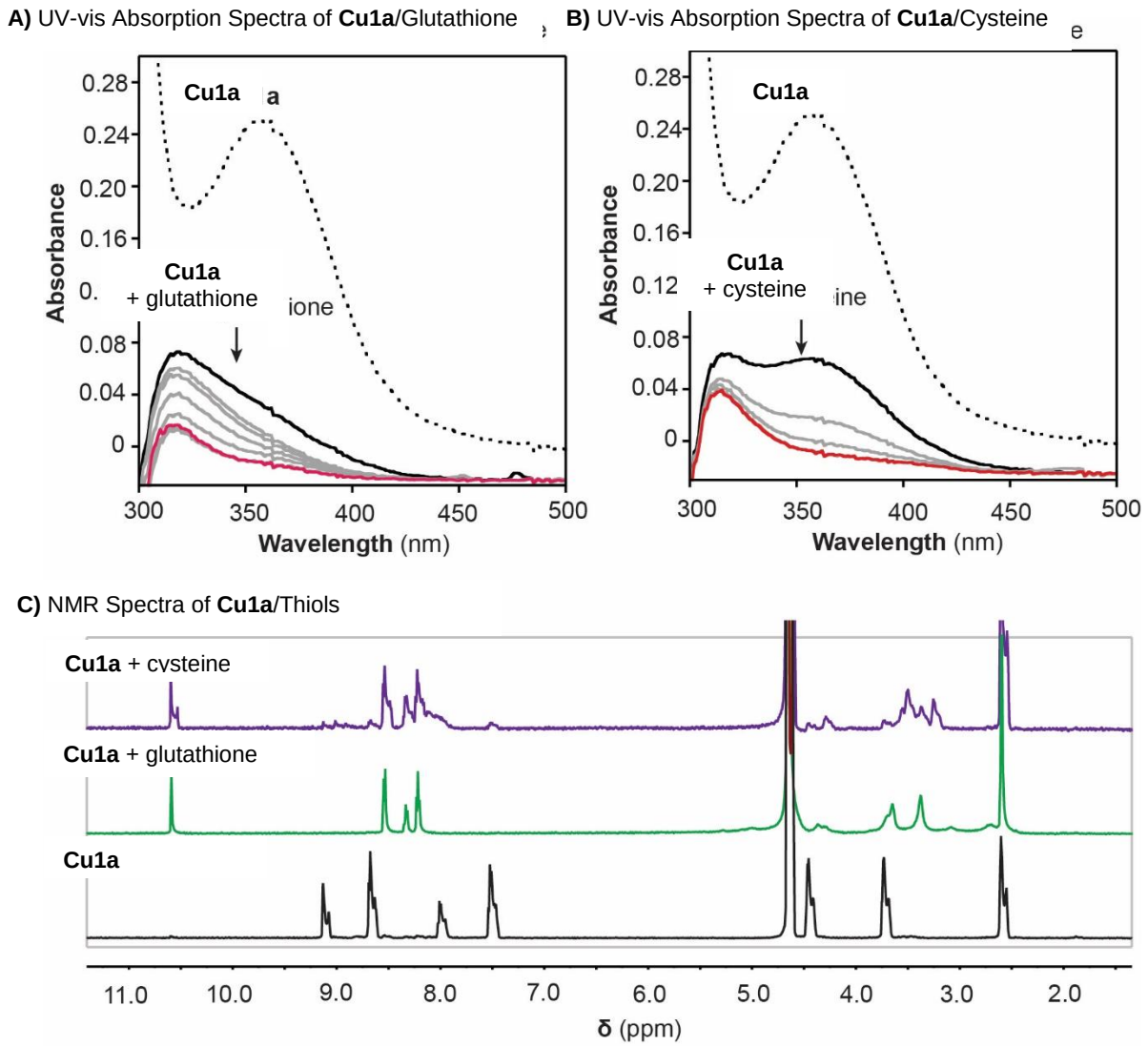

Figure 5.2. Reaction of complex **Cu1a** (50 µM) with biological thiols (100 µM). Plots A and B show the UV-vis absorption spectra (H_2O) of **Cu1a**/glutathione and **Cu1a**/cysteine, respectively. The dotted trace shows the spectrum of **Cu1a** without any additives. The solid black traces were obtained right after mixing **Cu1a** with either glutathione or cysteine and the solid red traces were obtained after ~60-80 min. Plot C shows the NMR spectra (D_2O, 500 MHz) of **Cu1a**, **Cu1a**/glutathione and **Cu1a**/cysteine as indicated.

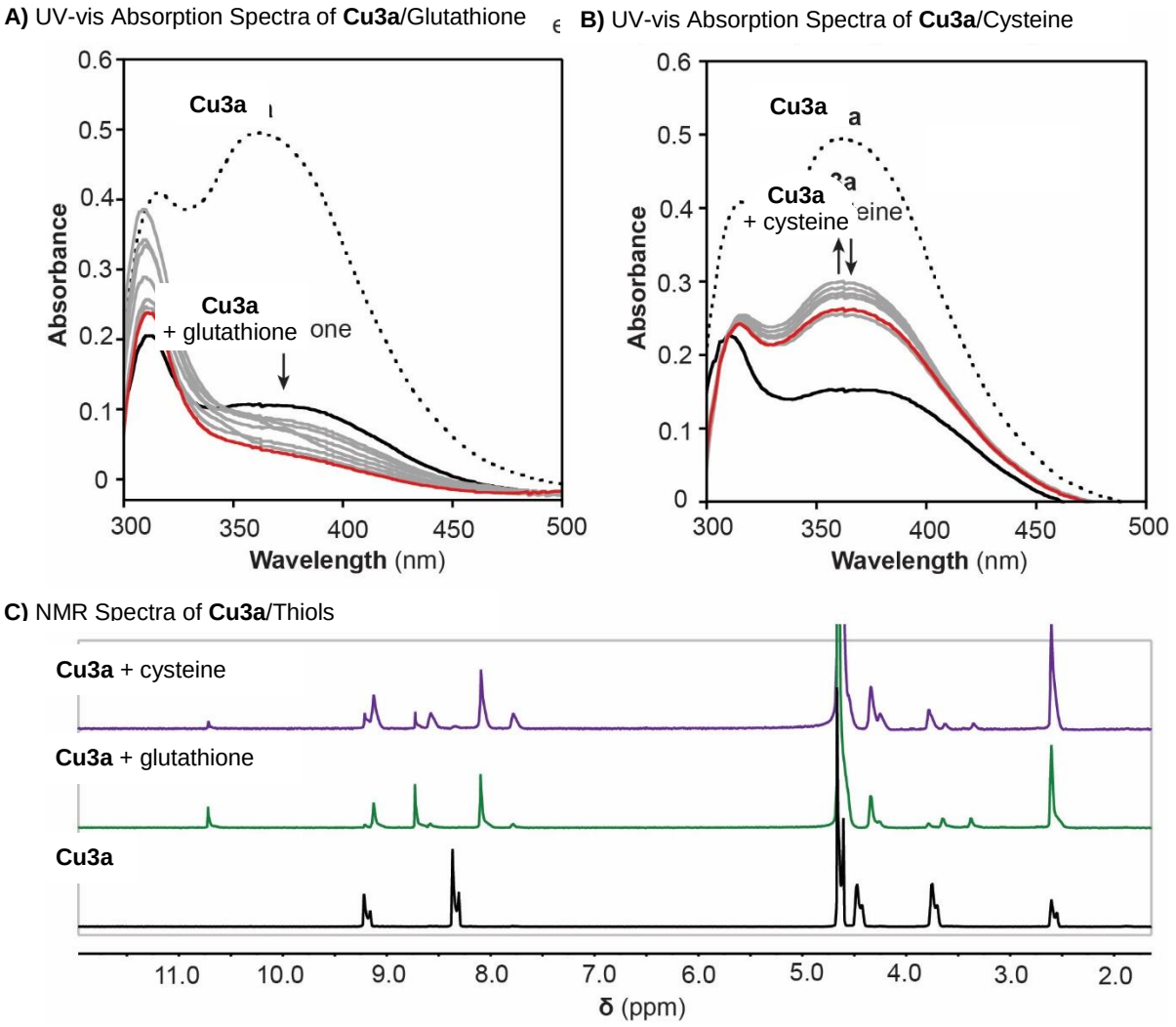

Figure 5.3. Reaction of complex **Cu3a** (50 µM) with biological thiols (100 µM). Plots A and B show the UV-vis absorption spectra (H_2O) of **Cu3a**/glutathione and **Cu3a**/cysteine, respectively. The dotted trace shows the spectrum of **Cu3a** without any additives. The solid black traces were obtained right after mixing **Cu3a** with either glutathione or cysteine and the solid red traces were obtained after ~60-80 min. Plot C shows the NMR spectra (D_2O, 500 MHz) of **Cu3a**, **Cu3a**/glutathione and **Cu3a**/cysteine as indicated.

5.6. Spectra Characterization

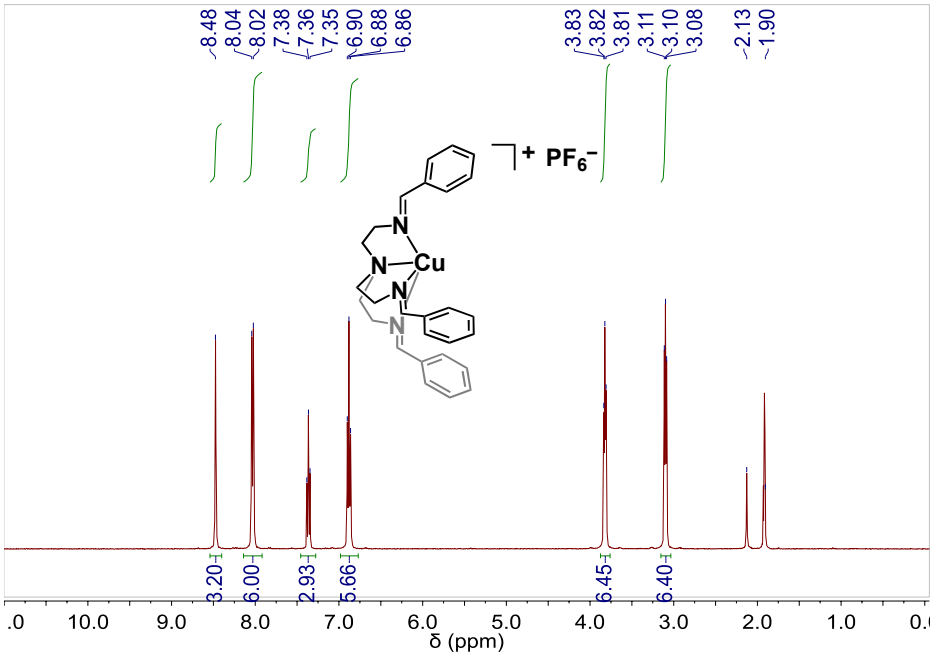

Figure 5.4. ^{1}H NMR spectrum ($CDCl_3$, 400 MHz) of complex **Cu1a**.

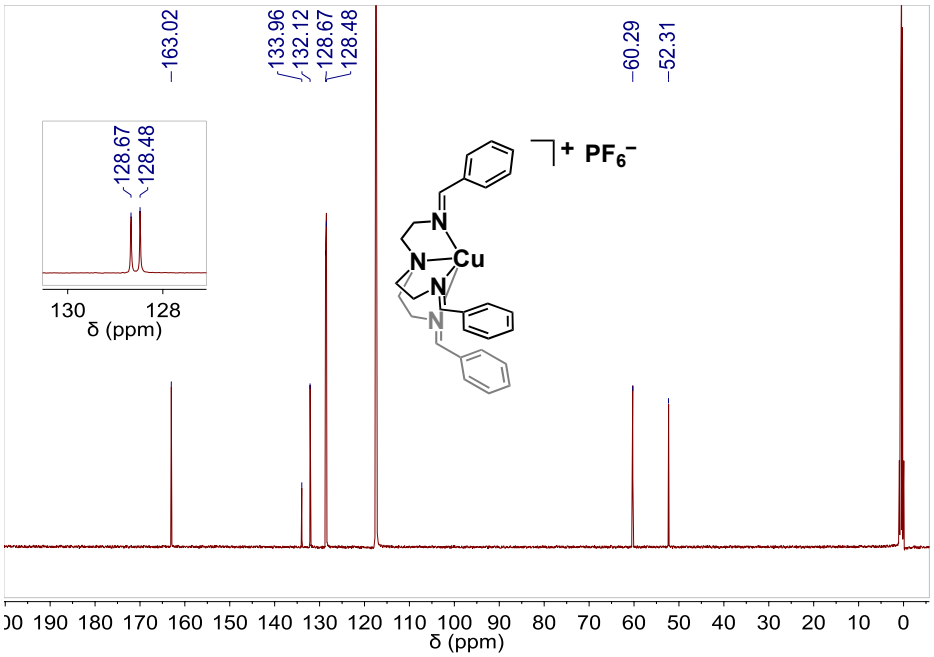

Figure 5.5. ^{13}C NMR spectrum (CD_3CN, 126 MHz) of complex **Cu1a**.

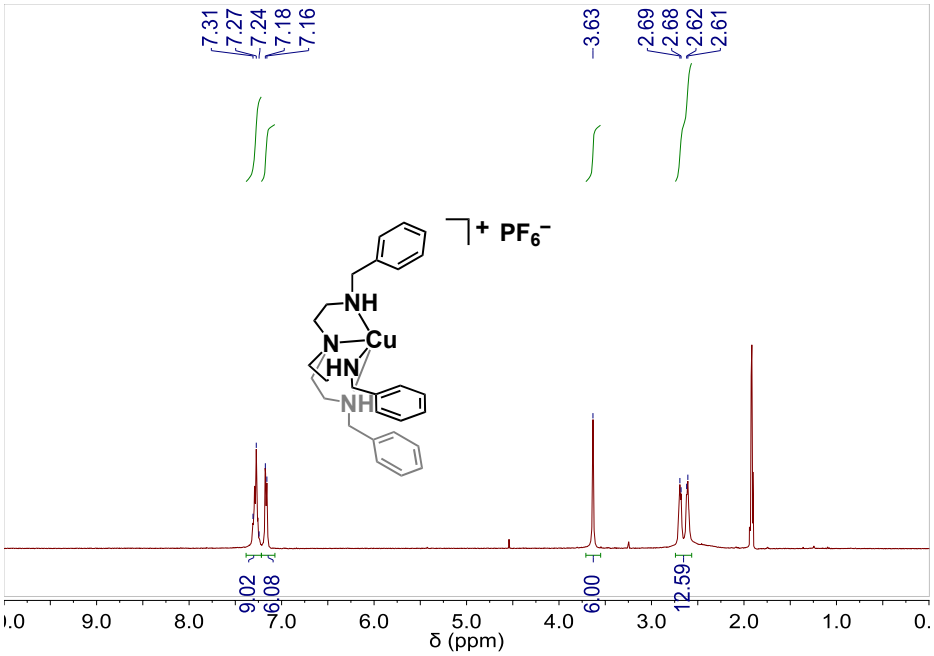

Figure 5.6. ^{1}H NMR spectrum (CD_3CN, 400 MHz) of complex **Cu1b.**

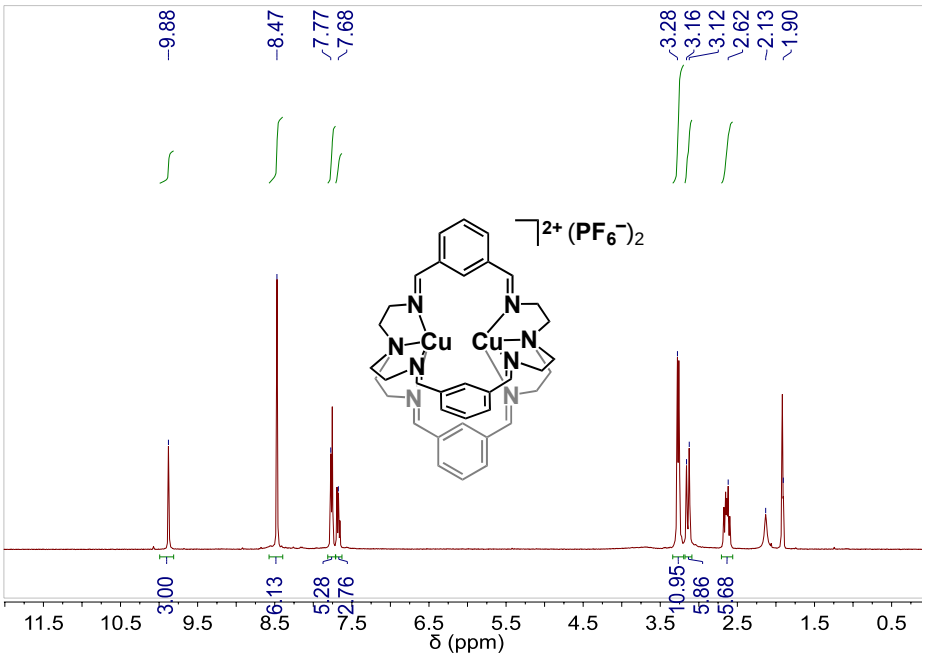

Figure 5.7. ^{1}H NMR spectrum (CD_3CN, 400 MHz) of complex **Cu2a**.

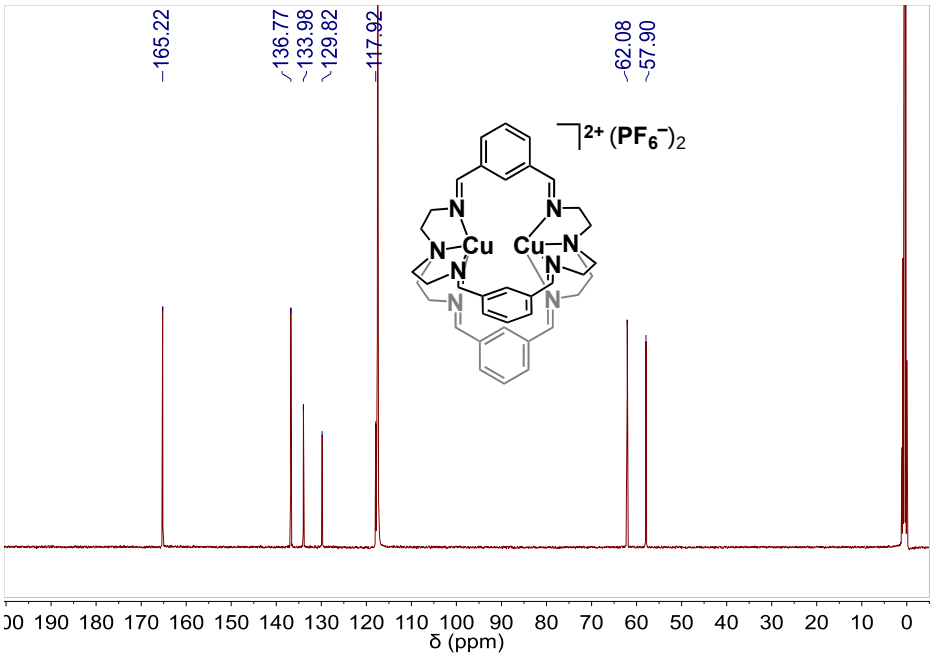

Figure 5.8. ^{13}C NMR spectrum (CD_3CN, 100 MHz) of complex **Cu2a**.

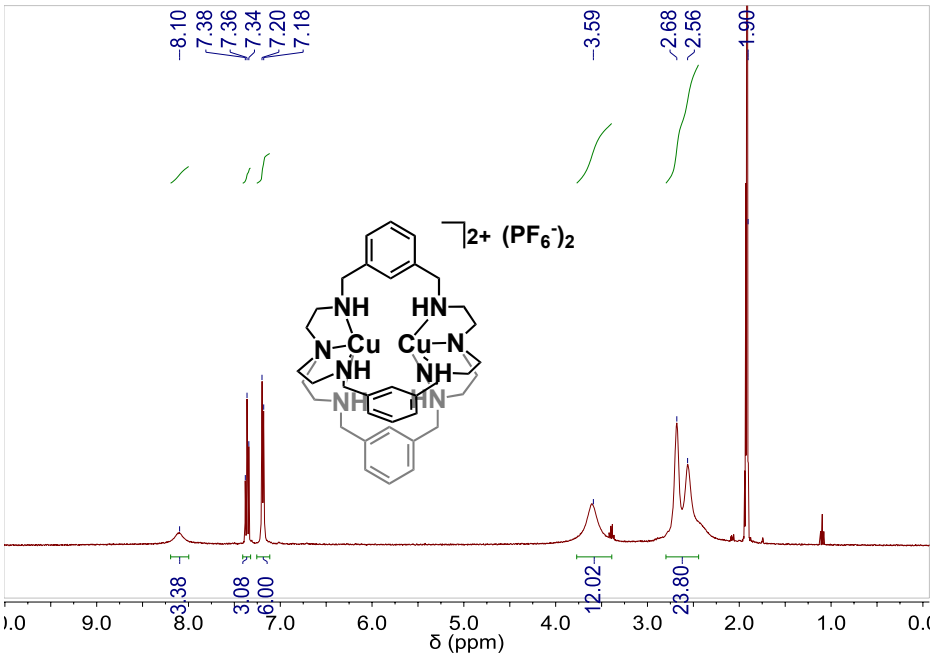

Figure 5.9. ^{1}H NMR spectrum (CD_3CN, 400 MHz) of complex **Cu2b**. The broad peaks suggest that the complex undergoes dynamic structural changes in solution.

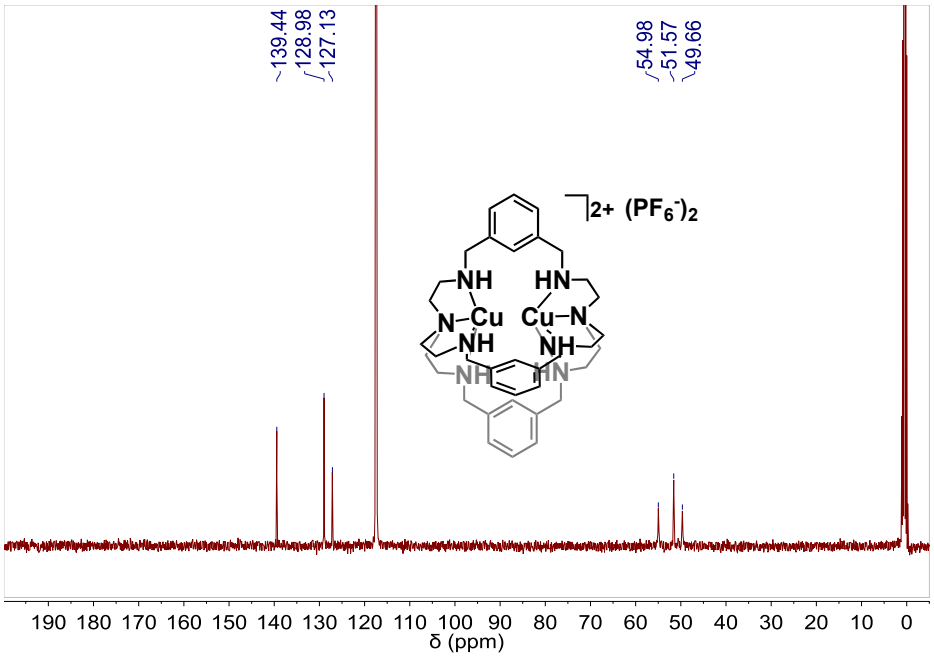

Figure 5.10. ^{13}C NMR spectrum (CD_3CN, 100 MHz) of complex **Cu2b**.

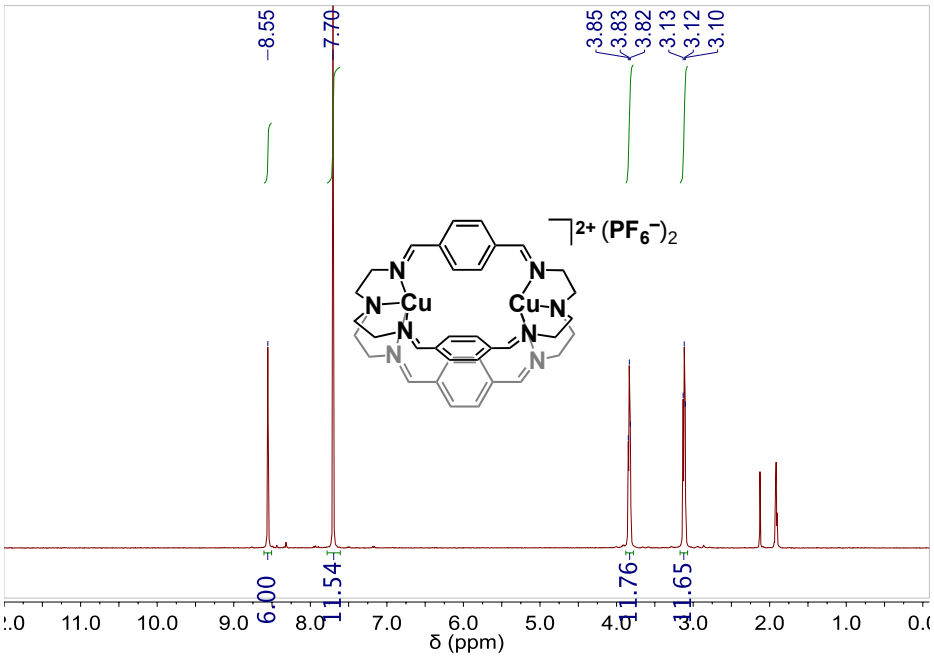

Figure 5.11. ^{1}H NMR spectrum (CD_3CN, 400 MHz) of complex **Cu3a**.

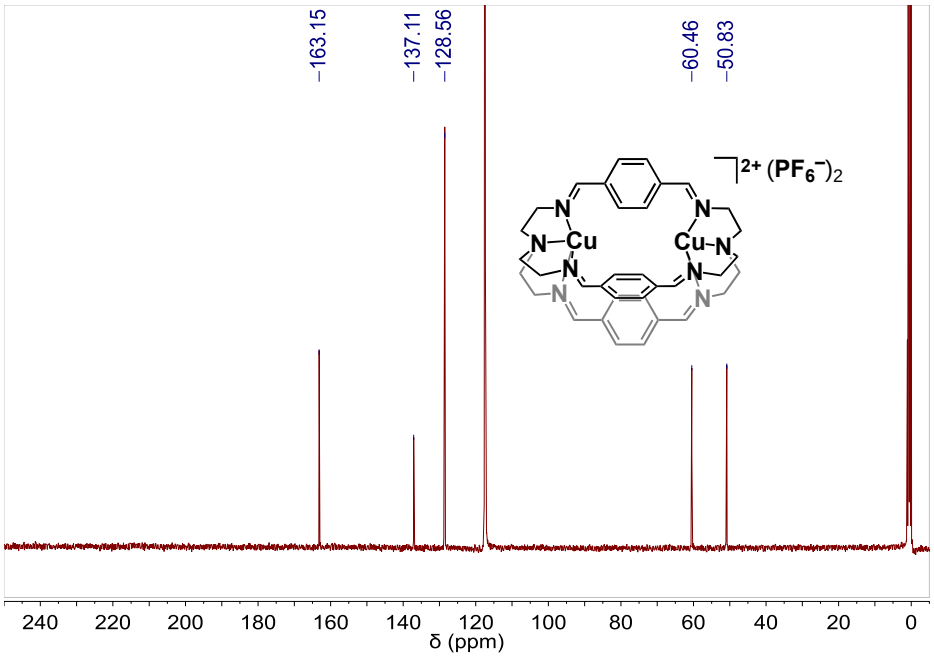

Figure 5.12. ^{13}C NMR spectrum (CD_3CN, 126 MHz) of complex **Cu3a**.

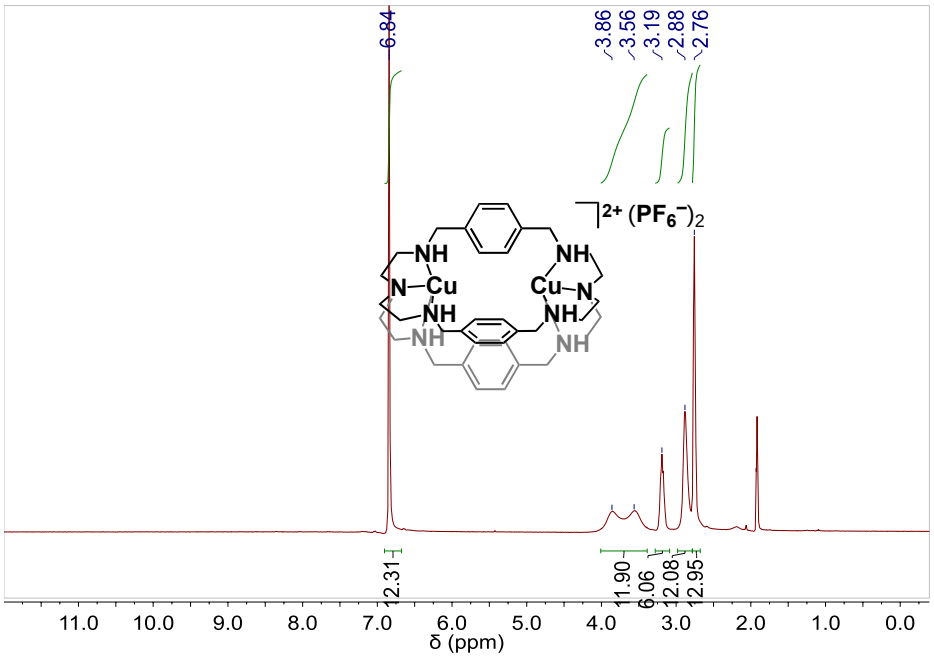

Figure 5.13. ^{1}H NMR spectrum (CD_3CN, 400 MHz) of complex **Cu3b.**

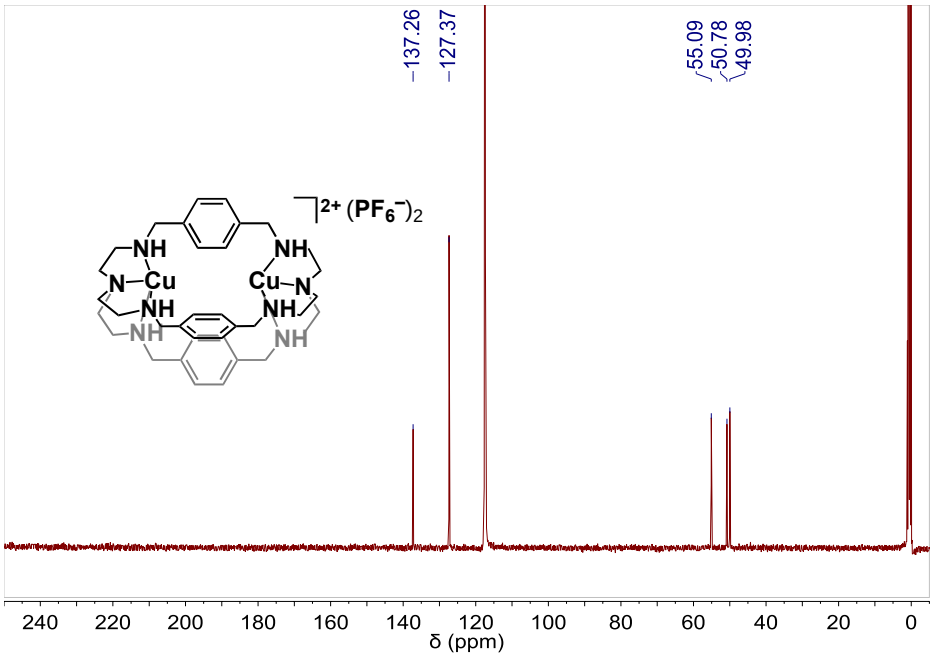

Figure 5.14. ^{13}C NMR spectrum (CD_3CN, 100 MHz) of complex **Cu3b**.

BIBLIOGRAPHY

1. Stürzel, M.; Mihan, S.; Mülhaupt, R., *Chemical Reviews* **2016,** *116* (3), 1398-1433.
2. Gentekos, D. T.; Sifri, R. J.; Fors, B. P., *Nature Reviews Materials* **2019,** *4* (12), 761-774.
3. Malpass, D. B., *Wiley, Hoboken, NJ, USA* **2010**, 85-97.
4. Mark A. Spalding, A. M. C., *Wiley-VCH, Weinheim* **2017**.
5. Mitchell, N. E.; Long, B. K., *Polymer International* **2019,** *68* (1), 14-26.
6. Geyer, R.; Jambeck, J. R.; Law, K. L., *Science Advances* **2017,** *3* (7), 1-5.
7. Sifri, R. J.; Padilla-Vélez, O.; Coates, G. W.; Fors, B. P., *Journal of the American Chemical Society* **2020,** *142* (3), 1443-1448.
8. Rosenbloom, S. I.; Gentekos, D. T.; Silberstein, M. N.; Fors, B. P., *Chemical Science* **2020,** *11* (5), 1361-1367.
9. Klosin, J.; Fontaine, P. P.; Figueroa, R., *Accounts of Chemical Research* **2015,** *48* (7), 2004-2016.
10. Nakamura, A.; Ito, S.; Nozaki, K., *Chemical Reviews* **2009,** *109* (11), 5215-5244.
11. Chen, Z.; Brookhart, M., *Accounts of Chemical Research* **2018,** *51* (8), 1831-1839.
12. Sauter, D. W.; Taoufik, M.; Boisson, C., *Polymers* **2017,** *9* (6), 185.
13. Chum, P. S.; Swogger, K. W., *Progress in Polymer Science* **2008,** *33* (8), 797-819.
14. Wang, Y.; Vignesh, A.; Qu, M.; Wang, Z.; Sun, Y.; Sun, W.-H., *European Polymer Journal* **2019,** *117*, 254-271.
15. Anderson, W. C.; Rhinehart, J. L.; Tennyson, A. G.; Long, B. K., *Journal of the American Chemical Society* **2016,** *138* (3), 774-777.
16. Stalzer, M. M.; Delferro, M.; Marks, T. J., *Catalysis Letters* **2015,** *145* (1), 3-14.
17. Liang, T.; Goudari, S. B.; Chen, C., *Nature Communications* **2020,** *11* (1), 372.
18. Zhang, D.; Nadres, E. T.; Brookhart, M.; Daugulis, O., *Organometallics* **2013,** *32* (18), 5136-5143.
19. Wang, F.; Chen, C., *Polymer Chemistry* **2019,** *10* (19), 2354-2369.
20. Padilla-Vélez, O.; O'Connor, K. S.; LaPointe, A. M.; MacMillan, S. N.; Coates, G. W., *Chemical Communications* **2019,** *55* (53), 7607-7610.
21. Luca, O. R.; Crabtree, R. H., *Chemical Society Reviews* **2013,** *42* (4), 1440-1459.
22. Kaiser, J. M.; Long, B. K., *Coordination Chemistry Reviews* **2018,** *372*, 141-152.
23. Wei, J.; Diaconescu, P. L., *Accounts of Chemical Research* **2019** *52* (2), 415-424.
24. Wang, X.; Thevenon, A.; Brosmer, J. L.; Yu, I.; Khan, S. I.; Mehrkhodavandi, P.; Diaconescu, P. L., *Journal of the American Chemical Society* **2014,** *136* (32), 11264-11267.
25. Broderick, E. M.; Guo, N.; Vogel, C. S.; Xu, C.; Sutter, J.; Miller, J. T.; Meyer, K.; Mehrkhodavandi, P.; Diaconescu, P. L., *Journal of the American Chemical Society* **2011,** *133* (24), 9278-9281.
26. Broderick, E. M.; Guo, N.; Wu, T.; Vogel, C. S.; Xu, C.; Sutter, J.; Miller, J. T.; Meyer, K.; Cantat, T.; Diaconescu, P. L., *Chemical Communications* **2011,** *47* (35), 9897-9899.
27. Biernesser, A. B.; Li, B.; Byers, J. A., *Journal of the American Chemical Society* **2013,** *135* (44), 16553-16560.
28. Gregson, C. K. A.; Gibson, V. C.; Long, N. J.; Marshall, E. L.; Oxford, P. J.; White, A. J. P., *Journal of the American Chemical Society* **2006,** *128* (23), 7410-7411.

29. Gibson, V. C.; Halliwell, C. M.; Long, N. J.; Oxford, P. J.; Smith, A. M.; White, A. J. P.; Williams, D. J., *Dalton Transactions* **2003,** (5), 918-926.
30. Gibson, V. C.; Gregson, C. K. A.; Halliwell, C. M.; Long, N. J.; Oxford, P. J.; White, A. J. P.; Williams, D. J., *Journal of Organometallic Chemistry* **2005,** *690* (26), 6271-6283.
31. Chen, M.; Yang, B.; Chen, C., *Angewandte Chemie International Edition* **2015,** *54* (51), 15520-15524.
32. Zhao, M.; Chen, C., *Acs Catalysis* **2017 - Ethylene,** *7* (11), 7490-7494.
33. Anderson, W. C.; Park, S. H.; Brown, L. A.; Kaiser, J. M.; Long, B. K., *Inorganic Chemistry Frontiers* **2017,** *4* (7), 1108-1112.
34. Kaiser, J. M.; Anderson, W. C.; Long, B. K., *Polymer Chemistry* **2018,** *9* (13), 1567-1570.
35. Yang, Q.; Xiao, W.-J.; Yu, Z., *Organic Letters* **2005,** *7* (5), 871-874.
36. Shen, Q.; Hartwig, J. F., *Journal of the American Chemical Society* **2007,** *129* (25), 7734-7735.
37. Jiang, Y. J.; Tu, Y. Q.; Zhang, E.; Zhang, S. Y.; Cao, K.; Shi, L., *Advanced Synthesis & Catalysis* **2008,** *350* (4), 552-556.
38. Hirata, Y.; Yada, A.; Morita, E.; Nakao, Y.; Hiyama, T.; Ohashi, M.; Ogoshi, S., *Journal of the American Chemical Society* **2010,** *132* (29), 10070-10077.
39. Bielinski, E. A.; Lagaditis, P. O.; Zhang, Y.; Mercado, B. Q.; Würtele, C.; Bernskoetter, W. H.; Hazari, N.; Schneider, S., *Journal of the American Chemical Society* **2014,** *136* (29), 10234-10237.
40. Tokmic, K.; Jackson, B. J.; Salazar, A.; Woods, T. J.; Fout, A. R., *Journal of the American Chemical Society* **2017,** *139* (38), 13554-13561.
41. Maity, A.; Teets, T. S., *Chemical reviews* **2016,** *116* (15), 8873-8911.
42. Becica, J.; Dobereiner, G. E., *Organic & Biomolecular Chemistry* **2019,** *17* (8), 2055-2069.
43. Delferro, M.; Marks, T. J., *Chemical Reviews* **2011,** *111* (3), 2450-2485.
44. Contrella, N. D.; Jordan, R. F., *Organometallics* **2014,** *33* (24), 7199-7208.
45. McInnis, J. P.; Delferro, M.; Marks, T. J., *Accounts of chemical research* **2014,** *47* (8), 2545-2557.
46. Cai, Z.; Xiao, D.; Do, L. H., *Journal of the American Chemical Society* **2015,** *137* (49), 15501-15510.
47. Chiu, H.-C.; Koley, A.; Dunn, P. L.; Hue, R. J.; Tonks, I. A., *Dalton Transactions* **2017,** *46* (17), 5513-5517.
48. Xiao, D.; Do, L. H., *Organometallics* **2018,** *37* (18), 3079-3085.
49. Chen, Y.; Boardman, B. M.; Wu, G.; Bazan, G. C., *Journal of Organometallic Chemistry* **2007,** *692* (21), 4745-4749.
50. Cai, Z.; Shen, Z.; Zhou, X.; Jordan, R. F., *ACS Catalysis* **2012,** *2* (6), 1187-1195.
51. Johnson, A. M.; Contrella, N. D.; Sampson, J. R.; Zheng, M.; Jordan, R. F., *Organometallics* **2017,** *36* (24), 4990-5002.
52. Wang, G.; Li, M.; Pang, W.; Chen, M.; Tan, C., *New Journal of Chemistry* **2019,** *43* (34), 13630-13634.
53. Tan, C.; Qasim, M.; Pang, W.; Chen, C., *Polymer Chemistry* **2020,** *11* (2), 411-416.

54. Johnson, L.; Wang, L.; McLain, S.; Bennett, A.; Dobbs, K.; Hauptman, E.; Ionkin, A.; Ittel, S.; Kunitsky, K.; Marshall, W.; McCord, E.; Radzewich, C.; Rinehart, A.; Sweetman, K. J.; Wang, Y.; Yin, Z.; Brookhart, M., Copolymerization of Ethylene and Acrylates by Nickel Catalysts. In *Beyond Metallocenes*, American Chemical Society: 2003; Vol. 857, pp 131-142.
55. Tanabiki, M.; Tsuchiya, K.; Motoyama, Y.; Nagashima, H., *Chemical Communications* **2005,** (27), 3409-3411.
56. Smith, A. J.; Kalkman, E. D.; Gilbert, Z. W.; Tonks, I. A., *Organometallics* **2016,** *35* (15), 2429-2432.
57. Cai, Z.; Do, L. H., *Organometallics* **2017 - Ethylene,** *36* (24), 4691-4698.
58. Tran, T. V.; Nguyen, Y. H.; Do, L. H., *Polymer Chemistry* **2019,** *10* (27), 3718-3721.
59. Cai, Z.; Do, L. H., *Organometallics* **2018,** *37* (21), 3874-3882.
60. Xiao, D.; Cai, Z.; Do, L. H., *Dalton Transactions* **2019 - Ethylene,** *48* (48), 17887-17897.
61. Xiao, D.; Do, L. H., *Organometallics* **2018,** *37* (2), 254-260.
62. Shen, Z.; Jordan, R. F., *Journal of the American Chemical Society* **2010,** *132* (1), 52-53.
63. Wei, J.; Shen, Z.; Filatov, A. S.; Liu, Q.; Jordan, R. F., *Organometallics* **2016,** *35* (20), 3557-3568.
64. Liu, Q.; Jordan, R. F., *Organometallics* **2018,** *37* (24), 4664-4674.
65. Liu, Q.; Jordan, R. F., *Journal of the American Chemical Society* **2019,** *141* (17), 6827-6831.
66. Xin, B. S.; Sato, N.; Tanna, A.; Oishi, Y.; Konishi, Y.; Shimizu, F., *Journal of the American Chemical Society* **2017,** *139* (10), 3611-3614.
67. Brookhart, M.; Grant, B.; Volpe, A. F., Jr., *Organometallics* **1992,** *11* (11), 3920-3922.
68. Hirose, K., *Journal of inclusion phenomena and macrocyclic chemistry* **2001,** *39* (3), 193-209.
69. Zhang, Y.; Mu, H.; Pan, L.; Wang, X.; Li, Y., *ACS Catalysis* **2018,** *8*, 5963-5976.
70. Gates, D. P.; Svejda, S. A.; Oñate, E.; Killian, C. M.; Johnson, L. K.; White, P. S.; Brookhart, M., *Macromolecules* **2000,** *33* (7), 2320-2334.
71. Rhinehart, J. L.; Brown, L. A.; Long, B. K., *Journal of the American Chemical Society* **2013,** *135* (44), 16316-16319.
72. Chen, M.; Chen, C., *Angewandte Chemie International Edition* **2018,** *57* (12), 3094-3098.
73. Zhou, X.; Bontemps, S.; Jordan, R. F., *Organometallics* **2008,** *27* (19), 4821-4824.
74. Delferro, M.; McInnis, J. P.; Marks, T. J., *Organometallics* **2010,** *29* (21), 5040-5049.
75. Kenyon, P.; Wörner, M.; Mecking, S., *Journal of the American Chemical Society* **2018,** *140* (21), 6685-6689.
76. Noda, S.; Kochi, T.; Nozaki, K., *Organometallics* **2009,** *28* (2), 656-658.
77. Kocen, A.; Brookhart, M.; Daugulis, O., *Nature Communications* **2019,** *10*, 438.
78. Dai, S.; Zhou, S.; Zhang, W.; Chen, C., *Macromolecules* **2016,** *49* (23), 8855-8862.
79. Younkin, T. R.; Connor, E. F.; Henderson, J. I.; Friedrich, S. K.; Grubbs, R. H.; Bansleben, D. A., *Science* **2000,** *287* (5452), 460-462.
80. Zhang, Y.-P.; Li, W.-W.; Li, B.-X.; Mu, H.-L.; Li, Y.-S., *Dalton Transactions* **2015,** *44* (16), 7382-7394.

81. Mokhadinyana, M. S.; Maumela, M. C.; Mogorosi, M. M.; Overett, M. J.; Van Den Berg, J.-A.; Janse Van Rensburg, W.; Blann, K. Tetramerisation of Ethylene. Int. Patent WO/2014/181250, November 12, 2014, 2014.
82. Egami, H.; Ide, T.; Kawato, Y.; Hamashima, Y., *Chemical Communications* **2015,** *51* (93), 16675-16678.
83. Carmona, E.; Paneque, M.; Poveda, M. L., *Polyhedron* **1989,** *8* (3), 285-291.
84. Kenyon, P.; Mecking, S., *Journal of the American Chemical Society* **2017,** *139* (39), 13786-13790.
85. Tao, W.-j.; Nakano, R.; Ito, S.; Nozaki, K., *Angewandte Chemie International Edition* **2016,** *55* (8), 2835-2839.
86. Tsuda, A.; Fukumoto, C.; Oshima, T., *Journal of the American Chemical Society* **2003,** *125* (19), 5811-5822.
87. Krebs, F. C.; Spanggaard, H., *The Journal of Organic Chemistry* **2002,** *67* (21), 7185-7192.
88. van Truong, N.; Norris, A. R.; Shin, H. S.; Buncel, E.; Bannard, R. A. B.; Purdon, J. G., *Inorganica Chimica Acta* **1991,** *184* (1), 59-65.
89. Nishi, N.; Murakami, H.; Imakura, S.; Kakiuchi, T., *Analytical Chemistry* **2006,** *78* (16), 5805-5812.
90. Collin, R. J.; Smith, B. C., *Dalton Transactions* **2005,** (4), 702-705.
91. Lang, P. F.; Smith, B. C., *Dalton Transactions* **2010,** *39* (33), 7786-7791.
92. Klabunde, U.; Mulhaupt, R.; Herskovitz, T.; Janowicz, A. H.; Calabrese, J.; Ittel, S. D., *Journal of Polymer Science Part A: Polymer Chemistry* **1987,** *25* (7), 1989-2003.
93. Klabunde, U.; Itten, S. D., *Journal of Molecular Catalysis* **1987,** *41* (1), 123-134.
94. Wang, C.; Friedrich, S.; Younkin, T. R.; Li, R. T.; Grubbs, R. H.; Bansleben, D. A.; Day, M. W., *Organometallics* **1998,** *17* (15), 3149-3151.
95. Gao, H.; Ke, Z.; Pei, L.; Song, K.; Wu, Q., *Polymer* **2007,** *48* (25), 7249-7254.
96. Zhang, Y.; Mu, H.; Pan, L.; Wang, X.; Li, Y., *ACS Catalysis* **2018,** *8* (7), 5963-5976.
97. Chen, Z.; Leatherman, M. D.; Daugulis, O.; Brookhart, M., *Journal of the American Chemical Society* **2017,** *139* (44), 16013-16022.
98. Connor, E. F.; Younkin, T. R.; Henderson, J. I.; Waltman, A. W.; Grubbs, R. H., *Chemical Communications* **2003,** (18), 2272-2273.
99. Ota, Y.; Ito, S.; Kuroda, J.-i.; Okumura, Y.; Nozaki, K., *Journal of the American Chemical Society* **2014,** *136* (34), 11898-11901.
100. Zhang, W.; Waddell, P. M.; Tiedemann, M. A.; Padilla, C. E.; Mei, J.; Chen, L.; Carrow, B. P., *Journal of the American Chemical Society* **2018,** *140* (28), 8841-8850.
101. Poater, A.; Cosenza, B.; Correa, A.; Giudice, S.; Ragone, F.; Scarano, V.; Cavallo, L., *European Journal of Inorganic Chemistry* **2009,** *2009* (13), 1759-1766.
102. Poater, A.; Ragone, F.; Giudice, S.; Costabile, C.; Dorta, R.; Nolan, S. P.; Cavallo, L., *Organometallics* **2008,** *27* (12), 2679-2681.
103. Poater, A.; Ragone, F.; Mariz, R.; Dorta, R.; Cavallo, L., *Chemistry – A European Journal* **2010,** *16* (48), 14348-14353.
104. Brown, I. D.; Skowron, A., *Journal of the American Chemical Society* **1990,** *112* (9), 3401-3403.

105. Delgado, M.; Ziegler, J. M.; Seda, T.; Zakharov, L. N.; Gilbertson, J. D., *Inorganic Chemistry* **2016,** *55* (2), 555-557.
106. Liang, T.; Chen, C., *Inorganic Chemistry* **2018,** *57* (23), 14913-14919.
107. Welch, G. C.; Holtrichter-Roessmann, T.; Stephan, D. W., *Inorganic Chemistry* **2008,** *47* (6), 1904-1906.
108. Noda, S.; Nakamura, A.; Kochi, T.; Chung, L. W.; Morokuma, K.; Nozaki, K., *Journal of the American Chemical Society* **2009,** *131* (39), 14088-14100.
109. Conley, M. P.; Jordan, R. F., *Angewandte Chemie International Edition* **2011,** *50* (16), 3744-3746.
110. Tran, Q. H.; Brookhart, M.; Daugulis, O., *Journal of the American Chemical Society* **2020**.
111. Chalmers, B. A.; Nejman, P. S.; Llewellyn, A. V.; Felaar, A. M.; Griffiths, B. L.; Portman, E. I.; Gordon, E.-J. L.; Fan, K. J. H.; Woollins, J. D.; Bühl, M.; Malkina, O. L.; Cordes, D. B.; Slawin, A. M. Z.; Kilian, P., *Inorganic Chemistry* **2018,** *57* (6), 3387-3398.
112. Konishi, Y.; Tao, W.-j.; Yasuda, H.; Ito, S.; Oishi, Y.; Ohtaki, H.; Tanna, A.; Tayano, T.; Nozaki, K., *ACS Macro Letters* **2018,** *7* (2), 213-217.
113. Zhang, Y.; Zhang, Y.; Chi, Y.; Jian, Z., *Dalton Transactions* **2020,** *49* (8), 2636-2644.
114. Tan, C.; Chen, C., *Angewandte Chemie International Edition* **2019,** *58* (22), 7192-7200.
115. Carreras, L.; Rovira, L.; Vaquero, M.; Mon, I.; Martin, E.; Benet-Buchholz, J.; Vidal-Ferran, A., *RSC Advances* **2017,** *7* (52), 32833-32841.
116. Shimizu, F. X., S.; Tanna, A.; Goromaru. S.; Matsubara, K., **2013**.
117. Camacho, D. H.; Salo, E. V.; Ziller, J. W.; Guan, Z., *Angewandte Chemie International Edition* **2004,** *43* (14), 1821-1825.
118. Liu, F.-S.; Hu, H.-B.; Xu, Y.; Guo, L.-H.; Zai, S.-B.; Song, K.-M.; Gao, H.-Y.; Zhang, L.; Zhu, F.-M.; Wu, Q., *Macromolecules* **2009,** *42* (20), 7789-7796.
119. Chen, M.; Chen, C., *ACS Catalysis* **2017,** *7* (2), 1308-1312.
120. Fu, X.; Zhang, L.; Tanaka, R.; Shiono, T.; Cai, Z., *Macromolecules* **2017,** *50* (23), 9216-9221.
121. Chen, Z.; Zhao, X.; Gong, X.; Xu, D.; Ma, Y., *Macromolecules* **2017,** *50* (17), 6561-6568.
122. Li, L.; Wang, Q., *Journal of Polymer Science Part A: Polymer Chemistry* **2004,** *42* (22), 5662-5669.
123. Moyassari, A.; Gkourmpis, T.; Hedenqvist, M. S.; Gedde, U. W., *Macromolecules* **2019,** *52* (3), 807-818.
124. Fan, Y.; Xue, Y.; Nie, W.; Ji, X.; Bo, S., *Polymer Journal* **2009,** *41* (8), 622-628.
125. Men, Y. F.; Rieger, J.; Enderle, H. F.; Lilge, D., *The European Physical Journal E* **2004,** *15* (4), 421-425.
126. Diop, M. F.; Burghardt, W. R.; Torkelson, J. M., *Polymer* **2014,** *55* (19), 4948-4958.
127. Kurtz, S. M.; Muratoglu, O. K.; Evans, M.; Edidin, A. A., *Biomaterials* **1999,** *20* (18), 1659-1688.
128. Nakayama, K.; Furumiya, A.; Okamoto, T.; Yagi, K.; Kaito, A.; Choe, C. R.; Wu, L.; Zhang, G.; Xiu, L.; Liu, D.; Masuda, T.; Nakajima, A., **1991,** *63* (12), 1793.
129. Ferry, J. D., *Viscoelastic properties of polymers*. John Wiley & Sons: 1980.

130. Rastogi, S.; Lippits, D. R.; Peters, G. W. M.; Graf, R.; Yao, Y.; Spiess, H. W., *Nature Materials* **2005,** *4* (8), 635-641.
131. Ahmad, M.; Wahit, M. U.; Kadir, M. R. A.; Dahlan, K. Z. M.; Jawaid, M., **2013,** *33* (7), 599.
132. Bin, Y.; Ma, L.; Adachi, R.; Kurosu, H.; Matsuo, M., *Polymer* **2001,** *42* (19), 8125-8135.
133. Ruff, M.; Lang, R. W.; Paulik, C., *Macromolecular Reaction Engineering* **2013,** *7* (7), 328-343.
134. Cho, K.; Lee, B. H.; Hwang, K.-M.; Lee, H.; Choe, S., *Polymer Engineering & Science* **1998,** *38* (12), 1969-1975.
135. Alt, F. P.; Böhm, L. L.; Enderle, H.-F.; Berthold, J., *Macromolecular Symposia* **2001,** *163* (1), 135-144.
136. Zacca, J. J.; Debling, J. A.; Ray, W. H., *Chemical Engineering Science* **1997,** *52* (12), 1941-1967.
137. Lopez-Linares, F.; Barrios, A. D.; Ortega, H.; Matos, J. O.; Joskowicz, P.; Agrifoglio, G., *J. Mol. Catal. A-Chem.* **2000,** *159* (2), 269-272.
138. Cho, H. S.; Chung, J. S.; Lee, W. Y., *Journal of Molecular Catalysis A: Chemical* **2000,** *159* (2), 203-213.
139. D'Agnillo, L.; Soares, J. B. P.; Penlidis, A., *Journal of Polymer Science Part A: Polymer Chemistry* **1998,** *36* (5), 831-840.
140. Liu, J.; Rytter, E., *Macromolecular Rapid Communications* **2001,** *22* (12), 952-956.
141. Cho, H. S.; Chung, J. S.; Han, J. H.; Ko, Y. G.; Lee, W. Y., *Journal of Applied Polymer Science* **1998,** *70* (9), 1707-1715.
142. Rostovtsev, V. V.; Green, L. G.; Fokin, V. V.; Sharpless, K. B., *Angew. Chem. Int. Ed.* **2002,** *41* (14), 2596-2599.
143. Tornøe, C. W.; Christensen, C.; Meldal, M., *J. Org. Chem.* **2002,** *67* (9), 3057-3064.
144. Yang, M.; Yang, Y.; Chen, P. R., *Top. Curr. Chem.* **2016,** *374* (1), 2.
145. Li, L.; Zhang, Z., *Molecules* **2016,** *21* (10), 1393.
146. Hein, J. E.; Fokin, V. V., *Chem. Soc. Rev.* **2010,** *39* (4), 1302-1315.
147. McKay, C. S.; Finn, M. G., *Chem. Biol.* **2014,** *21* (9), 1075-1101.
148. Zhong, W.; Sun, B.; Lu, C.; Yu, H.; Wang, C.; He, L.; Gu, J.; Chen, S.; Liu, Y.; Jing, X.; Bi, Z.; Yang, G.; Zhou, H.; Sun, T.; Yang, C., *Sci. Rep.* **2016,** *6*, 35579.
149. Beatty, K. E.; Xie, F.; Wang, Q.; Tirrell, D. A., *J. Am. Chem. Soc.* **2005,** *127* (41), 14150-14151.
150. Deiters, A.; Schultz, P. G., *Bioorgan. Med. Chem.* **2005,** *15* (5), 1521-1524.
151. Miguel-Ávila, J.; Tomás-Gamasa, M.; Olmos, A.; Pérez, P. J.; Mascareñas, J. L., *Chem. Sci.* **2018,** *9*, 1947-1952.
152. Clavadetscher, J.; Hoffmann, S.; Lilienkampf, A.; Mackay, L.; Yusop, R. M.; Rider, S. A.; Mullins, J. J.; Bradley, M., *Angew. Chem. Int. Ed.* **2016,** *55* (50), 15662-15666.
153. Li, S.; Wang, L.; Yu, F.; Zhu, Z.; Shobaki, D.; Chen, H.; Wang, M.; Wang, J.; Qin, G.; Erasquin, U. J.; Li, R.; Yingjun, W.; Chengzhi, C., *Chem. Sci.* **2017,** *8* (3), 2107-2114.
154. Lutz, J.-F., *Angew. Chem. Int. Ed.* **2008,** *47* (12), 2182-2184.
155. Fontecilla-Camps, J. C., *Structure and Mechanism of Metalloenzyme Active Sites*. Wiley-VCH Verlag GmbH & Co.: Weinheim, 2006.

156. Schwizer, F.; Okamoto, Y.; Heinisch, T.; Gu, Y.; Pellizzoni, M. M.; Lebrun, V.; Reuter, R.; Köhler, V.; Lewis, J. C.; Ward, T. R., *Chem. Rev.* **2018,** *118* (1), 142-231.
157. Kuijpers, P. F.; Otte, M.; Dürr, M.; Ivanović-Burmazović, I.; Reek, J. N. H.; de Bruin, B., *ACS Catal.* **2016,** *6* (5), 3106-3112.
158. Leung, D. H.; Fiedler, D.; Bergman, R. G.; Raymond, K. N., *Angew. Chem. Int. Ed.* **2004,** *43* (8), 963-966.
159. Fiedler, D.; Leung, D. H.; Bergman, R. G.; Raymond, K. N., *Acc. Chem. Res.* **2005,** *38* (4), 351-360.
160. Kaphan, D. M.; Levin, M. D.; Bergman, R. G.; Raymond, K. N.; Toste, F. D., *Science* **2015,** *350* (6265), 1235-1237.
161. Mouarrawis, V.; Plessius, R.; van der Vlugt, J. I.; Reek, J. N. H., *Frontiers Chem.* **2018,** *6*, 623.
162. Bond, A. D.; Derossi, S.; Harding, C. J.; McInnes, E. J.; McKee, V.; McKenzie, C. J.; Nelson, J.; Wolowska, J., *Dalton Trans.* **2005,** (14), 2403-2409.
163. Dussart, Y.; Harding, C.; Dalgaard, P.; McKenzie, C.; Kadirvelraj, R.; McKee, V.; Nelson, J., *J. Chem. Soc., Dalton Trans.* **2002,** (8), 1704-1713.
164. Drew, M. G. B.; Harding, C. J.; Howarth, O. W.; Lu, Q.; Marrs, D. J.; Morgan, G. G.; McKee, V.; Nelson, J., *J. Chem. Soc., Dalton Trans.* **1996,** (14), 3021-3030.
165. Chan, T. R.; Hilgraf, R.; Sharpless, K. B.; Fokin, V. V., *Org. Lett.* **2004,** *6* (17), 2853-2855.
166. Wilson, Y. M.; Dürrenberger, M.; Nogueira, E. S.; Ward, T. R., *J. Am. Chem. Soc.* **2014,** *136* (25), 8928-8932.
167. Ngo, A. H.; Bose, S.; Do, L. H., *Chem. Eur. J.* **2018,** *24* (42), 10584-10594.
168. Wang, C.; Wang, D.; Yu, S.; Cornilleau, T.; Ruiz, J.; Salmon, L.; Astruc, D., *ACS Catal.* **2016,** *6* (8), 5424-5431.
169. Presolski, S. I.; Hong, V.; Cho, S.-H.; Finn, M. G., *J. Am. Chem. Soc.* **2010,** *132* (41), 14570-14576.
170. Deraedt, C.; Pinaud, N.; Astruc, D., *J. Am. Chem. Soc.* **2014,** *136* (34), 12092-12098.
171. Bai, Y.; Feng, X.; Xing, H.; Xu, Y.; Kim, B. K.; Baig, N.; Zhou, T.; Gewirth, A. A.; Lu, Y.; Oldfield, E.; Zimmerman, S. C., *J. Am. Chem. Soc.* **2016,** *138* (35), 11077-11080.
172. Fu, F.; Martinez, A.; Wang, C.; Ciganda, R.; Yate, L.; Escobar, A.; Moya, S.; Fouquet, E.; Ruiz, J.; Astruc, D., *Chem. Commun.* **2017,** *53* (39), 5384-5387.
173. Lu, Q.; Latour, J.-M.; Harding, C. J.; Martin, N.; Marrs, D. J.; McKee, V.; Nelson, J., *J. Chem. Soc., Dalton Trans.* **1994,** (9), 1471-1478.
174. Qin, L.; McCann, M.; Nelson, J., *J. Inorg. Biochem.* **1993,** *51* (3), 633-639.
175. Drew, M. G. B.; Farrell, D.; Morgan, G. G.; McKee, V.; Nelson, J., *J. Chem. Soc., Dalton Trans.* **2000,** (9), 1513-1519.
176. Sato, T.; Suzuki, A.; Sakai, K.; Tsubomura, T., *Bull. Chem. Soc. Jpn.* **1996,** *69* (2), 379-388.
177. Youinou, M.-T.; Suffert, J.; Ziessel, R., *Angew. Chem. Int. Ed.* **1992,** *31* (6), 775-778.
178. Yang, L.-Z.; Li, Y.; Zhuang, X.-M.; Jiang, L.; Chen, J.-M.; Luck, R. L.; Lu, T.-B., *Chem. Eur. J.* **2009,** *15* (45), 12399-12407.
179. Schatz, M.; Becker, M.; Walter, O.; Liehr, G.; Schindler, S., *Inorganica Chim. Acta* **2001,** *324* (1), 173-179.

180. Donnelly, P. S.; Zanatta, S. D.; Zammit, S. C.; White, J. M.; Williams, S. J., *Chem. Commun.* **2008,** (21), 2459-2461.
181. Makarem, A.; Berg, R.; Rominger, F.; Straub, B. F., *Angew. Chem. Int. Ed.* **2015,** *54* (25), 7431-7435.
182. Presolski, S. I.; Hong, V. P.; Finn, M. G., *Curr. Protoc. Chem. Biol.* **2011,** *3*, 153-162.
183. Shin, J.-A.; Lim, Y.-G.; Lee, K.-H., *J. Org. Chem.* **2012,** *77* (8), 4117-4122.
184. Meldal, M.; Tornøe, C. W., *Chem. Rev.* **2008,** *108* (8), 2952-3015.
185. Ikhlef, D.; Wang, C.; Kahlal, S.; Maouche, B.; Astruc, D.; Saillard, J.-Y., *Comput. Theor. Chem.* **2015,** *1073*, 131-138.
186. Jin, L.; Tolentino, D. R.; Melaimi, M.; Bertrand, G., *Sci. Adv.* **2015,** *1* (5), e1500304.
187. Chen, H.; Soubra-Ghaoui, C.; Zhu, Z.; Li, S.; Albright, T. A.; Cai, C., *J. Catal.* **2018,** *361*, 407-413.
188. Chen, H.; Cai, C.; Li, S.; Ma, Y.; Luozhong, S.; Zhu, Z., *Chem. Eur. J.* **2017,** *23* (19), 4730-4735.
189. Rubino, J. T.; Chenkin, M. P.; Keller, M.; Riggs-Gelasco, P.; Franz, K. J., *Metallomics* **2011,** *3* (1), 61-73.
190. Poole, L. B., *Free Radical Biol. Med.* **2015,** *80*, 148-157.
191. Lushchak, V. I., *J. Amino Acids* **2012,** *736837*.
192. Brigham, M. P.; Stein, W. H.; Moore, S., *J. Clin. Invest.* **1960,** *39* (11), 1633-1638.
193. Lubineau, A.; Augé, J.; Scherrmann, M.-C., Organic Chemistry in Water. In *Aqueous Phase Oragnometallic Catalysis*, Cornils, B.; Herrmann, W. A., Eds. Wiley-VCH: Weinheim, 2004; pp 27-43.
194. Massoud, S. S.; Louka, F. R.; Ducharme, G. T.; Fischer, R. C.; Mautner, F. A.; Vančo, J.; Herchel, R.; Dvořák, Z.; Trávníček, Z., *J. Inorg. Biochem.* **2018,** *180*, 39-46.
195. Jopp, M.; Becker, J.; Becker, S.; Miska, A.; Gandin, V.; Marzano, C.; Schindler, S., *Eur. J. Med. Chem.* **2017,** *132*, 274-281.
196. Charalambidis, G.; Ladomenou, K.; Boitrel, B.; Coutsolelos, A. G., *Eur. J. Org. Chem.* **2009,** (8), 1263-1268.
197. MacDowell, D.; Nelson, J., *Tetrahedron Lett.* **1988,** *29* (3), 385-386.
198. Möller, F.; Merz, K.; Herrmann, C.; Apfel, U. P., *Dalton Trans.* **2016,** *45* (3), 904-907.
199. Whiteford, J. A. Bridged Polycyclic Compound Based Compositions for the Inibition and Amelioration of Disease. US 2008/0275141 A1, Nov. 6, 2008, 2008.
200. Chen, D.; Martell, A. E., *Tetrahedron* **1991,** *47* (34), 6895-6902.
201. Charalambidis, G.; Ladomenou, K.; Boitrel, B.; Coutsolelos, A. G., *Eur. J. Org. Chem.* **2009,** *2009* (8), 1263-1268.